AXISYMMETRIC AIR JET IMPINGING ON A CONVEX HEMISPHERICAL PLATE

BY

DAVID C. CHAN

A THESIS

PRESENTED IN PARTIAL FULFILLMENT OF

THE REQUIREMENT FOR THE DEGREE

OF

MASTER OF SCIENCE IN MECHANICAL ENGINEERING

AT

NEW JERSEY INSTITUTE OF TECHNOLOGY

Newark, New Jersey

1979

APPROVAL OF THESIS

AXISYMMETRIC AIR JET IMPINGING ON

A CONVEX HEMISPHERICAL PLATE

BY

DAVID C. CHAN

FOR

DEPARTMENT OF MECHANICAL ENGINEERING

NEW JERSEY INSTITUTE OF TECHNOLOGY

BY

FACULTY COMMITTEE

APPROVED: _____

_____

_____

NEWARK, NEW JERSEY

1979

TABLE OF CONTENTS

ACKNOWLEDGEMENT

The author wishes to express his utmost appreciation for the instruction and encouragement of his advisor, Dr. Peter Hrycak. Thanks is also due to Dr. Stefan Jachna who had given valuable suggestions and consultation during the course of this experimental work.

Acknowledgement is also due to the Mechanical Engineering Department of New Jersey Institute of Technology for the co-operation given to the author during the entire experiment.

ABSTRACT

Experimental investigation was conducted on an axisymmetric, submerged air jet impinging normally on a smooth convex hemisphere. Three nozzle diameters of 0.5" (12.7mm), 0.375" (9.525mm) and 0.25" (6.35mm) were used and tests were run at Reynolds number range of 14,700 to 84,000.

The results obtained in the free jet and deflection zones were found to confirm the works of previous investigators. As for the fully developed wall jet region, the following points are noted:

1) The maximum wall-velocity decay was found to possess a slightly higher rate than that of either the flat plate or the concave hemisphere.
2) The mean velocity profile at a given wall distance from the stagnation point follows the same profile as those of the flat plate and the concave hemisphere; but deviates from them at the outer envelope ($Z/Z_{\frac{1}{2}} > 1.2$) where it decays at the highest rate, followed by the curves of the flat plate and of the concave surface, in that order.
3) Both the inner boundary layer and the outer boundary were established. In comparison with the flat plate case, the inner boundary layer grows at a slightly higher rate (with respect to the wall distance), while the outer boundary layer grows at a slightly lower rate.

4) Negative static pressure distributions were found laterally across the wall jet. The maximum value occurs at $Z/Z_{\frac{1}{2}}$ equal 0.9 and is a function of nozzle diameter, distance of the nozzle exit from the impingement surface, and the distance from the stagnation point along the wall surface. The measurments of such negative static pressure serve as a verification of the Coanda Effect.

LIST OF SYMBOLS

Symbol	Definition	U.S. Engr. Units	International System of Units
b	width of jet, or the outer boundary thickness	inch	mm
C	defined in Fig. 6 and in Eq.(7)	dimensionless	
L	lip of the nozzle and defined in Fig. 6	"	
Re_D	Reynolds number based on nozzle diameter, air velocity and viscosity	"	
P	pressure	lbf/sq.in	N/m^2
P_s	static pressure	"	"
P_∞ , P_a	ambient pressure	"	"
P_c	static pressure along the jet centerline	"	"
P_{max}	maximum pressure	"	"
U	velocity in the x-direction	ft/sec	meter/sec
U_m	maximum axial velocity of the jet	"	"
U_{oc}	velocity at the center of nozzle exit	"	"
D	diameter of nozzle	inch	mm

Symbol	Definition	U.S. Engr. Units	International System of Units
V	velocity in the s-direction, along the circumference of the hemisphere	ft/sec	meter/sec
V_{rb}	reference boundary velocity	"	"
x	distance away from the nozzle along the centerline as defined in Fig. 1	inch	mm
y	distance normal to the nozzle centerline as defined in Fig. 1	"	"
$y_{\frac{1}{2}}$	y-location where $U = \frac{1}{2} U_m$	"	"
Z, z	distance normal to the circumference of the hemisphere as shown in Fig. 1	"	"
$Z_{\frac{1}{2}}$, $z_{\frac{1}{2}}$	z-location where $V = \frac{1}{2} V_m$	"	"
$\overline{Z}$	normal distance between the target plate and the nozzle	"	"
$S/\overline{Z}$	the ratio of the circumferential distance (s) to the nozzle exit from the impingement surface	dimensionless	
$\overline{Z}/D$	the ratio of the target plate distance from the nozzle to the nozzle diameter	"	

Symbol	Definition	U.S. Engr. Units	International System of Units
θ	angular distance from the stagnation point on the hemisphere	degree	radian
$\theta\sin\theta$	the product of the angle θ and its sine function	degree	radian
δ	boundary layer thickness, wall jet region	inch	mm
μ	dynamic viscosity	lbm/ft sec or lbm/ft hr	N-sec/m^2
$\nu = \frac{\mu}{\rho}$	kinematic viscosity	sq ft/hr or sq ft/sec	m^2/sec
ζ	$(z - \delta)/b$	dimensionless	
ρ	density	lbm/cu ft	Kg/cu m
η	$\frac{P_s - P_a}{\rho \, U_{oc}^2}$	dimensionless	

Subscript "o" indicates conditions at the origin (real or virtual).

Prime indicates differentiation with respect to s.

All other symbols are defined in the text.

CHAPTER 1

INTRODUCTION

A jet is defined as a quantity of fluid being discharged from a nozzle or orifice into a medium. When the jet is not confined and the medium is at rest, the jet is termed 'free'. When the flow of fluid of a free jet impinges upon a surface, the jet would be deflected and move outwardly along the surface, and a wall jet is formed. In analyzing jets, there are two main classes. When the jet issues from a slot, it is a two dimensional plane jet. When the jet issues from a circular nozzle or orifice, it is an axisymmetric radial jet. The present investigation deals with the latter--- axisymmetric type.

There are many applications of jets. Some of the common areas of such applications are:

1) A single jet or a row of jets is used in spot cooling of turbine blades, especially in high performance engines.
2) A Pelton wheel is powered by an impinging jet which converts kinetic energy to mechanical energy.
3) A blow torch utilizes a jet of combustible gaseous mixtures to deliver the required heat released in combustion to the work.
4) A rocket is powered by the momentum change carried by a jet.
5) A jet of water is used by a dentist to clean and polish the teeth of a patient.
6) In the glass industry, a matrix of jets is used for cooling intricate molds.

In summary, a jet is used as a heat transfer, momentum transfer or mass transfer carrier.

Historical Background

Early in 1925, Prandtl published his mixing length threory. Tollmien was the first man to apply this theory to theoretically solve for an axially symmetrical jet from a small nozzle[1]. In 1932, Taylor published his theory of free turbulence[1]. In 1942, Prandtl published a second theory based on viscous friction[1]. Based on this theory, Görtler obtained the solution for a free circular turbulent jet in a closed form. Furthermore, the problem of mixing zone at the boundary of parallel jets[10], and this was substantiated by the investigation of Reichardt[30]. The following is a list of researchers who had contibuted to the study of jets.

Researcher	Reference No.	Area of Interest
Glauert	8	Wall jet along a flat plate
Miller and Comings	12	The study of static pressure in jet
Gooderum, Wood and Brevoort	9	Investigation of free boundary of a free supersonic jet
Bakke	4	Experimentation with wall jet and essay on investigation technique
Poreh and Cermak	13	Investigation of Impinging jets
Hrycak, Lee, Gauntner and Livingood	20	Study of mass and heat transfers in impinging jets
Russell and Hatton	31	By use of both Pitot tube and hot wire measurements, impinging jet was studied and Pitot tube was found to give better results

Researcher	Reference #	Area of Interest
Beltaos and Rajaratnam	5	A presentation of compatible velocity distribution in the study of slot jet impinging on a flat plate
Krishnan and Glickman	22	The analysis of a two dimensional heated free jet
Tsuei	34	Investigated the boundary layer of a jet impinging on a smooth plate
Kim	21	Analytical research was done on the momentum, mass and heat transfer characteristics in the flow field produced by an axisymmetric jet impinging normally on an infinite plate
Wilson	35	Experimentation with a slot jet impinging on the outsde of a cylinder
Lee	23	Experimental investigation of an axisymmetric jet impinging on a flat plate
Hrycak	19	Investigation of heat transfer characteristics from a row of jet impinging on a concave semi-cylindrical surface
Jachna	33	Investigation of fluid characteristics of an axisymmetric jet impinging on the concave side of a hemisphere
Jit	32	An experimental and analytical investigation of the mass transfer

Researcher	Reference #	Area of Interest
Jit	32	of an air jet impinging on a flat surface saturated with a volatile liquid (methyl alcohol)

.....

CHAPTER 2

SUBJECT OF INVESTIGATION

This investigation was done experimentally on a turbulent, subsonic, axisymmetric submerged jet impinging on the convex side of a hemisphere. As shown in Figure 1, the impinging jet can be divided into four main regions.

I Potential Core

II Free Jet

III Deflection Zone

IV Wall Jet

The following is the list of specifics of which this investigation was done on.

I Velocity profile and static pressure distribution of free jet both along the axis and across the axis of the flow path.

II Velocity profile, static pressure distribution of wall jet both along and across the wall jet flow path.

III Velocity profile of the deflection zone.

IV Inner and outer boundary layers of the wall jet.

The range of Reynolds number was between 14,700 and 84,000 and based on the findings of (20) which stated that at Reynolds number over 4,000, fully turbulent flow would result. The flow in the present investigation is considered fully turbulent.

Since the Mach number of the wall jet was below 0.3, the flow was incompressible by virtue of reference (31). Compressibility was considered as part of the data analysis, and it was found that the effect was negligible.

The technique of this investigation followed the same path as those of Lee[23] and Jachna[33]. The results of this investigation were compared to theirs as well as those of Jit[32], Wilson[35] and Tsuei[34]. Analytical modeling on maximum velocity decay on the wall jet was based on the intergral momentum equation.

CHAPTER 3

EXPERIMENTAL APPARATUS AND PROCEDURE

3.1 Piping and Air Supply

A reciprocating compressor located directly underneath the laboratory is used to compress the intake ambient air to about 60 psig and the compressed air is then stored in a large reservoir to ensure a steady flow. Since it is essential to maintain constant pressure and flow rate of air during each run, a separate air supply such as the one referred is required. Its is for this reason that the use of the central plant air or branching of air supply to other outlets is not possible. A sketch is shown in Fig.(3)outlining the air supply from a rotometer to the testing nozzle. Moreover, the three manometers (one with mercury, one with water, and one a 0.797 S.G. oil) are shown in the same figure. The rotometer gives accurate flow rate measurement of the air to the nozzle. The accuracy of this instrument is better than 1 %. The inlet pressure at the rotometer inlet is registered by a Bourdon gage. The flow goes through the controlled section, then enters a $1\frac{1}{2}$ inch pipe and enters a plenum chamber through an orifice. In the plenum chamber, a thermocouple is placed to record the temperature of the air there. The plenum chamber is $2\frac{1}{2}$ inches in diameter and 35 inhes in length, and is connected to the $1\frac{1}{2}$ inch pipe by a 90 degrees, $1\frac{1}{2}$ to $2\frac{1}{2}$ inches reducer. At the outlet, an end plate is welded on, nozzles of various sizes may be fitted. In the present experiment, four different nozzle diameters (1/8, 1/4, 3/8, 1/2 inch) were used. A rubber seal is placed at the threaded end of the nozzle to ensure air tightness. The plenum chamber is directed vertically with the aid of three supporting guide wires.

3.2 Manometers

Two large manometer boards, one with mercury and the other with water are used. For low pressure measurement, such as low velocity at the end of the boundary layer or the static pressure of the wall jet, a micromanometer with an oil with 0.797 specific gravity is used. Readings are made by turning a dial which is divided into 0.001 inch by bringing the meniscus to zero. The oil is dyed blue for ease of reading.

3.3 Traversing Carriage

As shown in Fig.(2), the pressure probes are mounted on the carriage by a slide. The slide-carriage system can be moved in three dimensions so as to take pressure measurement at all points of interest of the jet. The slide travels vertically to a maximum of 24 inches while the carriage moves in either direction up to 6 inches in the horizontal plane. The probe can also be rotated about the axis of its tubing to enable the probe to pick up measurements of the flow patterns.

3.4 Impinging Surface

The convex hemisphere is of 7.48 inches in nomimal outer diameter and 0.05 inch in thickness. It is made of brass and fixed to three long threaded bolts as shown in Fig.(4). The height of the hemisphere can be adjusted by the threads of the bolts and also by means of an external fixture made of plywood. There are two rows of 16 holes of 1/64 inch in diameter. The two rows are at right angles to each other. They serve as pressure taps for static pressure measurements along the surface of the wall jet.

3.5 Pressure Probes

Fig.(3a)shows the details of the measuring probes. Four static pressure probes and two total pressure probes are used. The measurements of each probe are critically precise and conform to the recommended design by NASA. The unique lip feature of the nozzles used is equally critical so as to obtain the most precise pressure measurements with the least interference of the device present in the flow field.

3.6 Experimental Procedure

By means of the experiment set stated in the last section and illustrated in Figs. 2 to 4, measurements of total pressure and static pressure are taken in the desired areas of both free jet and wall jet. The axisymmetric, incompressible and turbulent jets issuing from nozzles of four different sizes are studied. The nozzles are 1/8, 1/4, 3/8, and 1/2 inch in diameters respectively. Due to the small quantity of flow obtained from the 1/8 inch nozzle, measurements in the wall jet zone, particularly when the impingement distance is large, pressure readings are too small to be measured accurately. So, in the study of wall jet, this nozzle size is omitted. This is also in agreement with the findings of Lee[23]. For nozzle alignment, the stagnation point is found on the impinging surface as a starting point. Although Snedeker[16] recommended the use of a drop of dark grease applied at the approximate stagnation point would spread out radially, giving a good indication of streamline patterns and the stagnation point, it is not used in the present experiment. The reason is---- there is a pressure tap at the center of the hemisphere, it is much neater and easier to just observe the maximum pressure reading at the tap while aligning the nozzle directly above this tap under the assumption

that this tap is at the geometric center of the impingement surface. The same procedure was undertaken by Jachna[33] in his investigation of jet impinging on a concave hemisphere.

The range of Reynolds number based on nozzle diameter is between 14,700 and 84,000 and with $\bar{Z}/D$ (impingement distance to nozzle diameter ratio) at 4, 7, 10 and 20. The total and static pressure probes shown in Fig.(3a) give velocity and static pressure profiles. At each point in space where measurement is required, the probe is rotated tangent to the streamline so that the true measurement can be obtained at all times. This technique was employed by Lee[23] and Jachna[33] and was suggested by Dr. Hrycak.

In the free jet zone, the velocity decay along the centerline is obtained to investigate the relationship between Reynolds number based on nozzle diameter and the resulting potential core. In the wall jet zone, the velocity profile and the maximum velocity decay along the surface are studied. In addition, the profile of the reference boundary layer velocity which is the hypothetical velocity at the centerline of an equivalent free jet is also obtained. The boundary layer of the wall jet is divided into two parts. The inner layer corresponds to the velocity of zero at the wall to a small distance from the wall where the local velocity reaches a maximum. The outer layer then takes over at the maximum velocity point to a distance far enough so that the velocity approaches that of the medium. The profile of those two boundary layers and the co-ordinate system are shown graphically in Fig.(5).

CHAPTER 4

ANALYTICAL MODEL

4.1 Free Jet Zone

In the presence of an impingement surface, the free jet zone was determined as 8/10 of the vertical distance between the nozzle and the stagnation point as shown in Fig. (1) by Poreh and Cermak[13] and was verified by Tani and Komatsu[17], and Lee[23]. The flow profiles of this zone are the same as in a free jet. Again, the free jet zone can be subdivided into the potential core where the centerline velocity remains constant and the fully developed region where the velocity begins to decay according to the relationship to be derived below.

By means of Prandtl's mixing length theory:

The shearing stress, $$\tau = l^2 \rho \left|\frac{\partial u}{\partial y}\right| \frac{\partial u}{\partial y} \qquad (1)$$

where, y = radial distance

l = length of the fluid element

and, $$\tau = \rho l^2 \frac{\partial u}{\partial y} \sqrt{\left(\frac{\partial u}{\partial y}\right)^2 + l_1^2 \left(\frac{\partial^2 u}{\partial y^2}\right)^2} \qquad (2)$$

where the mixing lengths l and l_1 are purely local functions, according to new theory,

$$\tau = \rho \epsilon \frac{\partial u}{\partial y} = \rho A b \left(U_{max} - U_{min} \right) \frac{\partial u}{\partial y} \qquad (3)$$

where b = width of mixing zone

A = empirical constant

ϵ = virtual kinematic viscosity

Re-arranging eq(3)

$$\epsilon = Ab\ (U_{max} - U_{min})$$

According to Schlichting[15],

change of width/change of distance from jet

= a constant

$$\frac{db}{dx} = B, \text{ a constant}$$

$$\text{or, } b = Bx \qquad (5)$$

The momentum of an axisymmetric jet, $J = \rho \int_A u^2\ dA$

= constant, by the conservation of momentum

$$J = C\ \rho\ U_m^2\ b^2$$

From eq. (5)

$$J = C\ \rho\ U_m^2\ (B^2 x^2)$$

$$= K\ \rho\ U_m^2\ x^2$$

So, $$U_m^2 = J/(K\ \rho\ x^2)$$

$$U_m = \frac{J^{\frac{1}{2}}}{(K\rho)^{\frac{1}{2}} x^{\frac{1}{2}}}$$

From the conservation of momentum,

$$J = \text{constant}$$

From incompressibility,

$$\rho = \text{constant}$$

$$U_m = \frac{K}{x} \qquad (6)$$

$$\frac{U_m}{U_{oc}} = \frac{K}{x\, U_{oc}}$$

But, $U_{oc} = \frac{Re\,\mu}{D}$

$$\frac{U_m}{U_{oc}} = \frac{K}{Re\,\mu(\frac{x}{D})}$$

For a given run, Re and μ are constant

so,

$$\frac{U_m}{U_{oc}} = \frac{K}{\text{constant}\ (\frac{X}{D})} \qquad \text{(where x and X are the same)}$$

$$\frac{U_m}{U_{oc}} = \frac{C}{\frac{X}{D}} \qquad (7)$$

This is the maximum centerline velocity decay of the jet and it is valid in the fully developed region at X/D from 8 to 16 in the present case. The coefficient C in the above equation is determined by Abramovich[1] to be independent of Reynolds number for the range of Re_D between 20,000 and 400,000 based on his analysis of the works by Trupel, Zimm, Turkus and Syrkin. From Lee's work, it is found that for Reynolds numbers below 20,000, the coefficient C is a weak function of Reynolds number. However, it is a constant just as stated by Abramovich for higher Reynolds numbers.

From Schlichting[15],

for a circular jet, the kinematic momentum,

$$K = 2\pi \int_0^\infty u^2 y \, dy = \frac{J}{\rho} \tag{8}$$

$$U = \frac{3K}{8\pi \epsilon_o X \left(1 + \frac{1}{4}\bar{\eta}^2\right)^2} \tag{9}$$

$$V = \frac{1}{4}\sqrt{\frac{3}{\pi}}\,\frac{\sqrt{K}}{X}\,\frac{\bar{\eta} - \frac{1}{4}\bar{\eta}^2}{\left(1 + \frac{1}{4}\bar{\eta}^2\right)^2} \tag{10}$$

$$V = \frac{1}{4}\sqrt{\frac{3}{\pi}}\,\frac{\sqrt{K}}{\epsilon_o}\,\frac{y}{X} \tag{11}$$

where U and V are the axial velocity of the free jet and wall jet velocity respectively.

For incompressible, low speed jet, the static pressure in the submerged jet, is always considered constant and equal to the ambient

pressure. However in this experiment and those of Lee and Jachna, static pressure has been found to vary as a function of Reynolds Numbers. In addition this pressure is negative (i.e. lower than ambient pressure throughout the developed region). This serves as a driving mechanism for the mass in the medium to come in and fill in the void created by the jet.

4.2 Deflection Zone

i) Non-viscous flow

Schlichting[15] obtained the three dimensional flow equation in stagnation flow by analyzing a fluid stream impinging on a wall at right angle to it and flowing away radially.

The Navier-Stokes equations in cylindrical co-ordinates for rotation symmetry, and incompressible flow:

$$u\frac{\partial u}{\partial r} + w\frac{\partial u}{\partial r} = -\frac{1}{\rho}\frac{\partial p}{\partial r} + \nu\left(\frac{\partial^2 u}{\partial r^2} + \frac{1}{r}\frac{\partial u}{\partial r} - \frac{u}{r^2} + \frac{\partial^2 u}{\partial z^2}\right)$$

$$u\frac{\partial w}{\partial r} + w\frac{\partial w}{\partial z} = -\frac{1}{\rho}\frac{\partial p}{\partial z} + \nu\left(\frac{\partial^2 w}{\partial r^2} + \frac{1}{r}\frac{\partial w}{\partial r} + \frac{\partial^2 w}{\partial z^2}\right)$$

$$\frac{\partial u}{\partial r} + \frac{u}{r} + \frac{\partial w}{\partial z} = 0$$

Assume at the wall, $z = 0$, the stagnation point is at the origin and that the flow is in the direction of the negative z-axis.

For non-viscous flow, the radial component of velocity = u

the axial component of velocity = w

For viscous flow, they are $u = u(r,z)$, radially

$w = w(r,z)$, axially

Boundary Conditions:

$z = 0$: $u = 0$, $w = 0$

$z = \infty$: $u = U$

The solution:

$$V = as \tag{12}$$

$$U = -2az \tag{13}$$

$$P_o - P = \tfrac{1}{2}\rho (U^2 + V^2) = \tfrac{1}{2}\rho a^2 (s^2 + 4z^2) \tag{14}$$

where r has been replaced by s, the circumferential distance

Because the deflection zone of the present investigation is not large and the hemispherical surface is well polished, the friction effect is not significant so that Eq. (12) to Eq. (14) apply.

It is seen that from Eq. (12), the radial velocity increases linearly from the point of stagnation. This is confirmed by the plots in Fig. (64) to Fig. (70).

As the flow reaches some place farther away, the viscous effect becomes predominant and the equation is no longer valid. The actual flow velocity reaches a maximum and starts to decrease. As s or r reaches oo, the velocity becomes zero. Equation (13) shows that the axial velocity of flow increases linearly from zero at stagnation to some distance z vertically above the surface of the plate, the velocity profile leaves the deflection zone and enters the free jet zone again. Equation (14) shows that the static pressure varies parabolically along the plate and the jet centerline.

ii) Viscous Flow

The equations in this case are:

$$V = s\, f'(z) \tag{15}$$

$$U = -2f(z) \tag{16}$$

$$P_o - p = \tfrac{1}{2}\rho a^2 (s^2 + F(z)) \tag{17}$$

A solution of these equations in the form of a power series was first obtained by F. Homann[29]. These equations were also solved by Schach[27], Strand[28], and Tani and Komatsu[17].

4.3 Radial Wall Jet

Abramovich[1] developed the velocity of a fan jet and this can be extended to describe the velocity profile of a wall jet. As stated in his text[1], a sector OAB with center angle ϕ_{AB} is considered. The projection of the momentum of the mass per unit time which passes, in the main region of the jet, through an element $d\phi$ of the sector on the plane of symmetry of this sector of a layer, is equal to the projection on the same plane of the initial momentum in the corresponding part of the nozzle. In equation form:

$$\rho_o u_o^2 b_o r_o \cos\phi \, d\phi = r \cos\phi \, d\phi \int_o^b u^2 \rho \, dy \qquad (18a)$$

Here, the value of velocity u at any radius r depends only on the distance y to the plane of symmetry of the jet.

$$\text{So, } \rho_o u_o^2 b_o r_o = r \int_o^b \rho u^2 \, dy = \rho_o r b u_m^2 \int_o^1 \left(\frac{u}{u_m}\right)^2 \frac{\rho}{\rho_o} \, d\zeta \qquad (18b)$$

where, $\zeta = y/b$

For the isothermal jet where the

$$\int_o^1 \frac{\rho}{\rho_o} \left(\frac{u}{u_m}\right)^2 d\zeta = 0.316 \qquad (18c)$$

From Eq. (18b)

$$\left(\frac{u_o}{u_m}\right)^2 = \frac{0.316 \, rb}{r_o b_o} \qquad (18d)$$

Using the growth law for the thickness of the basic region of a submerged jet

$$\frac{db}{dr} = k = 0.22$$

and denoting ($r - r_o$) by x, we have:

$$b = k(r - r_o - x_o) = k\,(x - x_o)$$

Upon substitution of the above relationship into Eq.(18d), it yields:

$$\left(\frac{u_m}{u_o}\right)^2 = \frac{b_o\, r_o}{0.316\, k\, (x - x_o)\, (x + r_o)} \qquad (18e)$$

At a great distance from the nozzle ($x \gg r_o$) and $x_o \approx 0$

$$\frac{u_m}{u} = \frac{1}{x}\sqrt{\frac{r_o\, b_o}{0.316k}}$$

$$\approx \frac{3.8\sqrt{r_o\, b_o}}{x} = \frac{3.8\, b_o}{x}\sqrt{\frac{r_o}{b_o}} \qquad (18f)$$

Extending the above to use for the wall jet, and putting in the applicable paramters:

$$\frac{V_m}{U_{oc}} = \frac{3.8\, b_o}{s}\sqrt{\frac{s_o}{b_o}}$$

$$V_m = \frac{\text{constant}}{s} \qquad (19)$$

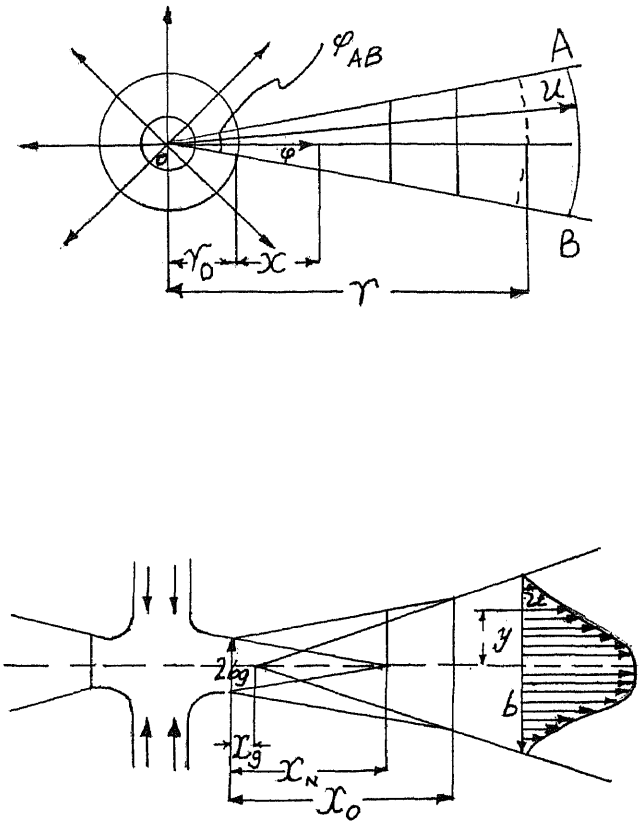

The diagram of a fan jet in two views[1]

Poreh and Cermak[14] assumed that the effect of the wall would be confined to the boundary layer near the wall and obtained an hypothetical parameter, V_{rb} , the reference boundary velocity

$$V_{rb} = \frac{\text{Constant}}{r} \qquad (20)$$

By use of Prandtl's second hypothesis,

$$\frac{V}{V_{rb}} = 1 - \tanh^2 \alpha \bar{\eta} \quad ; \quad \bar{\eta} = \frac{z}{s} \tag{21}$$

Similar to the analysis of two dimensional wall jets by Abramovich[1], the momentum balance equation is set up on a control volume with cross-section ABCD:

momentum in thru the surface AB − momentum out thru the surface AD
+ momentum in thru the surface BC − momentum out thru the surface DC
= momentum accumulation in control volume ABCD

(22)

Refer to Fig. 5

This equation is true only if $\tau_\alpha \frac{dv}{dz} = 0$ at $V = V_m$. Assume constant density, the ambient fluid is stationary, and the flow is in steady state; the above equation reduces to

$$2\pi s_o b_o \rho V_o^2 - \int_{s_o}^{s} \rho V_m \frac{\partial}{\partial s} \left(\int_0^{\delta} 2V\pi s \, dz \right) ds$$

$$= \int_{\delta}^{b+\delta} \rho 2V^2 \pi s \, dz \tag{23}$$

$$V_o^2 b_o s_o - \int_{s_o}^{s} V_m \frac{\partial}{\partial s} \left(\int_0^{\delta} V s \, dz \right) ds = \int_{\delta}^{b+\delta} s V^2 \, dz$$

(24)

Differentiate Eq. (24) with respect to s, and the following results:

$$V_m \int_0^{\delta} \frac{\partial s V}{\partial s} \, dz + \int_{\delta}^{b+\delta} \frac{\partial s V^2}{\partial s} \, dz = 0 \qquad (25)$$

In addition, introduce the following dimensionless parameters:

$$\bar{V} = \frac{V}{V_o} \qquad \bar{V}_m = \frac{V_m}{V_o}$$

$$\bar{z} = \frac{z}{\delta} \qquad \zeta = \frac{z - \delta}{b} \qquad (26)$$

$$d\bar{z} = \frac{1}{\delta} \, dz \qquad d\zeta = \frac{1}{b} \, dz$$

Upon substitution, Eq. (25) becomes

$$\bar{V}_m \delta \int_0^1 \left(\frac{\partial s \bar{V}}{\partial s}\right) d\bar{z} + b \int_0^1 \partial\left(\frac{s \bar{V}^2}{\partial s}\right) d = 0$$

$$\bar{V}_m \delta \int_0^1 s \frac{\partial \bar{V}}{\partial s} \, d\bar{z} + \bar{V}_m \int_0^1 s' \bar{V} \, d\bar{z} +$$

$$2b \int_0^1 s \bar{V} \frac{\partial \bar{V}}{\partial s} \, d\zeta + b \int_0^1 s' \bar{V}^2 \, d\zeta = 0 \qquad (27)$$

Near the wall, the normalized velocity distribution for the so called inner boundary layer is expressed by Schlichting's Power Law[15]

$$\bar{V} = \bar{V}_m \left(\bar{z} \right)^{\frac{1}{n}} \qquad (28)$$

and this is valid for $0 \leqslant z \leqslant \delta$

or $0 \leqslant \bar{z} \leqslant 1$

the index n is a positive integer and it varies from 7 to 15 as predicted by previous investigators[19].

Further away from the wall, in the region known as the outer boundary layer, Schlichting's formula for a two dimensional wake[16] can be used to describe the velocity profile of the wall jet with good results*.

$$\bar{V} = \bar{V}_m \left(1 - \zeta^{\frac{3}{2}} \right)^2 \qquad (29)$$

and this is valid for $\delta \leqslant z \leqslant \delta + b$

or $0 \leqslant \bar{z} \leqslant 1$

The use of this equation was proved to be satisfactory by Poreh and Cermak in their investigation[14] and by more recent researchers like Lee[23] and Jachna[33].

The approximate relations for the thickness of the wall jet, b

---

* See Appendix B

$$b = 0.202 \left(s - s_o \right) \qquad (30)$$

obtained experimentally as illustrated from Figs. (132) to (138)

s = circumferential distance

s_o = circumferential distance of the boundary of the impingement zone

Then for the boundary layer thickness or more specifically, the lower boundary layer thickness,

$$\frac{\delta}{z_{\frac{1}{2}}} = 0.22$$

obtained experimentally as illustrated from Figs. (93) to (120)

$$b = 2\left(z_{\frac{1}{2}} \right)$$

by the definition of wall jet thickness

So,

$$\delta = 0.22\, z_{\frac{1}{2}} = 0.22\left(\tfrac{1}{2}\, b \right) = 0.11\, b \qquad (31)$$

The above relations are empirical.

Taking derivatives of $\overline{V}$ and b from Eq. (29) to Eq. (30),

$$\frac{\partial \bar{V}}{\partial s} = \bar{z}^{\frac{1}{n}} \left(\bar{V}_m' - \frac{V_m \delta'}{n \delta} \right) \qquad (32)$$

$$\text{for} \quad 0 < \bar{z} < 1$$

$$\frac{\partial \bar{V}}{\partial s} = \bar{V}_m' \left(1 - \zeta^{1.5} \right)^2 + \frac{3 \bar{V}_m}{b} \delta' \left(\zeta \right)^{\frac{1}{2}} \left(1 - \zeta^{1.5} \right)$$

$$+ \frac{3 \bar{V}_m}{b} \left(b' \zeta^{1.5} \right) \left(1 - \zeta^{1.5} \right) \qquad (33)$$

$$\text{for} \quad 0 < \zeta < 1$$

And, for b'

$$\frac{db}{ds} = 0.202 \qquad (34)$$

The effects of curvature of the convex surface are included by means of Eqs. (31) and (34) which are obtained experimentally.

Therefore, using Eqs. (28), (29), (32) and (33), it yields:

$$\bar{V}_m \delta \left(\int_0^1 \frac{s \partial \bar{V}}{\partial s} \, d\bar{z} + \int_0^1 s' \, \bar{V} \, d\bar{z} \right)$$

$$= \bar{V}_m \delta \left[\int_0^1 s \left(\bar{z}^{\frac{1}{n}} \left(\bar{V}_m' - \frac{\bar{V}_m \delta'}{n \delta} \right) \right) d\bar{z} + \int_0^1 s' \bar{V}_m \bar{z}^{\frac{1}{n}} \, d\bar{z} \right]$$

$$= \bar{V}_m \delta \left[\frac{n}{n+1} s \left(\bar{V}_m' - \frac{\bar{V}_m \delta'}{n \delta} \right) + \frac{n}{n+1} s' V_m \right] \qquad (35)$$

$$b\left(2\int_0^1 s\,\bar{V}\,\frac{\partial \bar{V}}{\partial s}\,d\zeta + \int_0^1 s'\,\bar{V}^2\,d\zeta\right)$$

$$= b\,2s\int_0^1 \bar{V}_m\,\bar{V}_m'\,(1-\zeta^{1.5})^4 +$$

$$\frac{3\,\bar{V}_m^2}{b}\,\delta'\,\zeta^{\frac{1}{2}}(1-\zeta^{1.5})^3 + \left(\frac{3\,\bar{V}_m}{b}\,b'\,\zeta^{1.5}\right)$$

$$\times(1-\zeta^{1.5})^3\,d\zeta + \int_0^1 \bar{V}_m^2\,s'\,(1-\zeta^{1.5})^4\,d\zeta$$

$$= 0.6312\,\bar{V}_m'\,\bar{V}_m\,sb + \bar{V}_m^2\,\delta'\,s + 0.3156\,\bar{V}_m^2\,sb' +$$

$$0.3156\,\bar{V}_m^2\,s'b \qquad (36)$$

Now, upon substitution of Eqs. (35) and (36) into (27) yields

$$\frac{n}{n+1}\left(\bar{V}_m'\,\delta\,s + \bar{V}_m^2\,s\,\delta + \bar{V}_m\,s'\,\delta\right) + 0.6312\,\bar{V}_m'\,sb$$

$$+ 0.3156\,\bar{V}_m\,sb' + 0.3156\,\bar{V}_m\,s'\,b = 0 \qquad (37)$$

And, combining with Eqs. (30), (31), and (34):

$$\frac{n}{n+1}\left[0.11\, b\, \bar{V}'_m \left(\frac{b}{0.202} + s_o \right) + 0.11\, b'\, \bar{V}_m \left(\frac{b}{0.202} + s_o \right) + \frac{0.11\, b\, \bar{V}_m\, b'}{0.202} \right] + 0.6312\, b'\, \bar{V}_m \left(\frac{b}{0.202} + s_o \right)$$

$$+ 0.3156 \left(\frac{b}{0.202} + s_o \right) b'\, \bar{V}_m + 0.3156\, b\, \bar{V}_m \left(\frac{b'}{0.202} \right) = 0 \qquad (38)$$

After re-arrangement and simplication:

$$V_m\, b'\, s_o \left(\frac{0.11\, n}{n+1} + 0.3156 \right) + V'_m\, b\, s_o \left(\frac{0.11\, n}{n+1} + 0.6312 \right)$$

$$+ \bar{V}'_m\, b^2 \left(\frac{0.5445\, n}{n+1} + 3.1246 \right) + \bar{V}_m\, b'b \left(\frac{1.089\, n}{n+1} + 3.1246 \right)$$

$$= 0 \qquad (39)$$

Introducing a new set of symbols:

$$P\, \bar{V}_m\, b + Q\, \bar{V}_m\, b' + R\, \bar{V}_m\, bb' + T\, \bar{V}'_m\, b^2 = 0 \qquad (40)$$

By the method of separation of variables, the solution is obtained

$$\ln \bar{V}_m + \ln \left(K^e \times \frac{L^f}{K^f} \right) = C_1$$

Where $K = P + Tb$

$L = Tb$

$e = \frac{R}{T}$

$f = \frac{Q}{P}$

Solving for $\overline{V}_m$:

$$\overline{V}_m = \frac{C_1}{K^{e-f} \left(L \right)^f} \tag{41}$$

$$\frac{L^f}{K^f} = \left(1 - s_o / s \right)^f \tag{42}$$

$$K = \left(\frac{0.11\ n}{n + 1} + 0.6312 \right) s \tag{43}$$

Substitute Eqs. (42), (43) into (41),

$$\overline{V}_m = \frac{\text{Constant}}{s^g \left(1 - \frac{s_o}{s} \right)^h} \tag{44}$$

where $g = \frac{R}{T}$

$h = \frac{Q}{P}$

By comparing the constants in Eqs. (39) and (40), it can be shown that

$$\frac{R}{T} = 2\left(\frac{Q}{P}\right)$$

or,
$$g = 2h \tag{45}$$

and both g and h are functions of n which was defined in Eq. (28). As shown in Reference #19, n has been found by previous researchers to vary between 7 and 15.

Upon substituting various integral values of n as given in Eq. (39) and Eq. (40),

the following table is resulted:

Table 1

n	g
7	1.1323
9	1.1355
11	1.1378
13	1.1390
15	1.1400

Since n has been shown to be a function of Reynolds number g is also dependent on Reynolds number. However, due to its relationship with n as defined in Eq. (39), g is but a weak function of Reynolds number.

Lee[23] developed a similar analytical formula for the maximum velocity distribution for wall jet on a flat plate. However, for the same value of n, the power of the wall distance term (g, in the present case; α , in the flat plate case) is comparatively higher in the present convex surface. As a result, the maximum wall jet velocity decreases more rapidly in the present case. This agrees with the experimental results.

For $\frac{s}{s_o} \longrightarrow \infty$, far away from the stagnation point,

Eq. (44) reduces to a simplified version:

$$\overline{V}_m = \frac{V_m}{U_{oc}} = \frac{\text{Constant}}{s^g} = \frac{\text{Constant}}{(\frac{s}{D})^g} \qquad (46)$$

Since s = (radius of hemisphere) θ

θ = angular position in radians

radius of hemisphere = 7.48 inches

Alternatively,

$$s = 7.48\,\theta \qquad (47)$$

Upon substituting Eq. (47) into Eqs. (46) and (44)

$$\frac{V_m}{U_{oc}} = \overline{V}_m = \frac{\text{Constant}}{\theta^g\,(\,1 - \theta_o/\theta\,)^{\frac{1}{2}g}} \qquad (48)$$

For $\theta \gg \theta_o$, far away from the stagnation point,

$$\frac{V_m}{U_{oc}} = \bar{V}_m = \frac{\text{Constant}}{\theta^g} \tag{49}$$

This analytical model is plotted and compared with test results of the impinging jet on the convex hemisphere in Fig. (92).

According to Glauert[8], there are two regions in the wall jet zone. Close to the wall where the flow is influenced by the wall effect, the region is called the inner boundary layer. Then further away from the wall, there is an outer boundary layer which is characterized by the features of a free turbulent flow. The maximum velocity discussed in the preceeding pages occurs at the common boundary of these two layers.

In the deflection zone, the wall effect is the only dominating factor, so the inner layer is the only one present. From Schlichting[15], the thickness of this layer for an axisymmetric flow can be computed as shown:

$$\delta = \frac{2.8/\sqrt{2}}{\left(\frac{V_m\, r}{r^2 \nu}\right)^{\frac{1}{2}}}$$

$$\delta = \frac{1.98\, r^{\frac{1}{2}}}{\left(\frac{V_m}{\nu}\right)^{\frac{1}{2}}} \qquad (50)$$

Corresponding to an accuracy of 1 %

Since the deflection zone of a flat plate is similar to that of a convex surface, it is assumed that for small enough r

$$r = s$$

Furthermore, $z = \delta$ at $V/V_m = 0.99$

From Eq. (12)

$$V_m = a\, s \tag{12}$$

Upon substitution into Eq. (50), it yields

$$\delta = \frac{2.8/\sqrt{2}}{\sqrt{\frac{a}{D}}} \tag{51}$$

From the velocity distribution of maximum velocity of the deflection zone, the normalized $\overline{V}_m$ can be represented by

$$\frac{V_m}{U_{oc}} = a^* \left(s/D \right) \tag{52}$$

Combining Eqs. (12) and (51), it yields

$$a = \frac{a^* U_{oc}}{D} \tag{53}$$

Substitute Eq. (53) into Eq. (51) and re-arrange, it yields:

$$\frac{\delta}{D} = \frac{2.8/\sqrt{2}}{a^* Re_D} \tag{54}$$

Since it is shown in the present investigation that a* is a function of $\overline{Z}/D$, and δ is also a function of Re_D and $\overline{Z}/D$. With reference to Figs.(64) to (70), and from Figs. (125) to (131), the following results are noted:

$$a^* \propto \frac{1}{\frac{\bar{Z}}{D}}$$

$$\frac{\delta}{D} \propto \sqrt{\frac{\frac{\bar{Z}}{D}}{Re_D}} \qquad (55)$$

Table 2

$\frac{\bar{Z}}{D}$	a^*
4	0.9
7	0.56
10	0.38
20	0.24

In Lee's investigation of the flat plate[23], the same approach proved to be satisfactory.

CHAPTER 5

ANALYSIS OF EXPERIMENTAL RESULTS

5.1 Free Jet Zone

5.1.1 The potential core in the free jet zone is shown in Fig. (6).

a) Theoretical dimensionless length of the potential core, C

It is defined as the dimensionless S/D distance from the nozzle opening to the intersection of the tangent of the plot of center-line velocity decay in the fully developed region with the maximum velocity line (i.e., at $U_m / U_{oc} = 1$).

In the present experiment, C is found to be between 6.3 and 6.6 in the range of Re_D between 14,700 and 84,000 and for nozzle diameters of 0.125", 0.25", 0.375" and 0.5". Lee[23] reported C to be from 6.5 to 6.8 for the Re_D range between 1,000 and 100,000 for nozzle diameters of 0.125", 0.25" and 0.375". Other investigators had found various values of C.

Table 3

C	Investigators
5.2	Tani and Komatsu[17]
7.7	Poreh and Cermak[13]
7.0	Trentacoste and Sforza[18]

b) Actual potential core, L

It is defined as the actual dimensionless length where the

centerline velocity of the jet remains constant (i.e., near velocity ratio of one) since the velocity profile actually starts to decrease sooner than the intersection encountered in the theoretical potential core C. In the present experiment, L is found to be 4 and this is the same as Lee's[23].

5.1.2 Velocity across the free jet

Schlichting[15], Abramovich[1] and Trentacoste and Sforza[18] contributed to the study of velocity decay across free jet. Figs. (15) to (23) show plots of the velocity profiles at various dimensionless locations (X/D) and varied nozzle diameters. The results of the present investigation agree with the Schlichting's curve in the upper one-third portion as given by[15]

$$\left.\begin{aligned} u &= \frac{3}{8\pi\epsilon_o}\,\frac{K}{x}\,\frac{1}{\left(1+\frac{1}{4}\bar{\eta}^2\right)^2} \\ v &= \frac{1}{4}\sqrt{\frac{3}{\pi}}\,\frac{\sqrt{K}\left(\bar{\eta}-\frac{1}{4}\bar{\eta}^3\right)}{x\left(1+\frac{1}{4}\bar{\eta}^2\right)^2} \\ \bar{\eta} &= \frac{1}{4}\sqrt{\frac{3}{\pi}}\,\frac{\sqrt{K}}{\epsilon_o}\,\frac{y}{x} \end{aligned}\right\} \qquad (56)$$

In the lower one-third portion, the present test results are closer to the Tollmien solution[38].

All test locations are in the fully developed region and away from the impingement surface to ensure a true free turbulent jet.

5.1.3 Static Pressure along Jet Centerline

Theoretically, the static pressure is established to be that

of the ambient by the simplified boundary layer theory. In the present experiment as well as well as those of Lee[23] and Jachna[33], static pressure has been measured to be varied. In fact, it is less than the ambient pressure. The profiles of the dimensionless pressure ratio against the normalized centerline distance are plotted in Figs. (24) to (26). It is noted that the static pressure reaches a minimum at X/D close to 7 or 8. From this point onward, the pressure then increases to that of ambient gradually at X/D = 50.

5.1.4 Pressure Variation across Free Jet

The static pressure variations are shown in Fig. (27) to Fig. (29). This is the normalized pressure ratio versus $Y/Y_{\frac{1}{2}}$ where Y is the normal distance from the jet centerline and $Y_{\frac{1}{2}}$ is the distance at which the velocity reaches half of U_m at the X/D location in question. The minimum static pressure occurs at the centerline and then increases gradually to that of the ambient at the outer envelope of the profile. Ideally, it should be equal to the ambient pressure at $Y = 2\ Y_{\frac{1}{2}}$. For the same X/D distance, the curve is slightly steeper for larger nozzle diameter. So, based on the test results, it is noted that the static pressure ratio is a weak function of nozzle diameter. In general, the present investigation confirmed the findings in Lee[23].

In Fig. (44) the static pressure ratio * is plotted against Y/R where Y is the same as defined earlier and R is the radius of the nozzle. The result of Barat[4] is compared with a selected run of the

---

* this ratio is slightly modified as $\dfrac{P_s - P_a}{\frac{1}{2}\rho U_{oc}^2}$

present experiment for the sake of compatibility. In spite of the difference in Re_D (84,000 versus 400,000) and the difference in nozzle radii (1.27 cm versus 15 cm), the results are similar.

5.2 Deflection Zone

5.2.1 Pressure Distribution

The static pressure profiles in the deflection zone are represented by the steep portion of the curves in Figs. (30) to (41). This region occurs between S/D = 0 and S/D = 2, depending on the values of $\bar{Z}/D$. In general, for smaller $\bar{Z}/D$, the upper limit of S/D is smaller; and for larger $\bar{Z}/D$, this limit is larger. The equation given in Lee[23] is:

$$\frac{P_s - P_a}{\frac{1}{2}\rho U_{oc}^2} = A - B\left(\frac{r}{D}\right)^2 \qquad (57)$$

where r can be replaced by S without loss of accuracy in the deflection zone. Then this equation can be applicable to the present case of the convex surface.

In addition, the constants A and B determined empirically from the present investigation are:

Table 3

$\bar{Z}/D$	A	B
4	1	0.9
7	0.62	0.54
10	0.43	0.24
20	0.1	0.04

5.2.2 Velocity Profile

The variation of velocity profile in the deflection zone is shown in Figs. (64) to (70) corresponding to varied Re_D and $\bar{Z}/D$. The velocity increases from zero where the static pressure is at its peak to a maximum value at the edge of the deflection zone, according to the following equation:

$$\frac{V_m}{U_{oc}} = \text{Constant} \left(S/D \right) \qquad (58)$$

where the constant assumes the following values:

Table 4

$\bar{Z}/D$	S/D range	Constant
4	0 to 0.1	0.98
7	0 to 1.65	0.56
10	0 to 2.0	0.38
20	0 to 2.3	0.24

Alternatively, if V_m/U_{oc} is plotted against another parameter, $S/\bar{Z}$, the result is a straight line through the origin with a slope of 4.

$$\frac{V_m}{U_{oc}} = 4 \left(S/\bar{Z} \right) \qquad (60)$$

for all Re_D and $\bar{Z}/D$

The above results are shown in Figs. (57) to (63). The maximum velocity profile is compatible to the static pressure distribution. Basically, the maximum velocity is at its peak when the pressure approaches ambient; and conversely, the static pressure is at the maximum when the velocity is zero. It results from the fact that dissipation in the deflection zone can be neglected. This is in agreement with the assumption used to develope the analytical model in Chapter 4. Moreover, this also confirms the results in Lee's investigation[23]. Similar results were found by Tani and Komatsu[17], Brady and Ludwig[6], as well as Poreh and Cermak[14].

5.3 Wall Jet Zone

5.3.1 Velocity Profile across Wall Jet

The profiles of V/V_m versus $Z/Z_{\frac{1}{2}}$ are plotted in Figs. (93) to (120). For each run, V is the local wall jet velocity, V_m is the maximum velocity for a given station on the wall, Z is the normal distance from the surface of the plate, and $Z_{\frac{1}{2}}$ is the normal distance at which the velocity, V, reaches half the maximum value.

As Re_D increases the lower portion of the graph (corresponding to $Z/Z_{\frac{1}{2}} < 0.22$) becomes flatter. In addition, for small $\overline{Z}/D$ and (or) for small S/D, the measurements at the outer envelope are more precise since the total pressure is comparatively higher and more readily detected by the total pressure probe. Consequently, at such stations, the resulting curve tends to have a longer tail at large $Z/Z_{\frac{1}{2}}$. On the other hand, as S/D gets larger and (or) as $\overline{Z}/D$ increases, the total pressure measurements get smaller and make an accurate and precise plot at the outer boundary on the velocity profile more difficult.

The experimental dimensionless velocity profile obtained in the present investigation is similar to the results by Bakke[3] but slightly different from the results by Glauert[8]. Fig. (124) shows plots of their results.

Lee, Poreh and Cermak, and Tsuei obtained similar velocity profiles. Fig. (122) presents a comparison of the present investigation of a convex hemisphere with that of a flat plate by Lee[23] and that of a concave hemisphere by Jachna[33].

Similar comparison with the normalized height ($Z/Z_{\frac{1}{2}}$) modified to ($\zeta/\zeta_{\frac{1}{2}}$) is shown in Fig. (123). At the outer envelope of the curve, the results of the present investigation tend to decrease most rapidly, followed by the flat plate of Lee[23], the concave hemisphere of Jachna[33], and lastly, the formula derived from the solution of a wake by Schlichting[16] to apply on the wall jet zone*,

$$\overline{V} = \overline{V}_m \left(1 - \zeta^{1.5} \right)^2 \qquad (29)$$

$$V = V_m \left(1 - \zeta^{1.5} \right)^2 \qquad (60)$$

In particular, there are two applicable sets of empirical equations derived from the present investigation of the convex plate. They are:

$$\left.\begin{aligned} \frac{V}{V_m} &= 1.01\, e^{-0.287\, B} && 0 \leqslant B < 0.45 \\ \frac{V}{V_m} &= 1.196 - 0.696\, B && 0.45 \leqslant B < 1.6 \end{aligned}\right\} \qquad (61a)$$

and,

$$\left.\begin{aligned} \frac{V}{V_m} &= 1.000538 - 0.3886932\, B + 10.99342\, B^2 \\ &\quad -129.7117\, B^3 + 734.8\, B^4 - 2402.882\, B^5 \\ &\quad + 4747.511\, B^6 - 5718.57\, B^7 + 4091.051\, B^8 \\ &\quad - 1592.255\, B^9 + 258.9473\, B^{10} && 0 \leqslant B < 1.0 \\ \frac{V}{V_m} &= 1.196 - 0.696\, B && 1.0 \leqslant B < 1.6 \end{aligned}\right\} \qquad (61b)$$

---

* See Appendix B

In the above equation,

$$\left.\begin{aligned} B &= \frac{\zeta}{\zeta_{\frac{1}{2}}} \quad ; \quad \zeta = (z - \delta)/b \\ \zeta_{\frac{1}{2}} &= (z_{\frac{1}{2}} - \delta)/b \quad ; \quad b = \text{width of jet} \end{aligned}\right\} \qquad (61c)$$

Physically, the comparison in Fig. (123) illustrates the high dissipating effect of the local velocity possessed by the wall jet formed by the impinging convex surface.

Jit[32] developed a computer model of a wall jet along a flat plate. This analytical graph is reproduced in Fig. (121) and compared with the present investigation. The most striking disagreement is at the lower boundary layer where Jit's solution starts at the origin and increases linearly to $V/V_m = 1$ at $Z/Z_{\frac{1}{2}} = 0.2$, whereas the present experimental results show that the profile begins at some value of V/V_m larger than zero and increases linearly to V/V_m at $Z/Z_{\frac{1}{2}}$ of 0.22. At the end of the outer boundary layer, the computer solution maintains $V/V_m = 0.2$ asymptotically for larger $Z/Z_{\frac{1}{2}}$. However, in the present experiment, the graph decrease to zero velocity at $Z/Z_{\frac{1}{2}} = 1.6$.

5.3.2 Maximum Velocity Decay Along The Wall

This parameter is shown in Figs. (71) to (83). The empirical equation is :

$$\frac{V_m}{U_{oc}} = \frac{1.4}{(S/D)^{1.17} \quad (\bar{Z}/D)^{k}} \qquad (62)$$

or $$V_m = \frac{K}{(S)^{1.17} \; (\bar{Z}/D)^k} \qquad (63)$$

where the index, k, is given as follows:

Table 5

$\bar{Z}/D$	k
4	0
7	-0.0087
10	-0.018
20	-0.025

Alternatively,

$$\frac{V_m}{U_{oc}} = \frac{\text{Constant}}{(\theta \sin\theta)^{0.683}} \qquad (63a)$$

as shown in Figs. (139) to (145).

Equation (62) is compatible to Equation (46). Different values for the power of the wall distance (r, in the case of a flat plate) were found by various investigators:

Table 6

Investigator	Power
Poreh[14]	1
Brady[6]	1.14
Bakke[3]	1.12
Lee[23]	1.12

The power of S or r being larger than one implies that the decay of the wall jet is faster than that of a comparable free jet with identical physical parameters such as Re_D and D.

5.3.3 The Decay of V_{rb}, the Reference Boundary Layer Velocity

This quantity is defiend by Poreh and Cermak[13] as the hypothetical local velocity at the imaginery free jet centerline existing at the surface of the wall whose effect is neglected. Fig. (84) to Fig. (90) show the profiles of V_{rb}/U_{oc} versus $S/\overline{Z}$ with an empirical equation as follows:

$$\frac{V_{rb}}{U_{oc}} = \frac{0.0625}{\frac{S}{\overline{Z}}} \qquad (64)$$

for all values of $\overline{Z}/D$

for $14{,}700 \leqslant Re_D \leqslant 84{,}000$

When V_{rb} is plotted against another parameter $\theta \sin\theta$ as shown in Fig. (146) to Fig. (151), the following results:

$$\frac{V_{rb}}{U_{oc}} = \frac{\text{Constant}}{(\theta \sin\theta)^{0.635}} \qquad (65)$$

5.3.4 The Growth of Half Valued Width of Wall Jet

The spread or growth of the half valued width of wall jet is shown in Fig. (131a). It is found that $(\overline{Z}/D)$ varies to some power. Based on all the cases investigated in this study of the impinging convex surface, the following relationship is developed:

$$\frac{Z_{\frac{1}{2}}}{D} = \text{Constant} \left(\overline{Z}/D \right)^{n} \qquad (66)$$

where the values for the constant are given:

Table 7

$\overline{Z}/D$	n	Constant
4	0.98	0.0920
7	0.98	0.0935
10	0.98	0.0950
20	0.98	0.1030

Moreover, if the above equation is re-written using r in place of S, the following table based on the work of previous investigators is composed:

Table 6

Investigator	n
Lee[23]	0.95
Poreh, Tsuei and Cermak[14]	0.90
Bakke[3]	0.94
Brady[6]	1.028

In conclusion, the spread of a wall jet is at a slightly lower rate than that of a free jet.

5.3.4 Static Pressure Variations

Along the wall, the distribution of the static pressure is presented from Fig. (30) to Fig. (41). This is independent of Re_D but slightly dependent on the impingement plate distance to the nozzle diameter ratio. The profile flattens with increasing $\bar{Z}/D$. In general, at S/D larger than 3.5, the graph decreases asymptotically to some value slightly less than the ambient pressure. Lee[23] and Jachna[33] reported similar findings for the flat plate and the convex hemisphere.

Laterally across the wall jet, static pressure profiles are plotted in Figs. (45) to (56). The following points are noted:

i) For all Re_D , $\bar{Z}/D$, and S/D, the static pressure increases negatively from some value close to ambient at the wall surface to a peak value

at $Z/Z_{\frac{1}{2}}$ of about 0.9 before it rises to ambient at $Z/Z_{\frac{1}{2}}$ greater than 5.

ii) The peak value of static pressure is a function of S/D and a weak function of $\overline{Z}/D$.

iii) By definition, the tendency of a jet of fluid issuing from a nozzle to become attached to an adjacent surface is called the Coanda Effect, named after the man who helped to discover this phenomenon. Observation of this effect can be readily seen by pouring tea or coffee from a pot, by pouring liquid specimen from a test tube, or by the inward blowing from the curtain when the shower is running (even when the door and window are closed). Many schools of thought for the mechanism governing this jet attachment were established, of which the most plausible one is that developed by Squire[38]. Briefly, the process is explained to be undergone as follows:

> When a jet is flowing next to a surface, it entrains fluids from the surrounding. This entrained fluid will be replaced by the mass in the jet along the surface from downstream. The driving force for such motion is a negative pressure gradient.

Wilson[35] gave a comprensive description of the Coanda Effect.

The measurement of negative static pressure in the present investigation further supports the above theory.

5.3.5 Boundary Layer Thickness

i) Inner Boundary Layer

It is shown in Figs. (125) to (131) and the following empirical equation is established:

$$\frac{\delta}{D} = I \left(\frac{S}{D} \right)^{0.98} \qquad (67)$$

where $0.019 \leqslant I \leqslant 0.025$, as Re_D increases

This shows that the inner boundary layer thickness grows at a higher rate than that of an impinging wall jet over a flat plate, when it is compared with Lee's equation[23] :

$$\frac{\delta}{D} = 0.0175 \left(\frac{S}{D} \right)^{0.95} \qquad (68)$$

ii) Outer Boundary Layer

The distribution of the outer boundary layer thickness is shown in Figs. (132) to (138). It is approximated by a straight line:

$$\frac{b}{D} = 0.202 \left(\frac{S}{D} \right) \qquad (69)$$

For the same relationship, Lee[23] and Jachna[33] reported slopes of 0.22 and 0.226 respectively.

CONCLUSION

The characteristics of incompressible, turbulent and three dimensional fluid flows formed by impinging jets upon a convex hemisphere were investigated in the three zones (the free jet zone, the deflection zone and the wall jet zone).

In the free jet zone, the theoretical potential core was found to be between 6.3 and 6.8 X/D (the ratio of the axial distance along the free jet centerline to the nozzle diameter), while the actual potential core was 4 X/D. This agrees with the results of the previous investigators.

In the deflection zone, the velocity growth follows the same pattern as predicted by Schlichting and confirms the results of the other investigators in that the flow in this region is non-viscous. Moreover, since the deflection zone is small compared to the other zones, this area can be treated as flat in spite of the curvature.

The velocity profile across the wall jet is similar to that of the free jet except at $Z/Z_{\frac{1}{2}}$ of less than 0.22. In this region, the velocity increases from some small value at the wall to a maximum at $Z/Z_{\frac{1}{2}}$ of 0.22. From this point onward, the velocity profile follows the Schlichting's formula for a two dimensional wake. Compared to wall jets on flat plate and concave hemisphere, it is seen that the velocity profile on the convex surface tends to decay at a higher rate at the edge of the outer boundary layer.

The decay of maximum velocity along the wall is not dependent on either the Reynolds number or the impingement plate distance to nozzle diameter while the growth of half-valued width of the wall jet is independent of Reynolds number but slightly dependent on $\overline{Z}/D$.

Consistent with the findings of the previous investigators, particularly, Lee and Jachna, negative static pressure has been found in the free jet zone and along the wall of the impingement surface. In addition, negative static pressure is also observed laterally across the wall jet flow path. It is due to the presence of such pressure gradient that the fluid from the surroundings is being drawn in to replace the fluid which is entrained by the motion of the jet flowing next to the convex hemisphere. This lateral negative pressure distribution serves as further verification of the Coanda Effect.

RECOMMENDATION

1. Larger nozzle diameters are recommended for further investigation. The advantage of larger nozzle diameter is twofold. First, for the same Reynolds number and $\bar{Z}/D$, larger mass of fluid is ejected by the jet, making measurements for boundary layers and velocity profiles easier, even at large S/D. Secondly, since the flow field is bigger, the effect of interference due to the presence of the pressure probes is highly reduced. However, the air supply system has to be modified.

2. A heated convex surface would result in changes in the boundary layers and the velocity profiles. Since the application of impinging jets lies chiefly on the heat transfer aspects, it is advisable to extend the present investigation to study the impact of impinging jet on heated convex surface. On the other hand, heated jets impinging on convex surface at room temperature are worth studying because of the potential use of impinging jets for spot heating or melting purposes.

3. Rows or matrix of impinging jets upon a convex surface are recommended in order to study the interaction of such arrangements which have various applications.

4. Since negative static pressure distribution was found laterally across the wall jet in the present investigation, it is appropriate to duplicate similar effects for other impinging surfaces such as flat, concave or hyperbolic. Static pressure distributions resulting from them can be used to correlate with the present data for further study of Coanda Effect.

APPENDIX A

A 1 Evaluation of Experimental Error

a. The effect of directional fluctuation of flow field with respect to the pressure probes.

From Barat[36], the maximum correction factor for total pressure measurements is found to be less than 0.002%; similarly, for the static pressure, it is less than 0.005%.

However, during the experiment, the pressure probes (both static and total) were oriented by turning about the axis of the probe to align the tip of the probe in the direction of a streamline. In short, the tip of the probe was "head-on" against the direction of the flow. As a result, it can be assumed that the effect due to directional fluctuation can be neglected.

b. The velocity formula in terms of total pressure head is[33]

$$V = \sqrt{2gh \left(\rho_f / \rho_a - 1 \right)} \qquad \text{(A-1)}$$

where

$$\rho_a = \frac{144 \; P_a}{Z \; R \; T} \qquad \text{(A-2)}$$

g = gravity acceleration in ft/sec

h = manometer fluid column in inches of fluid

ρ_f = density of manometer fluid in lbm/ft^3

ρ_a = density of air in lbm/ft^3

P_a = ambient pressure in psia

Z = compressibility factor of air

R = gas constant for air, lbf/lbm deg. R

T = air temperature in deg. R

From Eqs. (A-1), (A-2)

$$V = \sqrt{\frac{2\ gh\ Z\ R\ T_f}{144\ P_a}} \qquad \text{(A-3)}$$

$$V = \text{Constant}\sqrt{\frac{\rho_f\ T\ h}{P_a}}$$

The maximum relative error

$$C_v = \tfrac{1}{2}\left(C_f + C_T + C_h + C_{P_a} \right)$$

For water in the range of temperature between $60^{\circ}F$ and $90^{\circ}F$

$$\rho_{60^{\circ}F} = 62.3\ \text{lbm/ft}^3$$

$$\rho_{90^{\circ}F} = 62.1\ \text{lbm/ft}^3$$

$$C_f = \frac{62.3-62.1}{62.1}\ 100\% = 0.25\ \% \qquad \text{(A-4)}$$

Assume a maximum temperature error of $2^{\circ}F$ and an average temperature of $75^{\circ}F$ or 535° R

$$C_T = \frac{2}{535} = 0.4\ \% \qquad \text{(A-5)}$$

The maximum in the manometer reading is 0.1 inch at an average V_{nozzle} of 300 ft/sec

$$C_h = \frac{0.1}{19.95} = 0.5\ \% \qquad \text{(A-6)}$$

The maximum error in the barometric reading is 0.03 inch

$$C_{P_a} = \frac{0.03}{30} = 0.1\ \% \qquad \text{(A-7)}$$

Combining Eqs. (A-4) to (A-7)

$$C_v = \tfrac{1}{2} (0.25 + 0.4 + 0.5 + 0.1) \% \qquad \text{(A-8)}$$

$$= 0.625 \%$$

c. Compressibility of air

Since the highest velocity measured in the wall jet was about 400 ft/sec corresponding to a Mach number of 0.36, the effect of compressible flow should be considered.

Modifying the Bernoulli Equation to account for compressibility[25],

$$P_t - P_s = \tfrac{1}{2} V^2 \rho \left(1 + \tfrac{1}{4} (M^2) + (\tfrac{2 - k}{24}) M^2 + ... \right)$$

where P_t, P_s and M are the stagnation pressure, static pressure and Mach number respectively.

Considering the first two terms in the series, for the above Mach number (M = 0.36), the maximum error due to compressibility of air is

$$C_c = 3.56 \% \qquad \text{(A-9)}$$

d. Total Error

This is obtained by the summation of all the errors,

$$C_{Total} = C_v + C_c = 4.185 \% \qquad \text{(A-10)}$$

However, the factor C_c is only applicable in a few runs at $Re_D > 56{,}000$ with D = 0.25 inch and at the region of wall jet near the deflection zone. For the rest of the runs, Mach numbers are much below 0.3 in the wall jet region

At Mach number of 0.3

$$C'_c = \frac{1}{4} (0.3)^2 + \left(\frac{2 - 1.4}{24} \right) (0.3)^2$$

$$= 2.475\ \%$$

So,

The maximum error correction for wall jets

$$C_{Total} = C_v + C'_c = 3.1^{-}\ \%$$

APPENDIX B

From Schlichting[15], pp. 691-695

The velocity distribution in a two-dimensional wake behind a cylinder is obtained from the solution of an appropriate differential equation:

$$\frac{u_1}{U_\infty} = \frac{\sqrt{10}}{18\beta} \left(\frac{x}{C_D d} \right)^{-\frac{1}{2}} \left(1 - \left(\frac{y}{b} \right)^{1.5} \right)^2 \qquad \text{(B-1)}$$

where u_1 = local velocity at a cross section of the wake

U_∞ = free stream velocity

d = thickness of the cylinder

b = the total wake width at a cross section

y = the distance from the centerline, measured on the width axis

C_D = coefficient of drag

β = a constant

x = the distance from the cylinder

Combining terms,

$$\frac{U}{U_m} = \left(1 - \zeta^{1.5} \right)^2 \qquad \text{(B-2)}$$

where U_m = the maximum velocity at a cross section

$\zeta = y/b$

U = the local velocity, same as u_1

When the above equation is applied to describe the velocity profiles at cross sections of the wall jet in the outer boundary layer zone, the

following is obtained:

$$\frac{V}{V_m} = \left(1 - \zeta^{1.5} \right)^2 \qquad \text{(B-3)}$$

This equation gives good correlation with measured data for the impinging axisymmetric jets. The same approach was used by Lee[23] and Jachna[33] with good results.

BIBLIOGRAPHY

1. Abramovich, G. N., The Theory of Turbulent Jets, MIT Press, Cambridge, Mass., 1963.

2. Albertson, M. L., Dai, Y. B., Jensen, R. A., and Rouse, H., Diffusion of Submerged Jets, ASCE Trans., vol. 115, 1950, pp.639-697.

3. Bakke, P., An Experimental Investigation of a Wall Jet, J. of Fluid Mech., vol. 12, 1957, pp. 467-472.

4. Barat, M., Variation de pression statique dans un jet libre subsonique, Mecanique Des Fluides, Comptes rendus, Seance du 25 Janvier 1954, pp. 445-447.

5. Beltaos, S., and Rajaratnam, N., Plane Turbulent Impinging Jets, J. of Hydr. Res., vol. 11.1, 1973, pp. 29-59.

6. Brady, W. G., and Ludwig, G., Theoretical and Experimental Studies of Impinging Uniform Jets, J. of American Helicopter Society, vol. 8.2, 1963, pp. 1-13.

7. Bradshaw, P. and Gee, M. T., Turbulent Wall Jets with and without an External Stream, Aeronaut. Res. Council R and M 3252, 1962.

8. Glauert, M. B., The Wall Jet, J. of Fluid Mech., vol. 1, 1963, pp. 625-643.

9. Gooderum, P. B., Wood, G. P. and Brevoort, M. J., Investigation with An Interferometer of the Turbulent Mixing of a Free Supersonic Jet, NACA Rep. 963, 1950.

10. Görtler, H., Berechung von Aufgaben der freien Turbulenz auf Grund eines neuen Näherungsansatzes, ZAMM, vol. 22, 1942, pp. 244-254.

11. Kaufmann, W., Fluid Mechanics, McGraw-Hill Book Co., Inc., New York, 1963.

12. Miller, David R. and Comings, Edward W., Static Pressure Distribution in the Free Turbulent Jet, J. of Fluid Mech., vol. 3, Pt. 1, Oct. 1957, pp. 1-6.

13. Poreh, M. and Cermak, J. E., Flow Characteristics of a Circular Submerged Jet Impinging Normally on a Smooth Boundary, Proc. 6th Midw. Conf. on Fluid Mech., 1959.

14. Poreh, M., Tsuei, Y. G., and Cermak, J. E., Investigation of a Turbulent Wall Jet, ASME Paper No. 67-APM-10, 1967.

15. Schlichting, H., Boundary Layer Theory, 6th ed., McGraw-Hill Book Co., New York, 1968.

16. Snedeker, R. S. and Donaldson, C. du P., Experiments on Free and Impinging Underexpanded Jets from a Convergent Nozzle, Ad 461622, 1964.

17. Tani, I. and Komatsu, Y., Impingement of a Round Jet on a Flat Surface, Proc. XI Int. Cong. of Appl. Mech., 1964, pp. 672-676.

18. Trentacoste, N. and Sforza, P. M., An Experimental Investigation of Three-Dimensional Free Mixing in Incompressible Turbulent, Free Jets, PIBAL Report, No. 17, 1966.

19. Hrycak, Peter, Heat Transfer from Impinging Jets, A Literature Review, prepared under Grant NGR-31-009-004, Newark College of Engineering, Newark, New Jersey, August 1968.

20. Hrycak, P., Lee, D. T., Gauntner, J. W. and Livingood, J. N. B., Experimental Flow Characteristics of a Single Turbulent Jet Impinging on a Flat Plate, NASA TND-5690, March 1970.

21. Kim, T. S., Analysis of Flow Characteristics in Circular, Submerged, Impinging Jets, Ph. D. Dissertation, Illinois Institute of Technology, 1967.

22. Krishnan, S. and Glickman, L. R., A Two Dimensional Analysis of a Heated Free Jet at Low Reynolds Numbers, ASME paper 70-WA/FE-3.

23. Lee, David T. H., Experimental Investigation of Submerged Incompressible Turbulent Impinging Jets, Master Thesis, Newark College of Engineering, 1969.

24. NASA facsimile reproduction of N65-19287.

25. Binder, R. C., Fluid Mechanics, 2nd ed., Prentice-Hall, Inc., New York, New York, 1949.

26. McNaughton, K. J. and Sinclair, C. G., Jets in Cylindrical Flow Vessels, J. of Fluid Mechanics, vol. 25, 1966, p.371.

27. Schach, W., Deflection of Circular Fluid Jet by a Flat Plate Perpendicular to the Flow Direction, Ing. Archiv, vol. 6, 1935, pp. 51-59.

28. Strand, T., On the Theory of Normal Ground Impingement of Axisymmetric Jets in Inviscid Incompressible Flow, AIAA Paper 64-424, 1964.

29. Homann, F., Der Einfluse grosser Zähigkeit bei der Strömung un den Zylinder und um die Kugel, ZAMM, vol. 16, 1936, pp. 153-164, and Forschg. Ing.-Wes. vol 7, 1968, pp. 1-10.

30. Reichardt, H., Gesetzmässigkeiten der freien Turbulenz, VDI-Forschunsheft 414, 1942.

31. Russell, P. J. and Hatton, A. P., Turbulent Flow Characteristics of an Impinging Jet, Proc. Instn. Mech. Eng. 186, 52/72, 1972, pp. 635-644.

32. Jit, I., Mass Transfer Studies in Some Types of Turbulent Flow, Ph. D. Dissertation, Indian Institute of Science, Bangalore, India, 1976.

33. Jachna, Stefan, Axisymmetric Air Jet Impinging on A Hemispherical Concave Plate, Sc. D. Dissertation, New Jersey Institute of Technology, Newark, New Jersey, 1978.

34. Tsuei, Y., Axisymmetric Boundary Layer of a Jet Impinging on a Smooth Plate, Ph. D. Dissertation, Colorado State University, 1963.

35. Wilson, D. J., An Experimental Investigation of the Mean Velocity, Temperature and Turbulence Fields in Plane and Curved Two-Dimensional Wall Jets: Coanda Effect, Ph. D. Dissertation, University of Minnesota, 1970.

36. Barat, Marc, Pressure Measurements in Highly Turbulent Flows, Heat and Mass Transfer in Boundary Layers, vol. 2, Proceedings of the International Summer School, Heat and Mass Transfer in Turbulent Boundary Layers, Herceg Novi, September, 1968; and Selected Papers and Abstracts of the International Seminar, Heat and Mass Transfer in Flows with Separated Regions, Herceg Novi, September, 1969, Pergamon Press, Oxford, New York,

Toronto, Sydney, Braunschweig.

37. Tollmien, W., Berechnung turbulenter Ausbreitungsvorgänge, ZAMM 6, pp. 468-478 (1926) NACA TM 1085 (1945).

38. Squire, M. A., Jet Flow and Its Effects on Aircraft, Aircraft Engineering, vol. 22, 1950, p. 62.

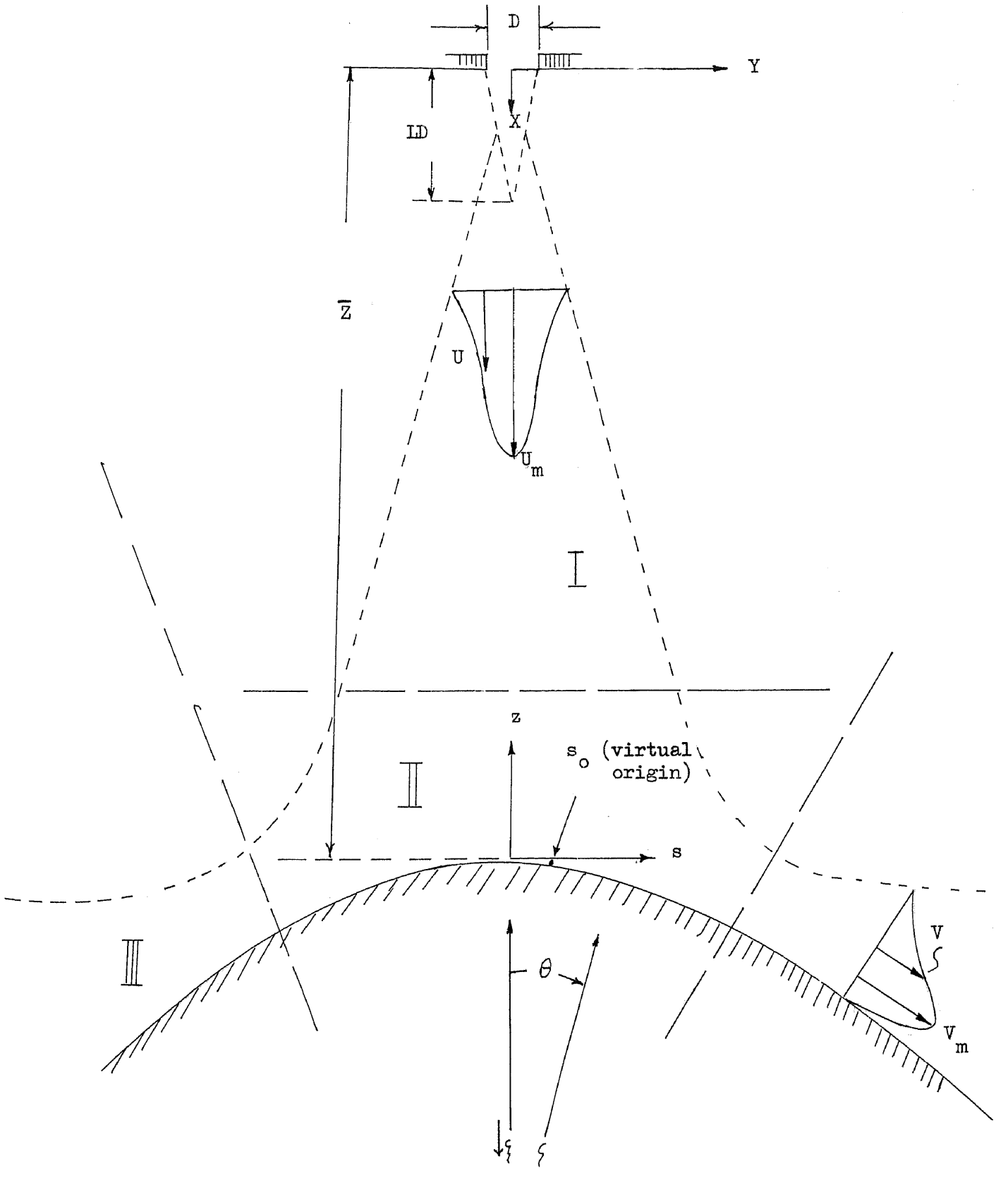

Fig. 1 Coordinate System and Flow Configuration

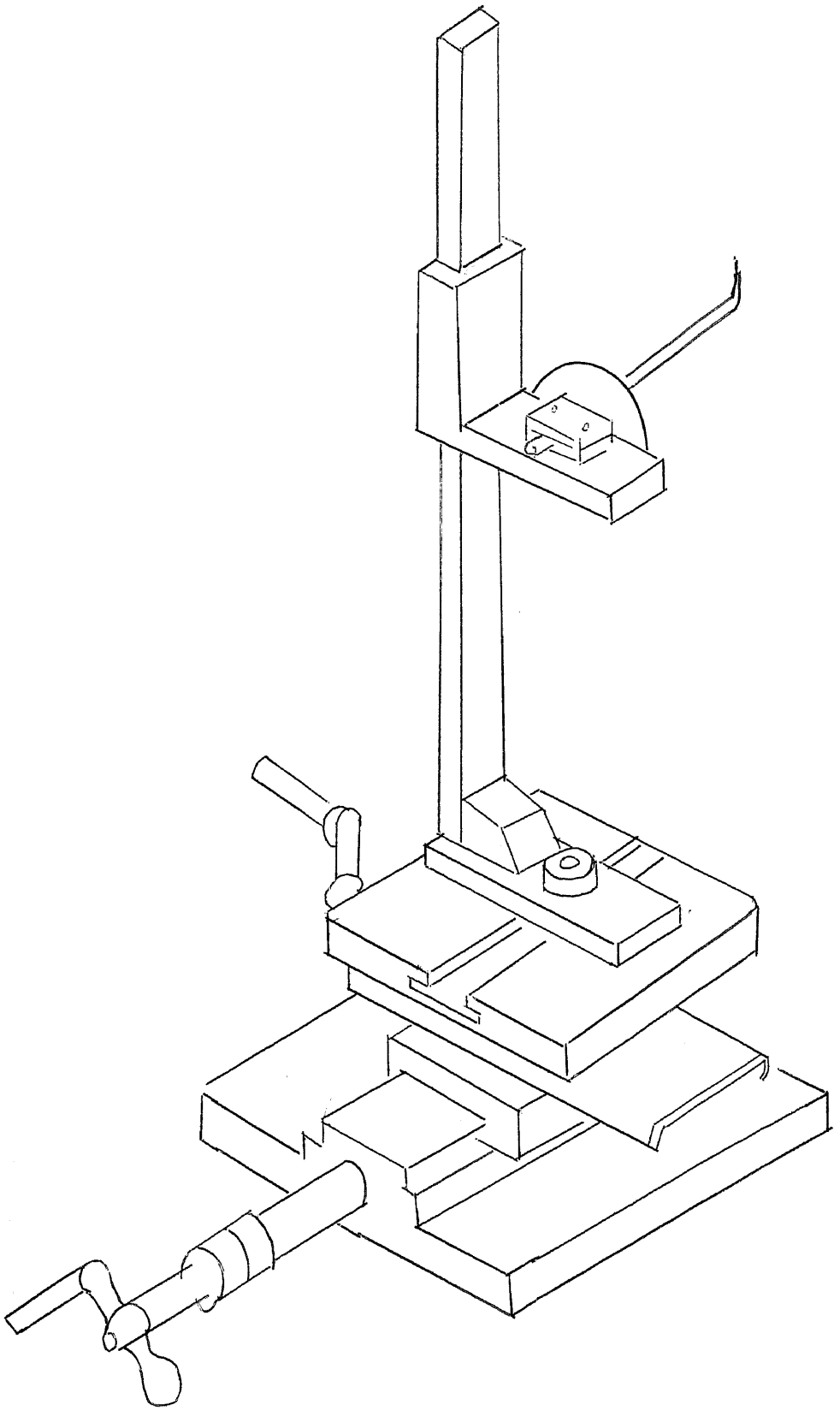

Three Dimensional Carriage

Fig. 2

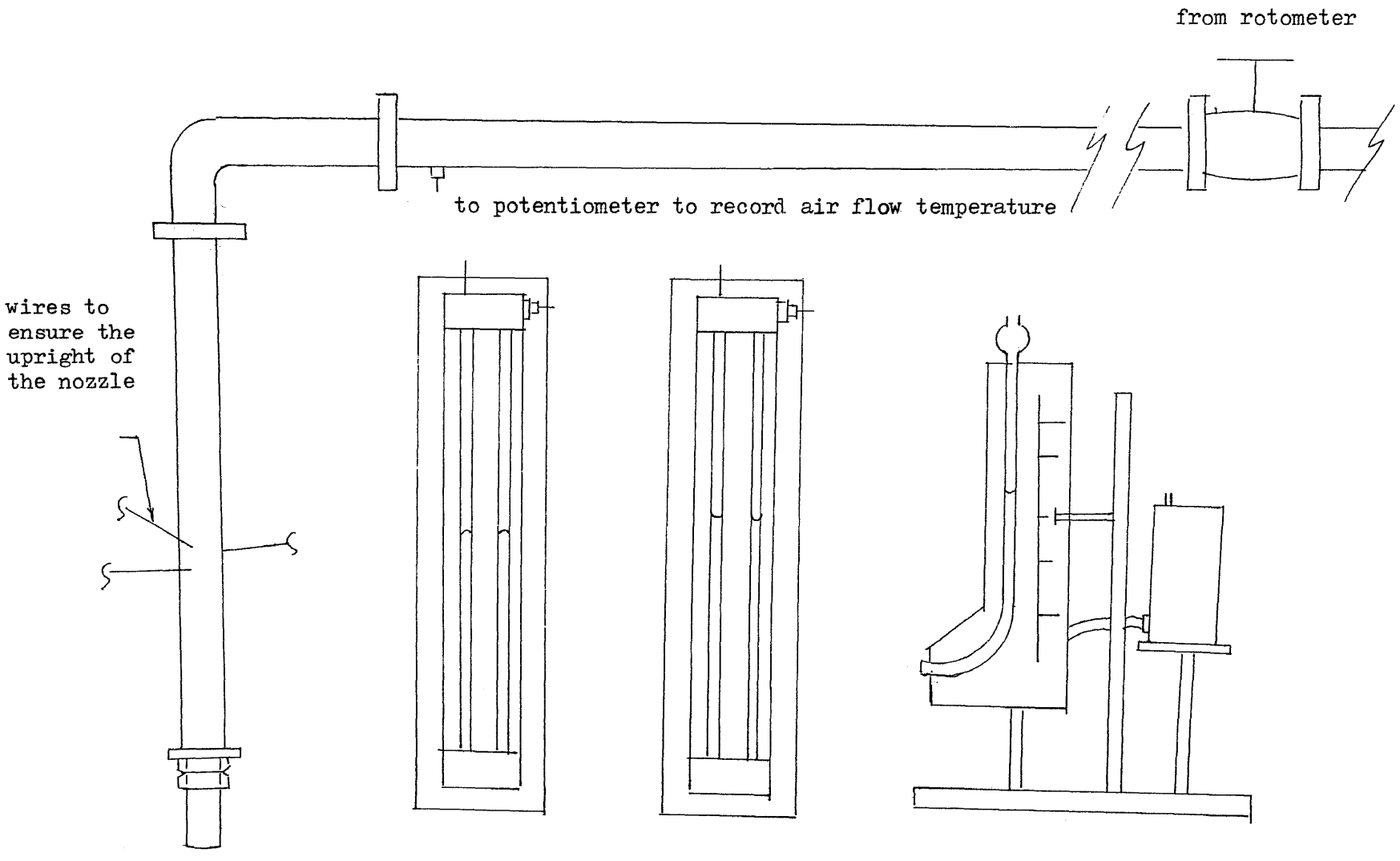

Fig. 3 Piping System and Manometers

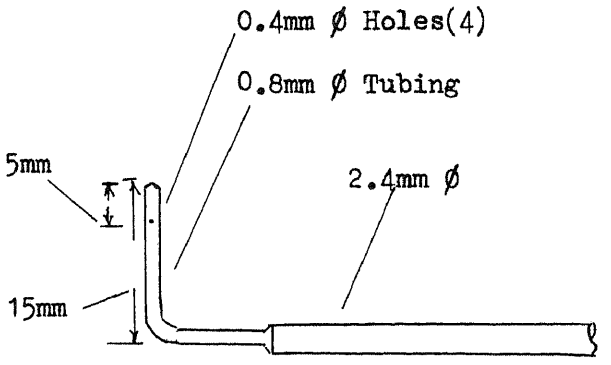

Static Pressure Probe

a = 2.2mm
b = 3.5mm
c = 7.5mm

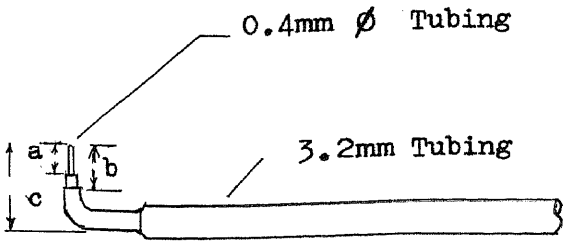

Total Pressure Probe

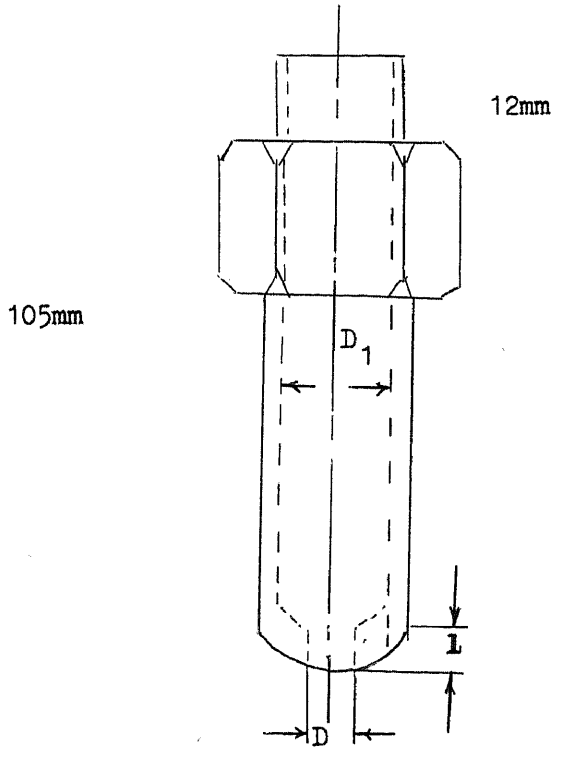

D=L D_1 2 D

Nozzle

Nozzle Size

3.175mm

6.35mm

9.525mm

12.7mm

Fig. 3a

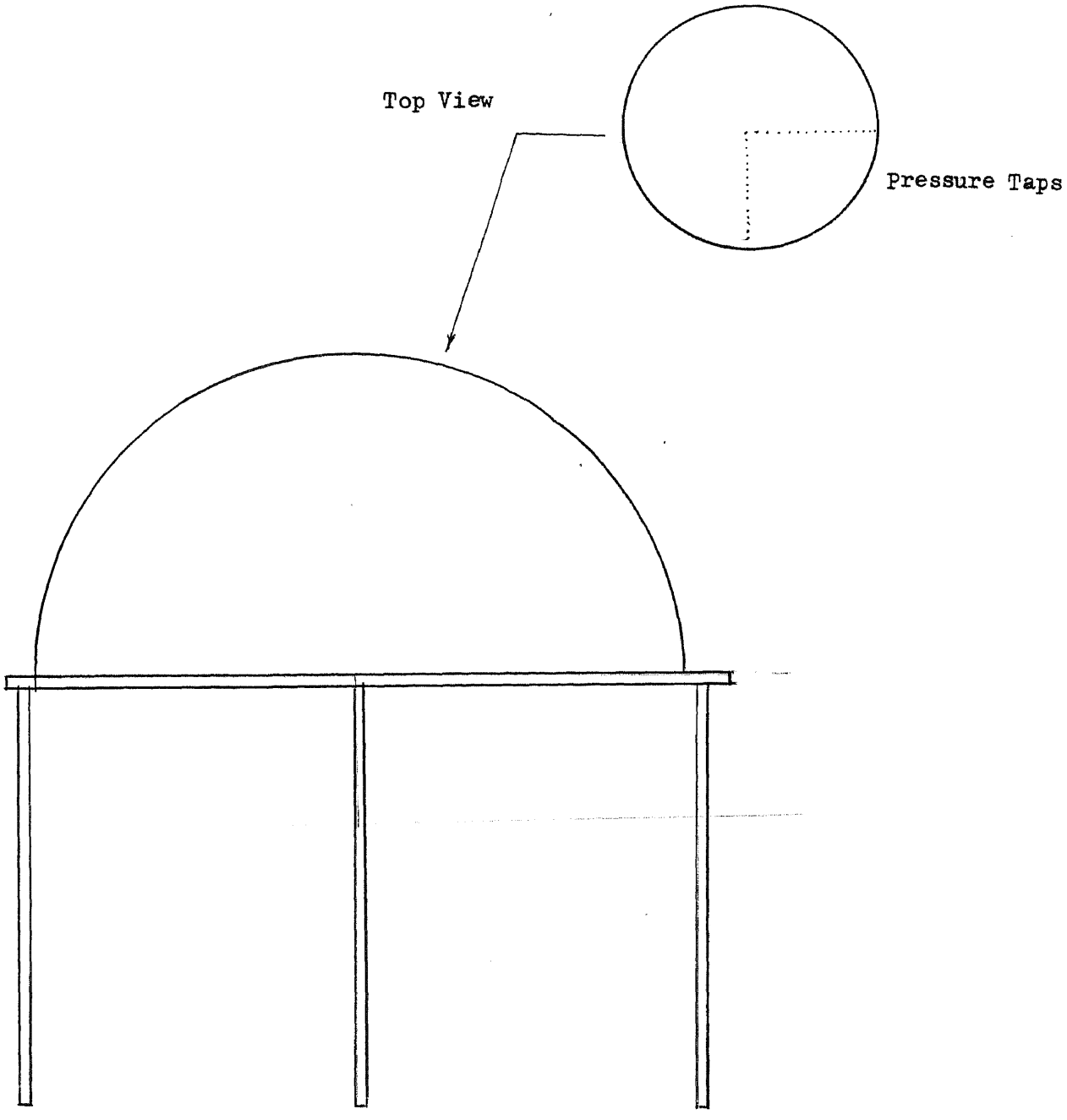

Impinging Hemisphere

Fig. 4

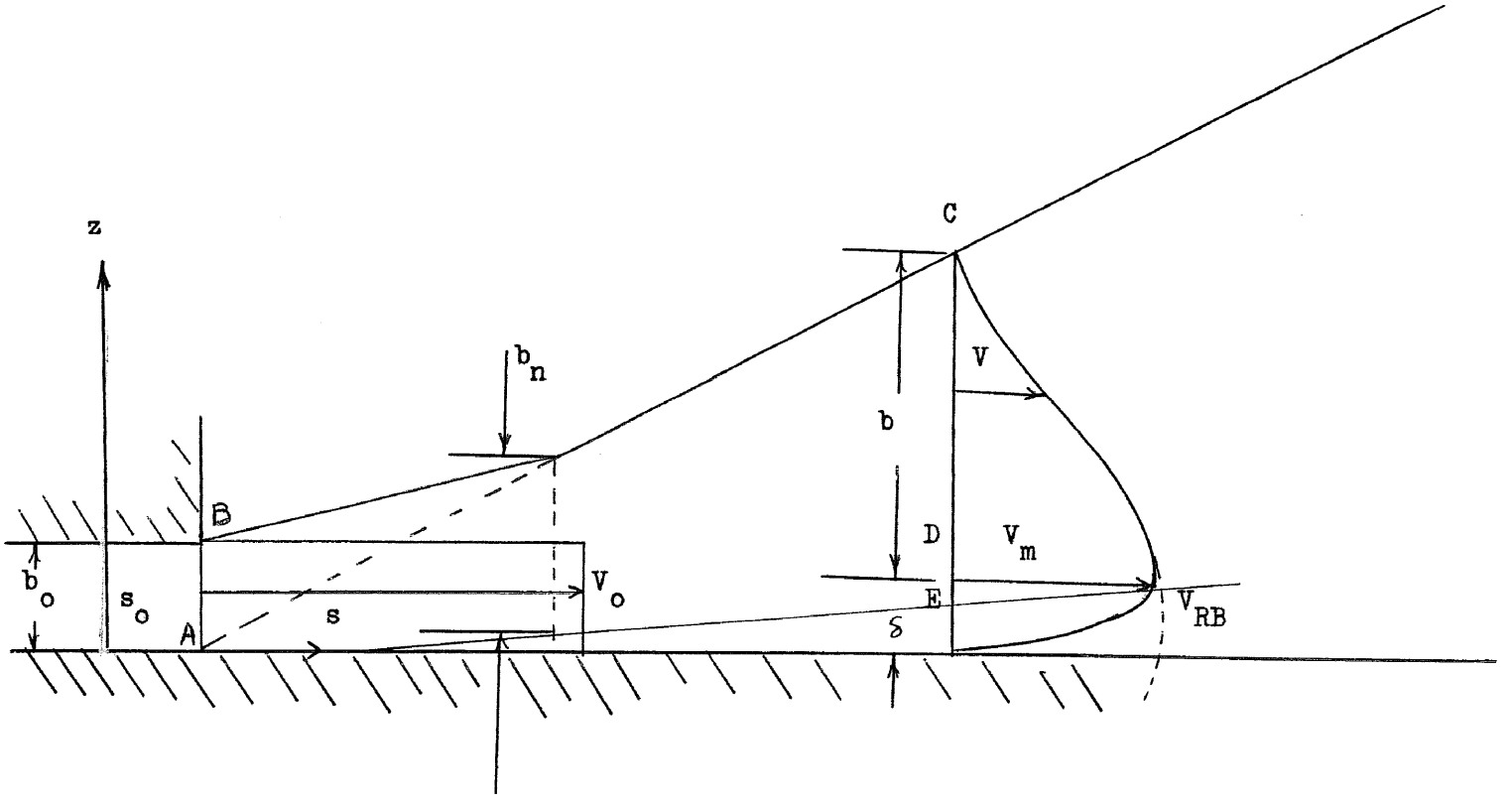

Coordinate System of a Radial Wall Jet

Fig. 5

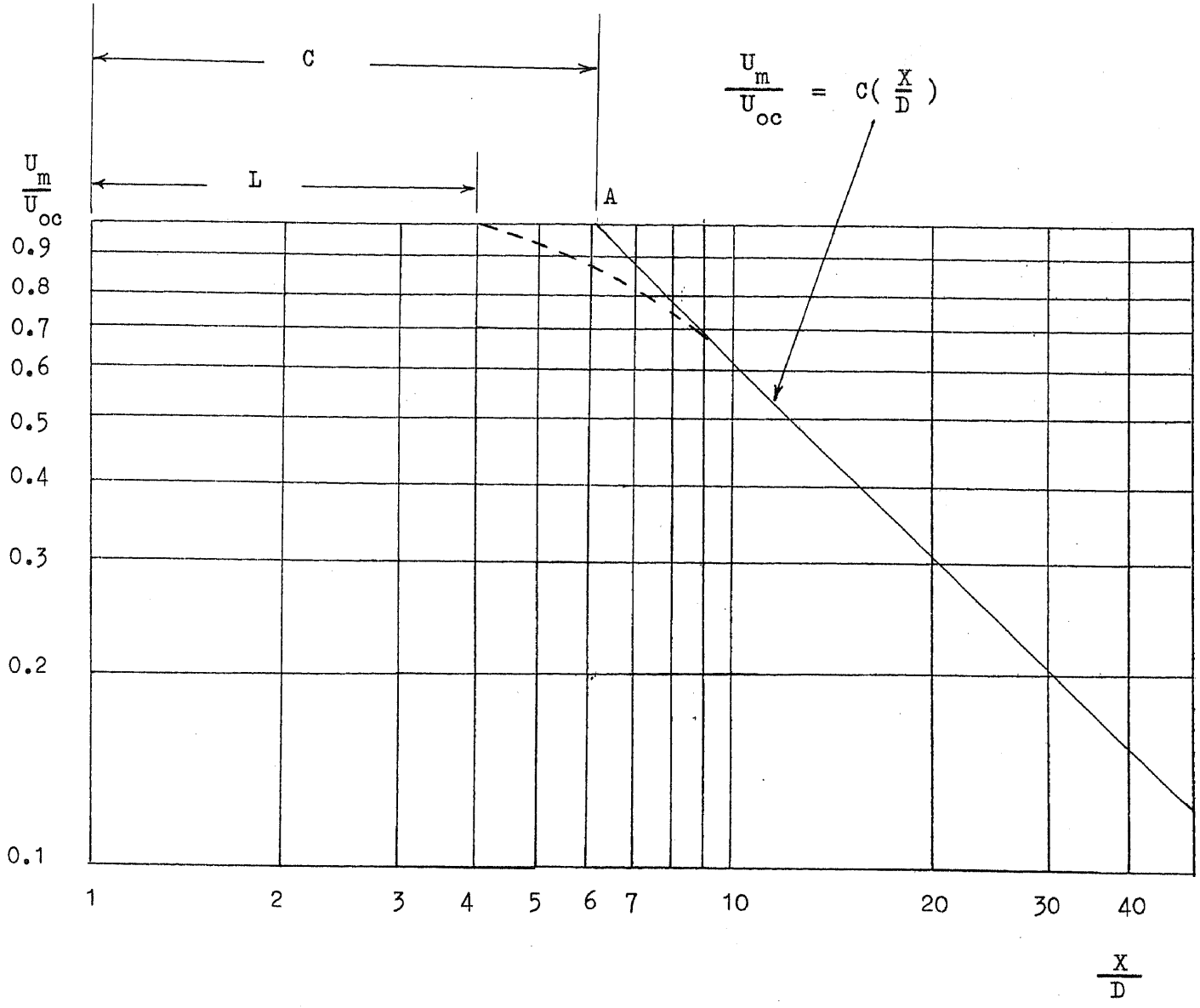

Fig. 6 Definition of C and L

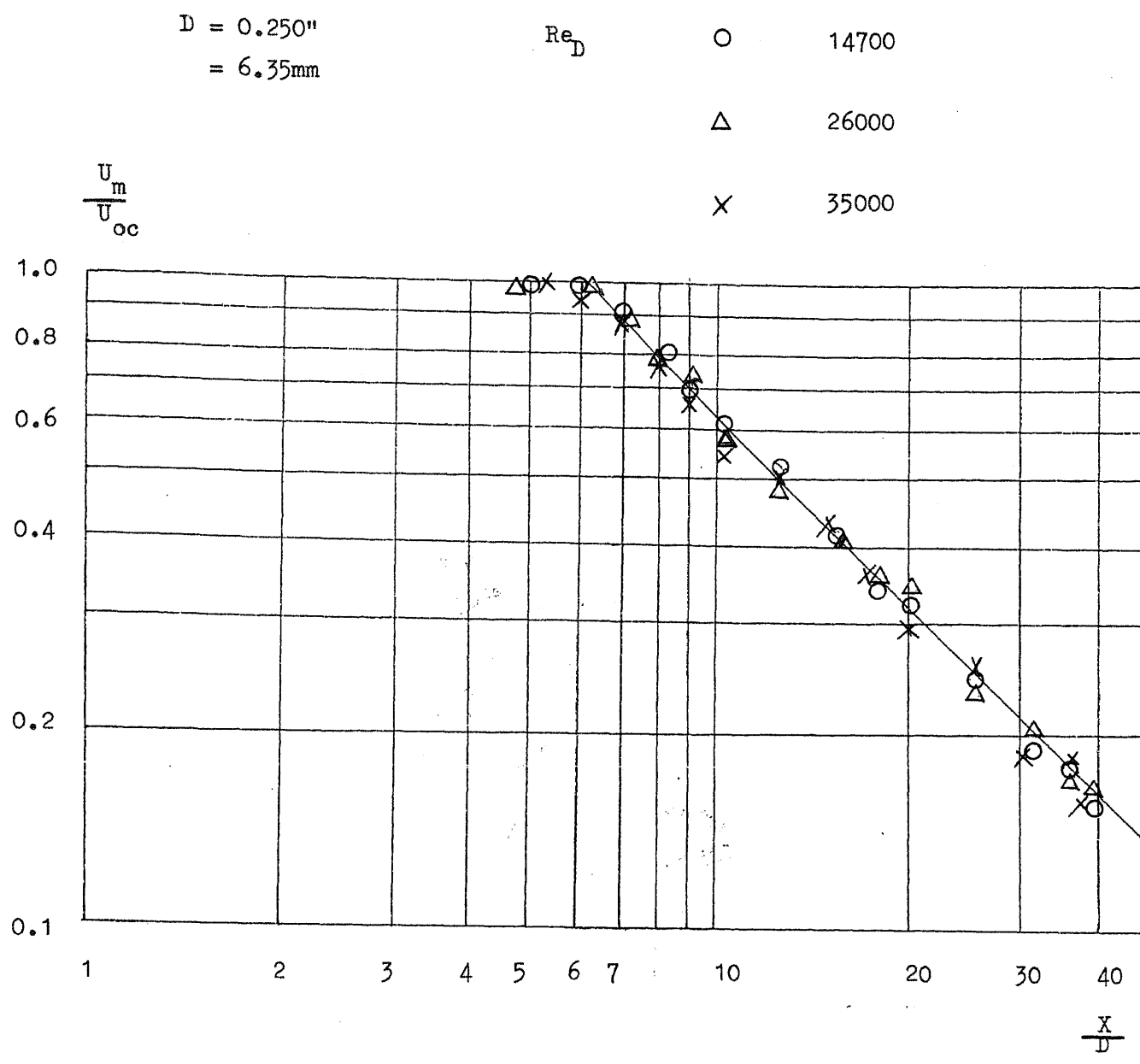

Fig. 7 Centerline Velocity Decay of Free Jet

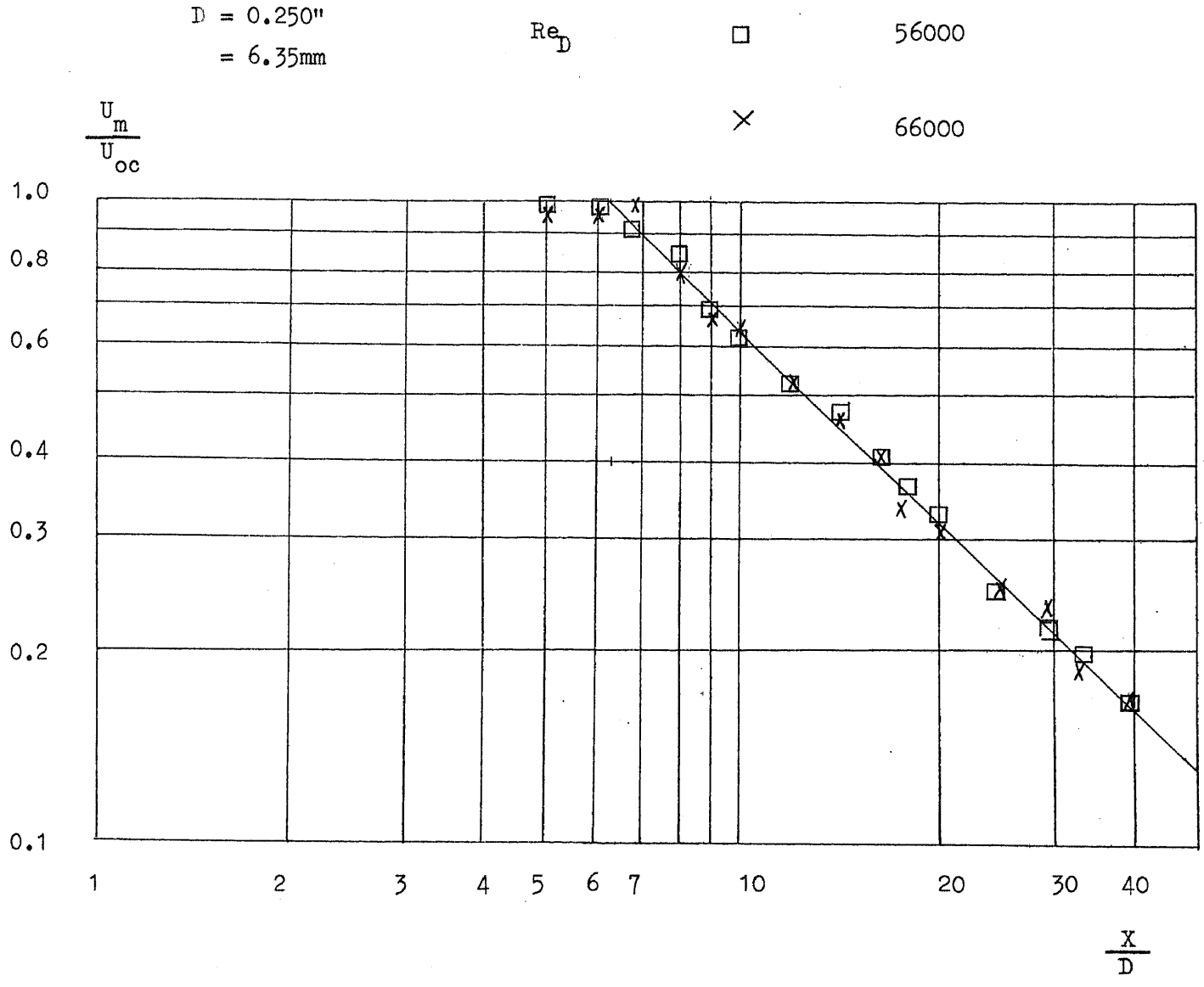

Fig. 8 Centerline Velocity Decay of Free Jet

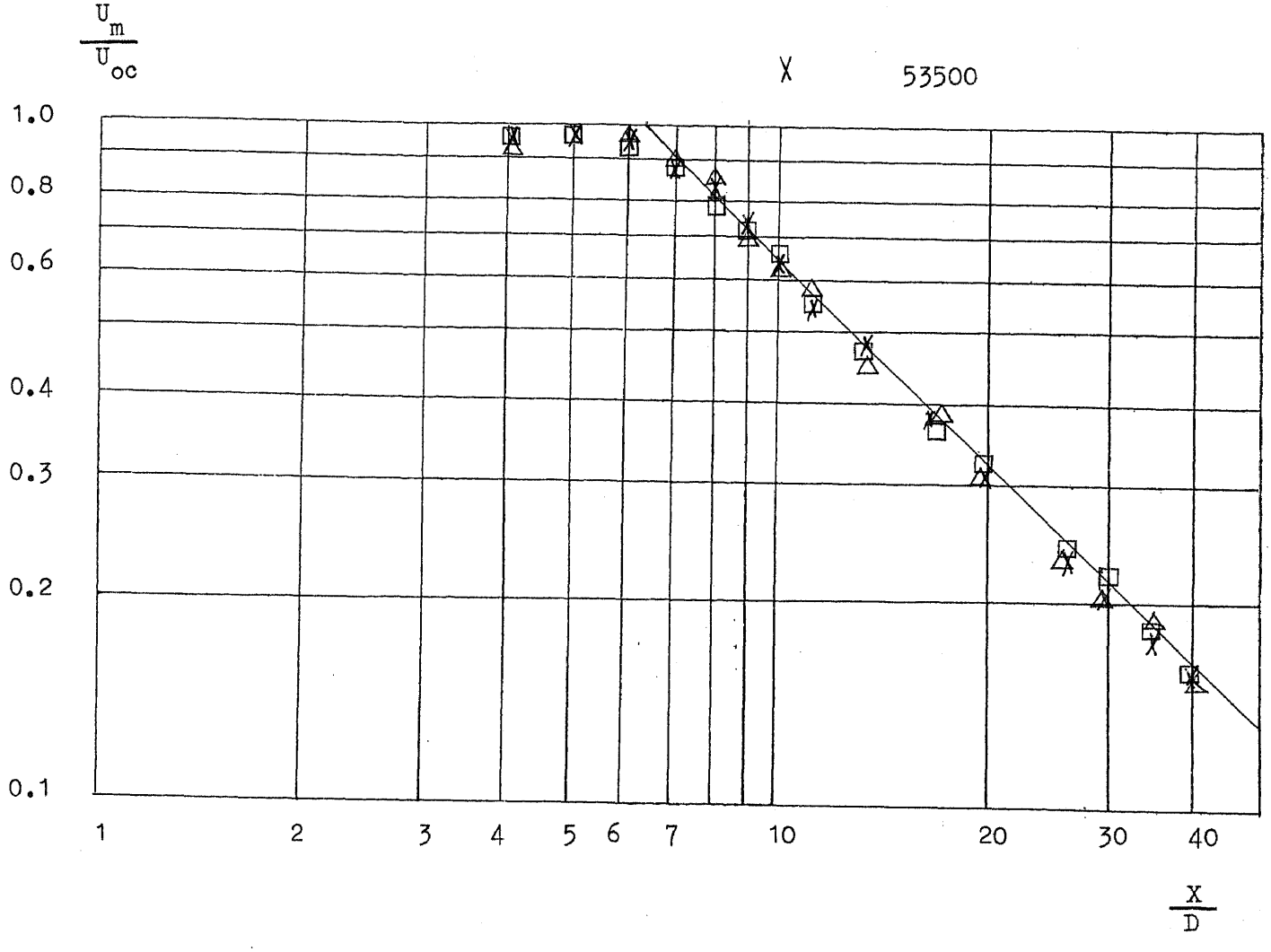

Fig. 9 Centerline Velocity Decay of Free Jet

D = 0.125"
= 3.175mm

Re_D □ 32000
△ 40000
X 62000

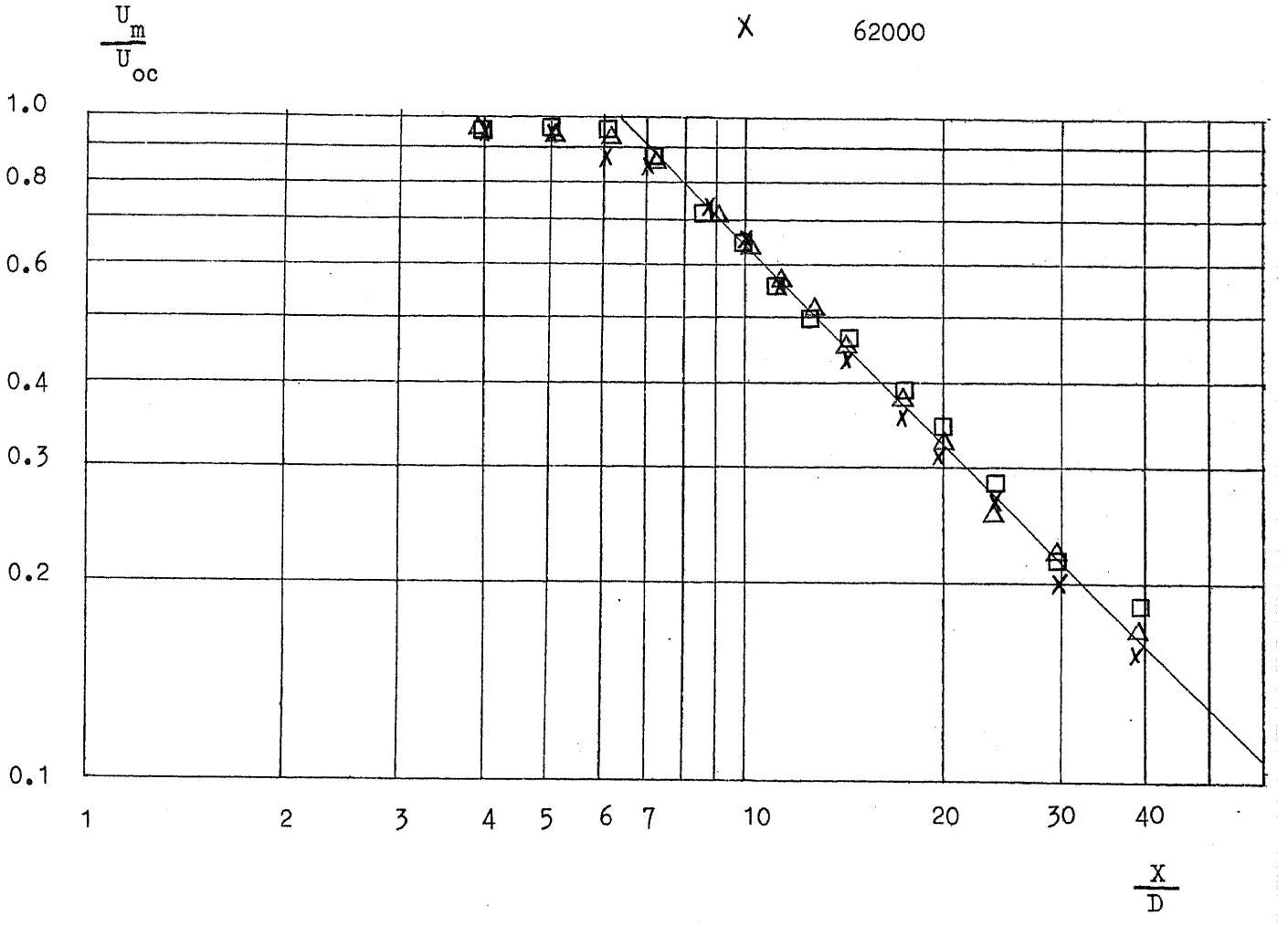

Fig. 10 Centerline Velocity Decay of Free Jet

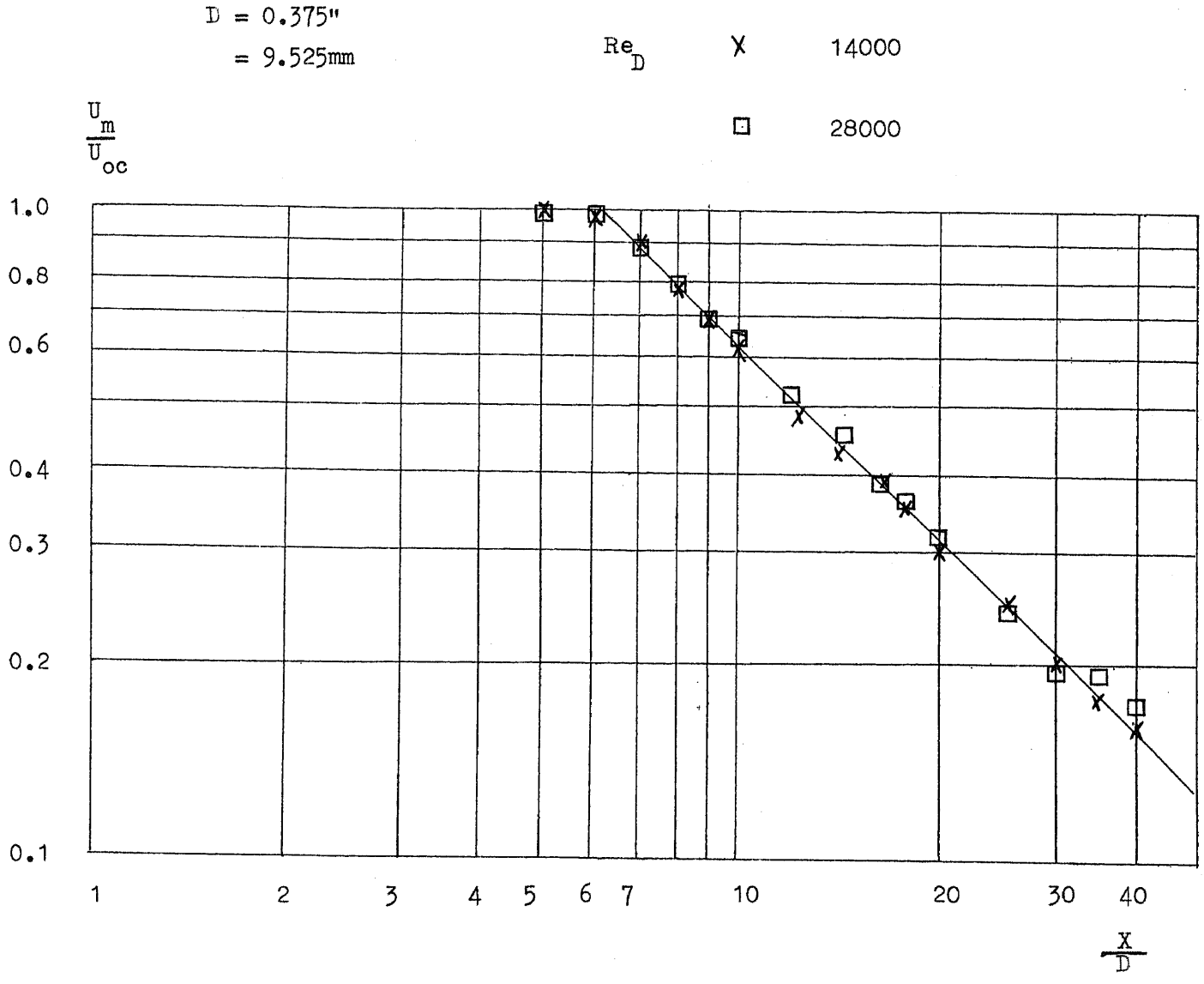

Fig. 11 Centerline Velocity Decay of Free Jet

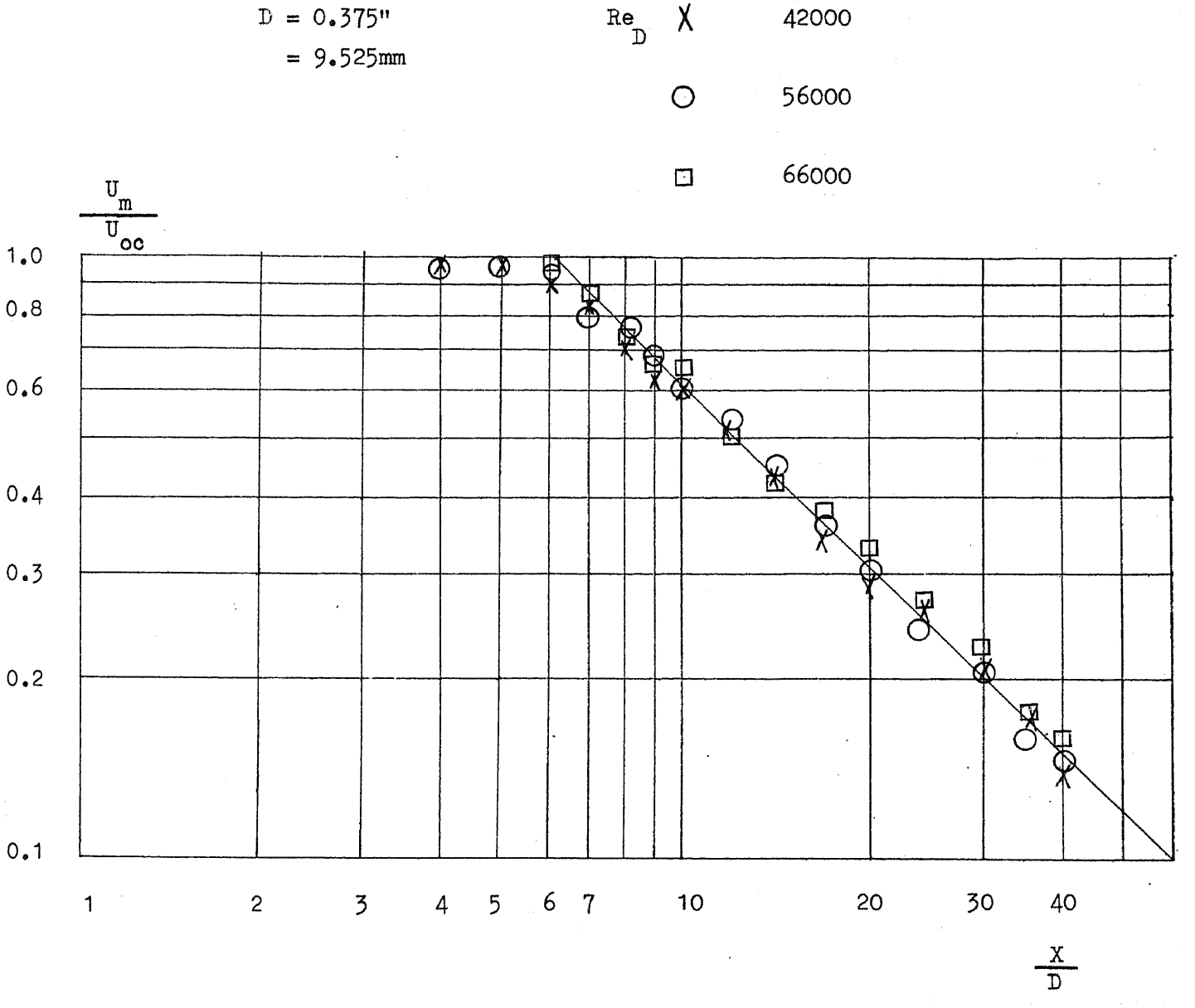

Fig. 12 Centerline Velocity Decay of Free Jet

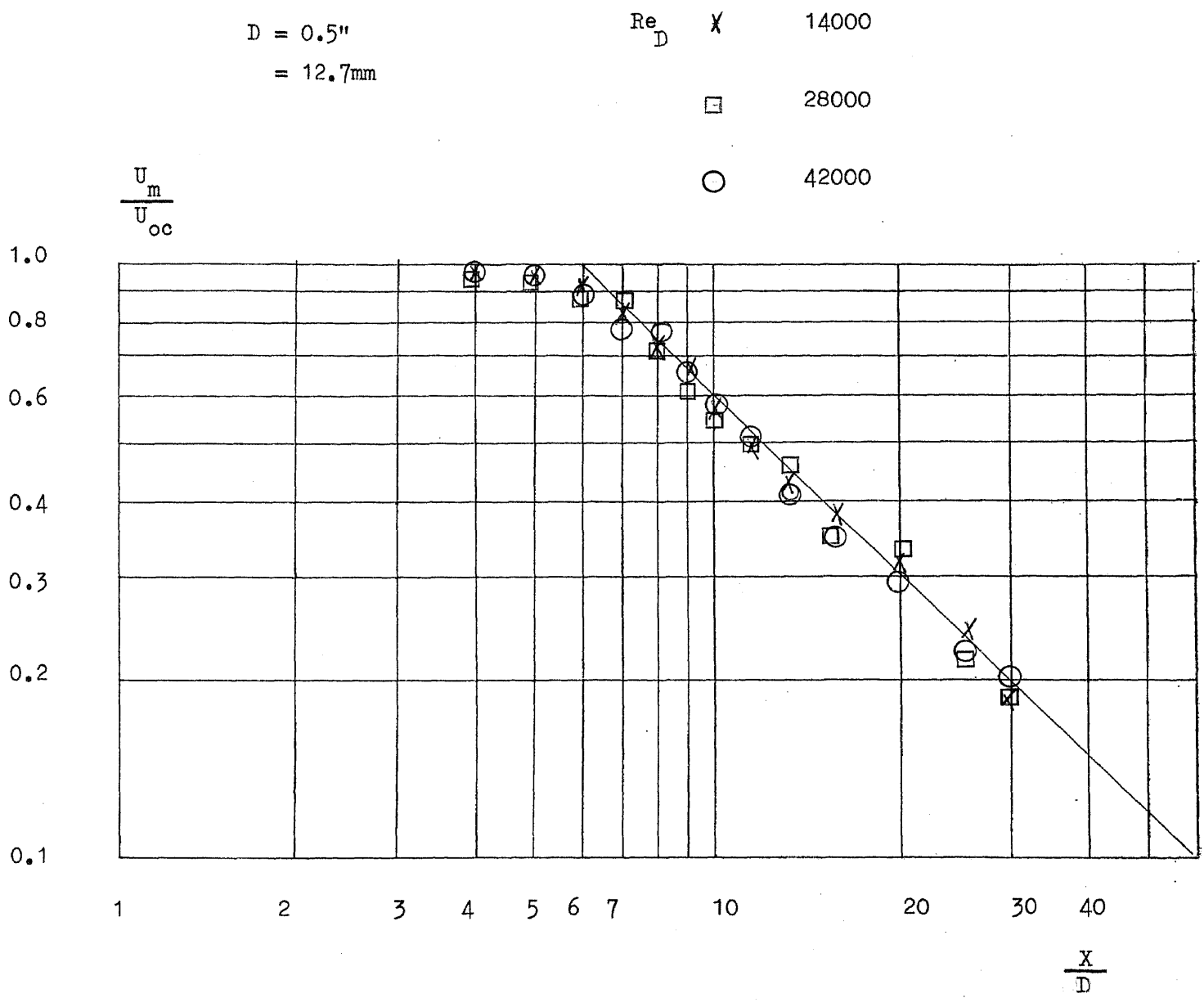

Fig. 13 Centerline Velocity Decay of Free Jet

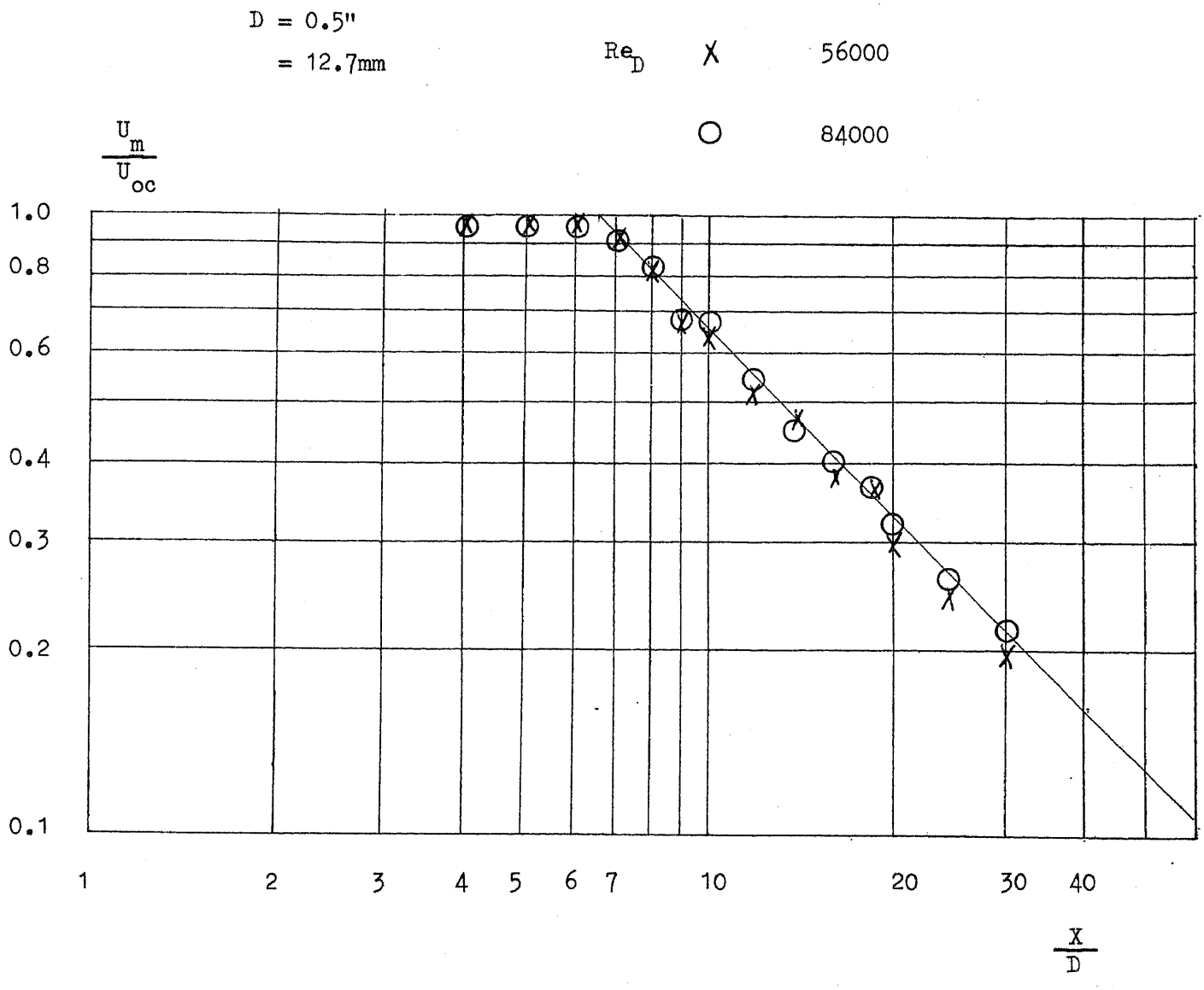

Fig. 14 Centerline Velocity Decay of Free Jet

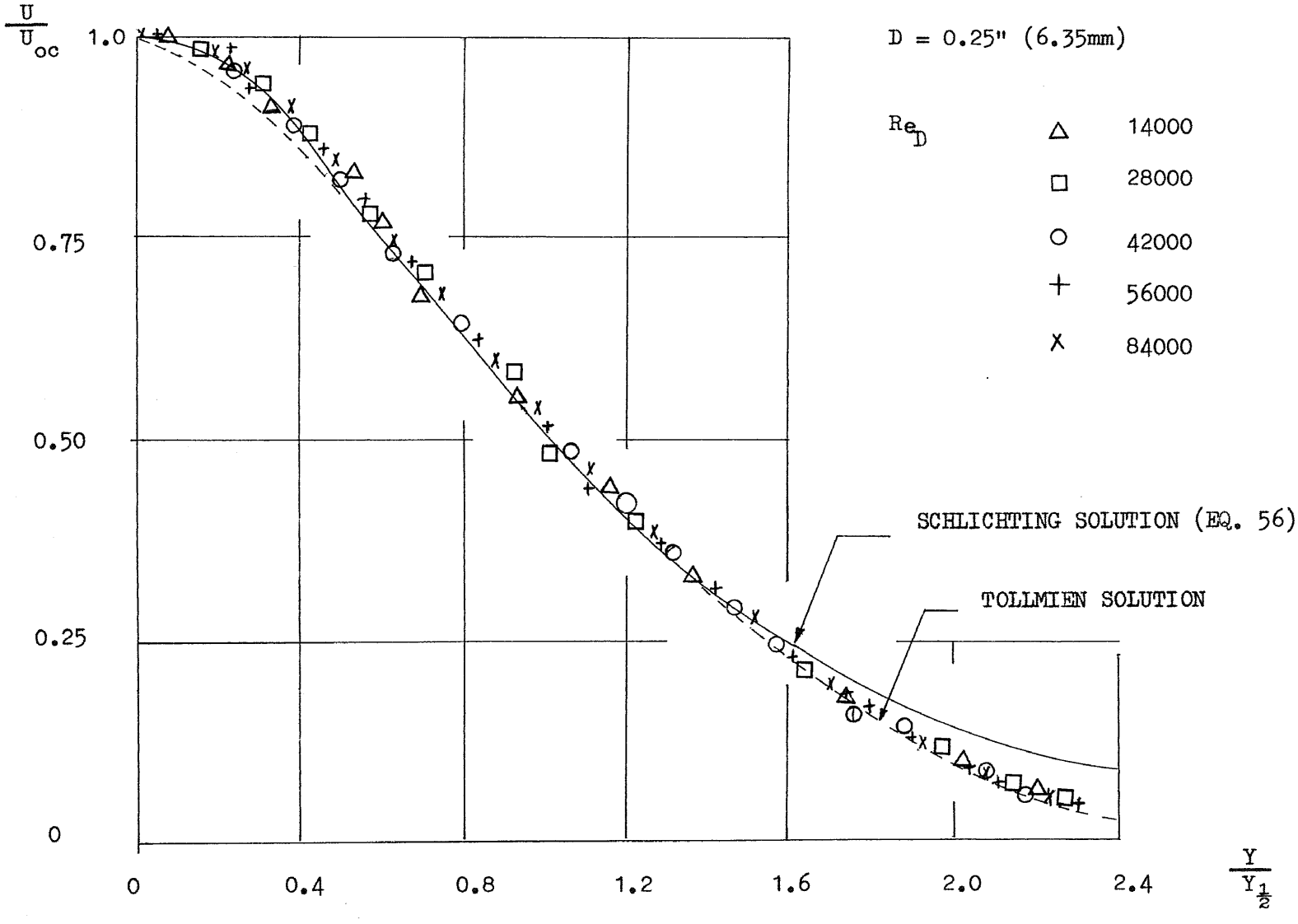

Fig. 15 Free Jet Velocity Distribution, X/D = 16

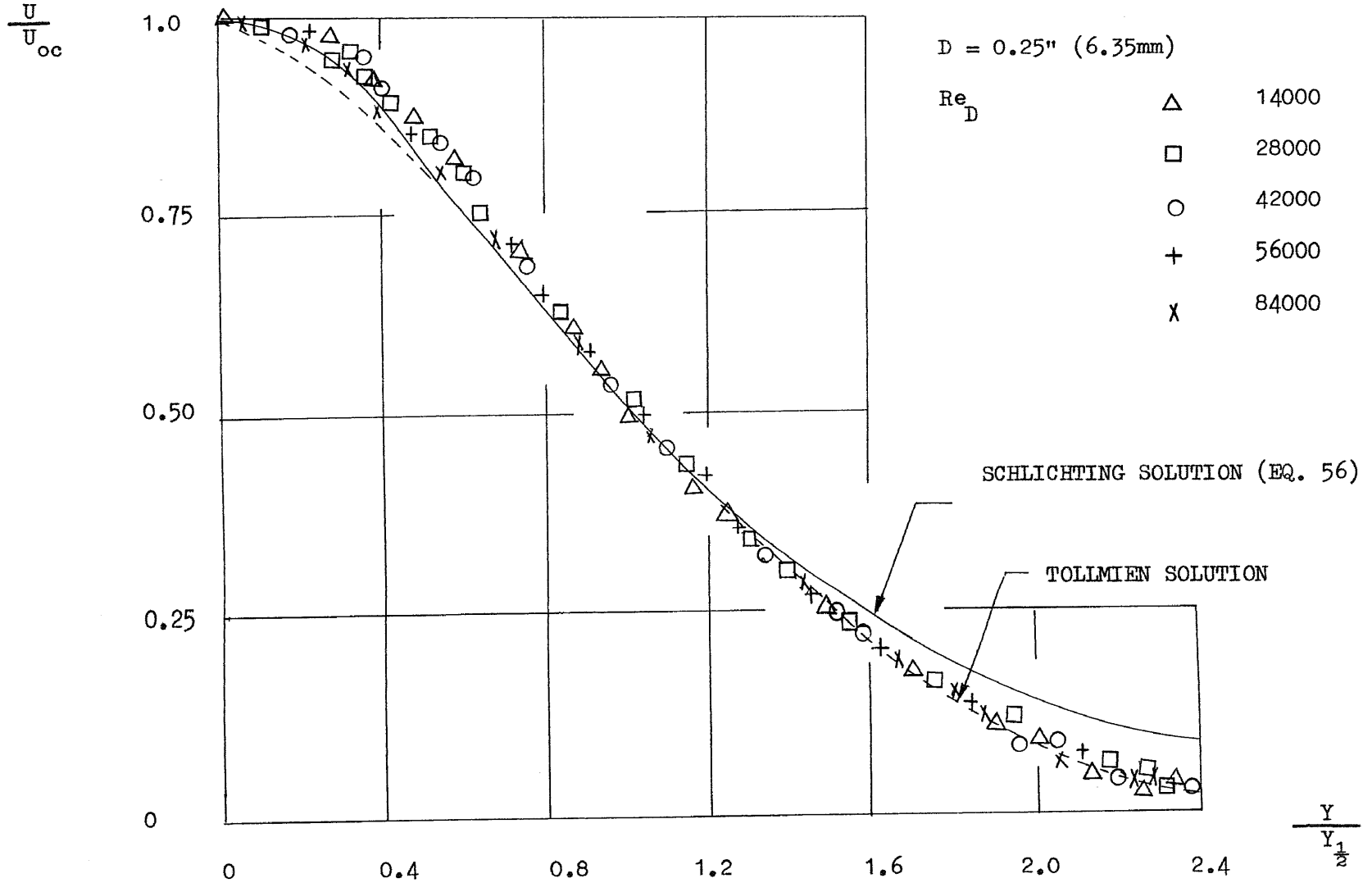

Fig. 16 Free Jet Velocity Distribution, X/D = 12

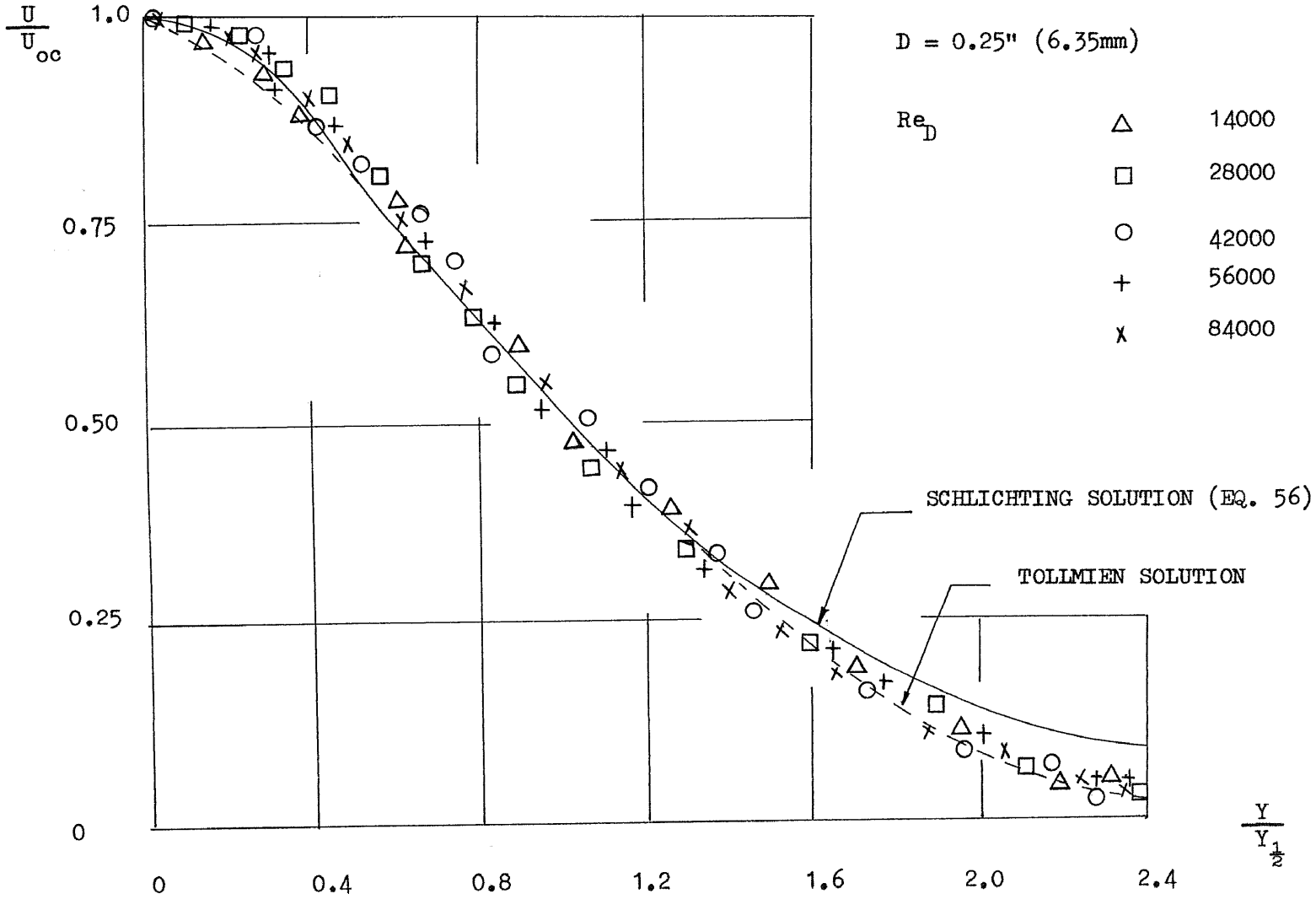

Fig. 17 Free Jet Velocity Distribution, X/D = 8

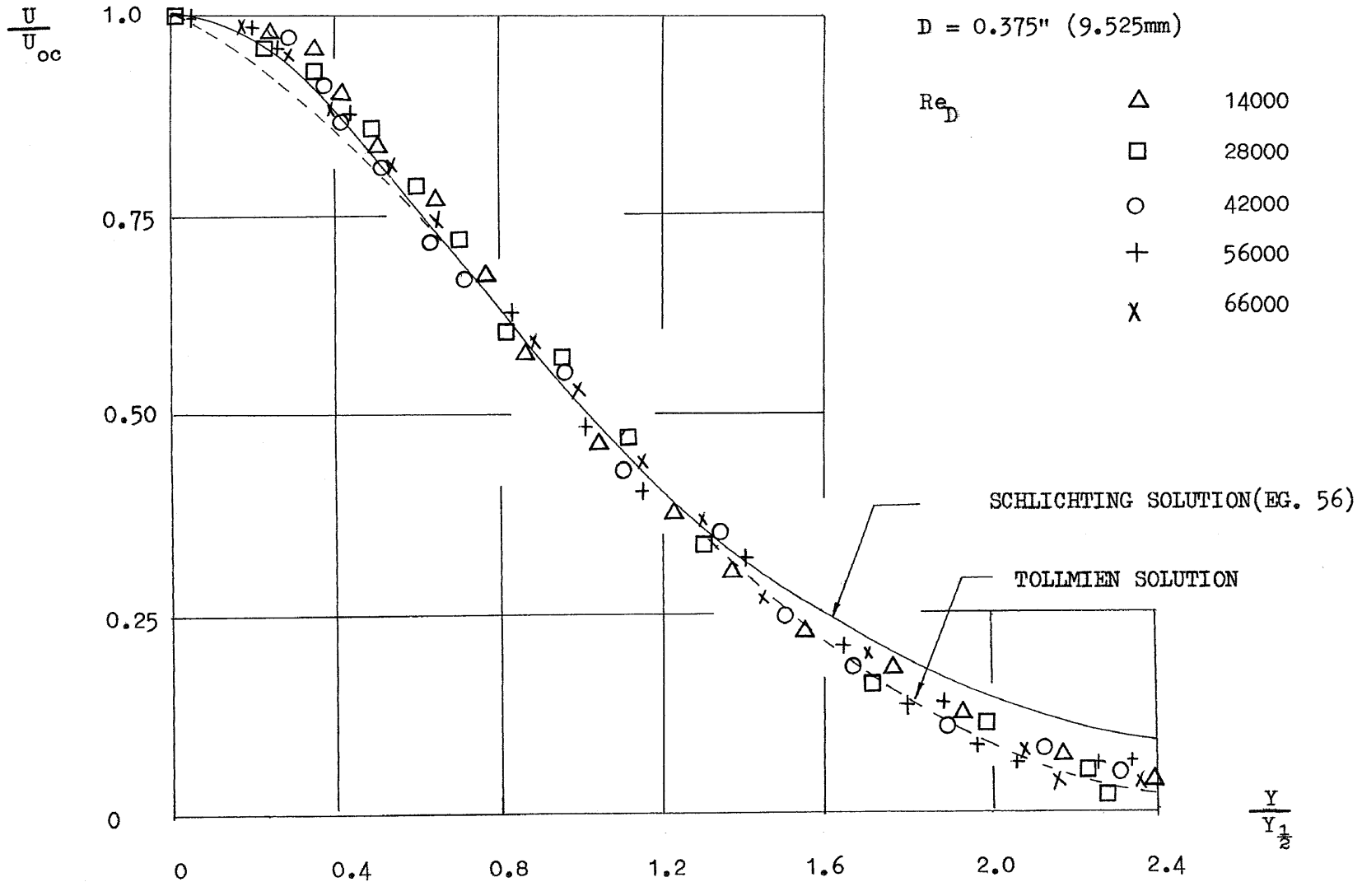

Fig. 18 Free Jet Velocity Distribution, X/D = 16

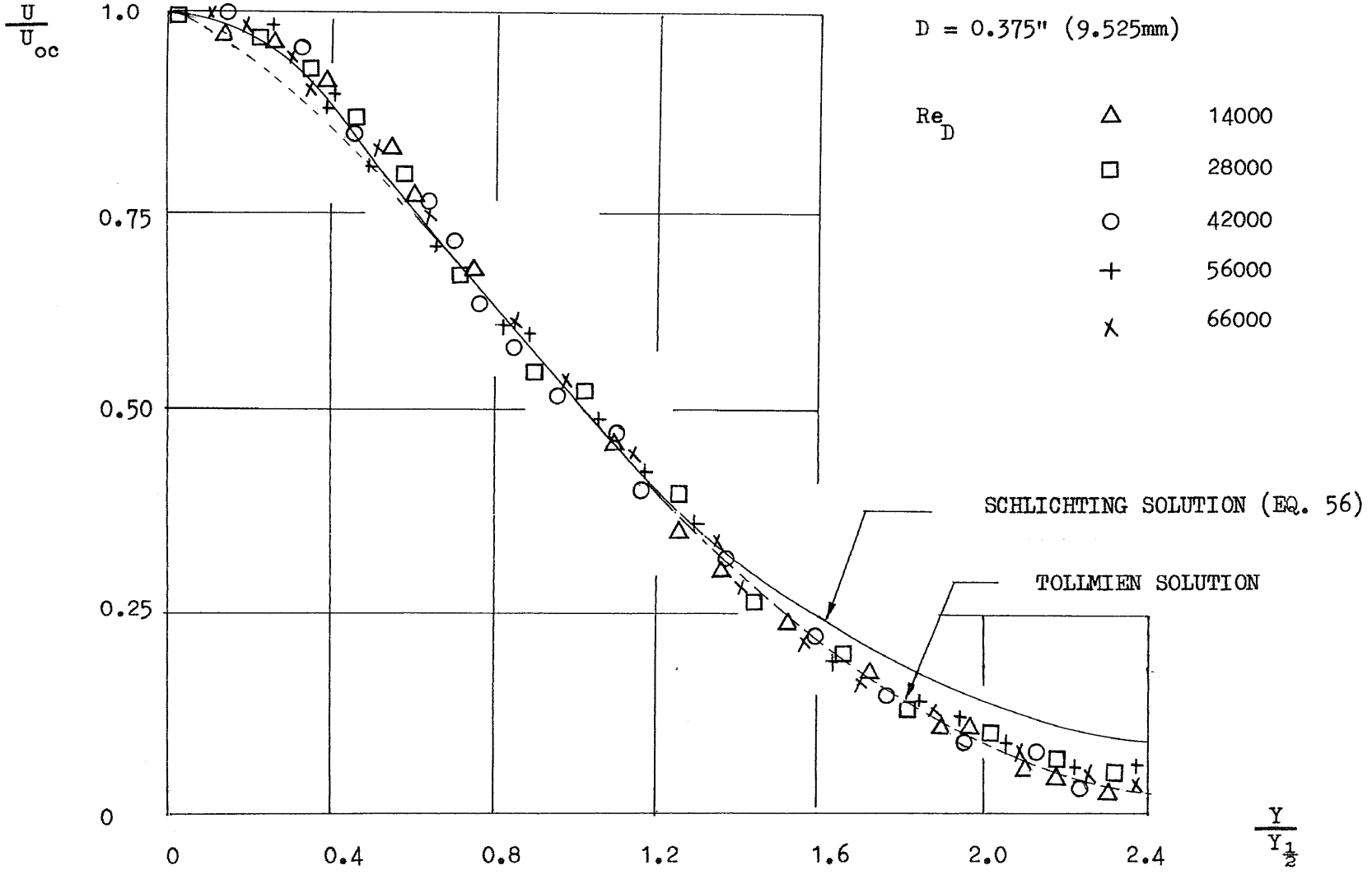

Fig. 19 Free Jet Velocity Distribution, X/D = 12

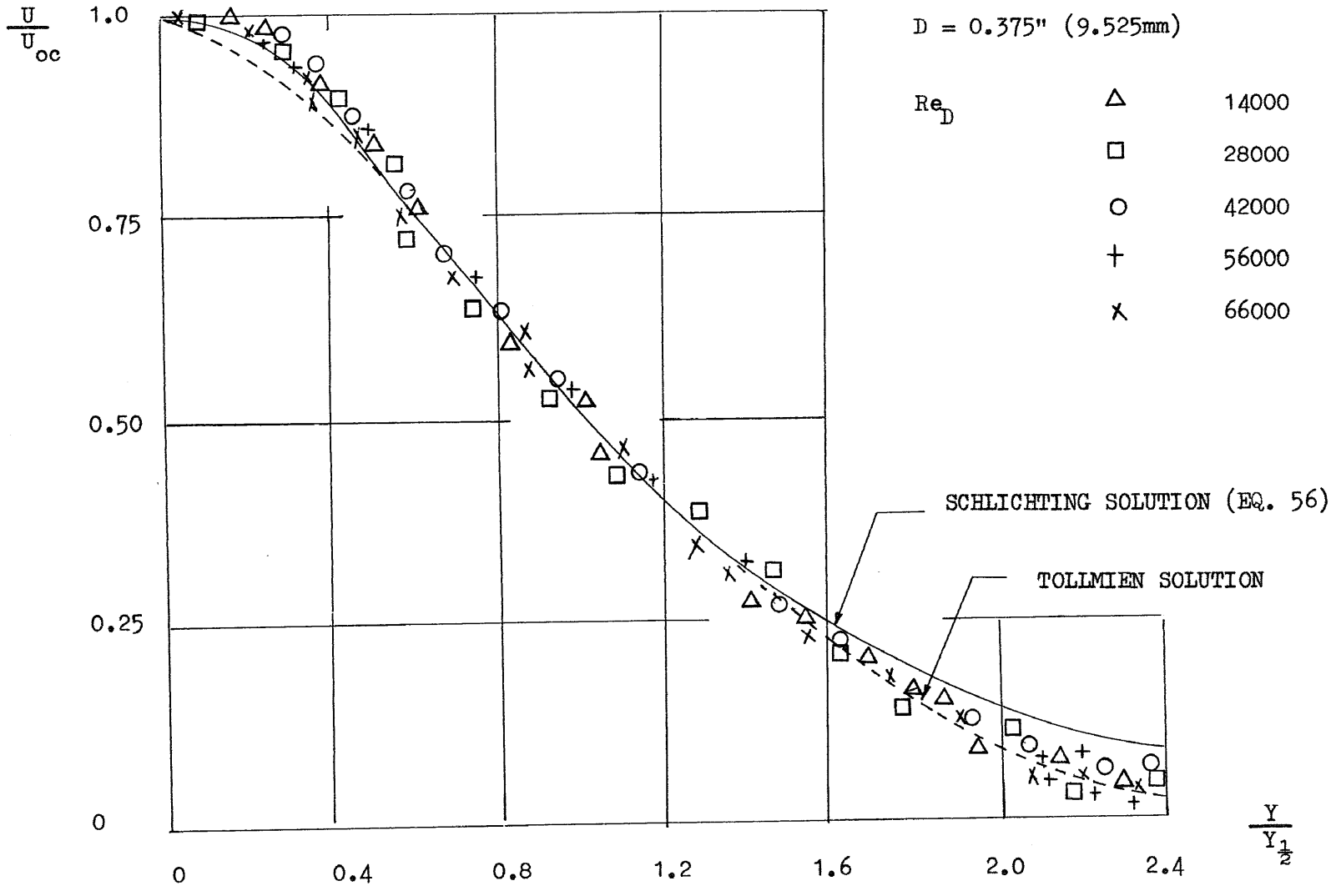

Fig. 20 Free Jet Velocity Distribution, X/D = 8

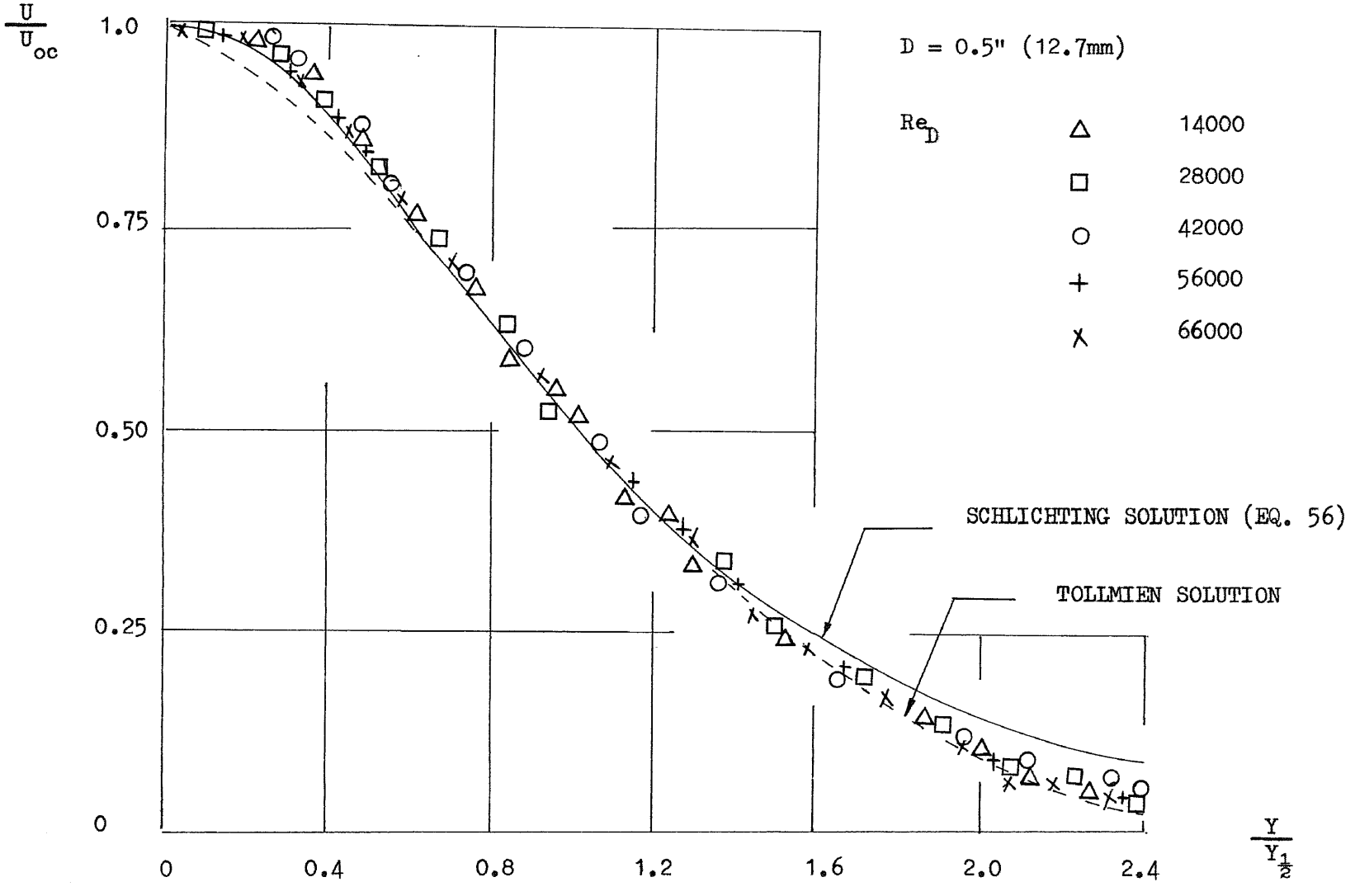

Fig. 21 Free Jet Velocity Distribution, X/D = 16

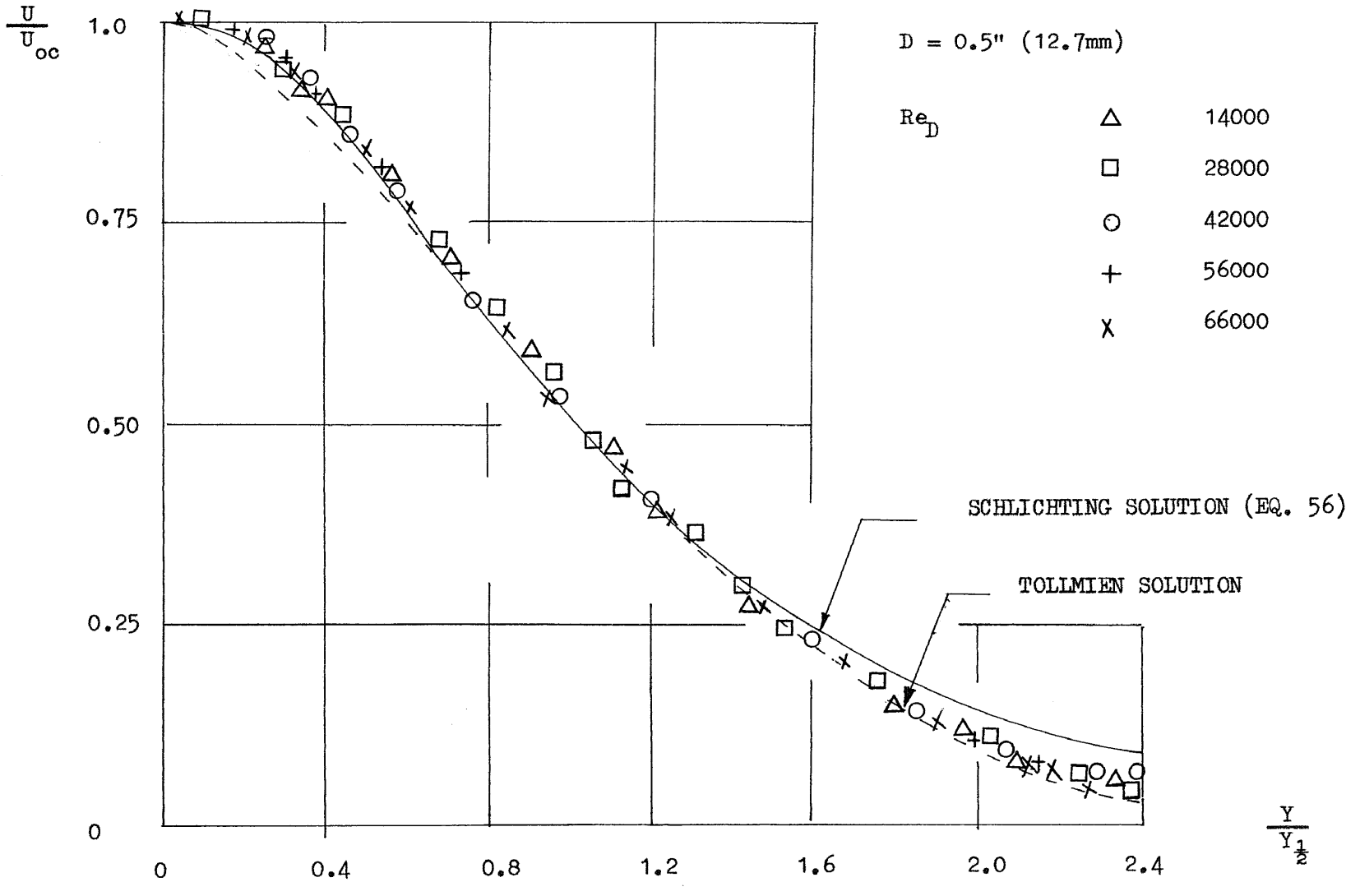

Fig. 22 Free Jet Velocity Distribution, X/D = 12

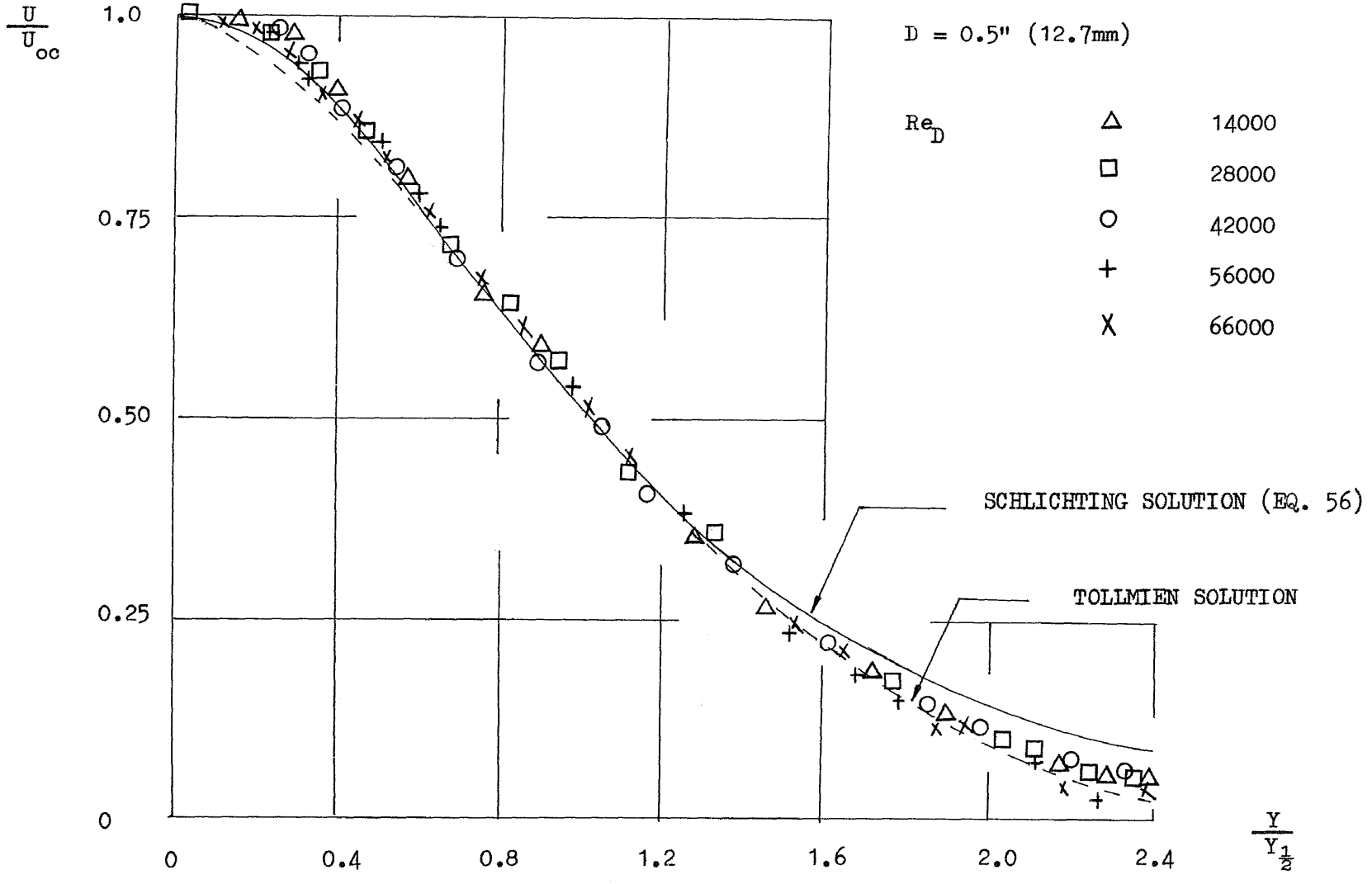

Fig. 23 Free Jet Velocity Distribution, X/D = 8

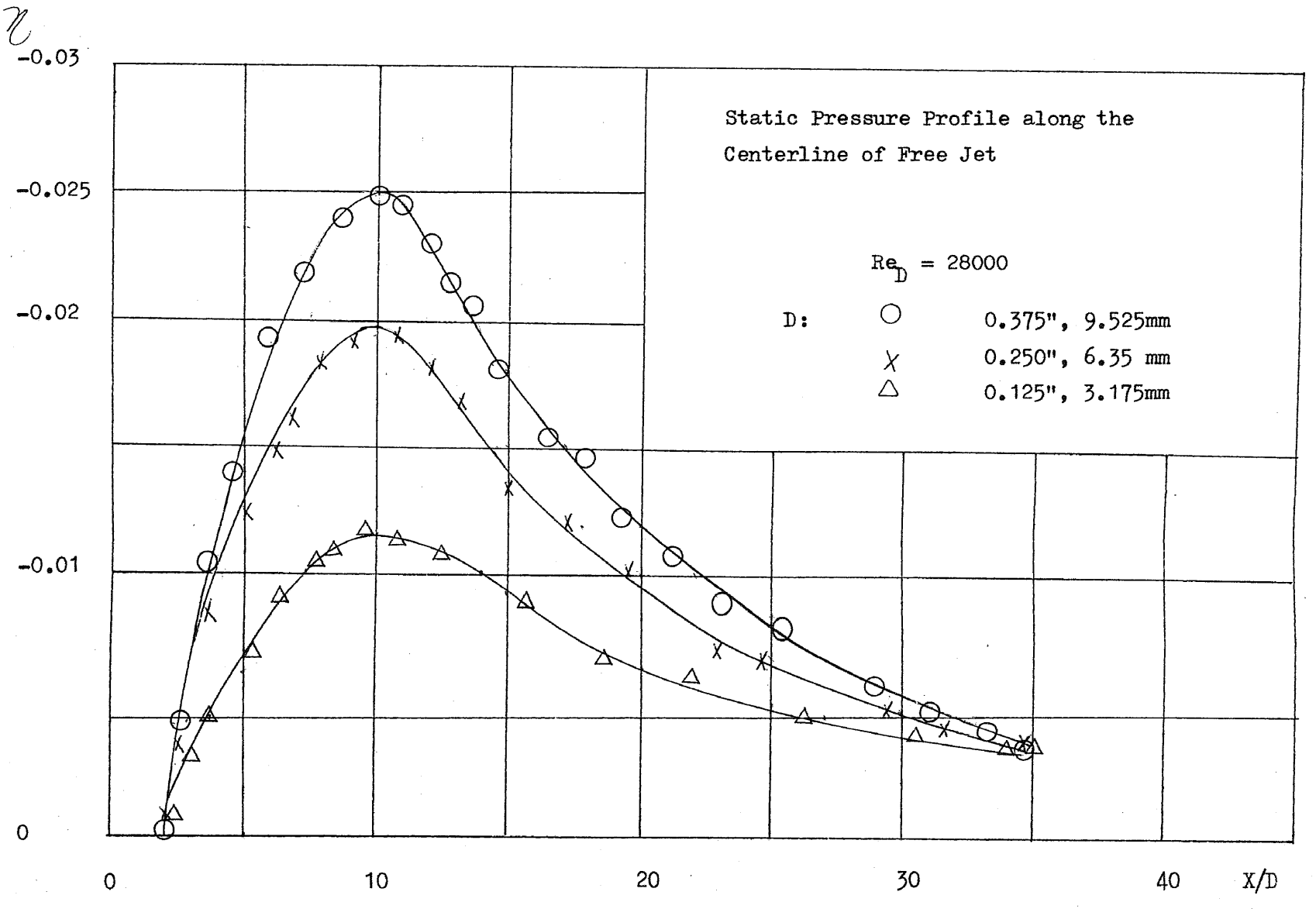
η
-0.03
-0.025
-0.02
-0.01
0
0
10
20
30
40
X/D
Static Pressure Profile along the
Centerline of Free Jet
Re_D = 28000
D:
0.375", 9.525mm
0.250", 6.35 mm
0.125", 3.175mm

Fig. 24

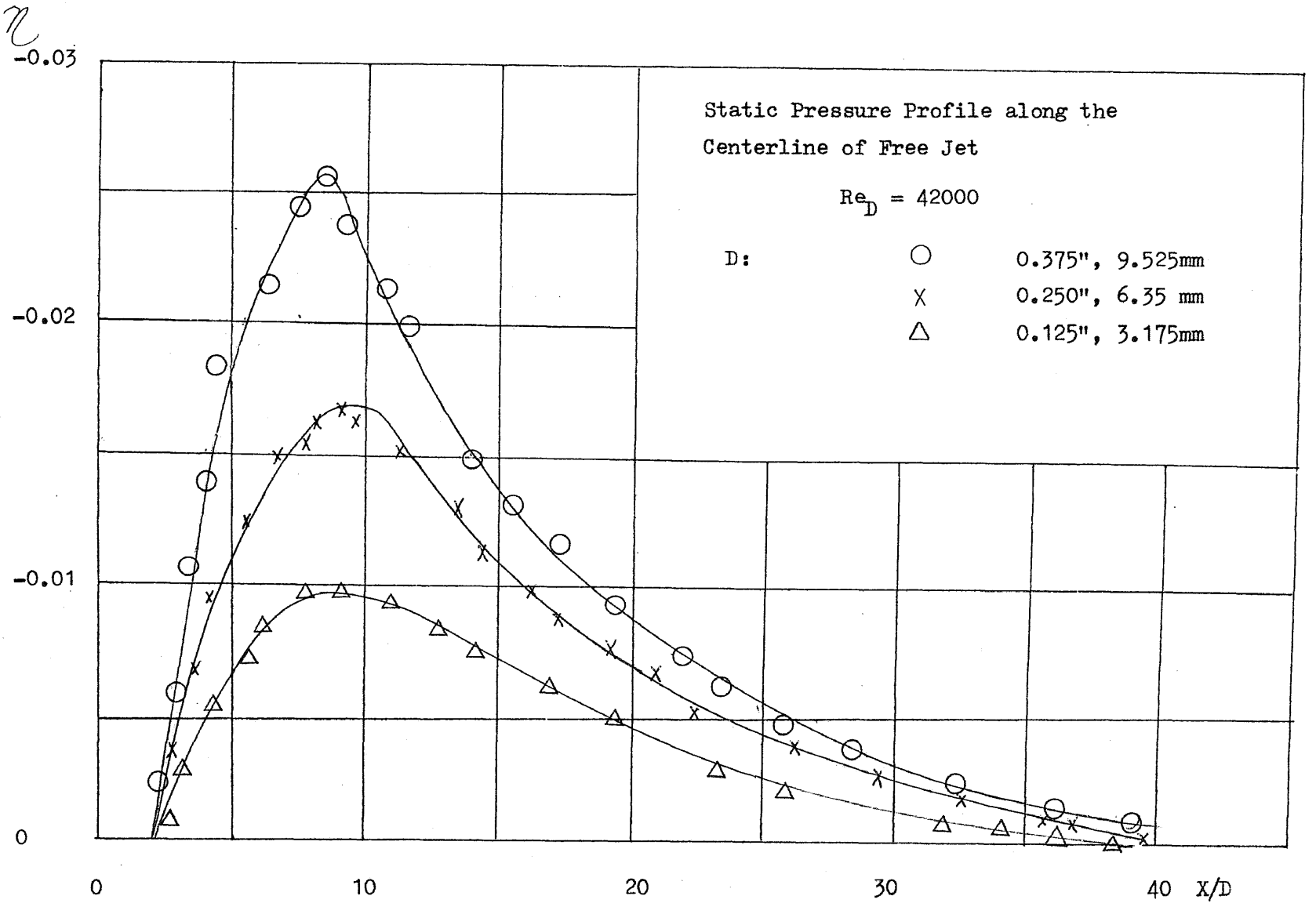
η
-0.03
-0.02
-0.01
0
Static Pressure Profile along the
Centerline of Free Jet
Re_D = 42000
D:
○ 0.375", 9.525mm
X 0.250", 6.35 mm
△ 0.125", 3.175mm
0
10
20
30
40
X/D

Fig. 25

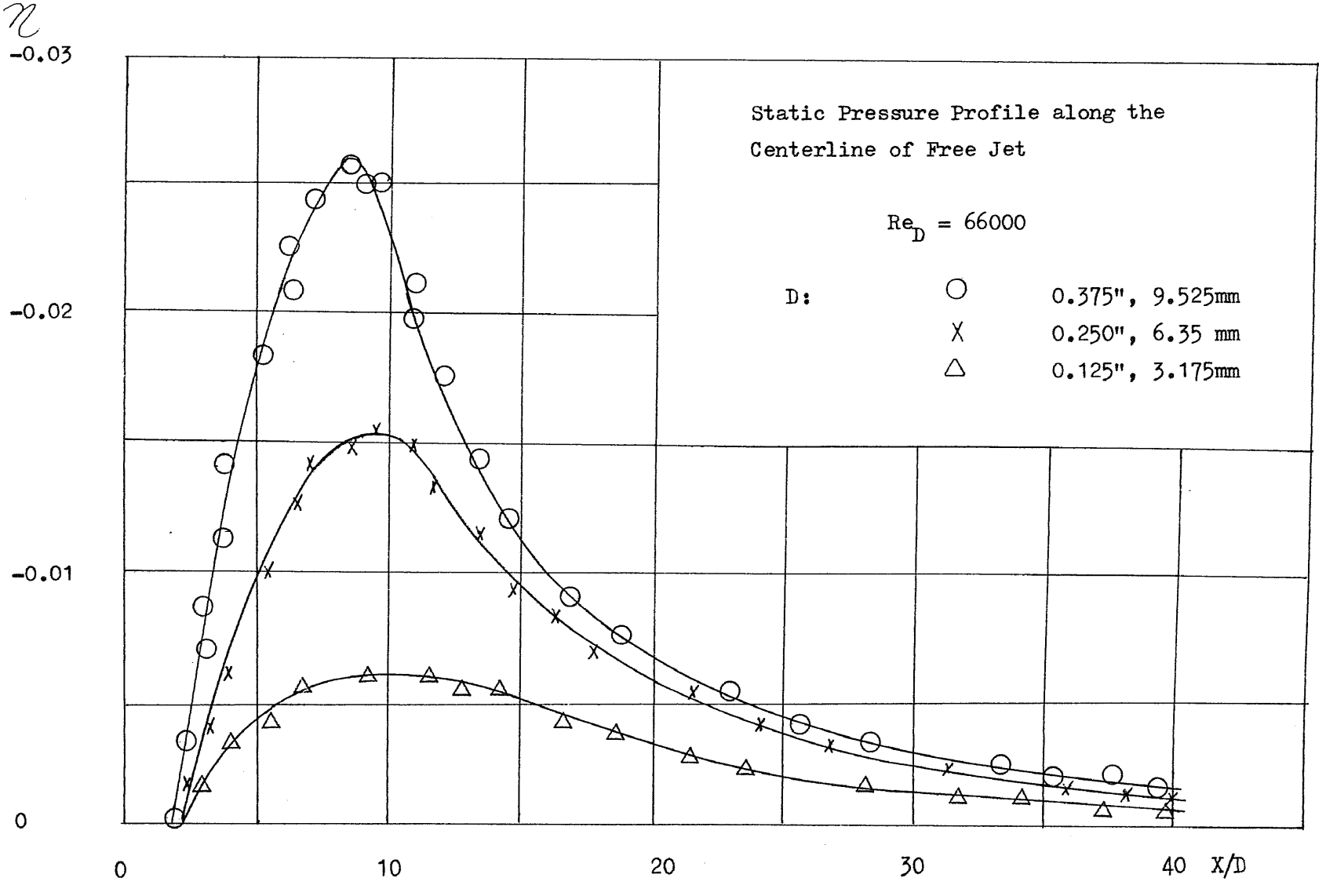
η
-0.03
-0.02
-0.01
0
0
10
20
30
40
X/D
Static Pressure Profile along the
Centerline of Free Jet
Re_D = 66000
D:
0.375", 9.525mm
0.250", 6.35 mm
0.125", 3.175mm

Fig. 26

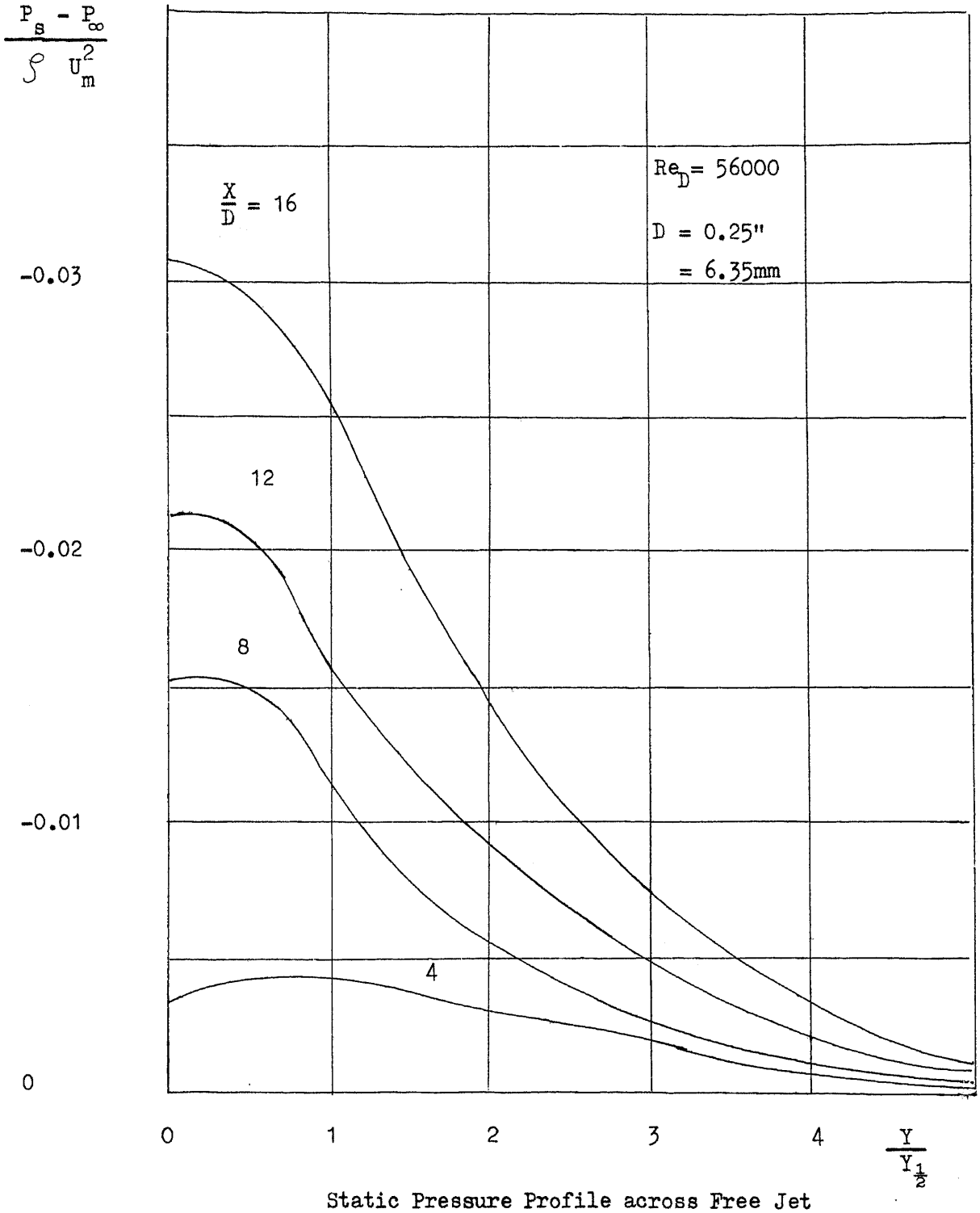

Static Pressure Profile across Free Jet

Fig. 27

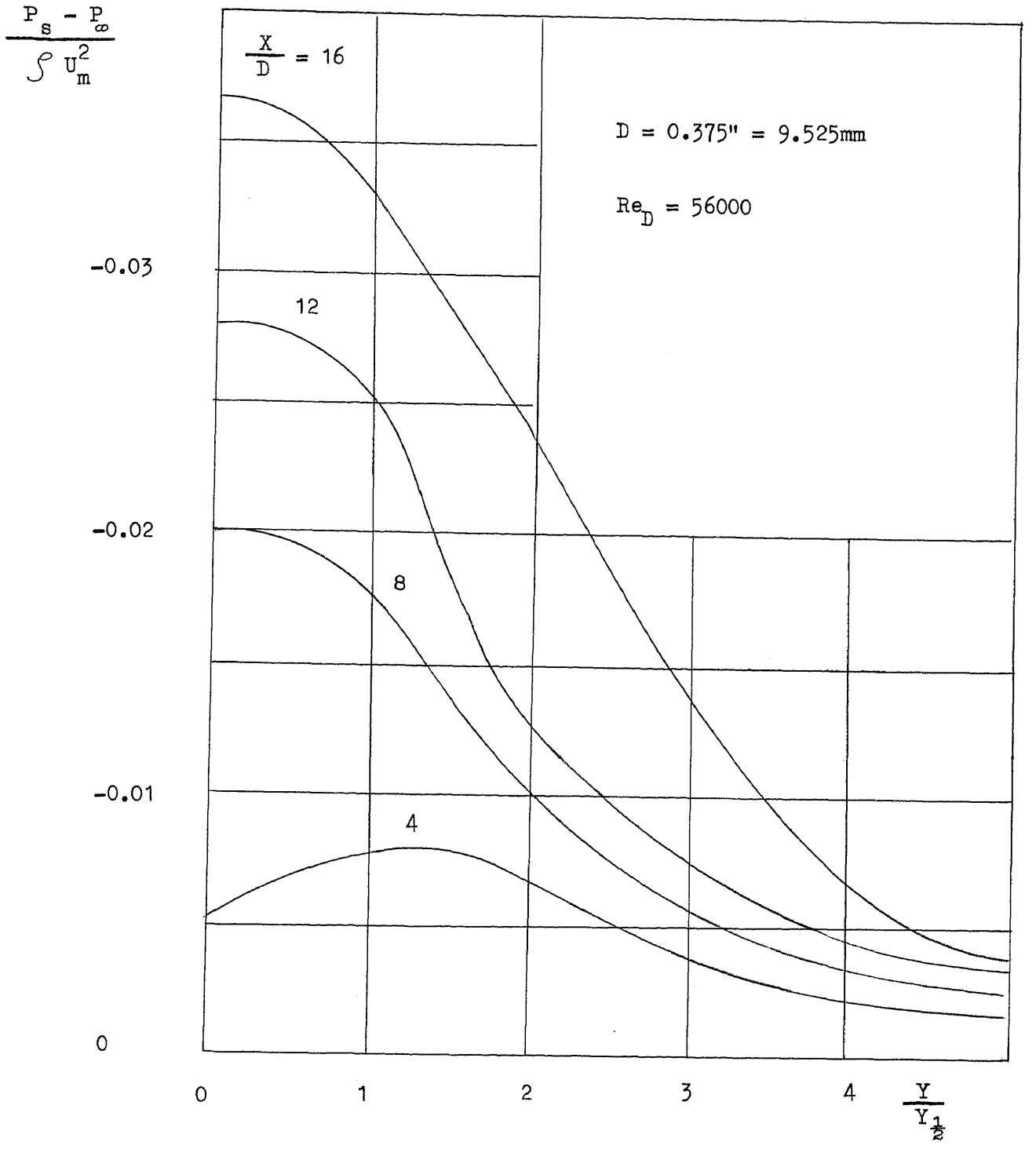

Fig.28 Static Pressure Profile across Free Jet

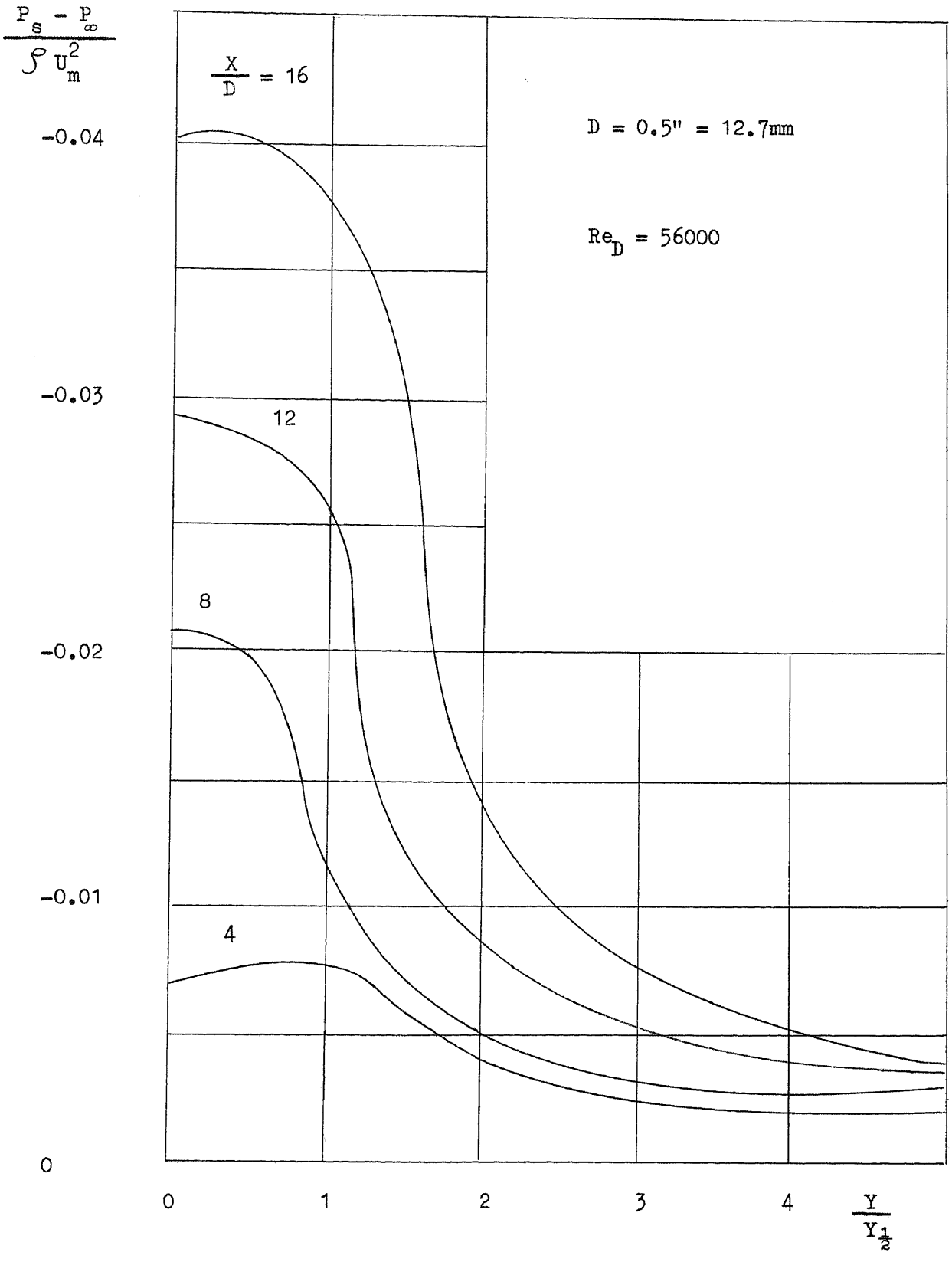

Fig. 29 Static Pressure Profile across Free Jet

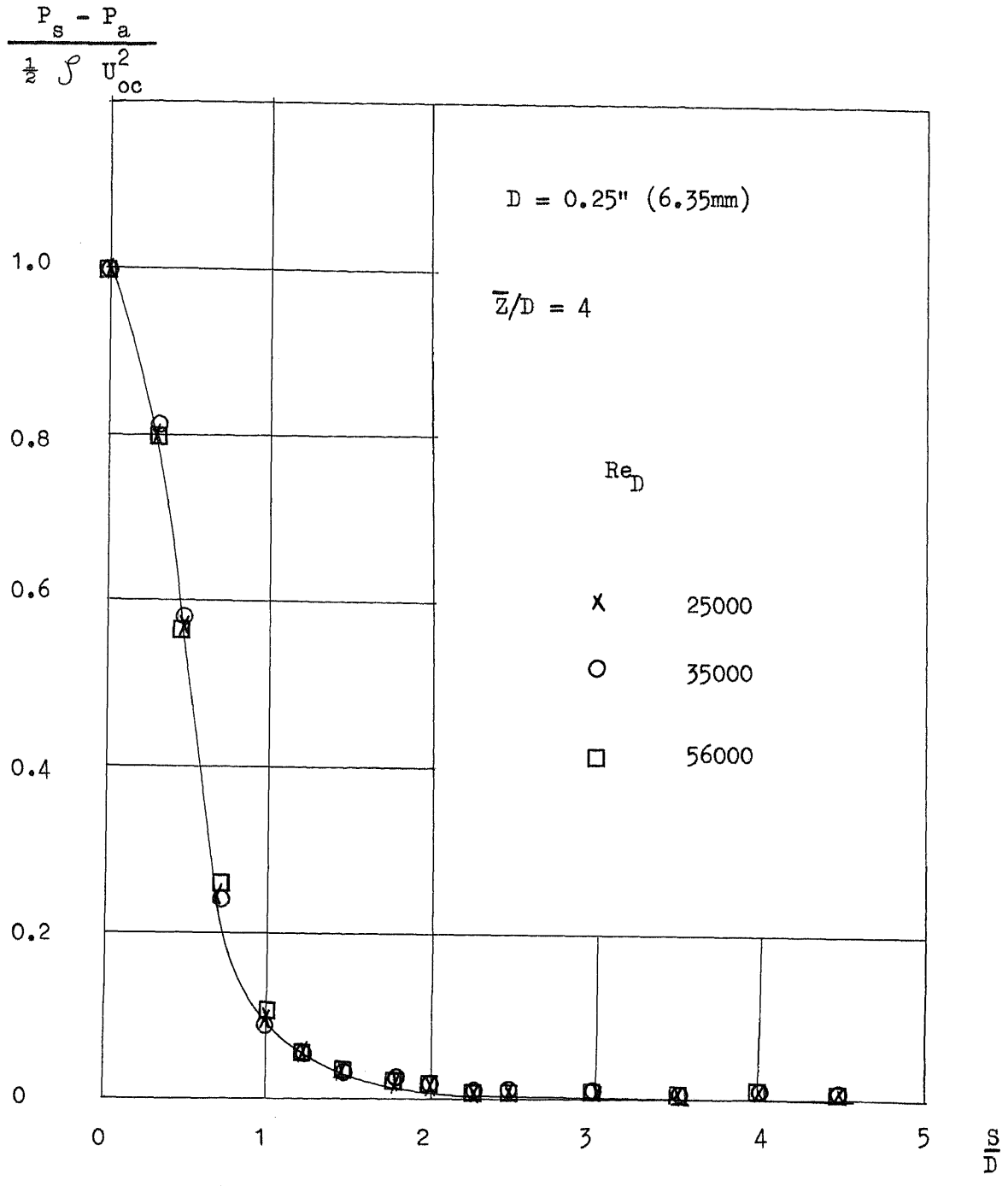

Fig. 30 Wall Pressure Distribution

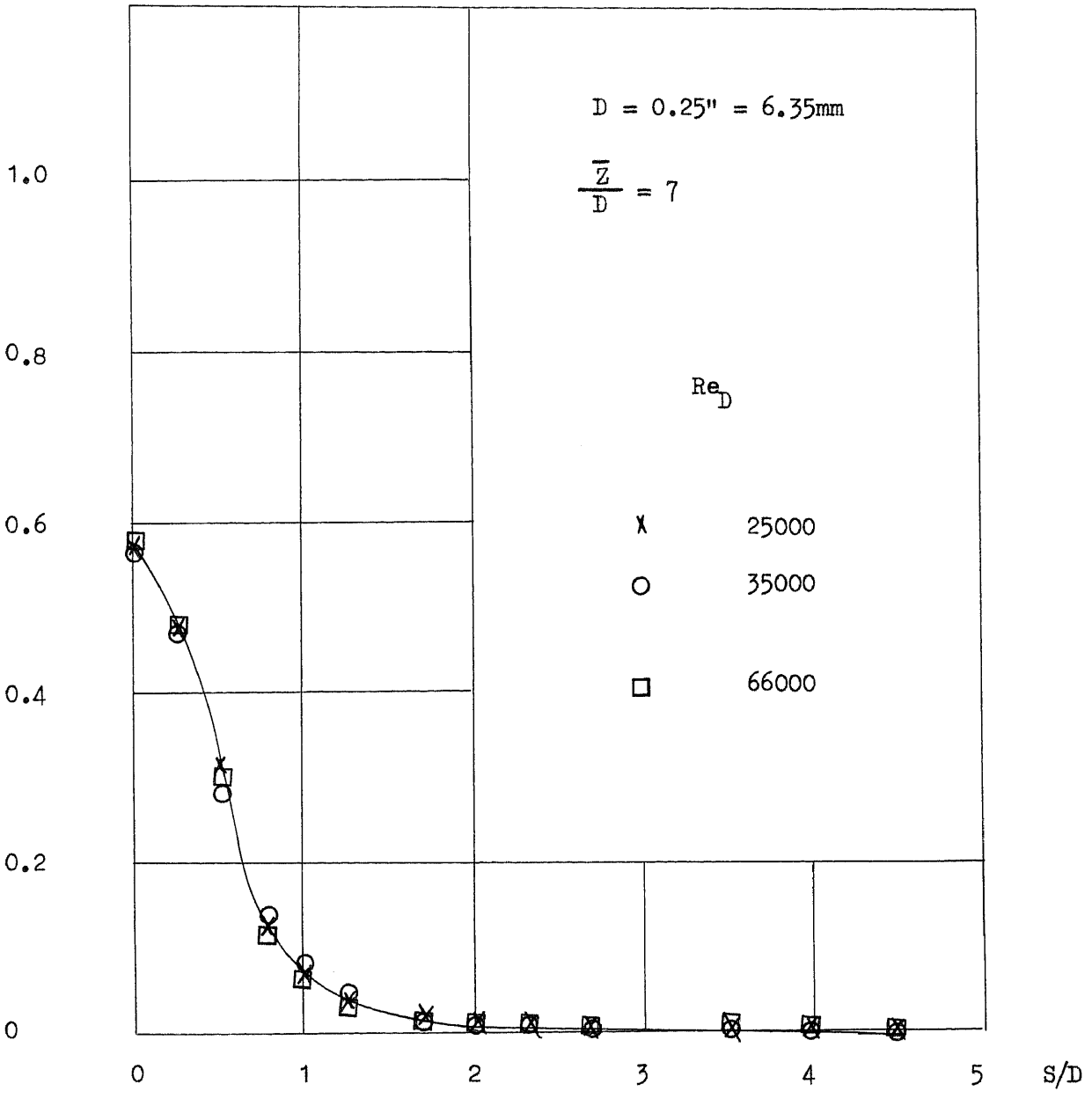

Wall Pressure Distribution

Fig. 31

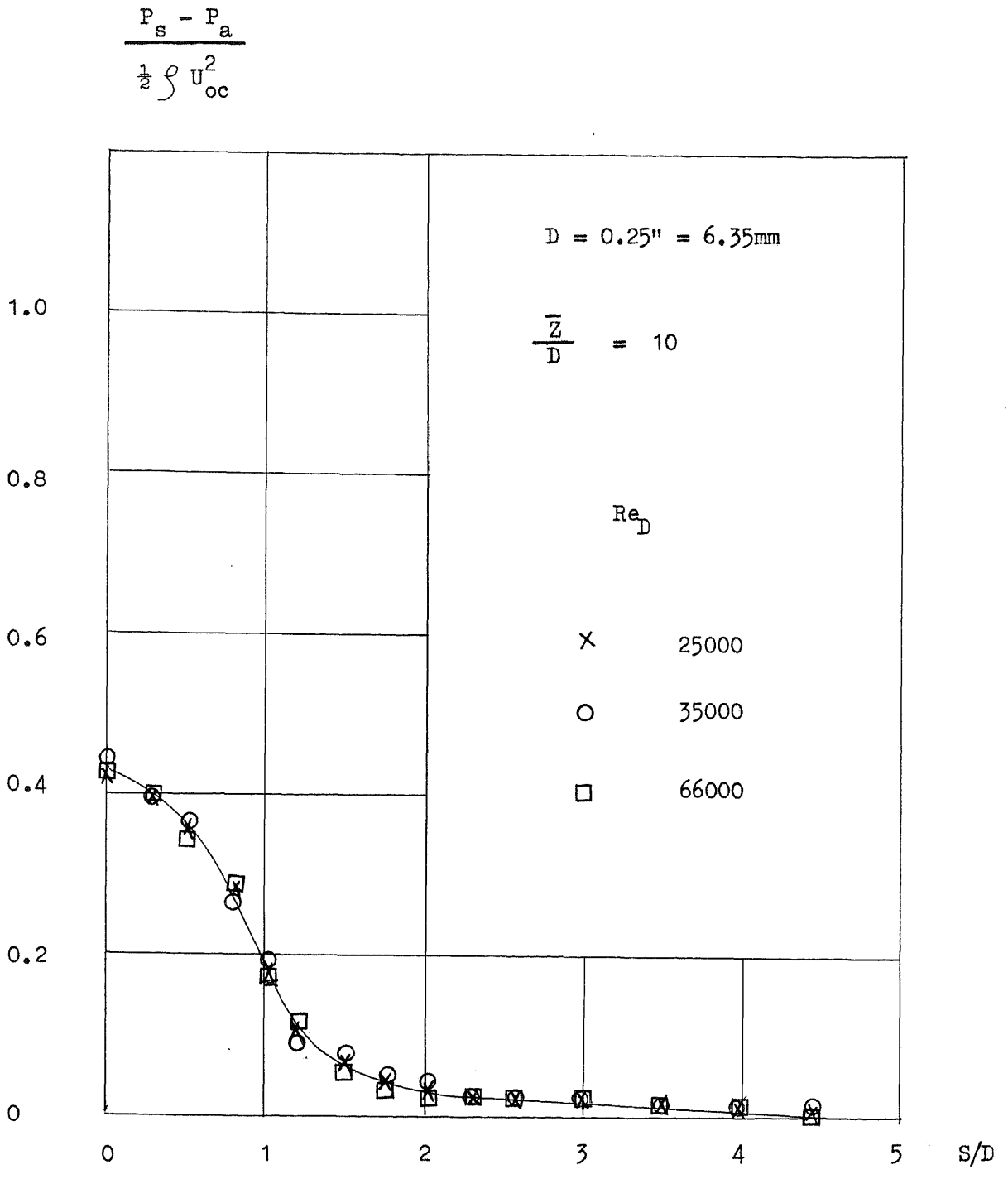

Wall Pressure Distribution

Fig. 32

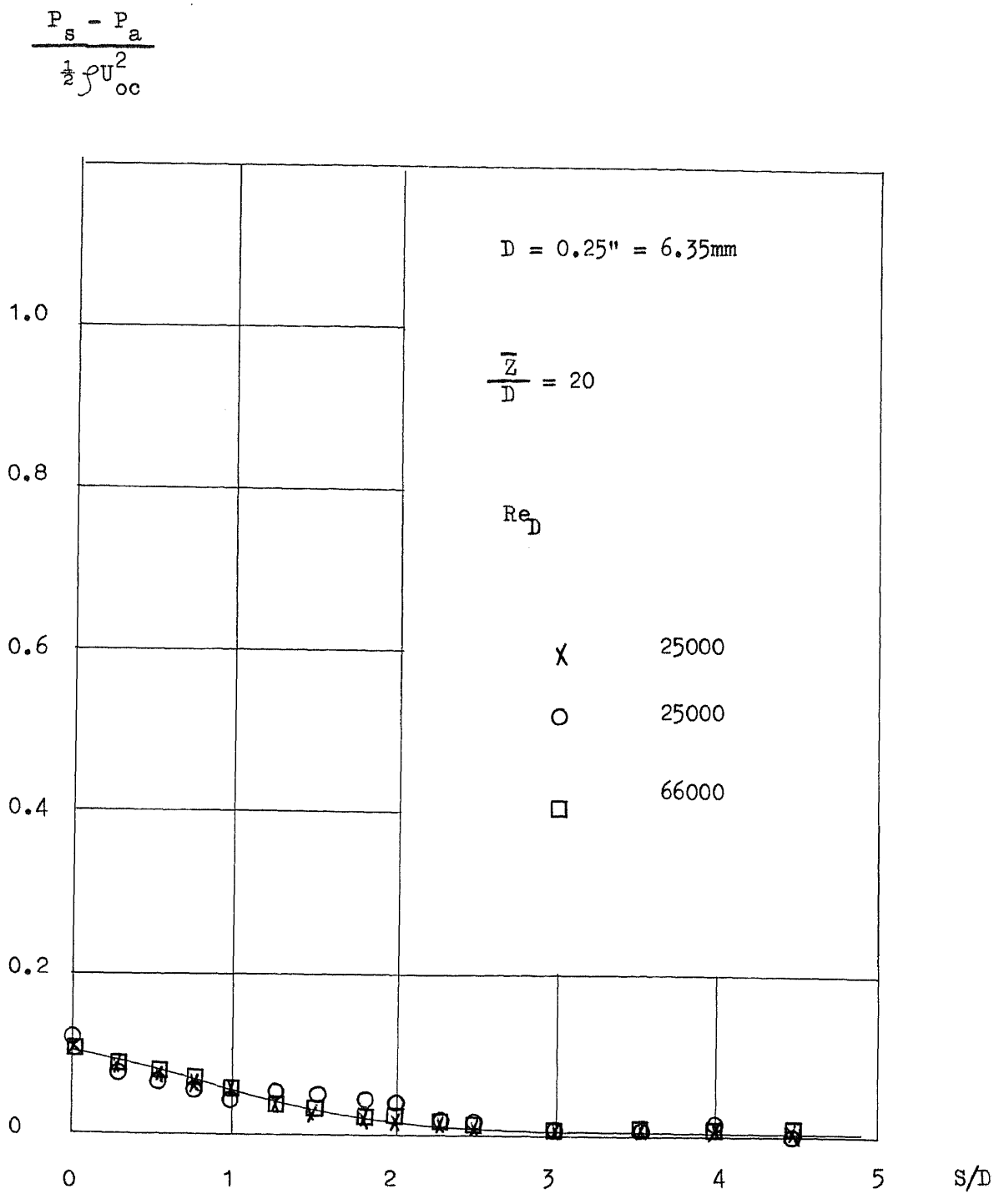

Wall Pressure Distribution

Fig. 33

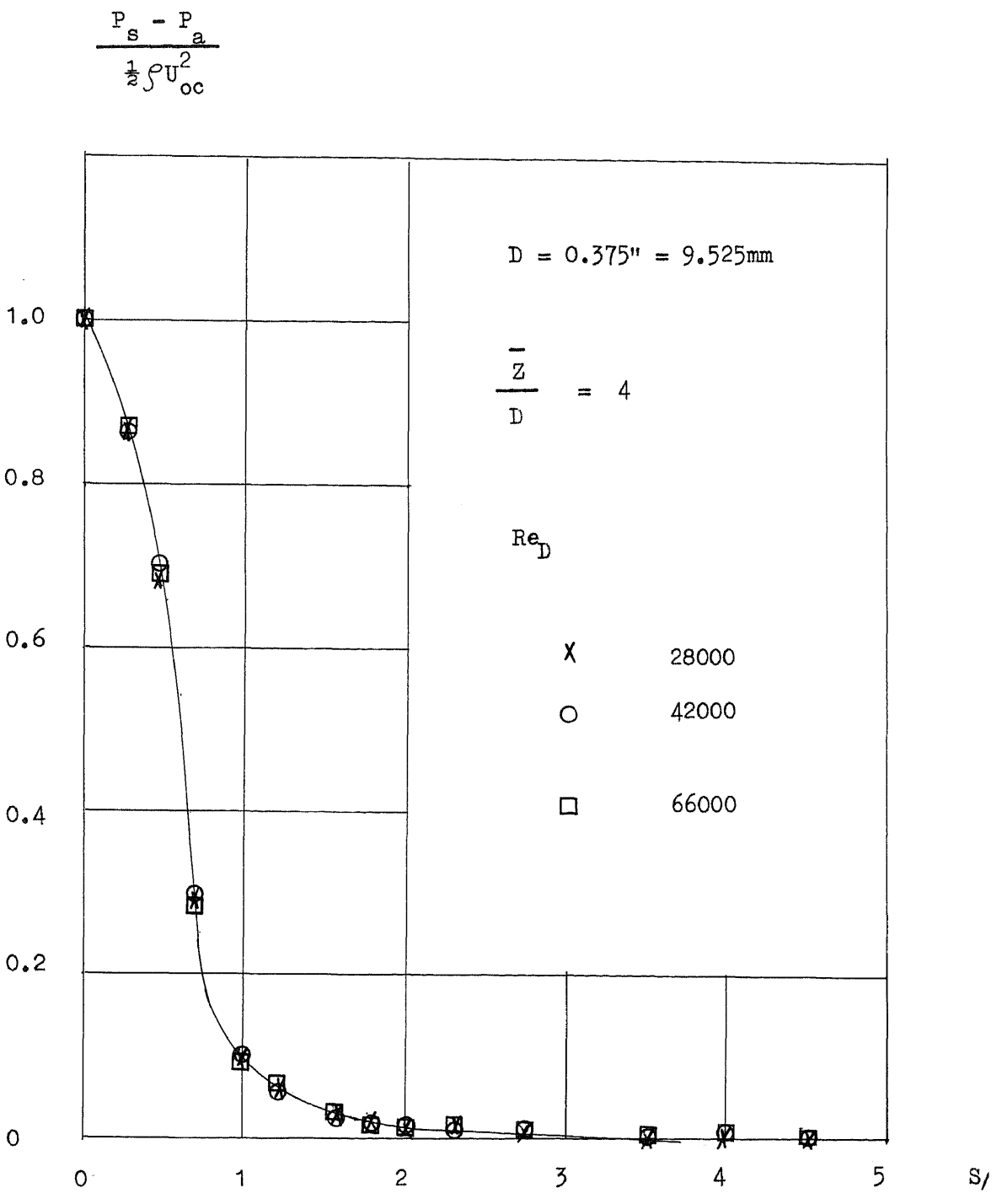

Wall Pressure Distribution

Fig. 34

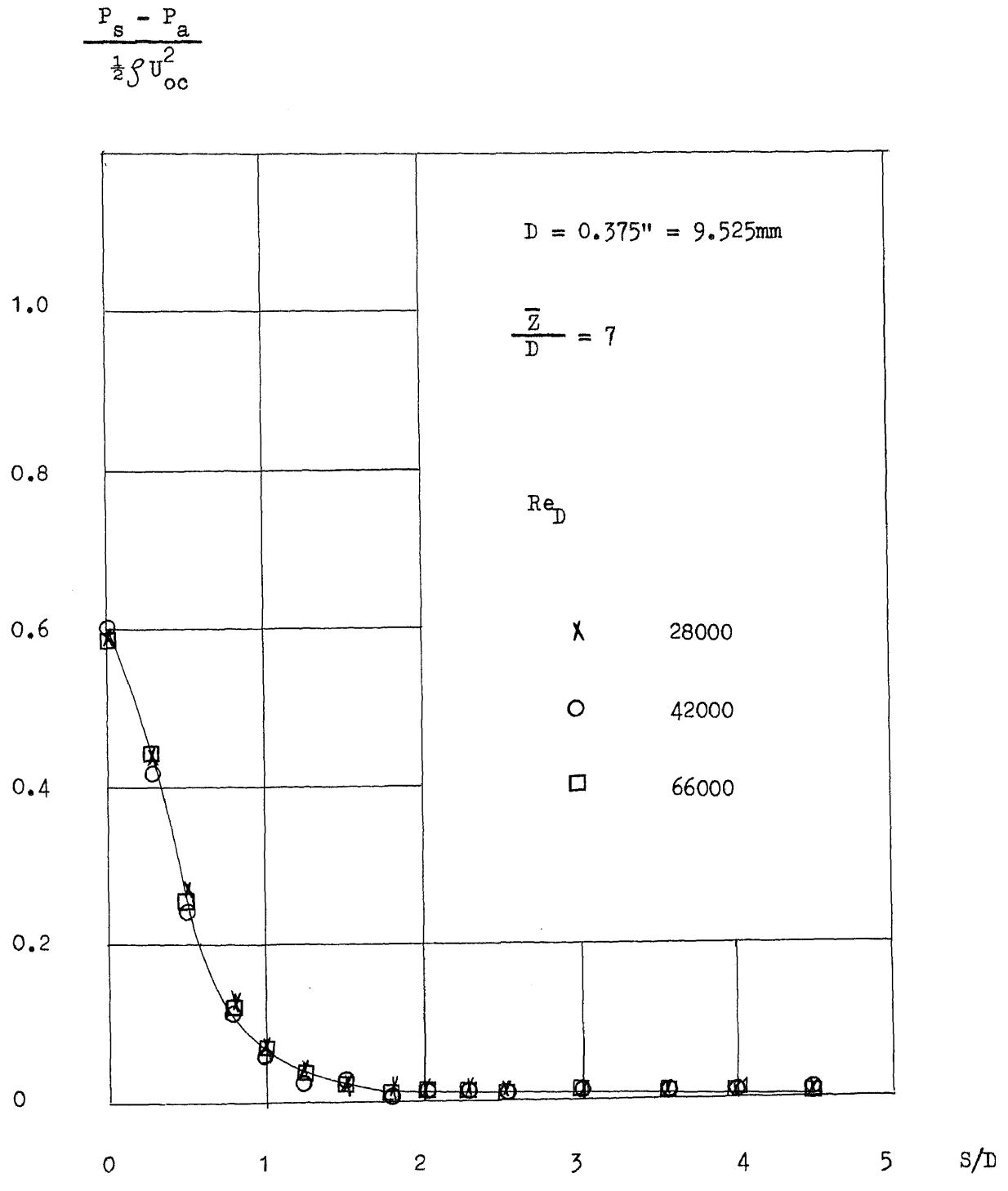

Wall Pressure Distribution

Fig. 35

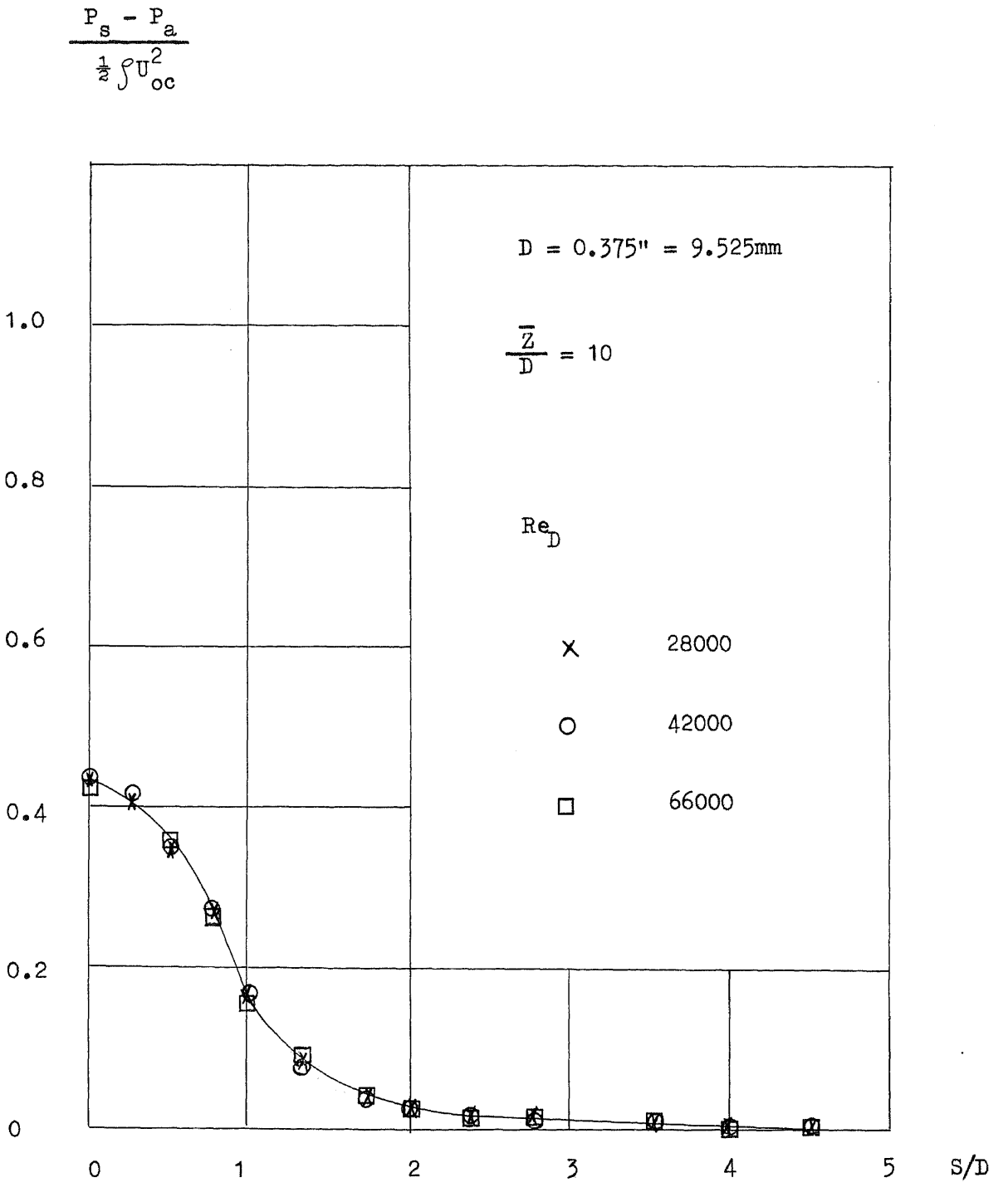

Wall Pressure Distribution

Fig. 36

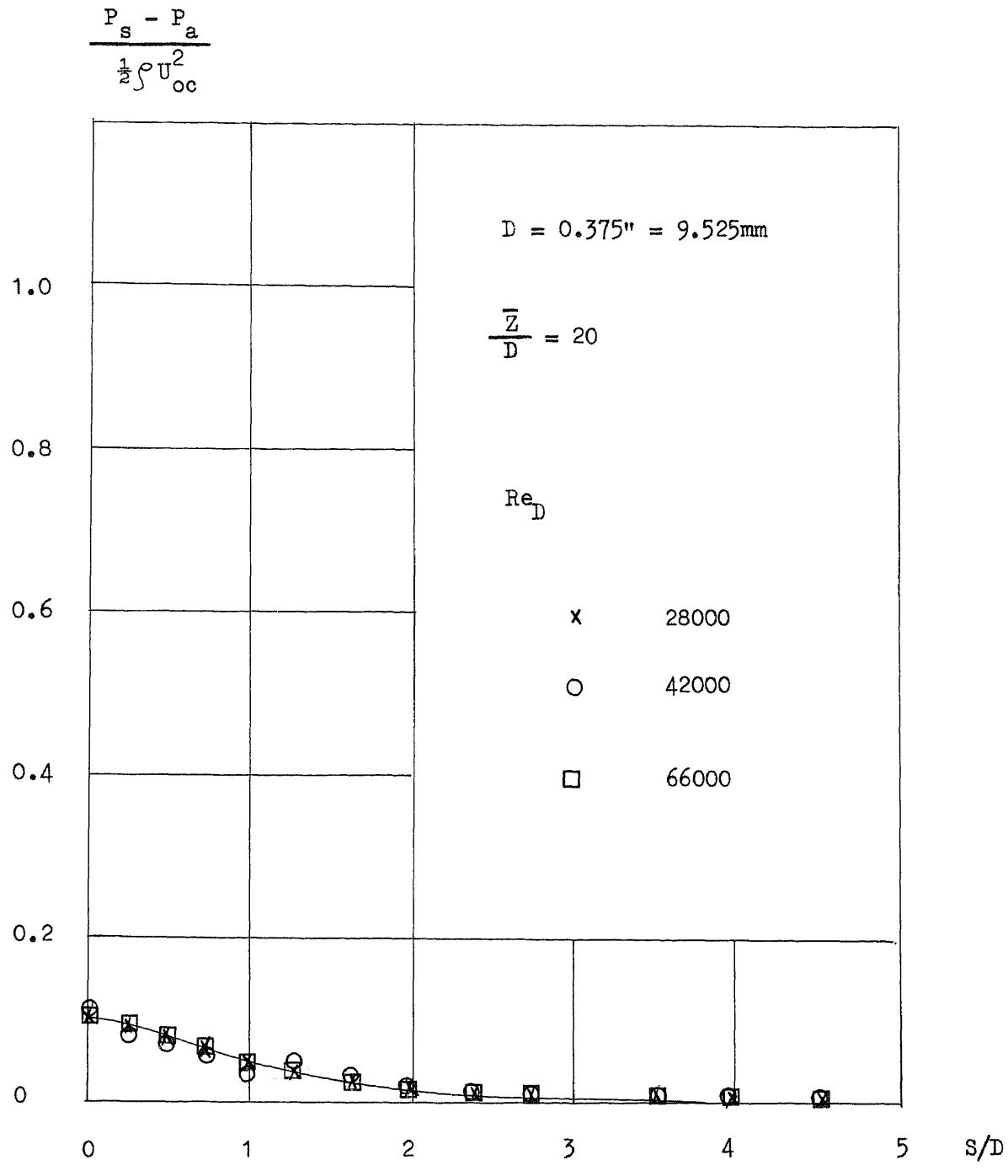

Wall Pressure Distribution

Fig. 37

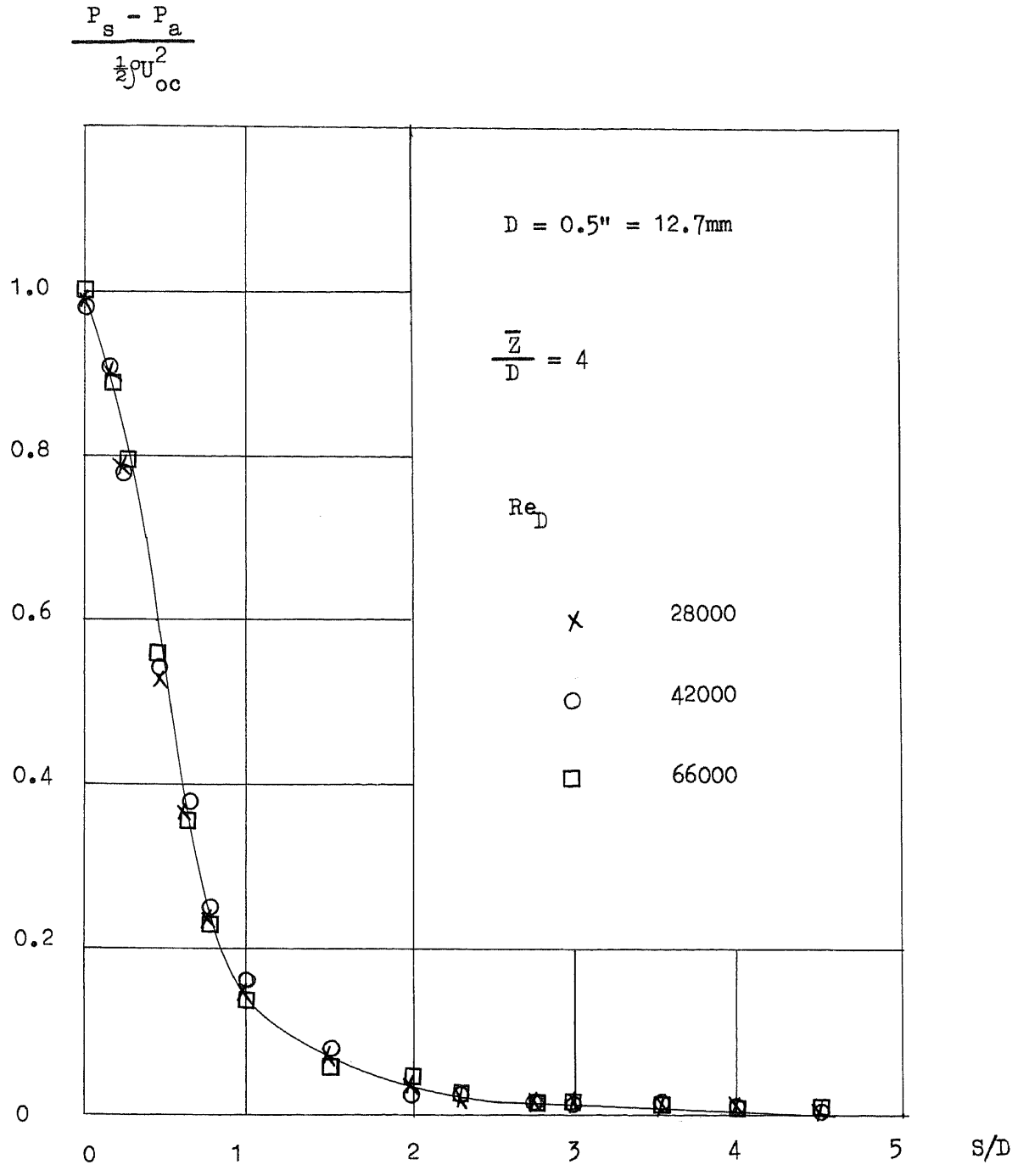

Wall Pressure Distribution

Fig. 38

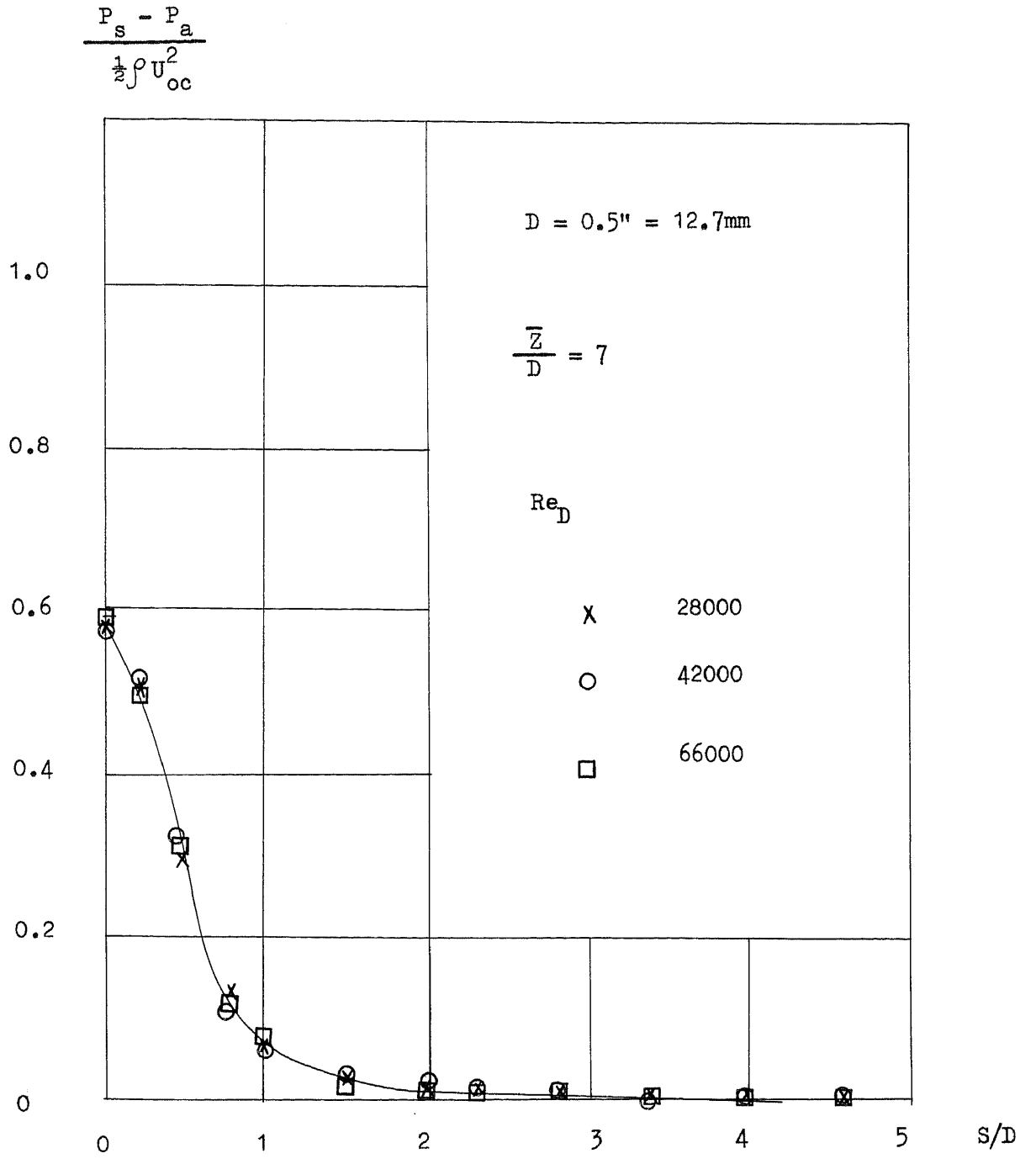

Wall Pressure Distribution

Fig. 39

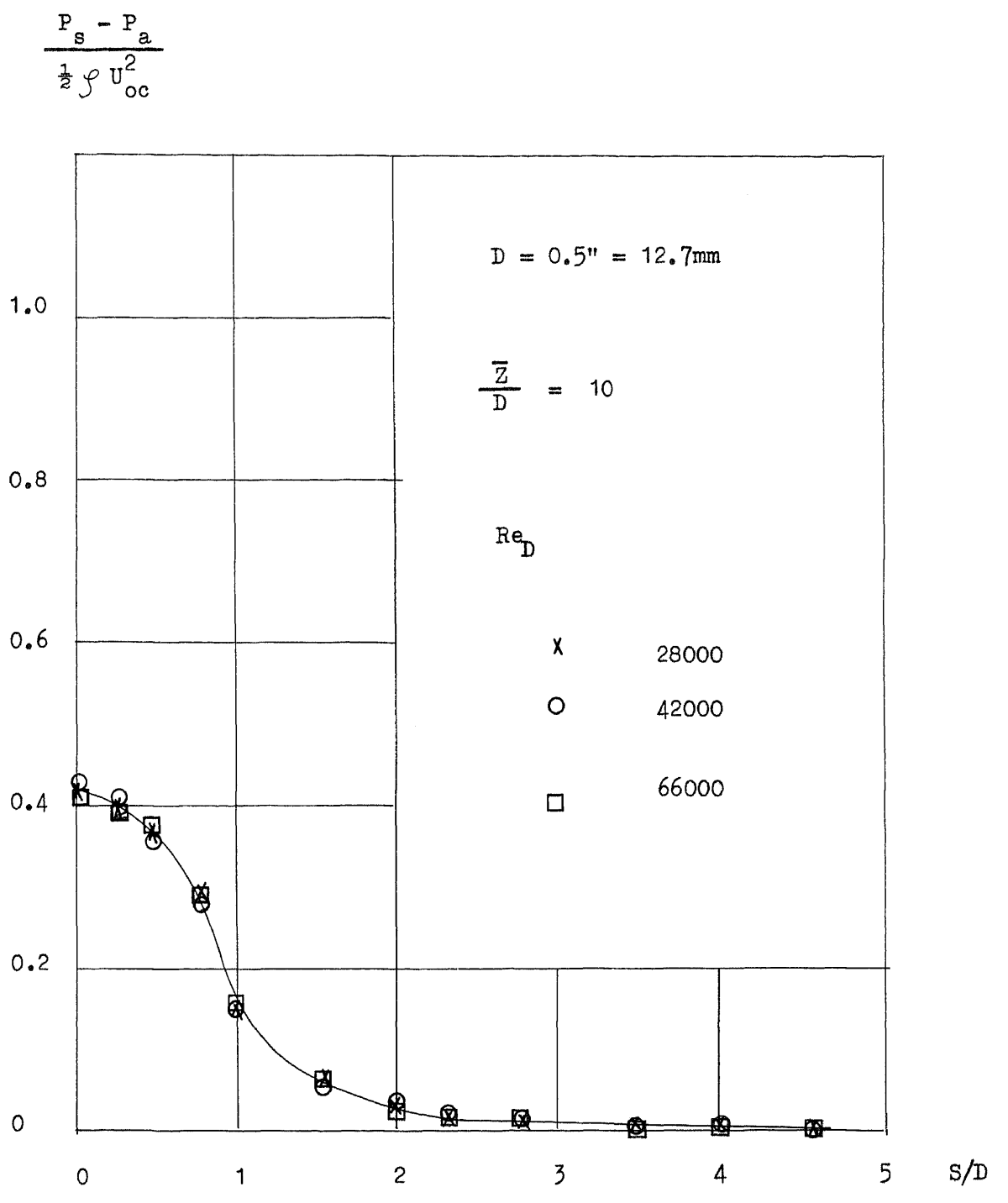

Wall Pressure Distribution

Fig. 40

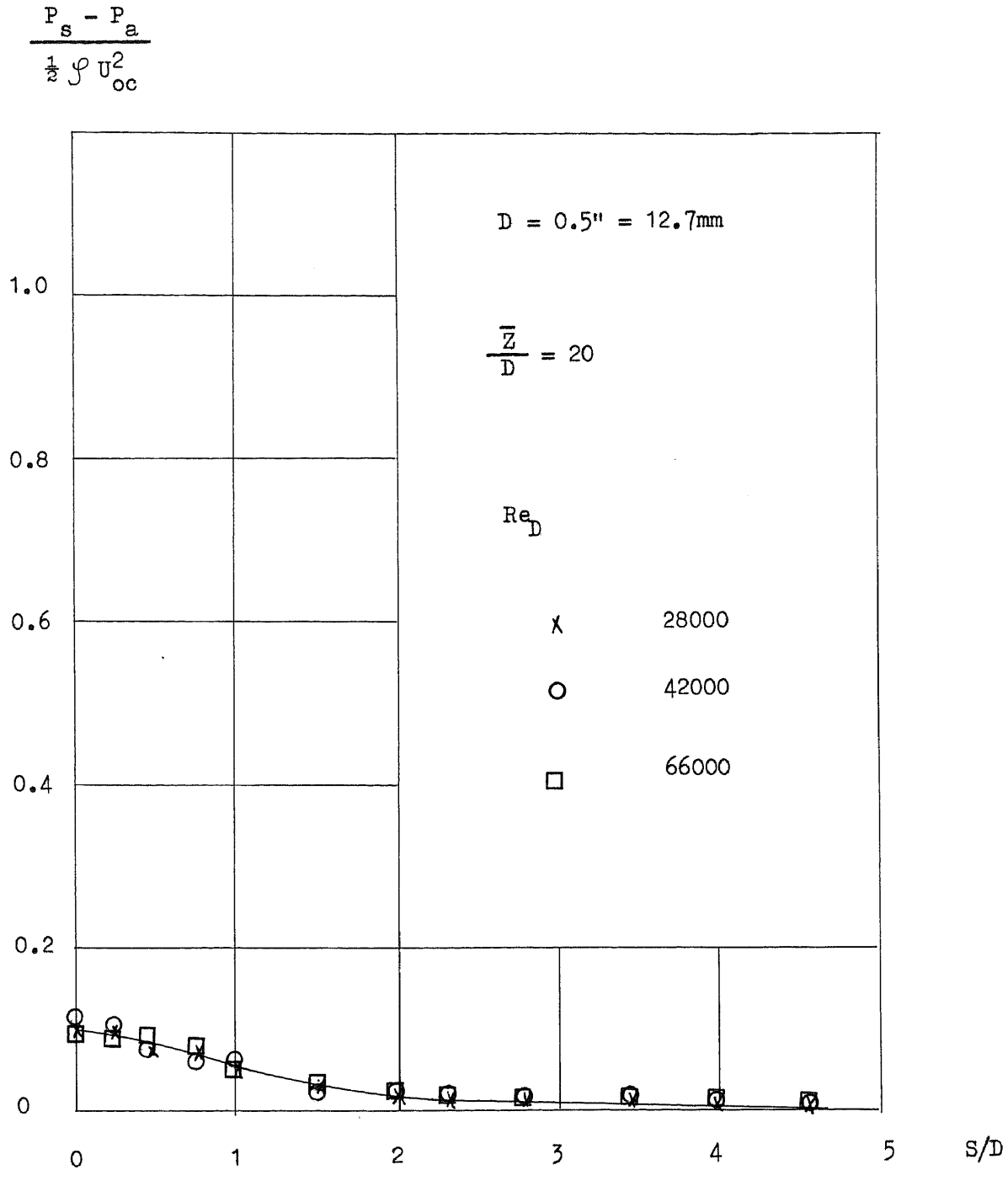

Wall Pressure Distribution

Fig. 41

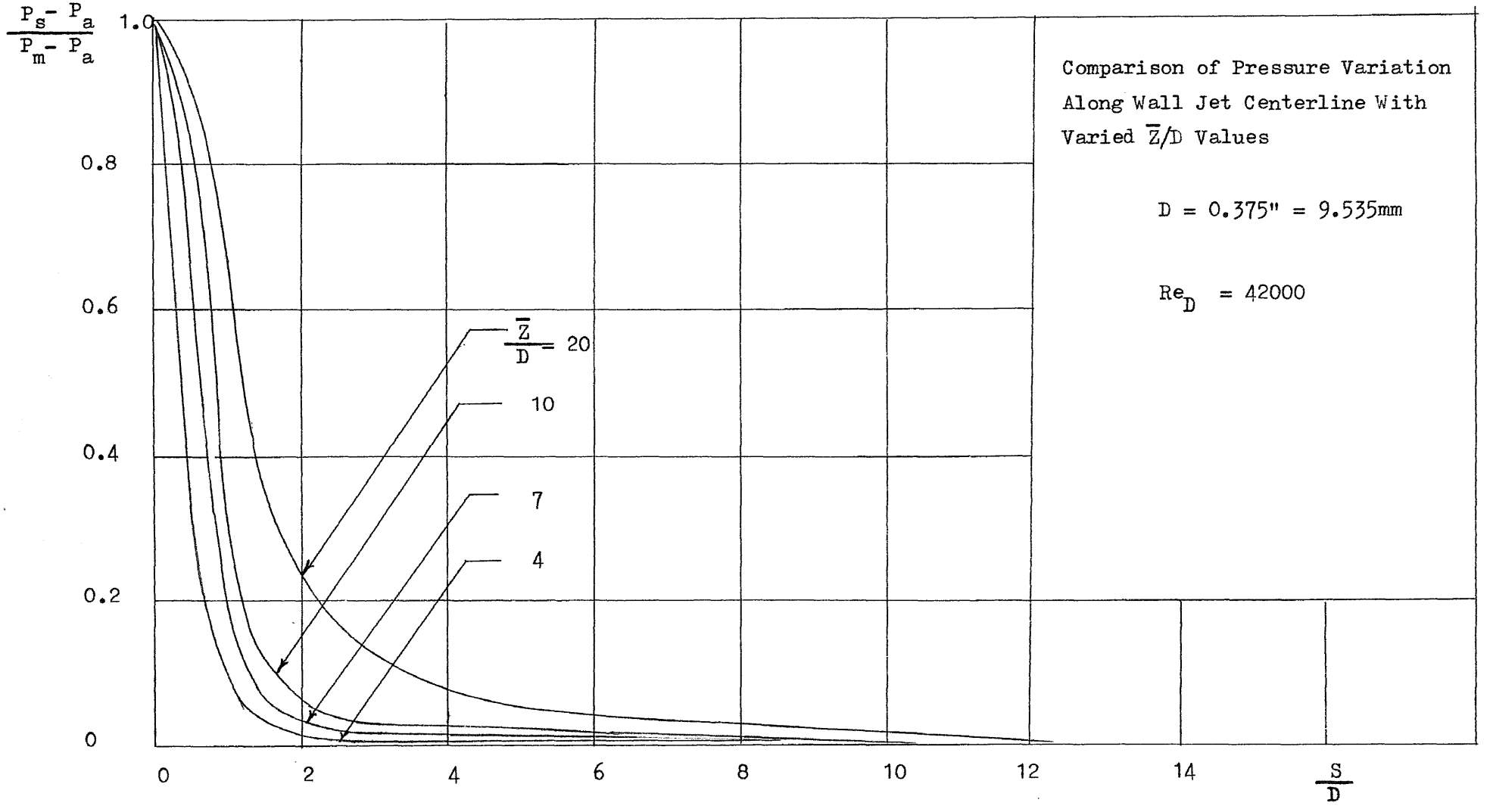

Wall Pressure Distribution

Fig. 42

$$\frac{P_s - P_a}{\frac{1}{2} \rho U_{oc}^2}$$

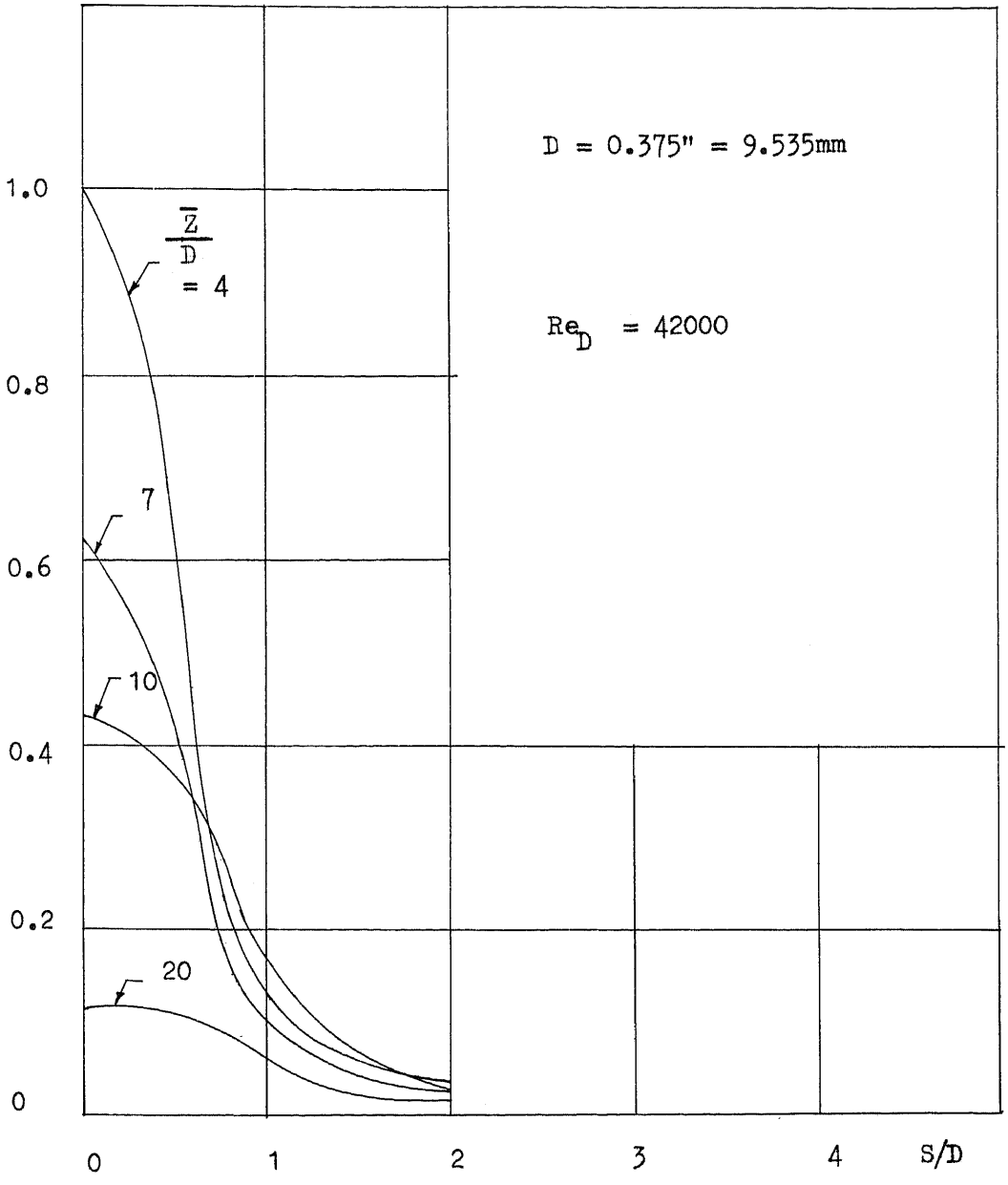

Comparison of Static Pressure along the Wall with Varied $\overline{Z}/D$

Fig. 43

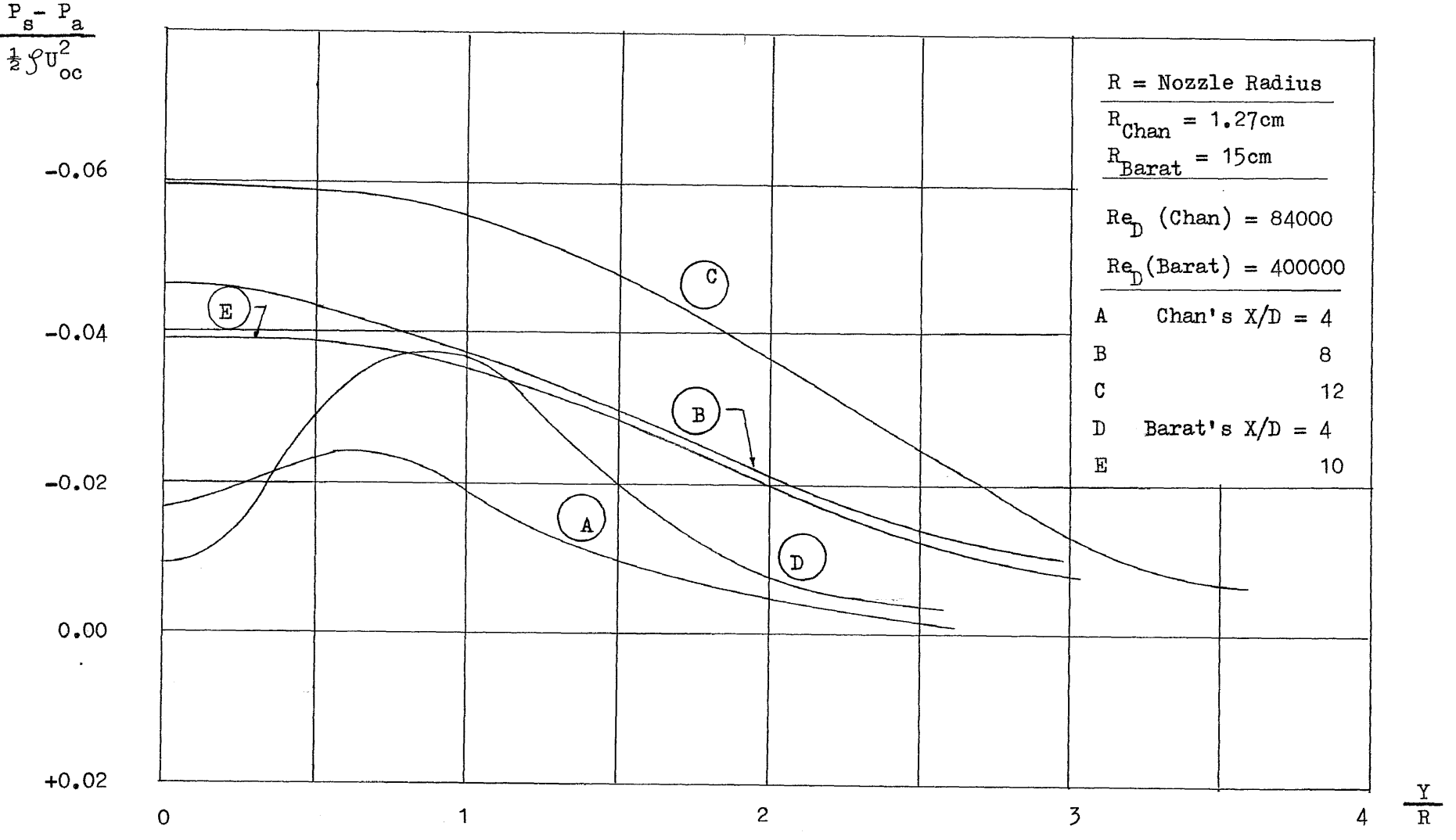

Static Pressure Profile across Free Jet (A Comparison)

Fig. 44

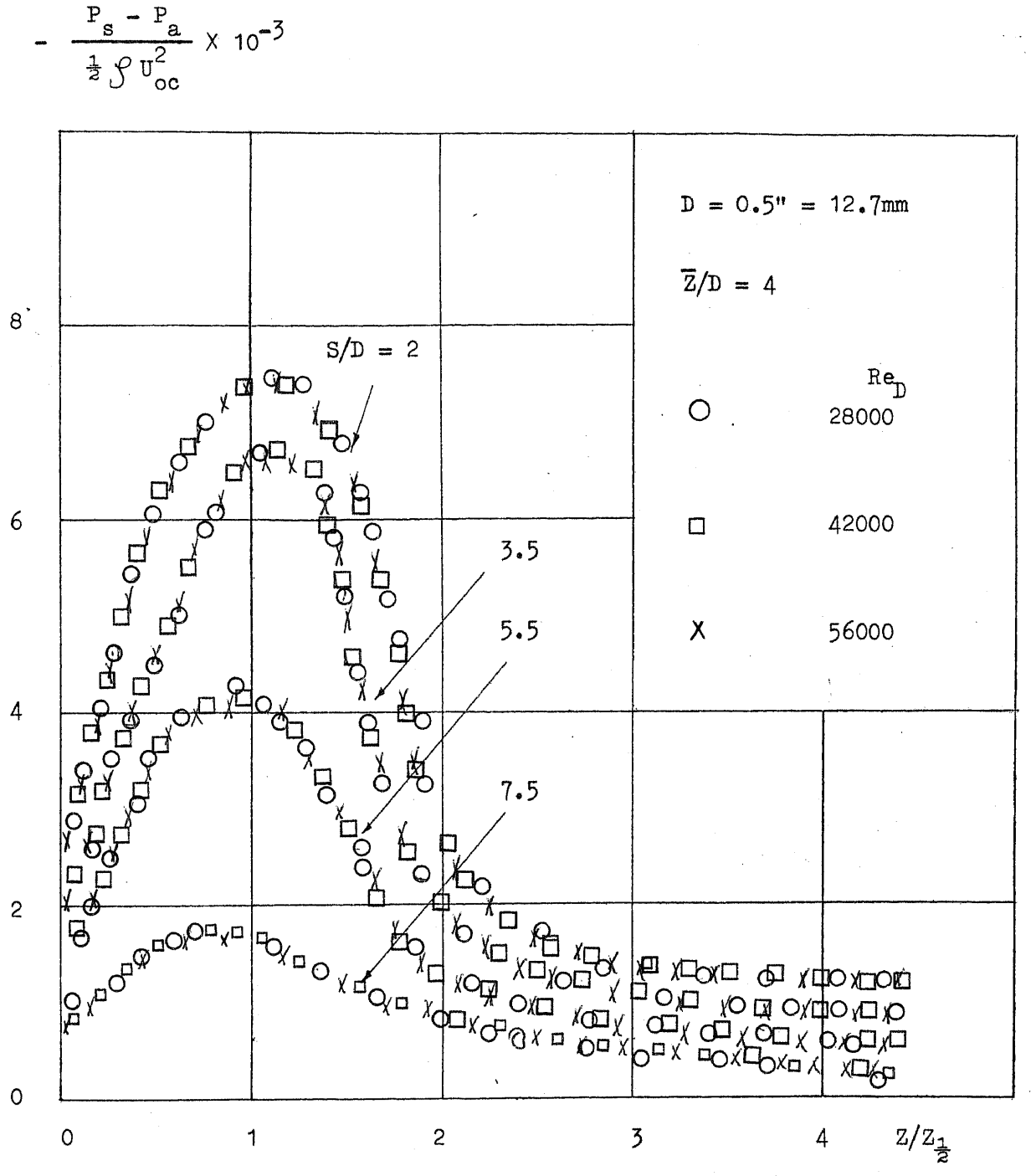

Profile of Static Pressure across Wall Jet

Fig. 45

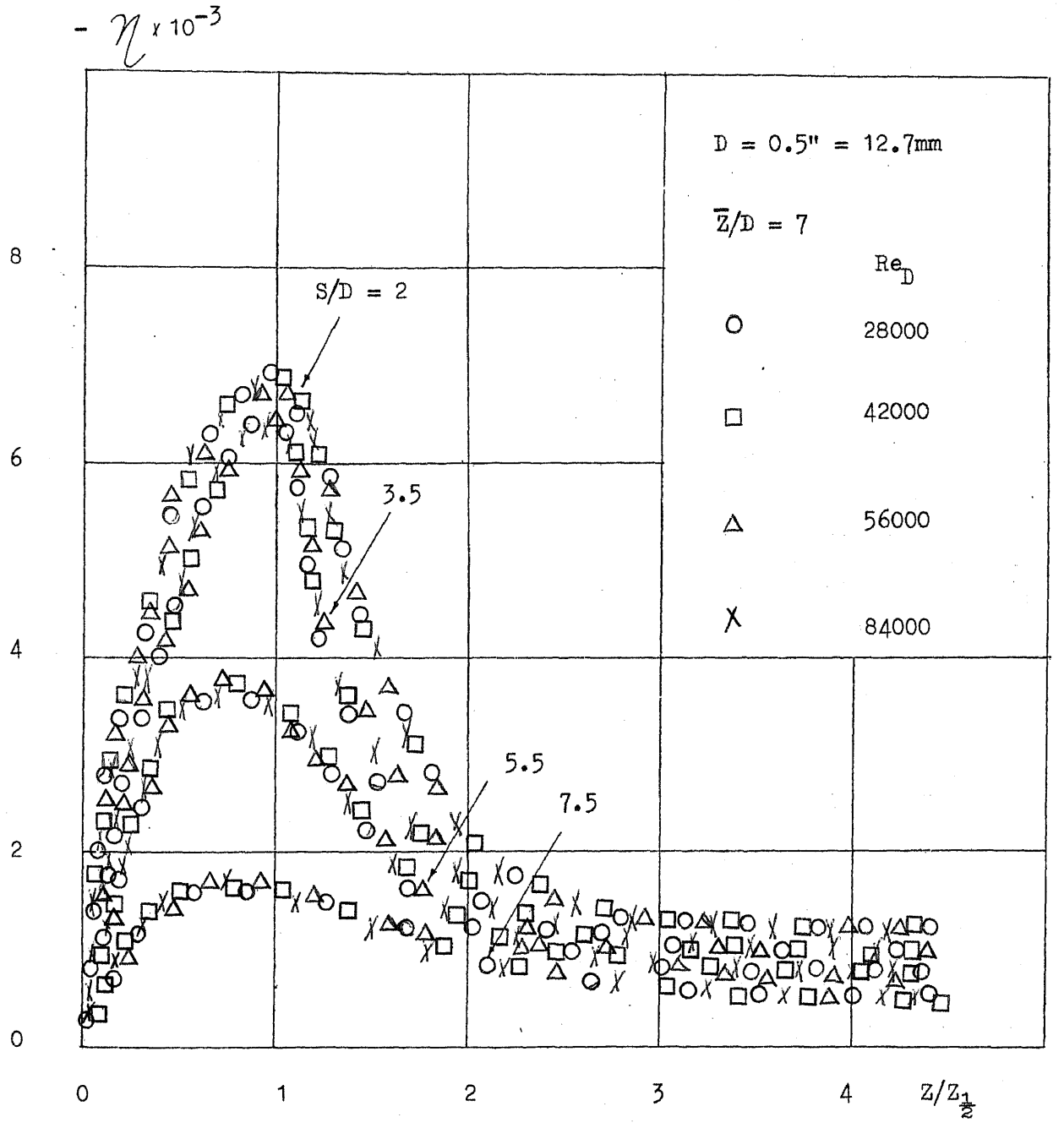

Profile of Static Pressure across Wall Jet

Fig. 46

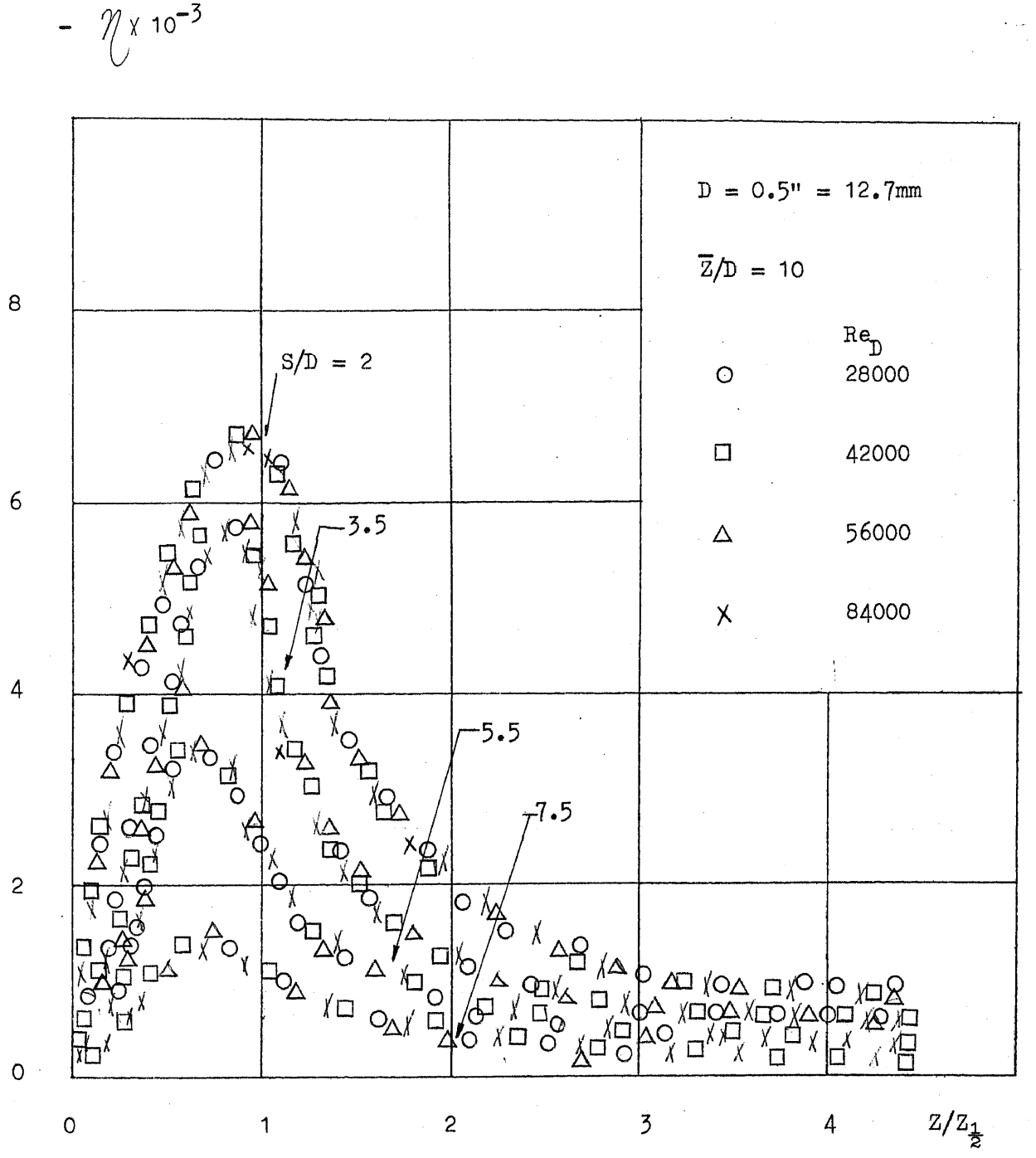

Profile of Static Pressure across Wall Jet

Fig. 47

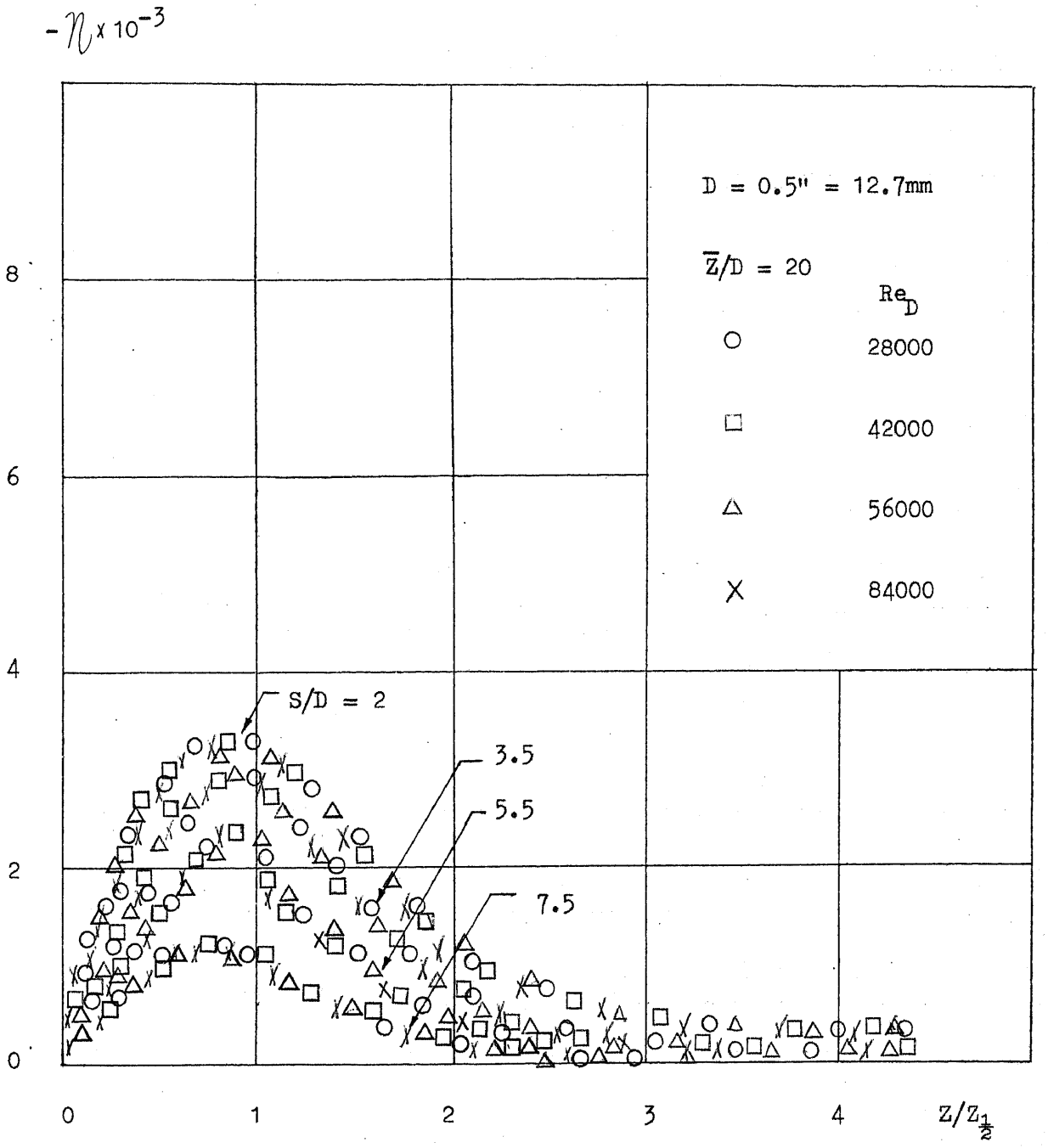

Profile of Static Pressure across Wall Jet

Fig. 48

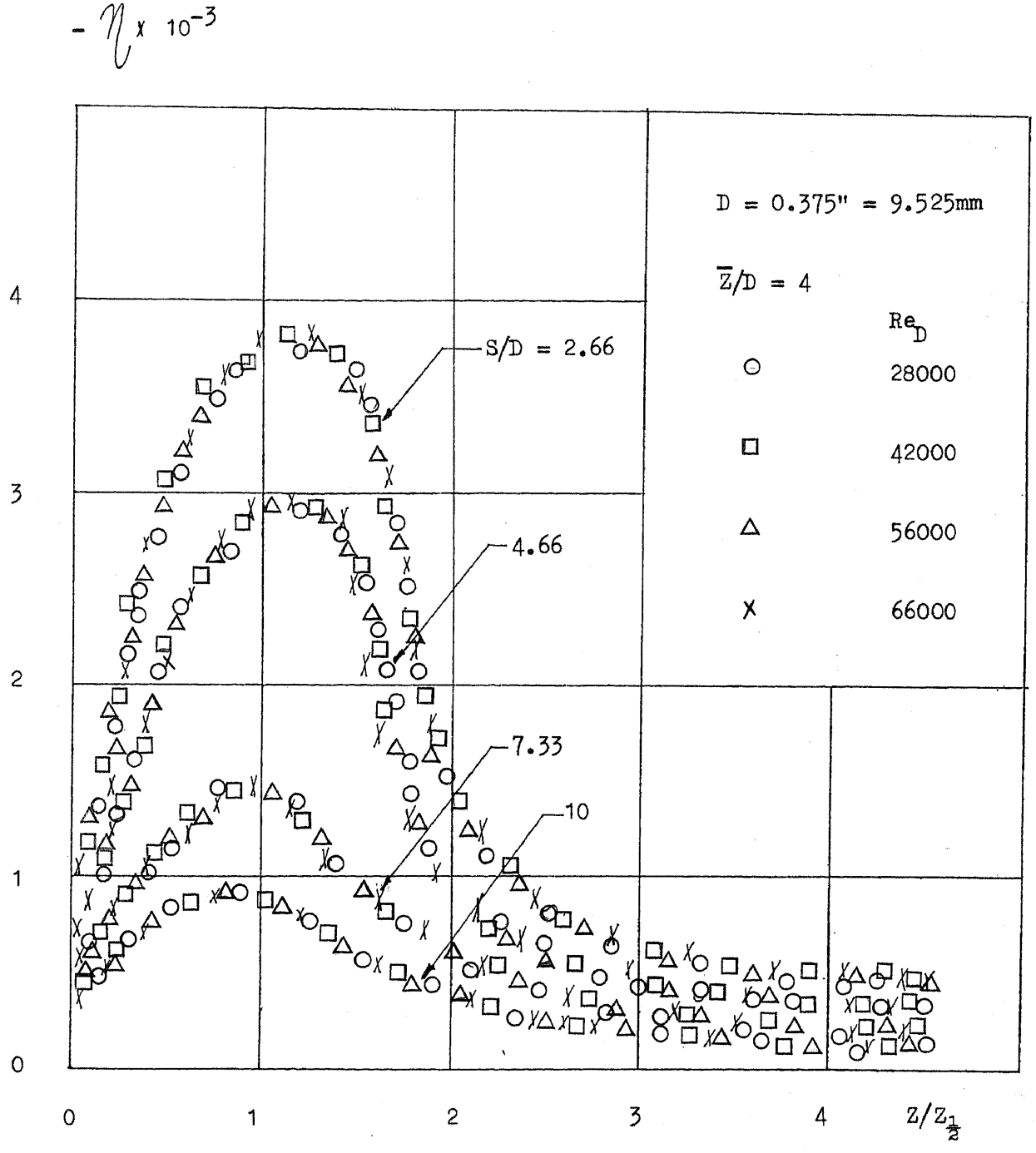

Profile of Static Pressure across Wall Jet

Fig. 49

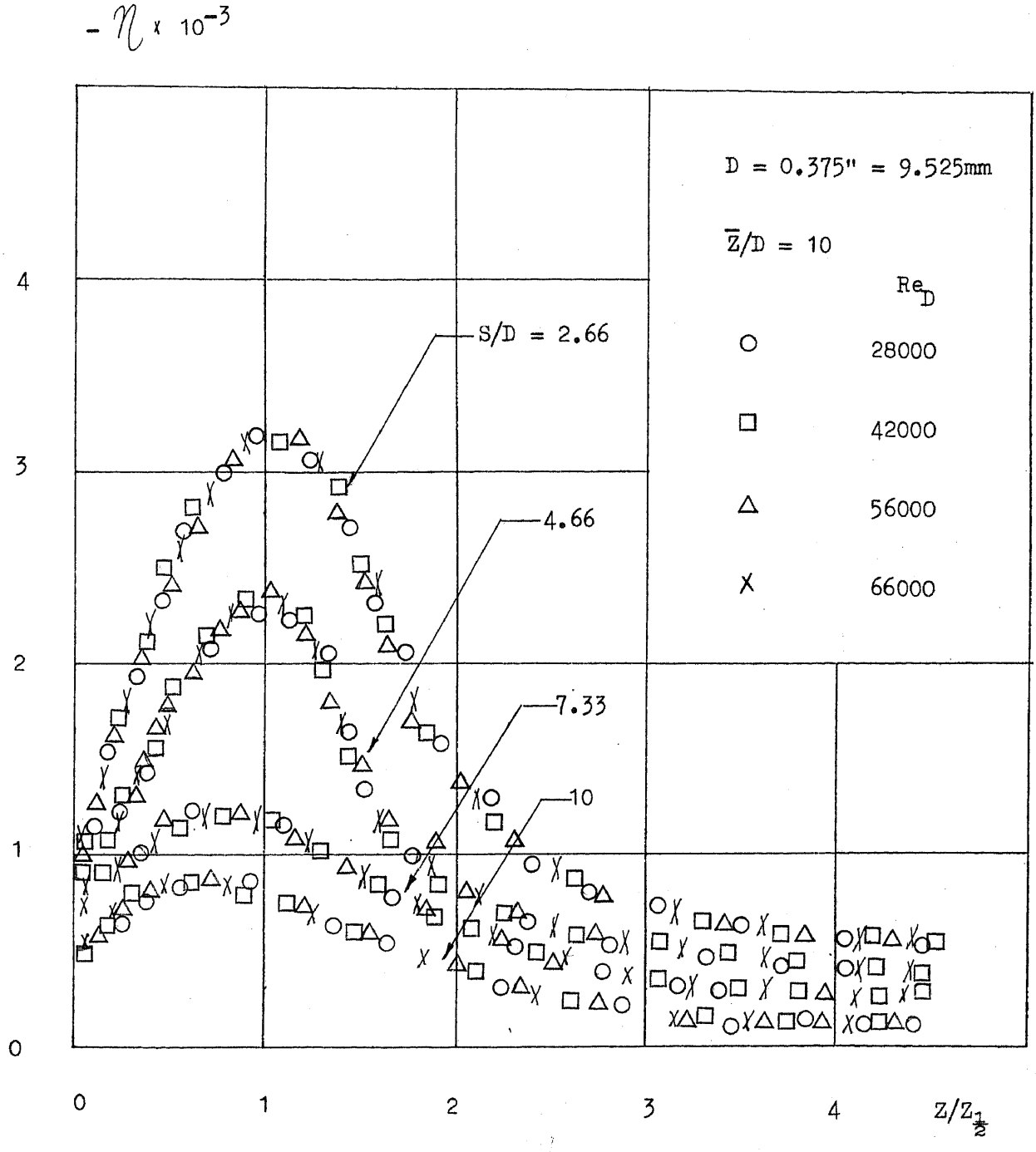

Profile of Static Pressure across Wall Jet

Fig. 50

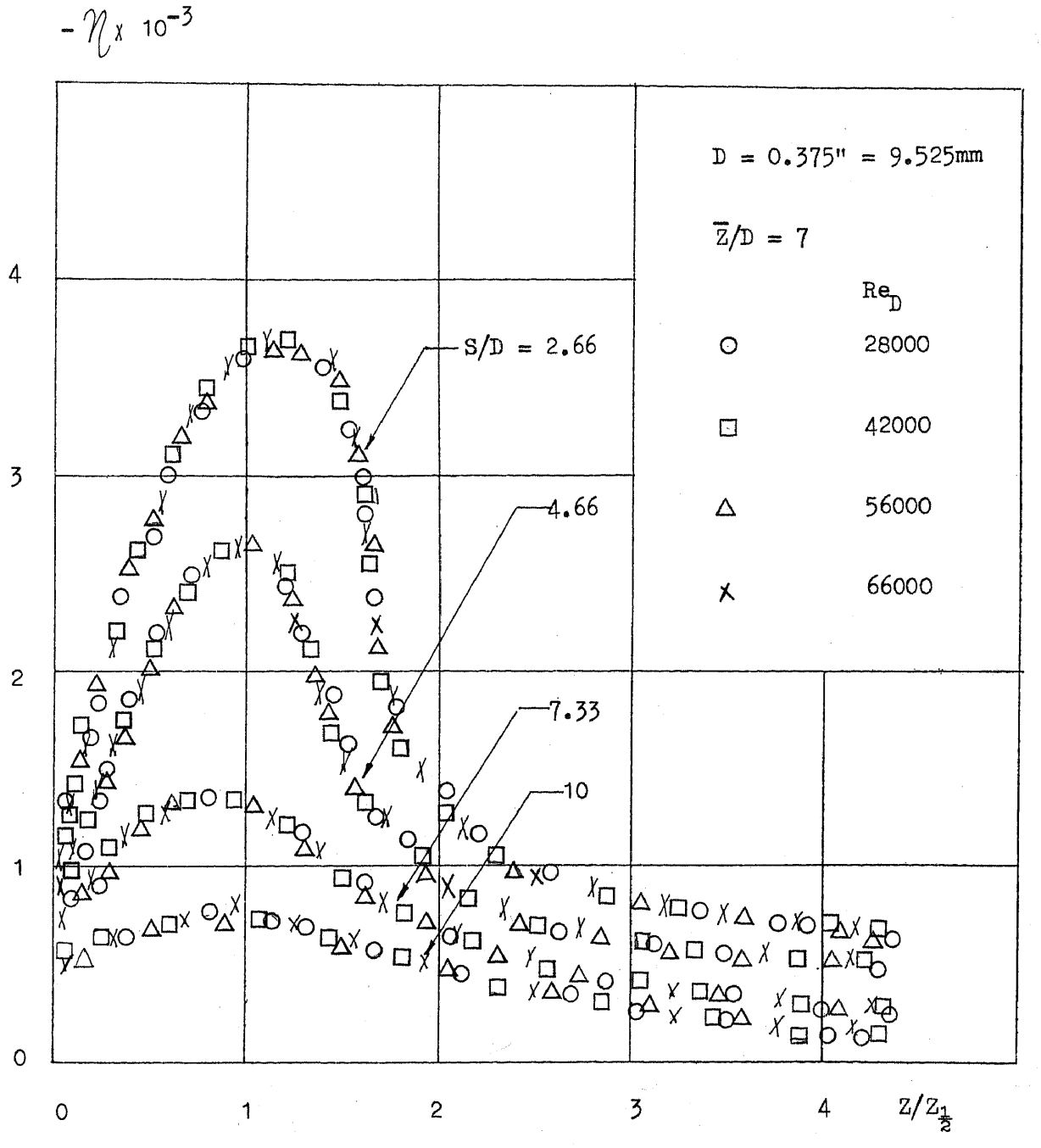

Profile of Static Pressure across Wall Jet

Fig. 51

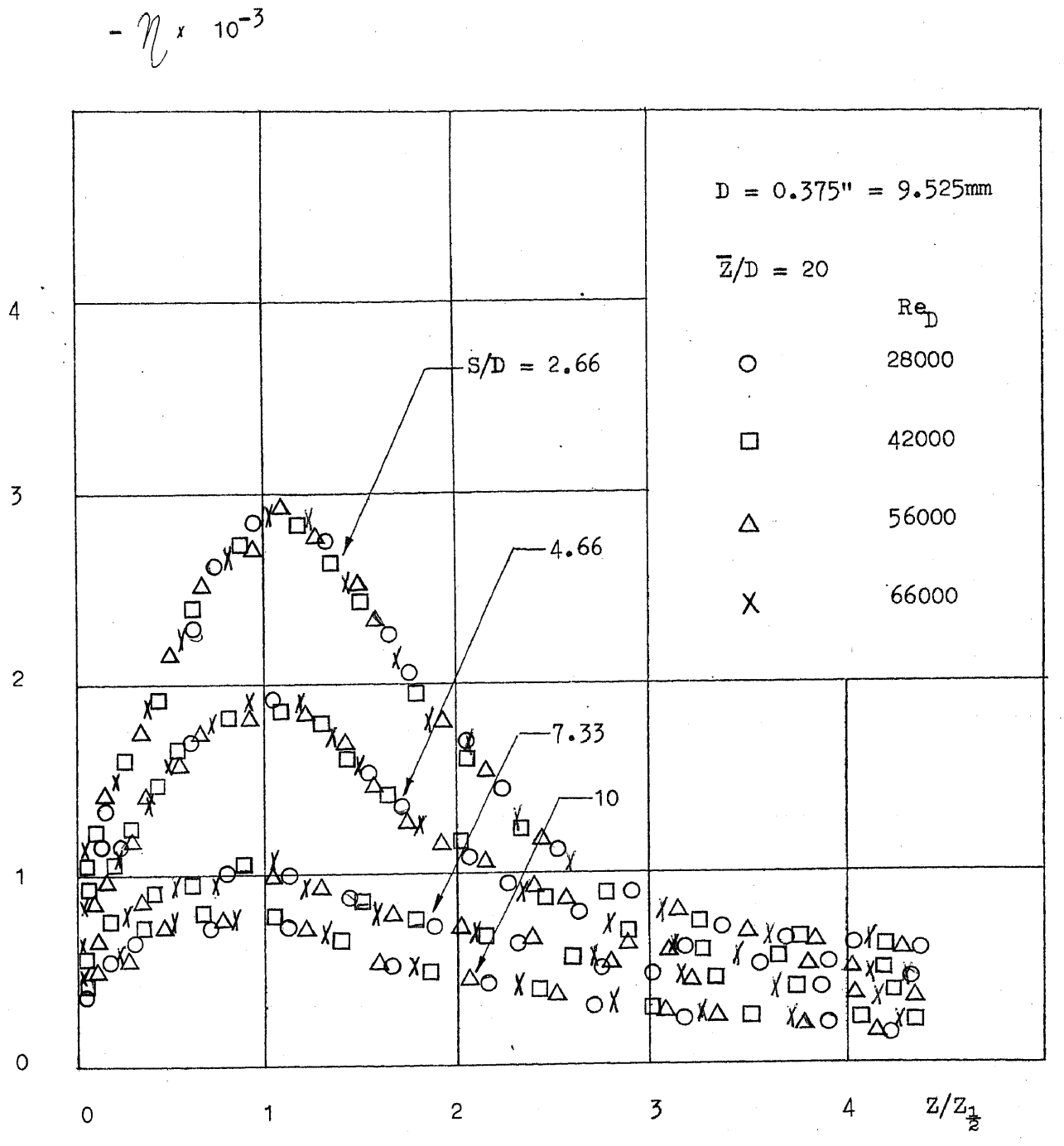

Profile of Static Pressure across Wall Jet

Fig. 52

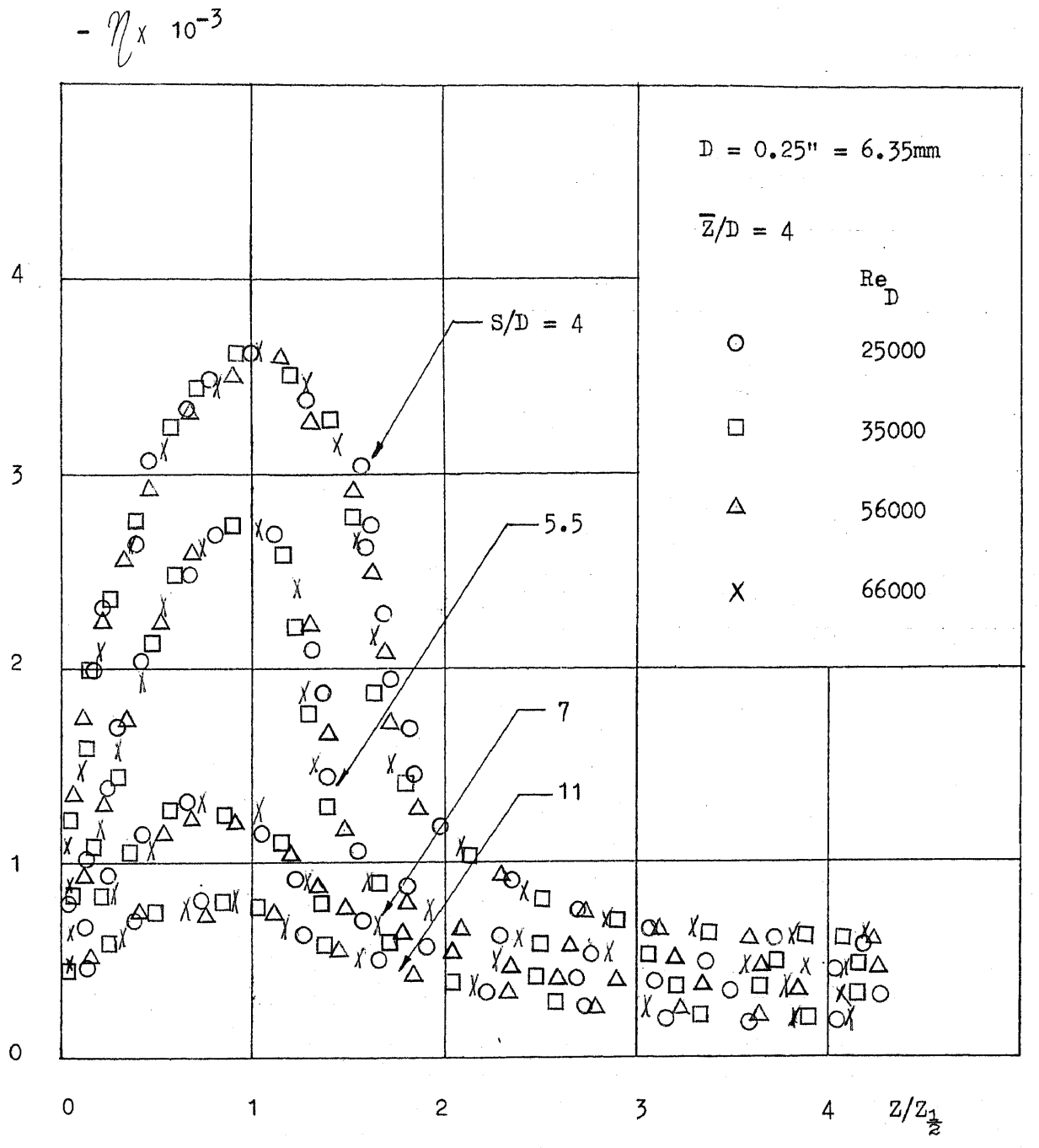

Profile of Static Pressure across Wall Jet

Fig. 53

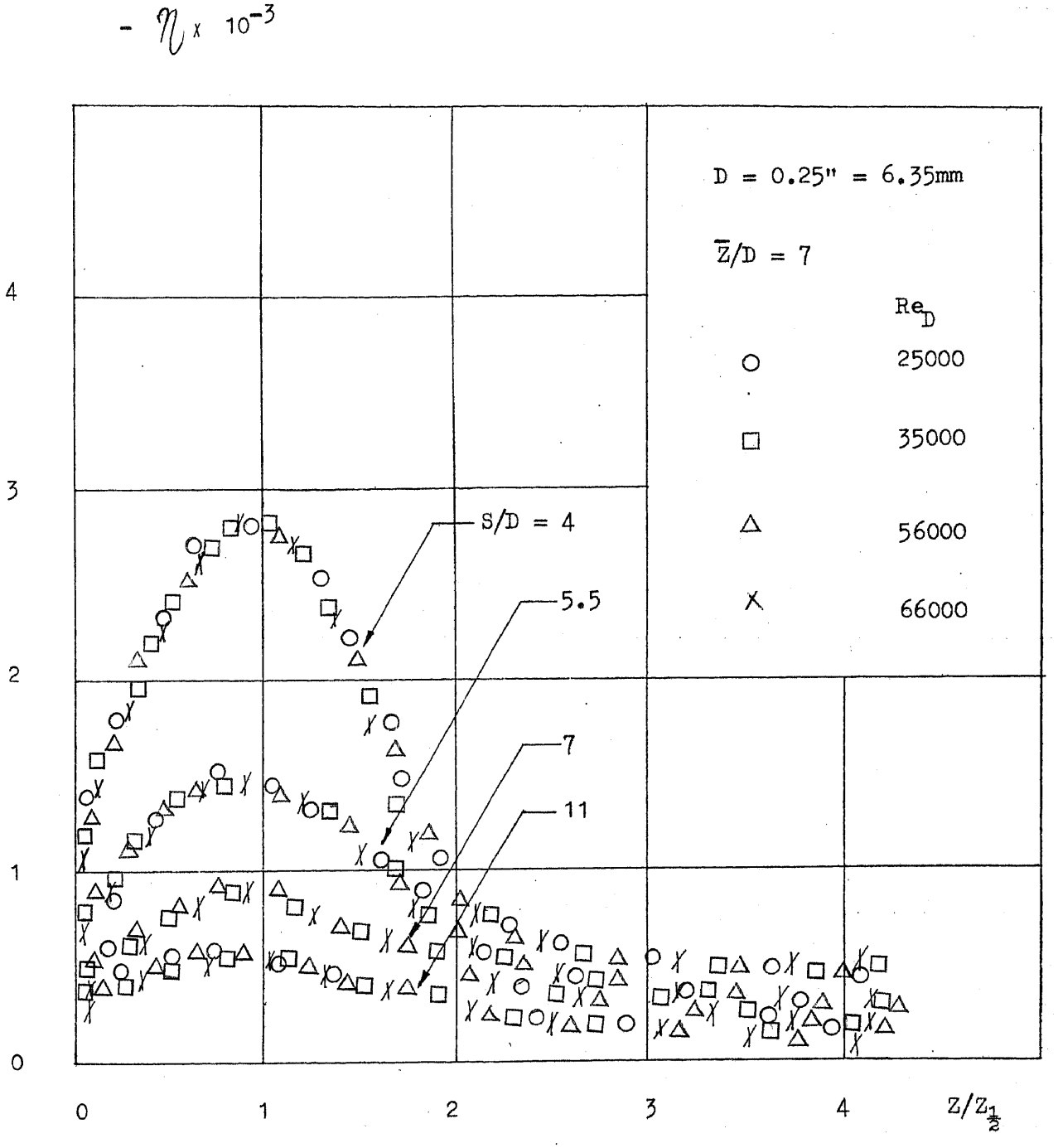

Profile of Static Pressure across Wall Jet

Fig. 54

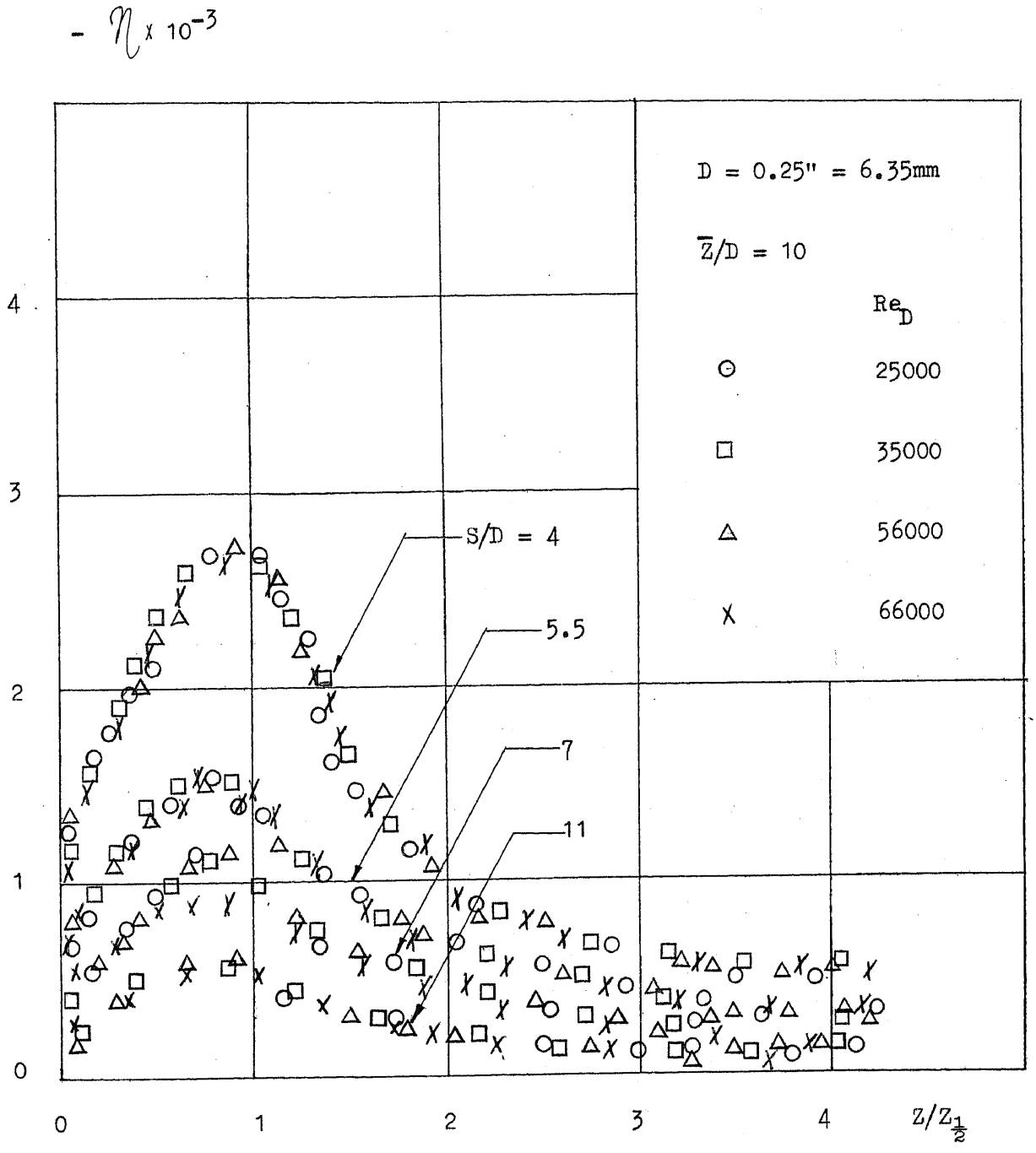

Profile of Static Pressure across Wall Jet

Fig. 55

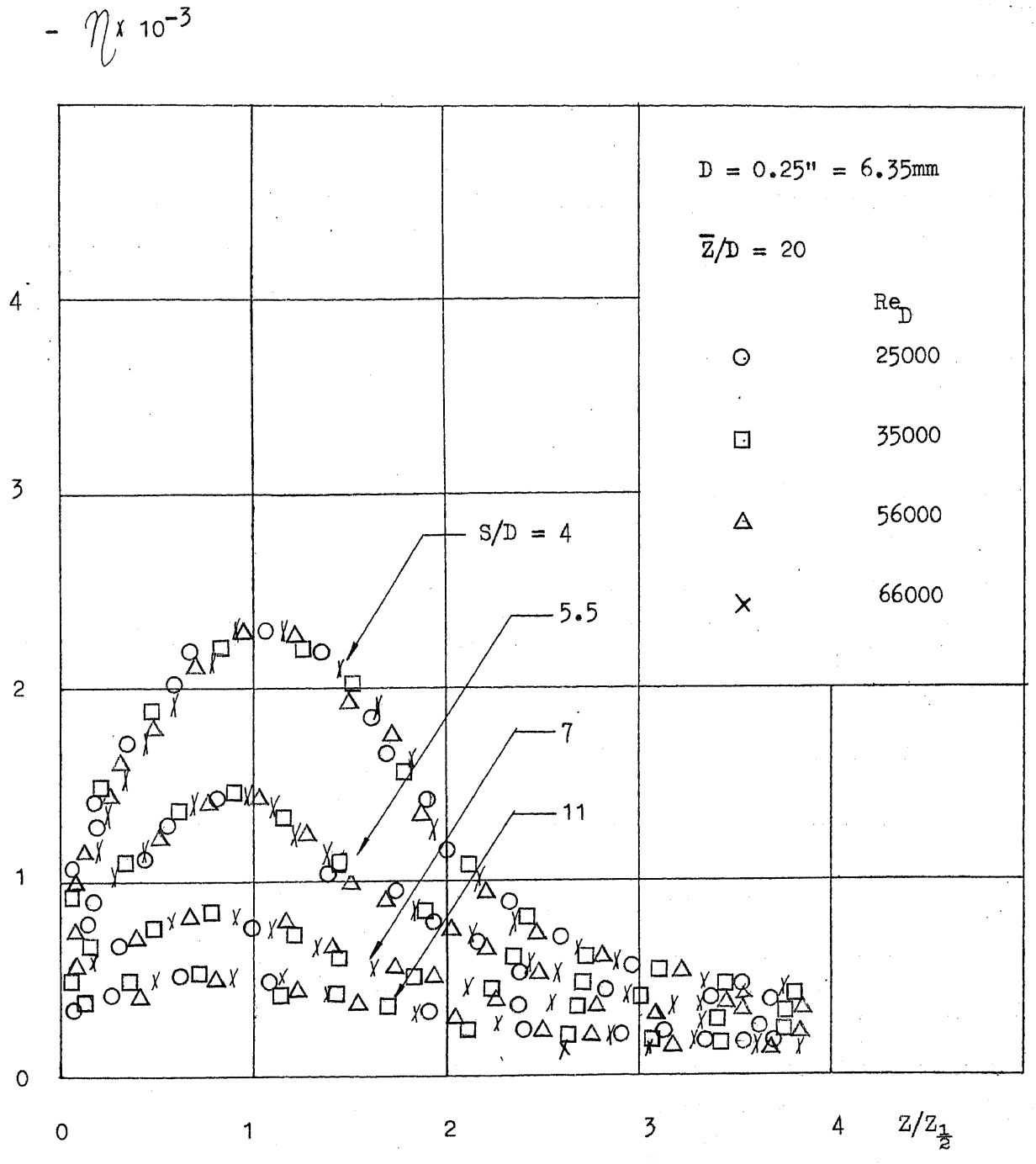

Profile of Static Pressure across Wall Jet

Fig. 56

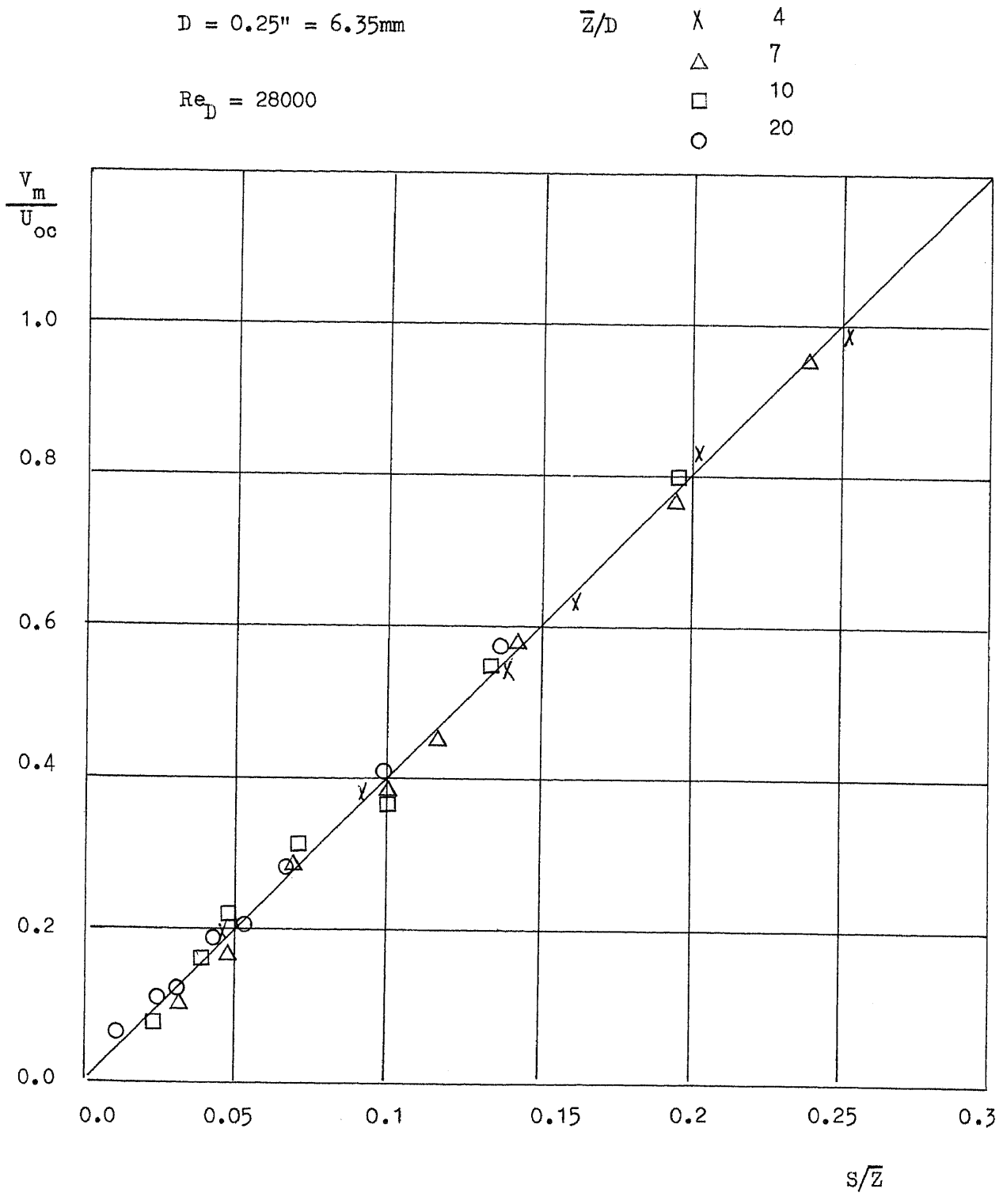

Distribution of Maximum Velocity in the Impingement Zone

Fig. 57

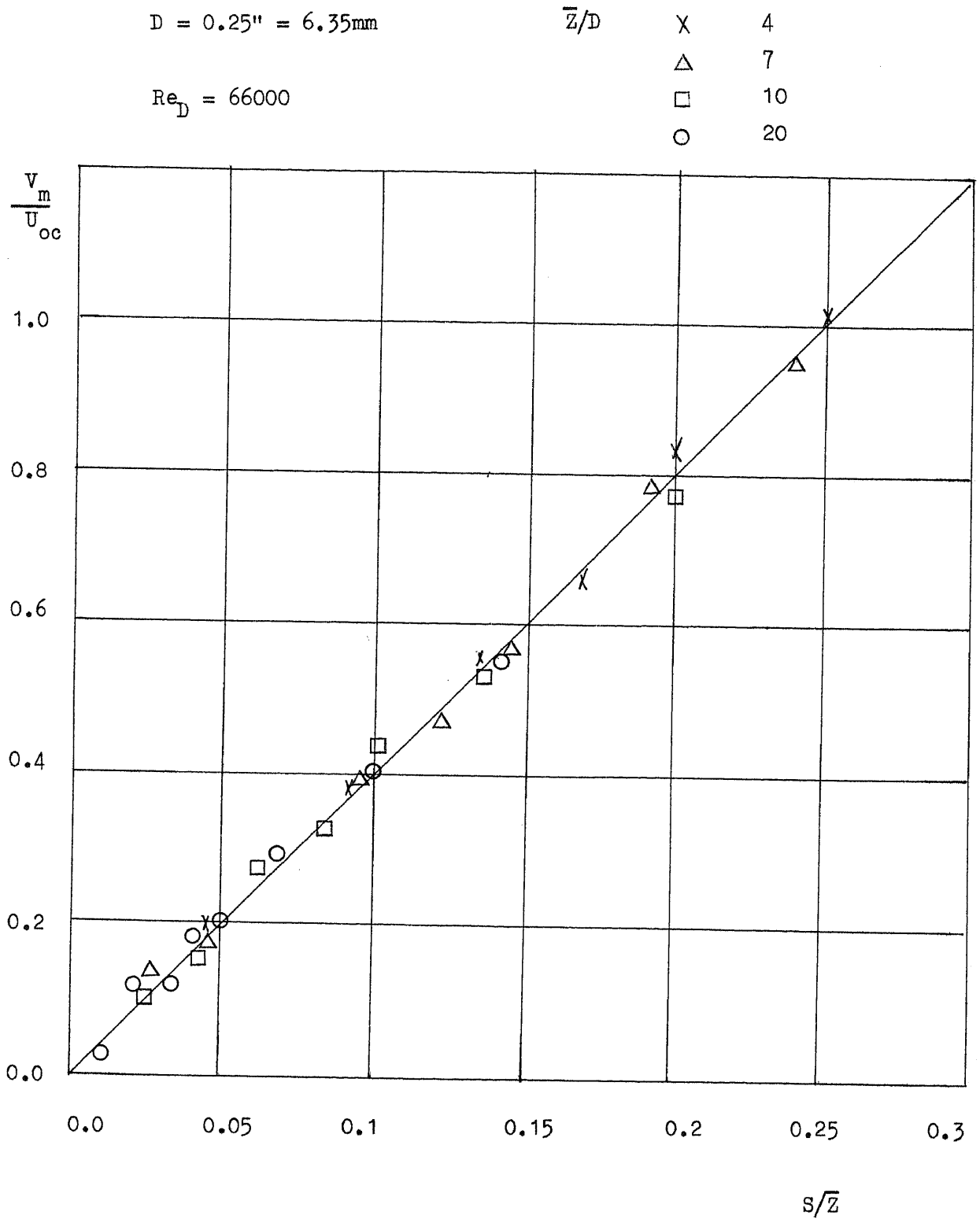

Distribution of Maximum Velocity in the Impingement Zone

Fig. 58

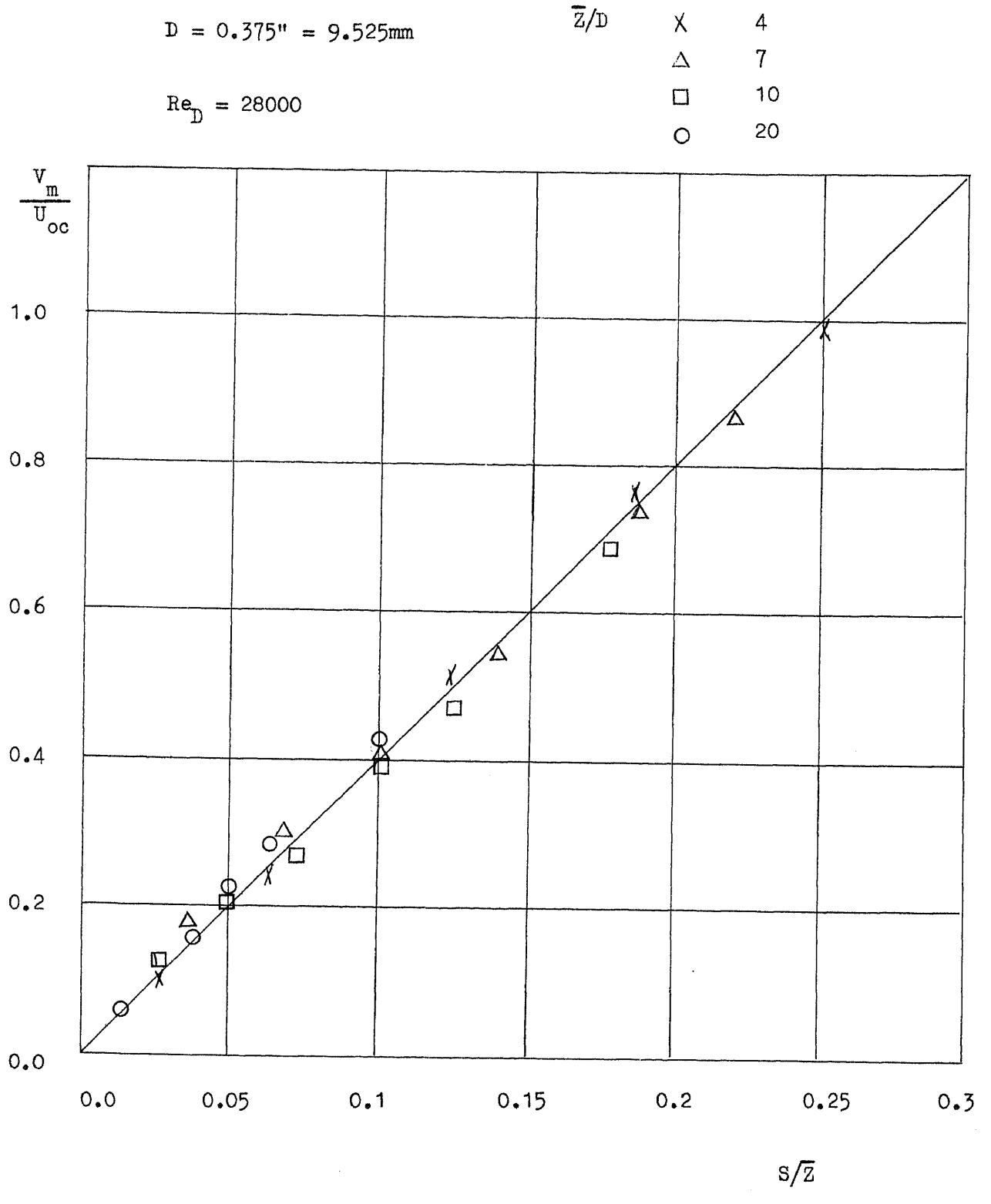

Distribution of Maximum Velocity in the Impingement Zone

Fig. 59

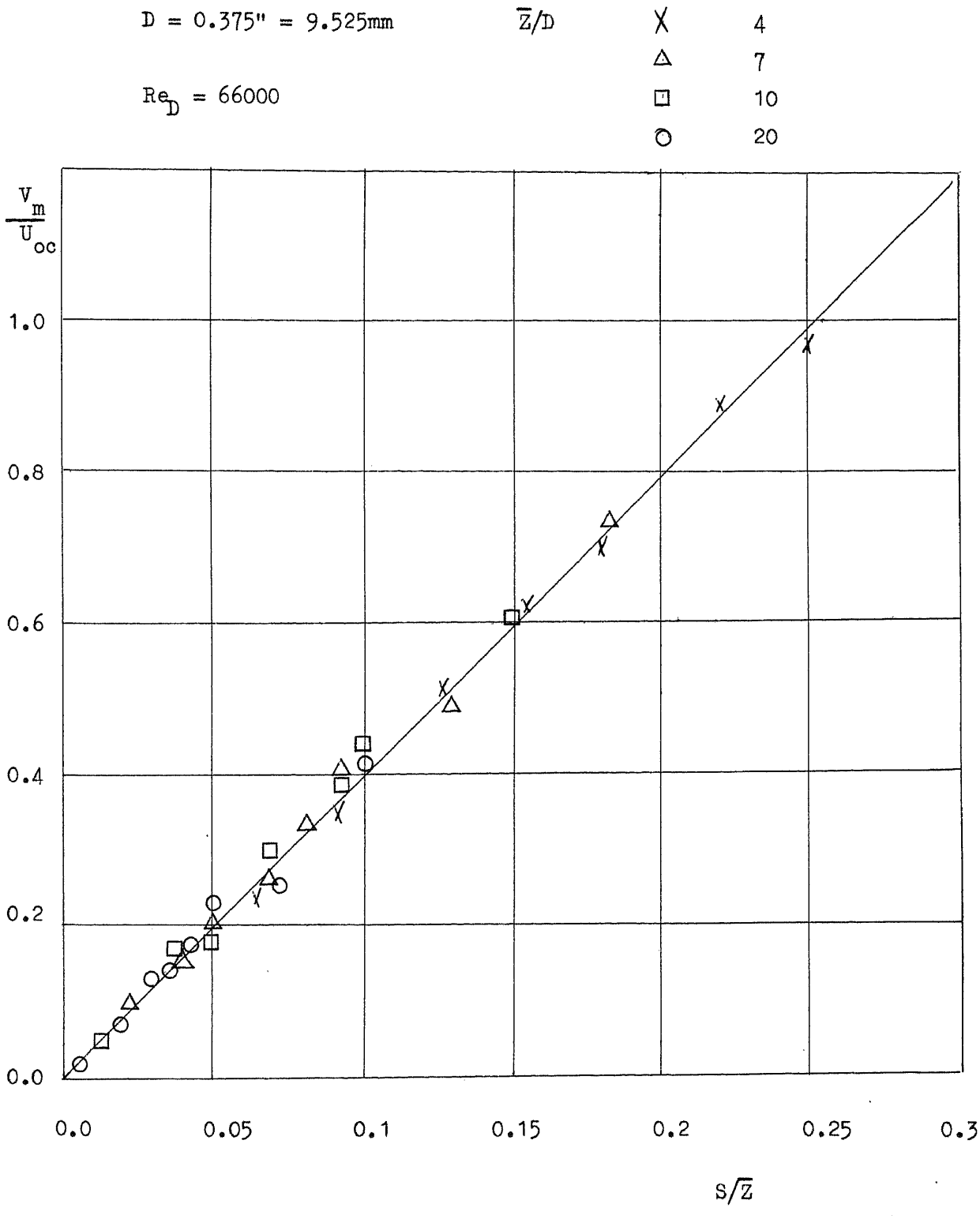

Distribution of Maximum Velocity in the Impingement Zone

Fig. 60

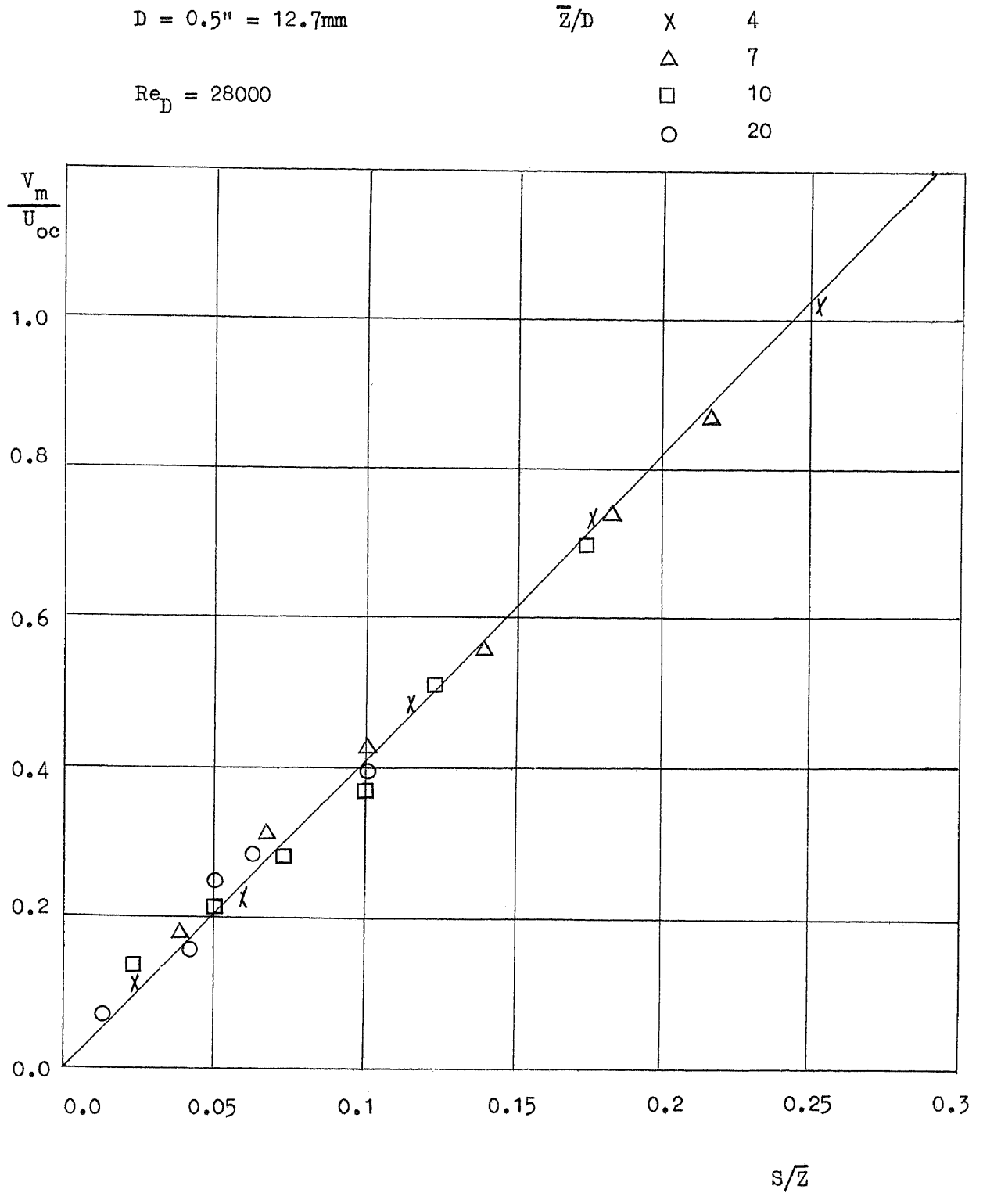

Distribution of Maximum Velocity in the Impingement Zone

Fig. 61

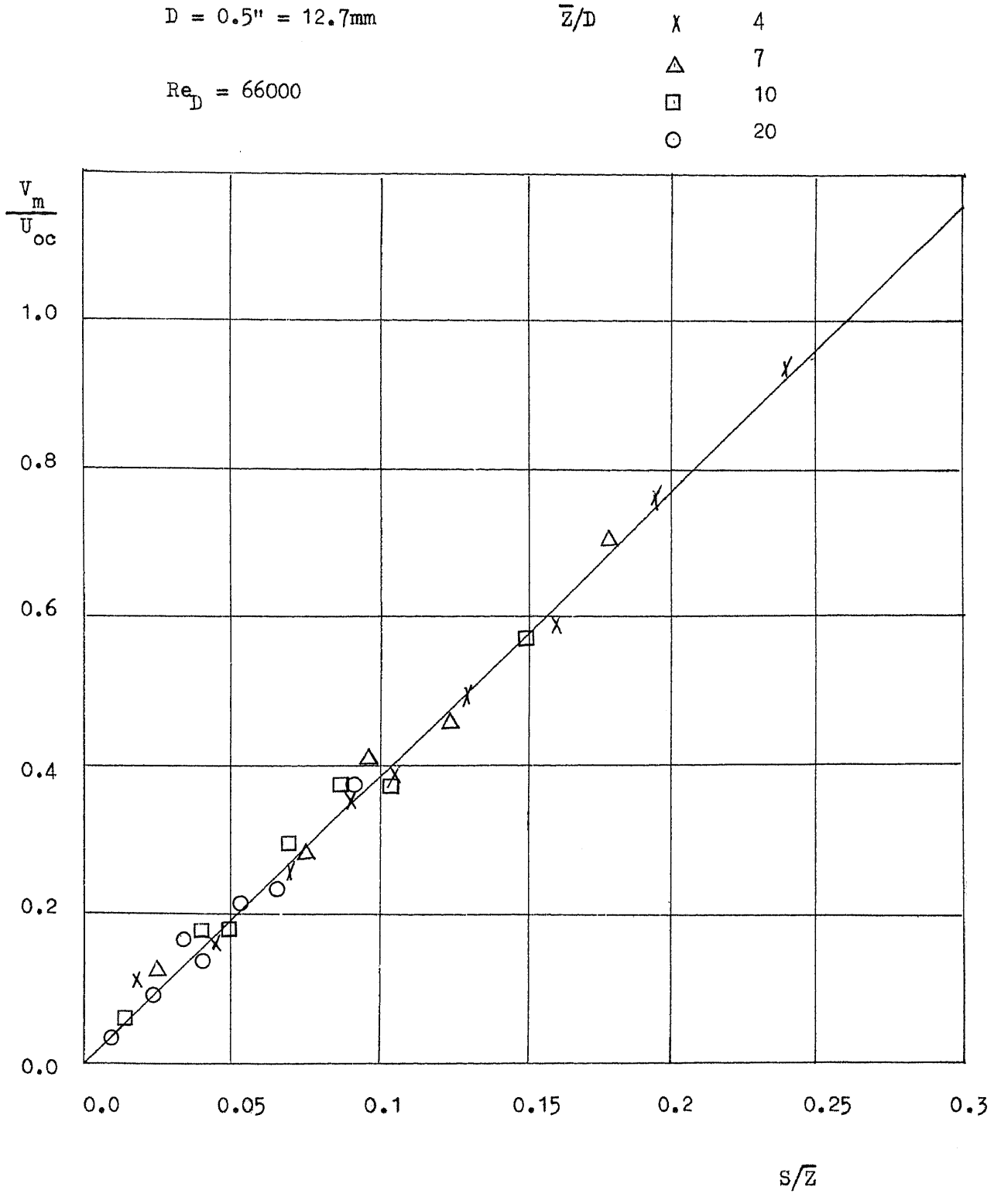

Distribution of Maximum Velocity in the Impingement Zone

Fig. 62

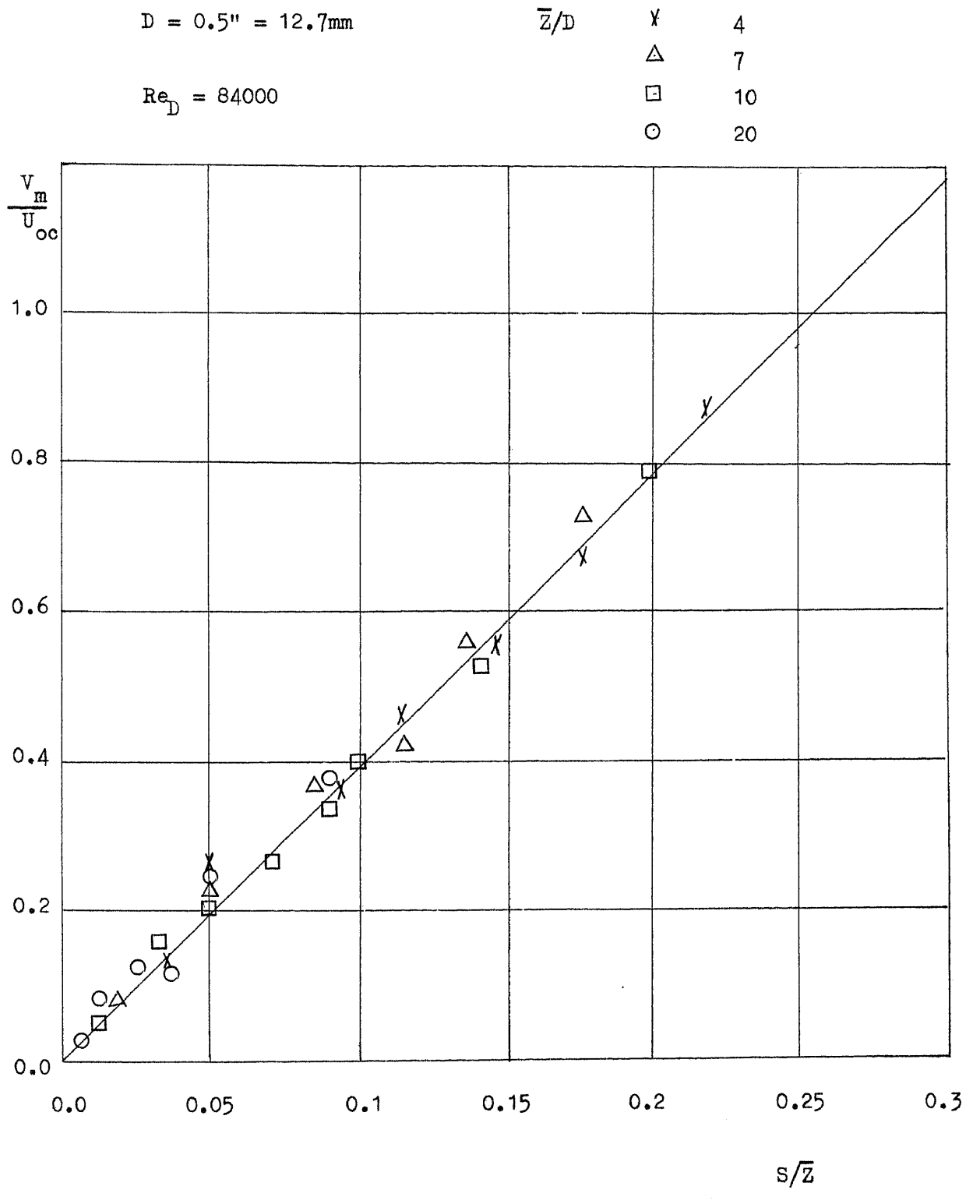

Distribution of Maximum Velocity in the Impingement Zone

Fig. 63

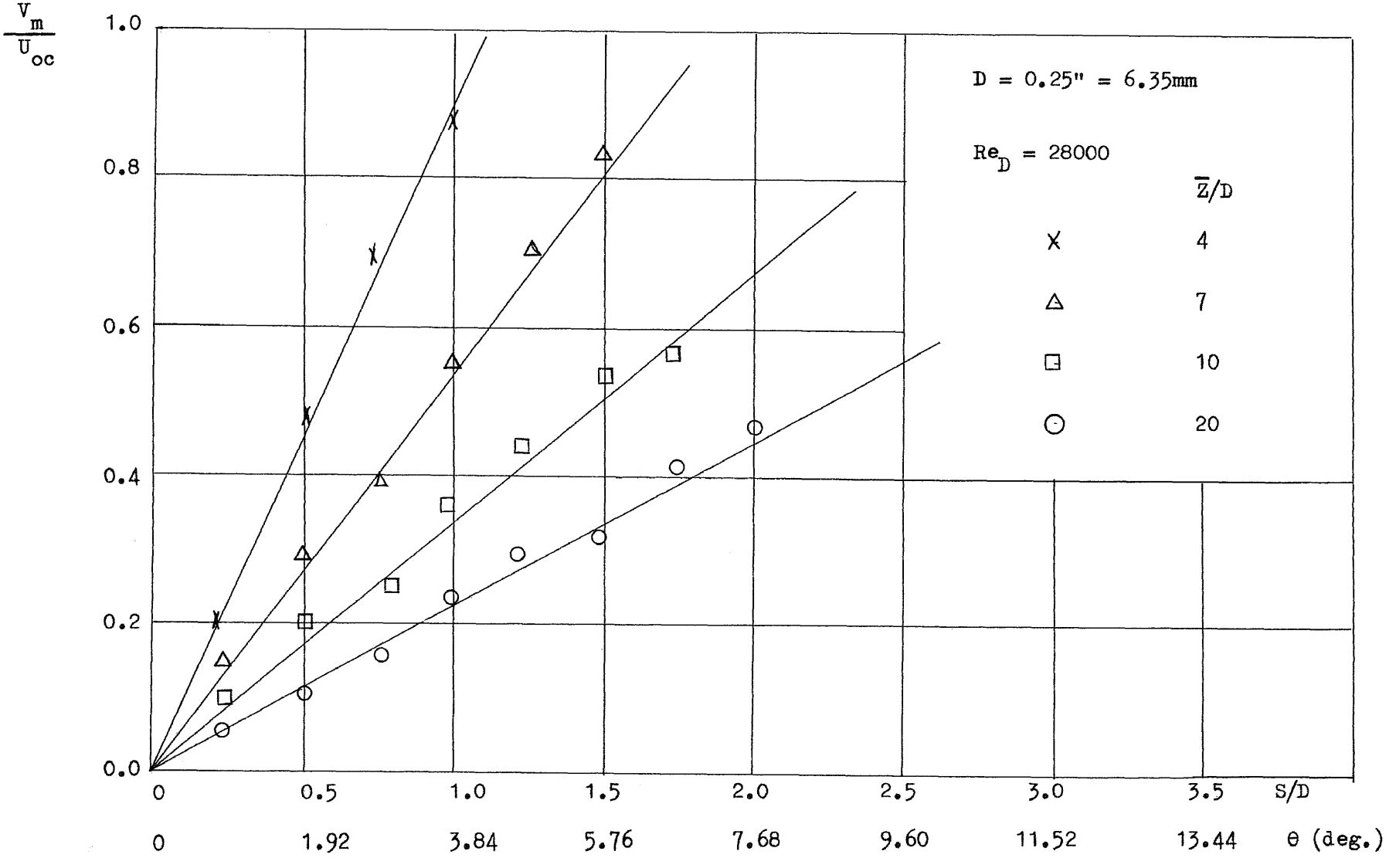

Fig. 64 Maximum Velocity Distribution of the Impingement Zone

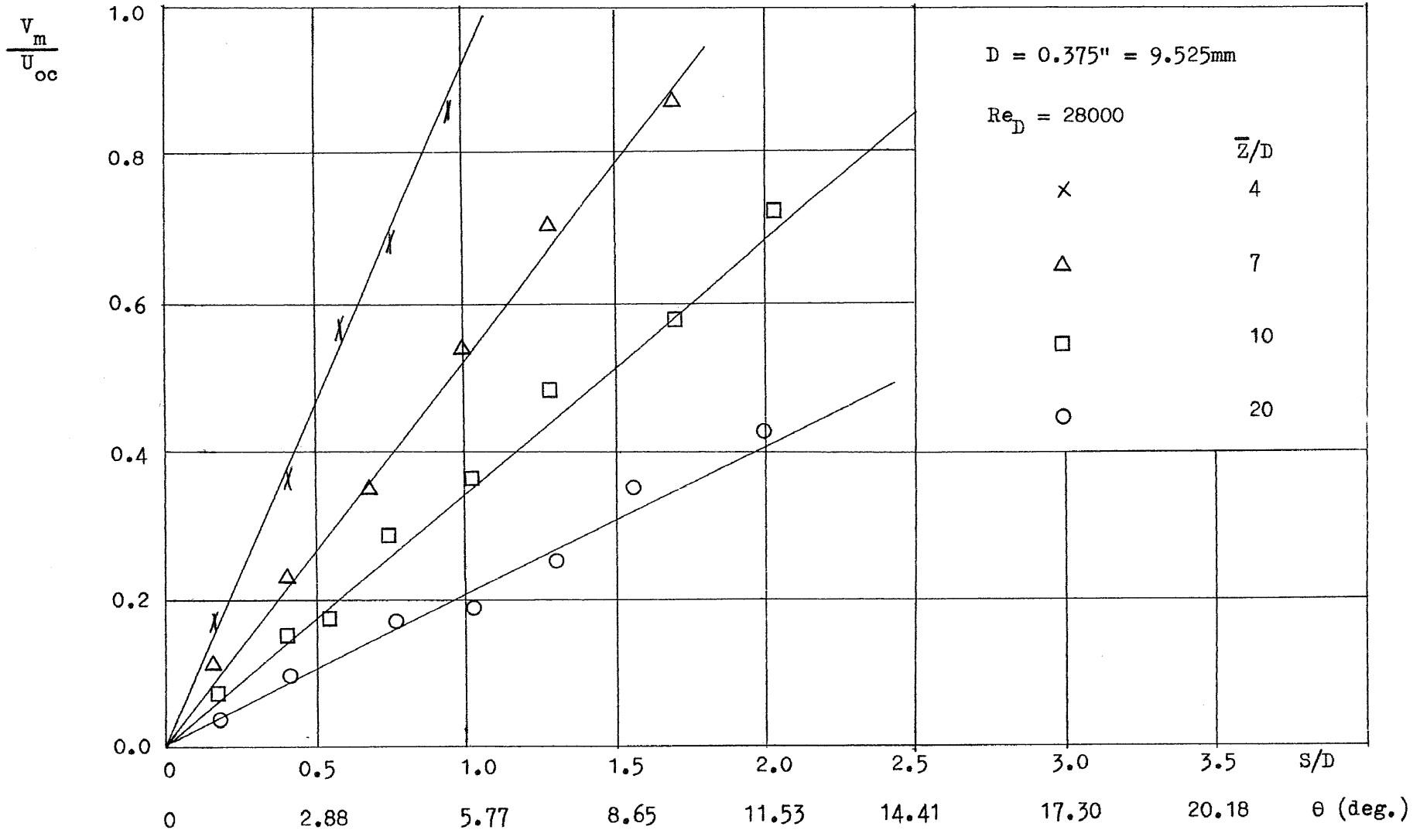

Fig. 65 Maximum Velocity Distribution of the Impingement Zone

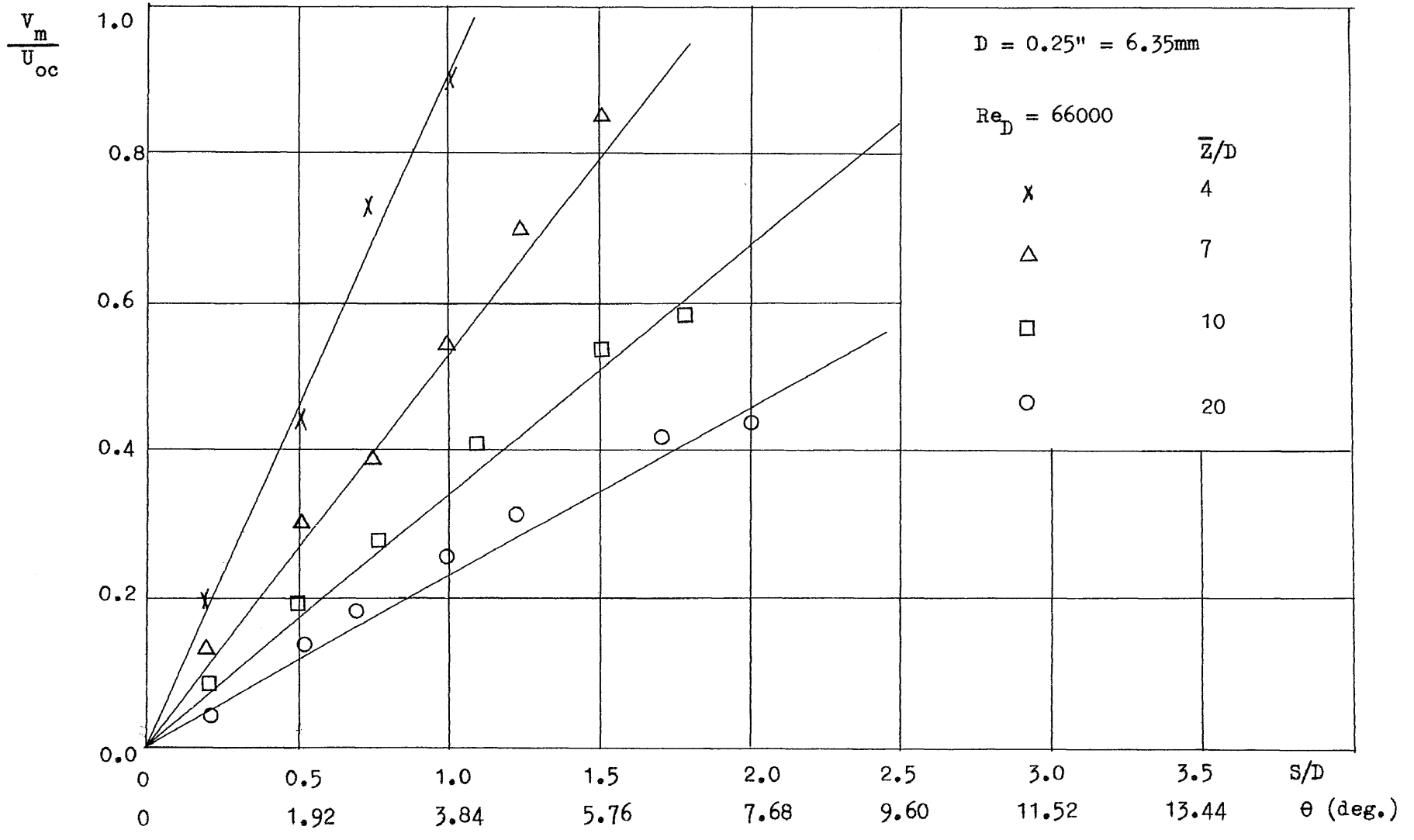

Fig. 66 Maximum Velocity Distribution of the Impingement Zone

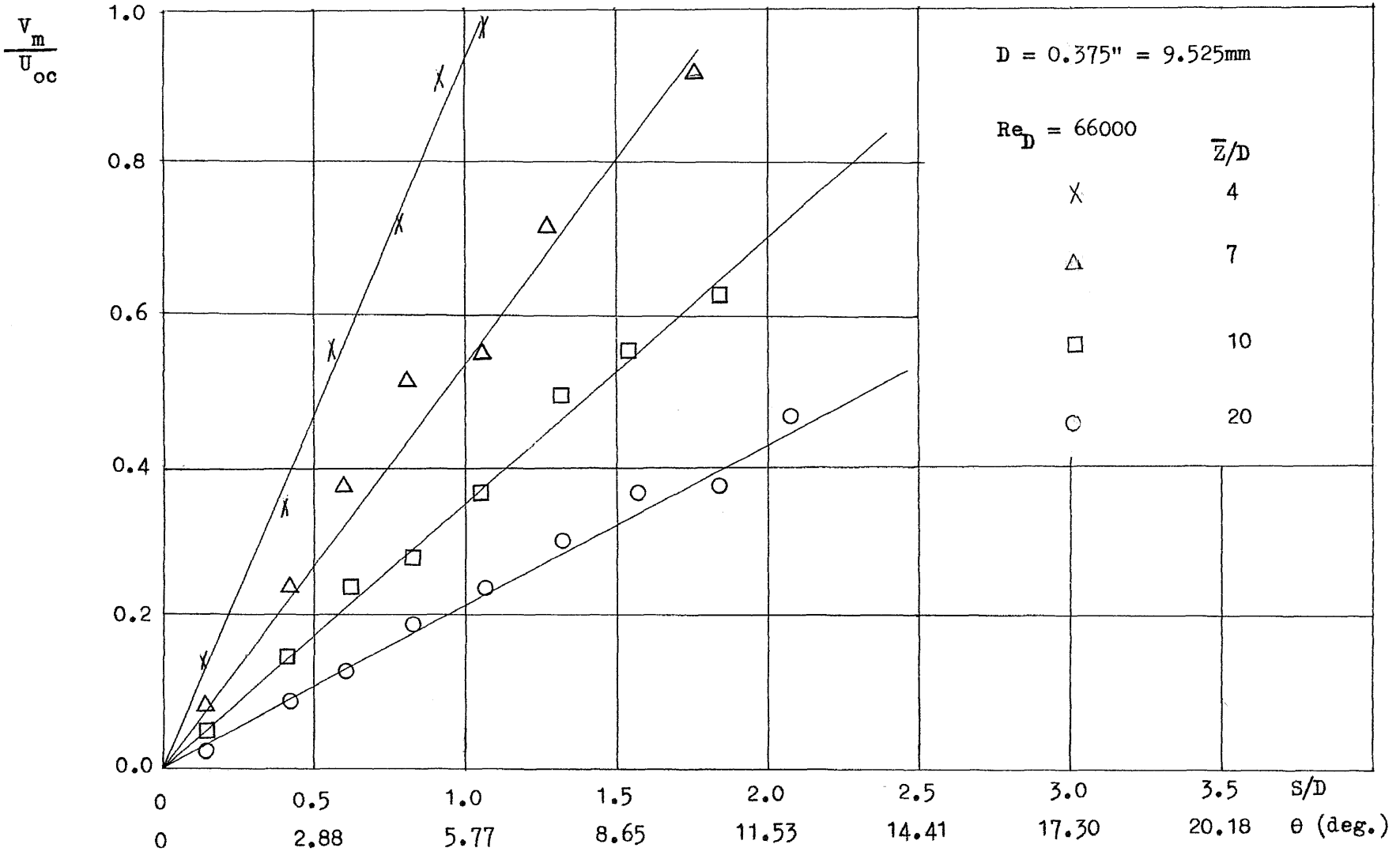

Fig. 67 Maximum Velocity Distribution of the Impingement Zone

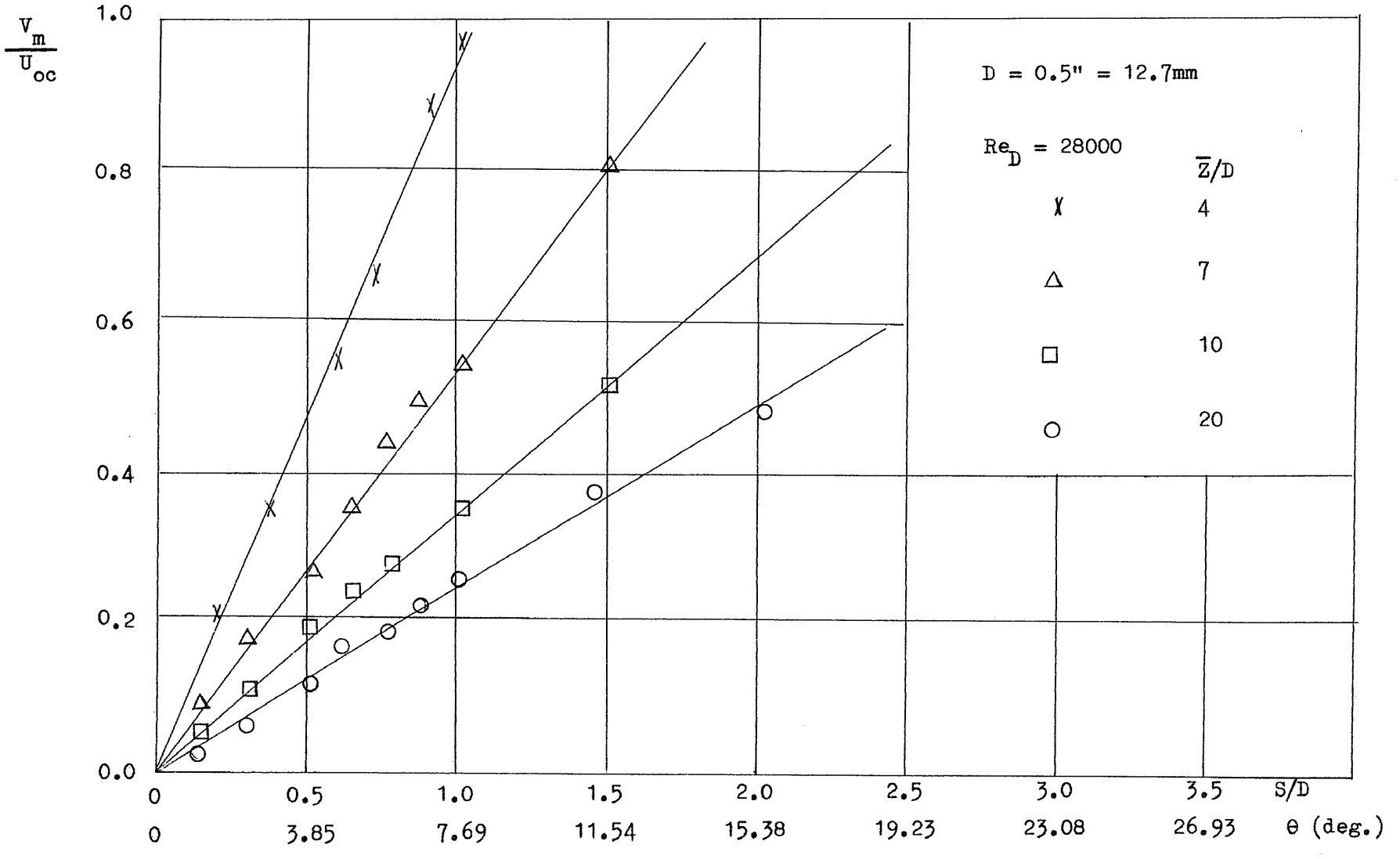

Fig. 68 Maximum Velocity Distribution of the Impingement Zone

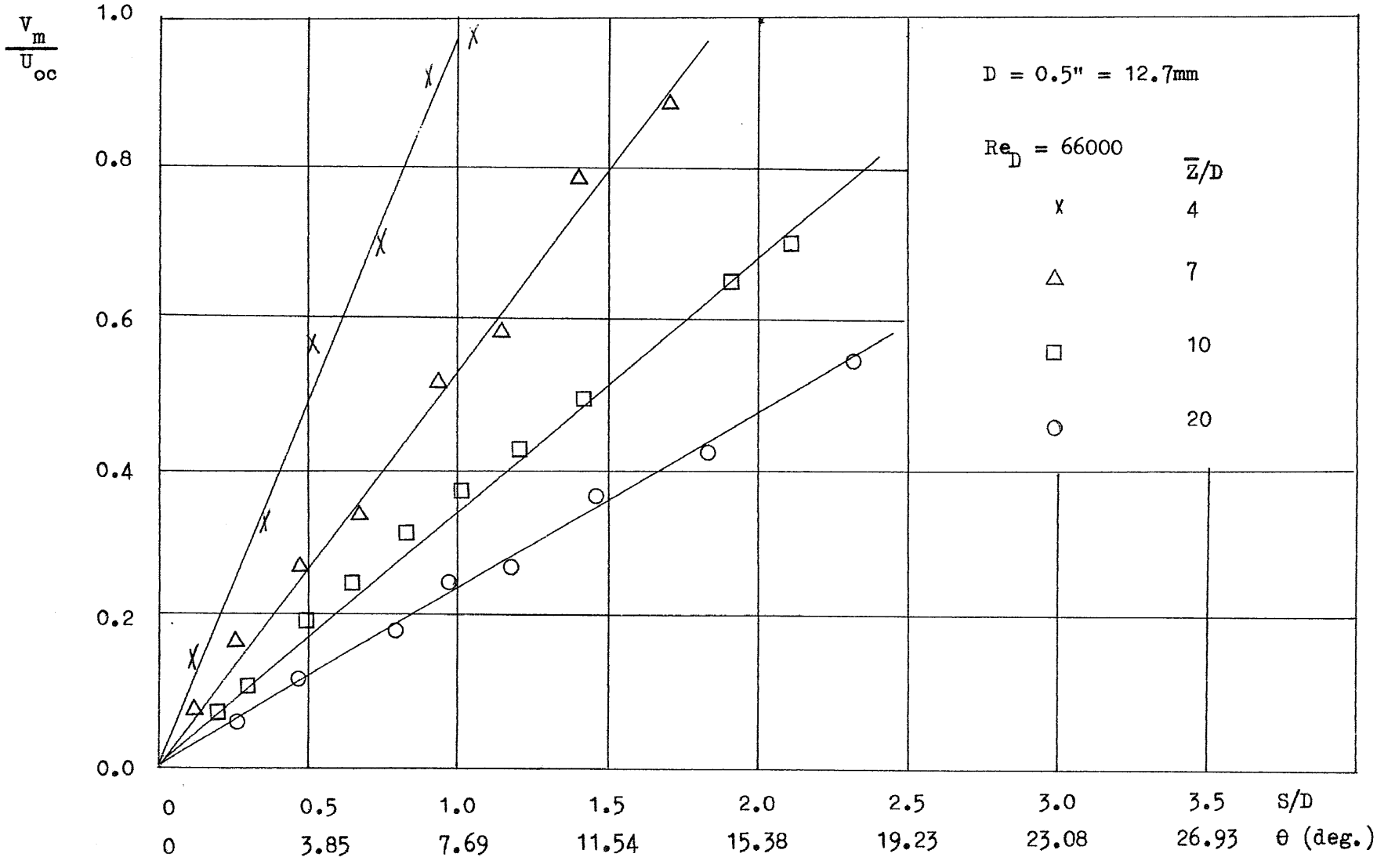

Fig. 69 Maximum Velocity Distribution of the Impingement Zone

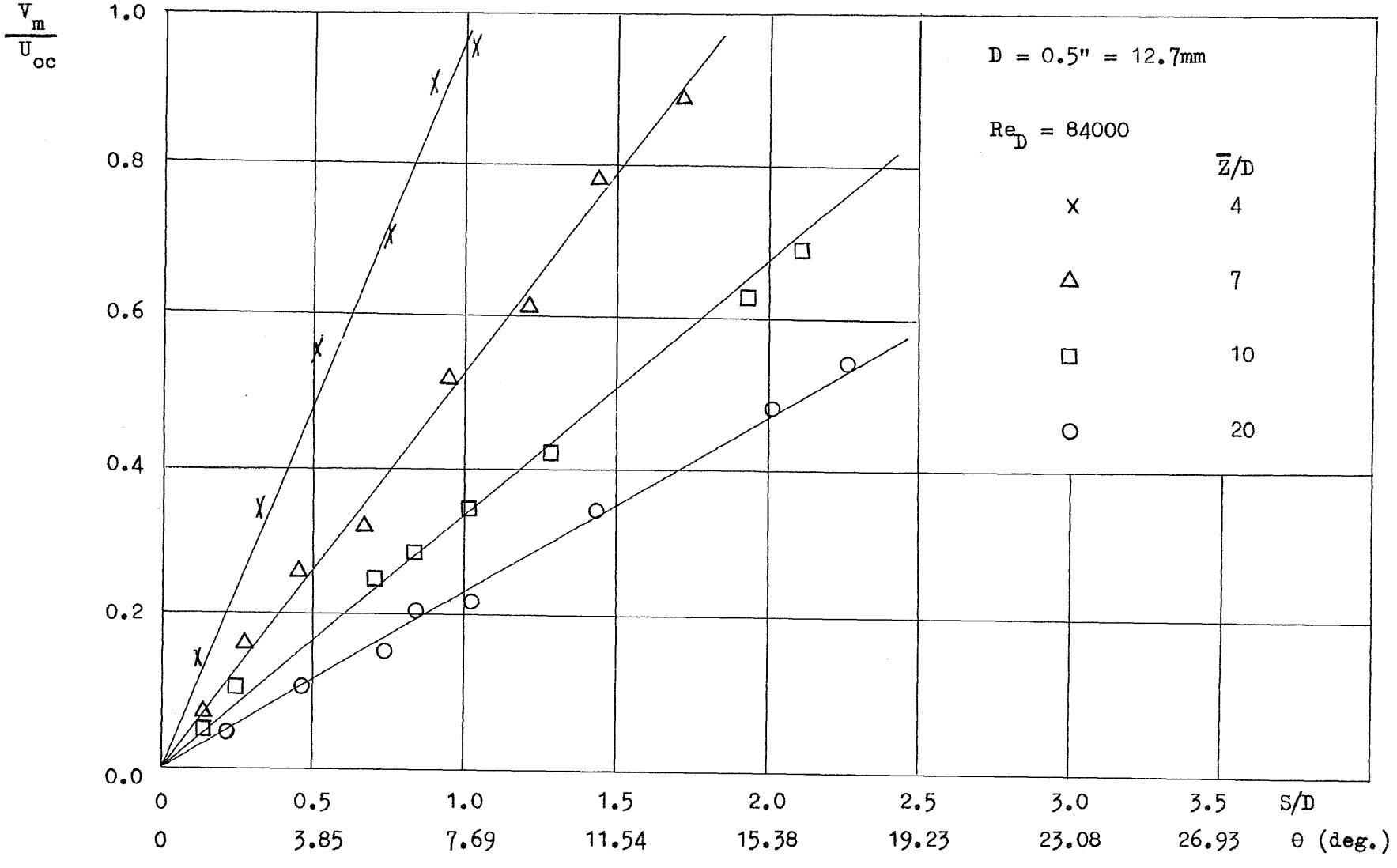

Fig. 70 Maximum Velocity Distribution of the Impingement Zone

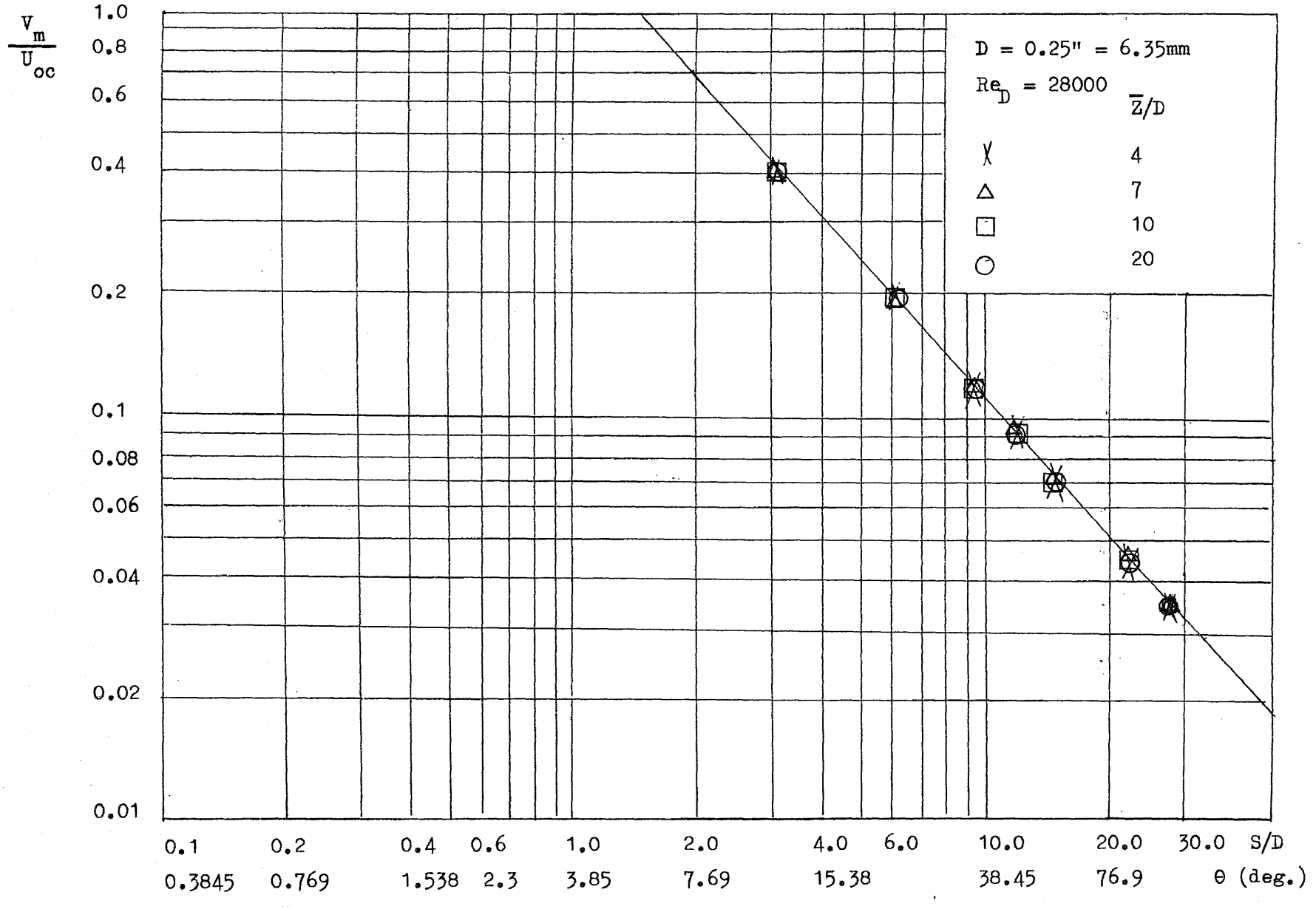

Fig. 71 Max. Velocity Decay along the Wall

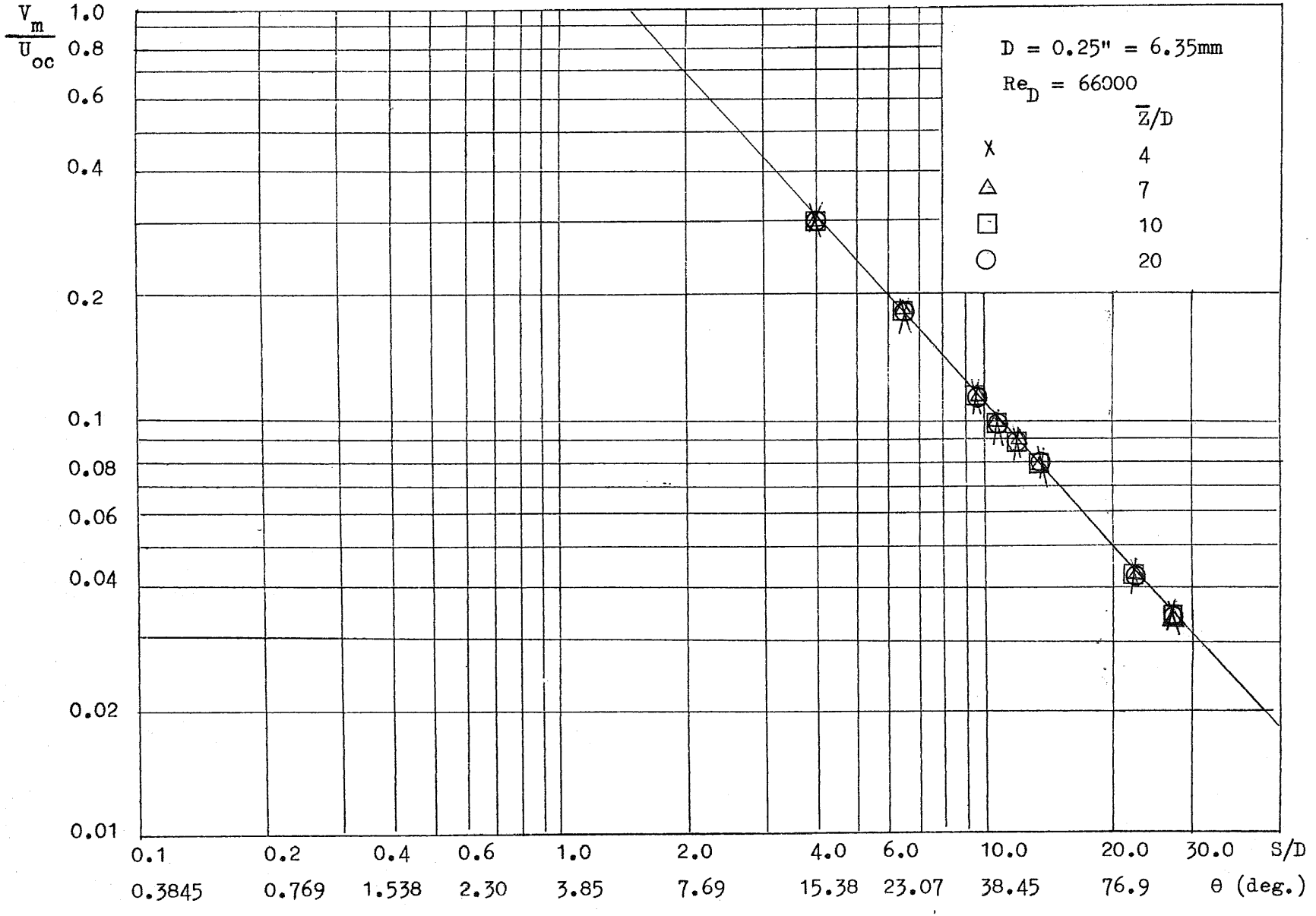

Fig. 72 Maximum Velocity Distribution along the Wall

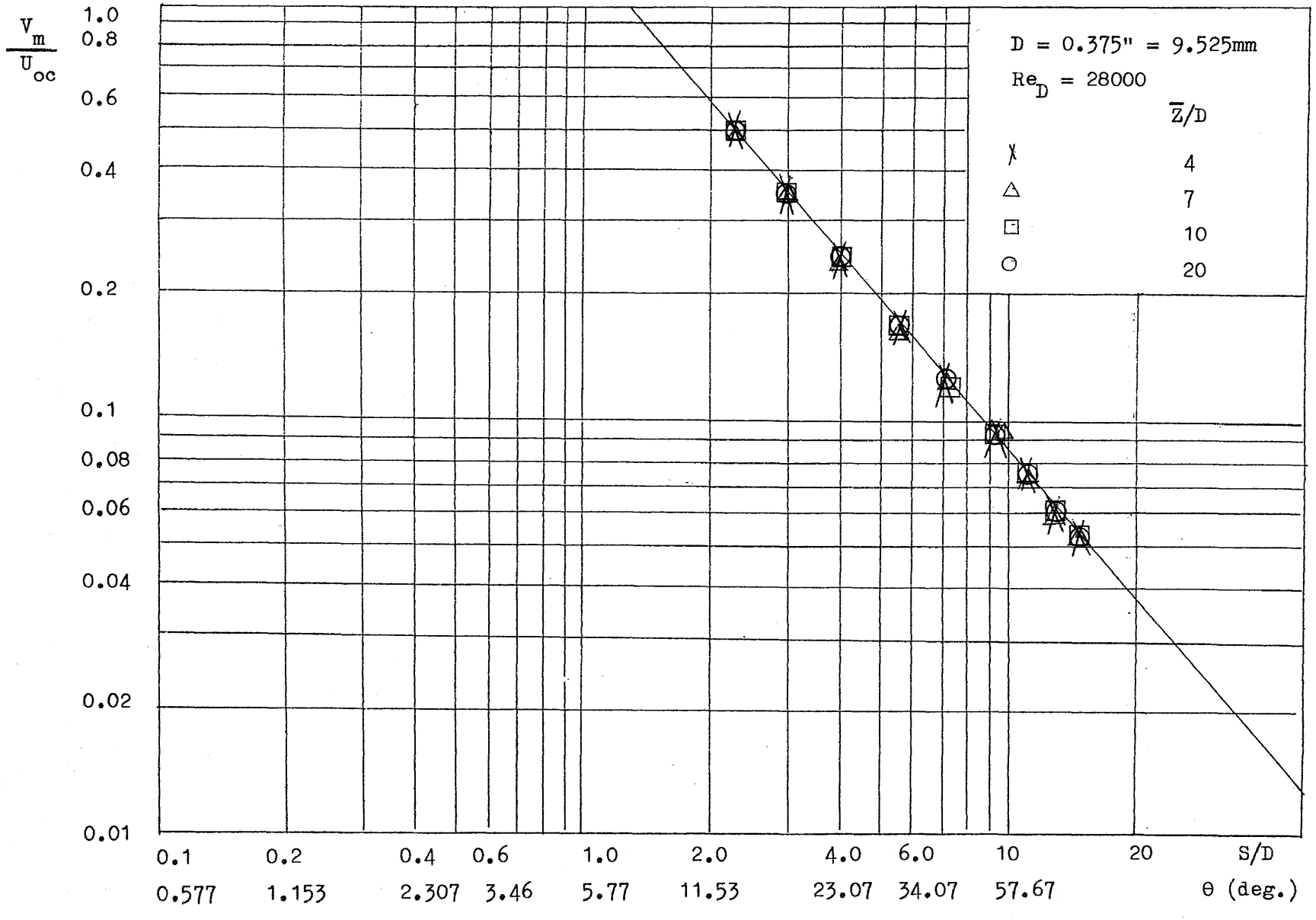

Fig. 73 Maximum Velocity Distribution along the Wall

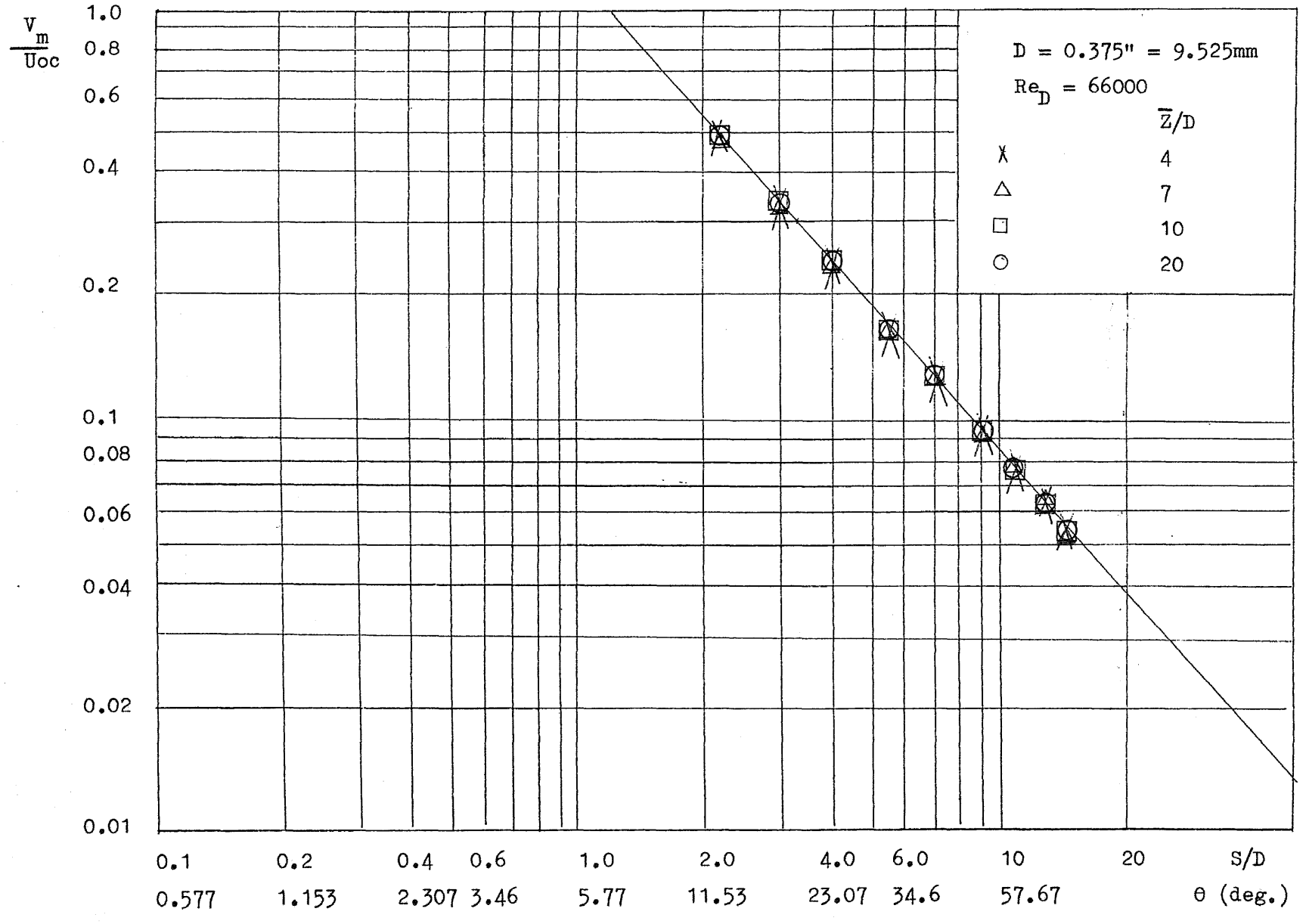

Fig. 74 Max. Velocity Decay along the Wall

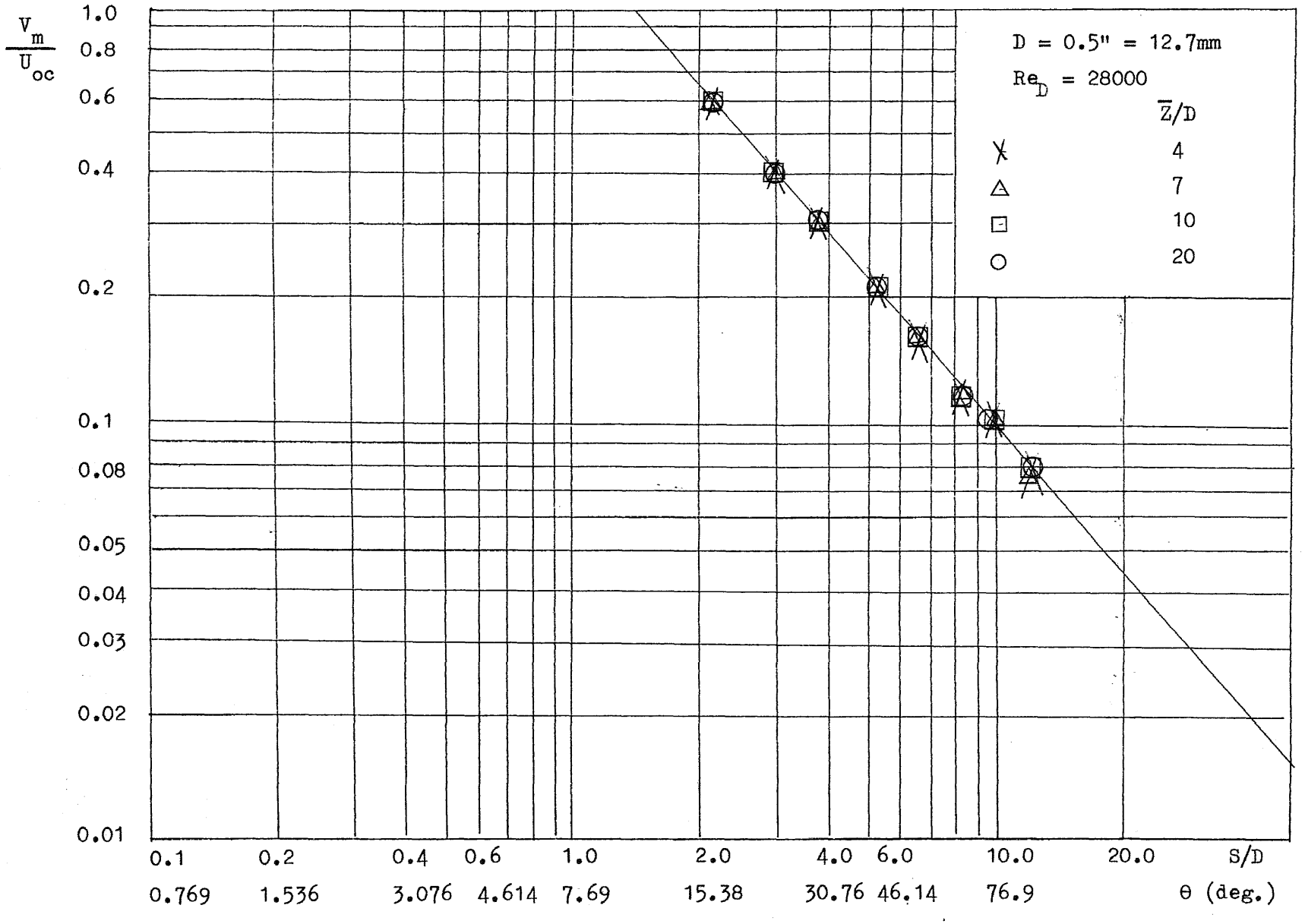

Fig. 75 Maximum Velocity Decay along the Wall

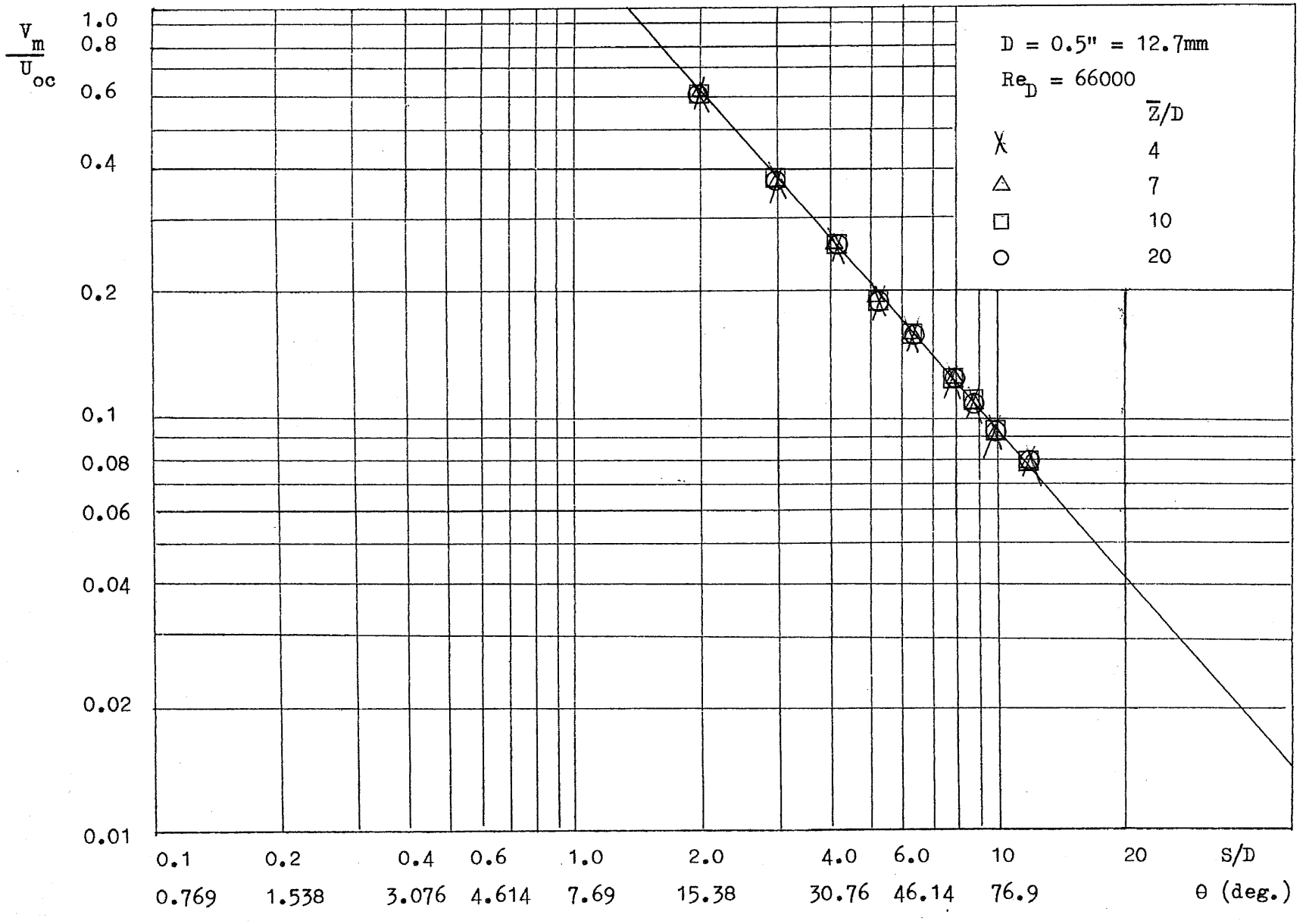

Fig. 76 Maximum Velocity Decay along the Wall

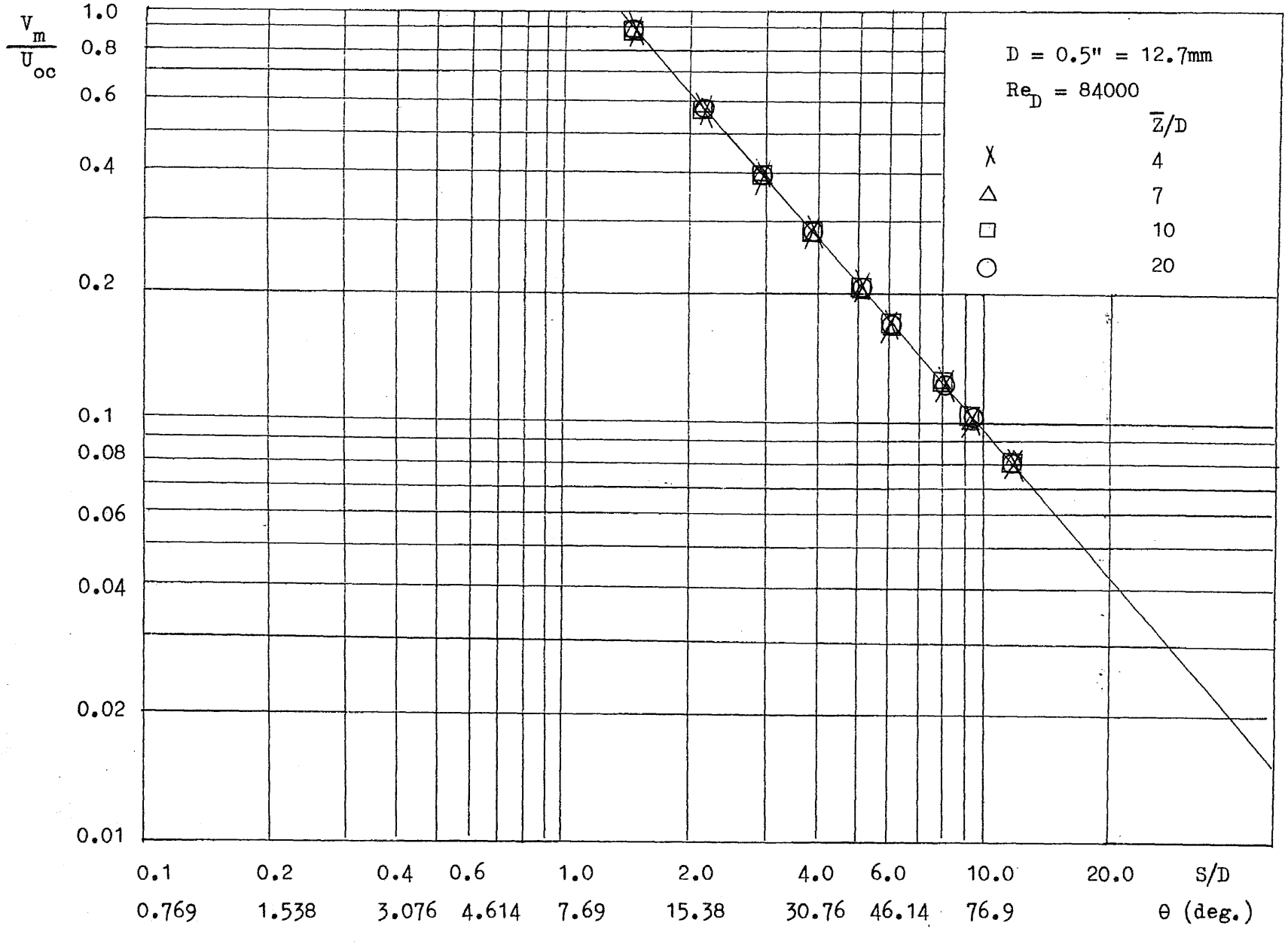

Fig. 77 Maximum Velocity Decay along the Wall

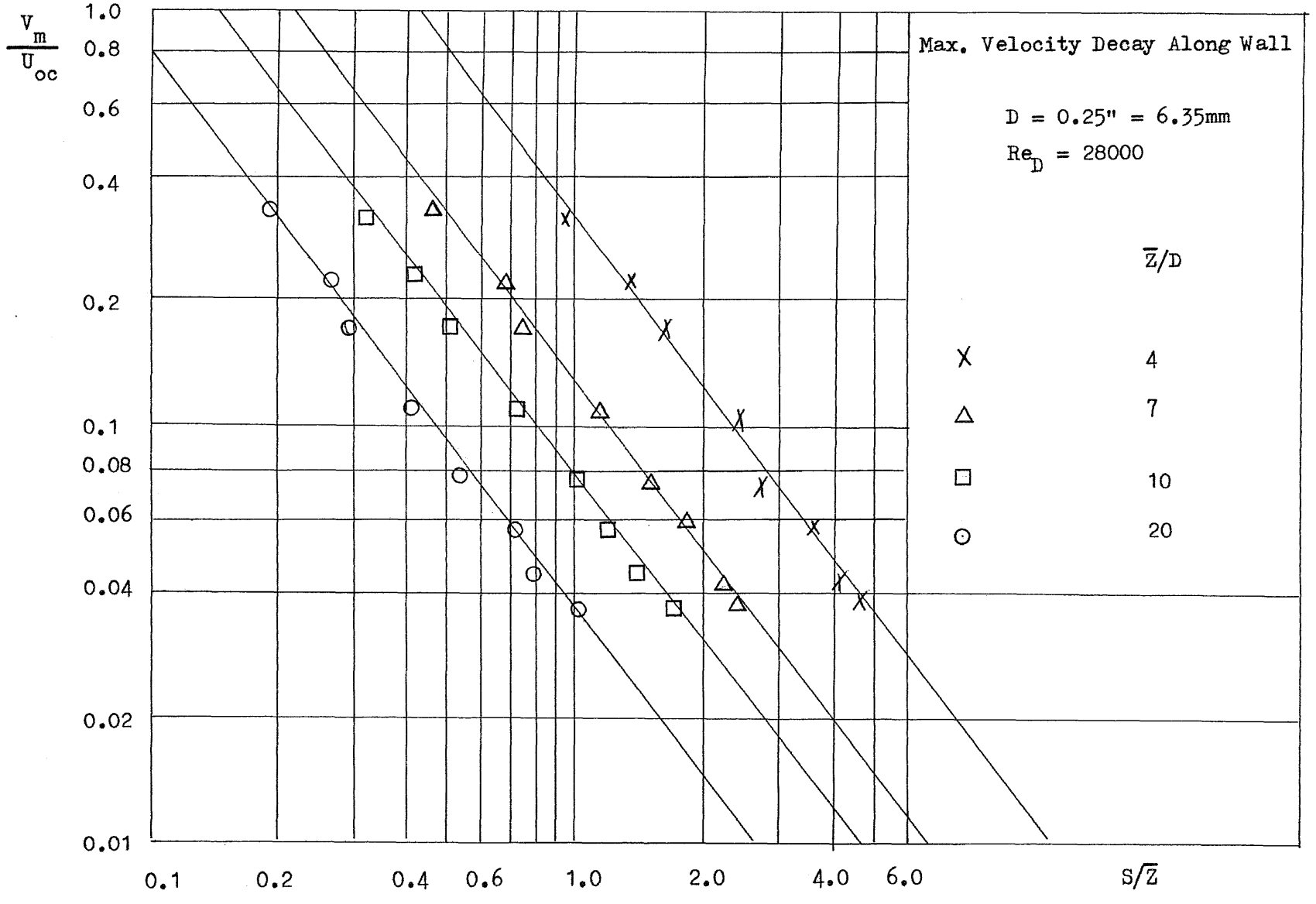
$\frac{V_m}{U_{oc}}$
1.0
0.8
0.6
0.4
0.2
0.1
0.08
0.06
0.04
0.02
0.01
0.1
0.2
0.4
0.6
1.0
2.0
4.0
6.0
S/Z̄
Max. Velocity Decay Along Wall
D = 0.25" = 6.35mm
Re_D = 28000
Z̄/D
4
7
10
20

Fig. 78

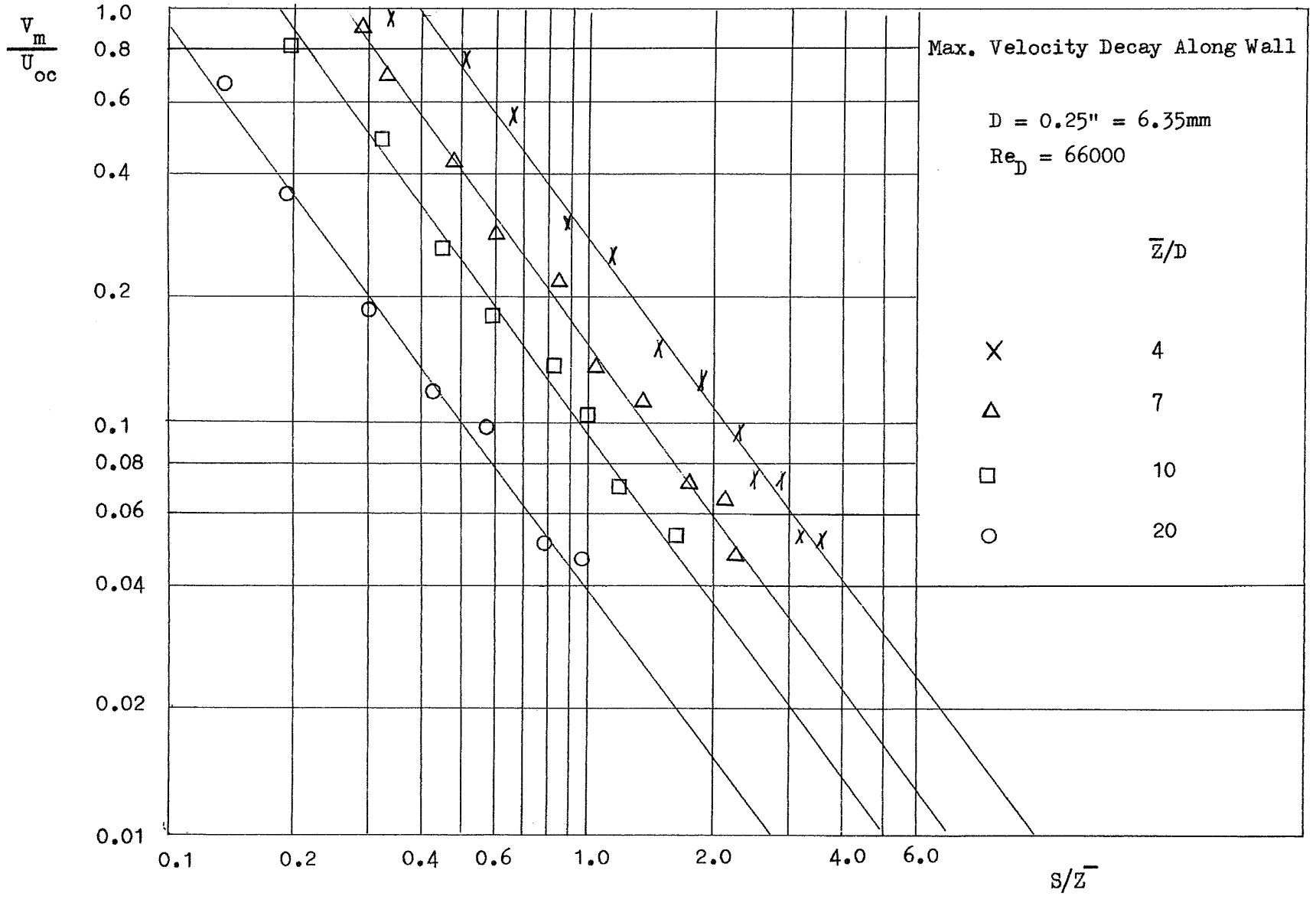
$\frac{V_m}{U_{oc}}$
1.0
0.8
0.6
0.4
0.2
0.1
0.08
0.06
0.04
0.02
0.01
0.1
0.2
0.4
0.6
1.0
2.0
4.0
6.0
$S/\bar{Z}$
Max. Velocity Decay Along Wall
D = 0.25" = 6.35mm
Re_D = 66000
$\bar{Z}/D$
4
7
10
20

Fig. 79

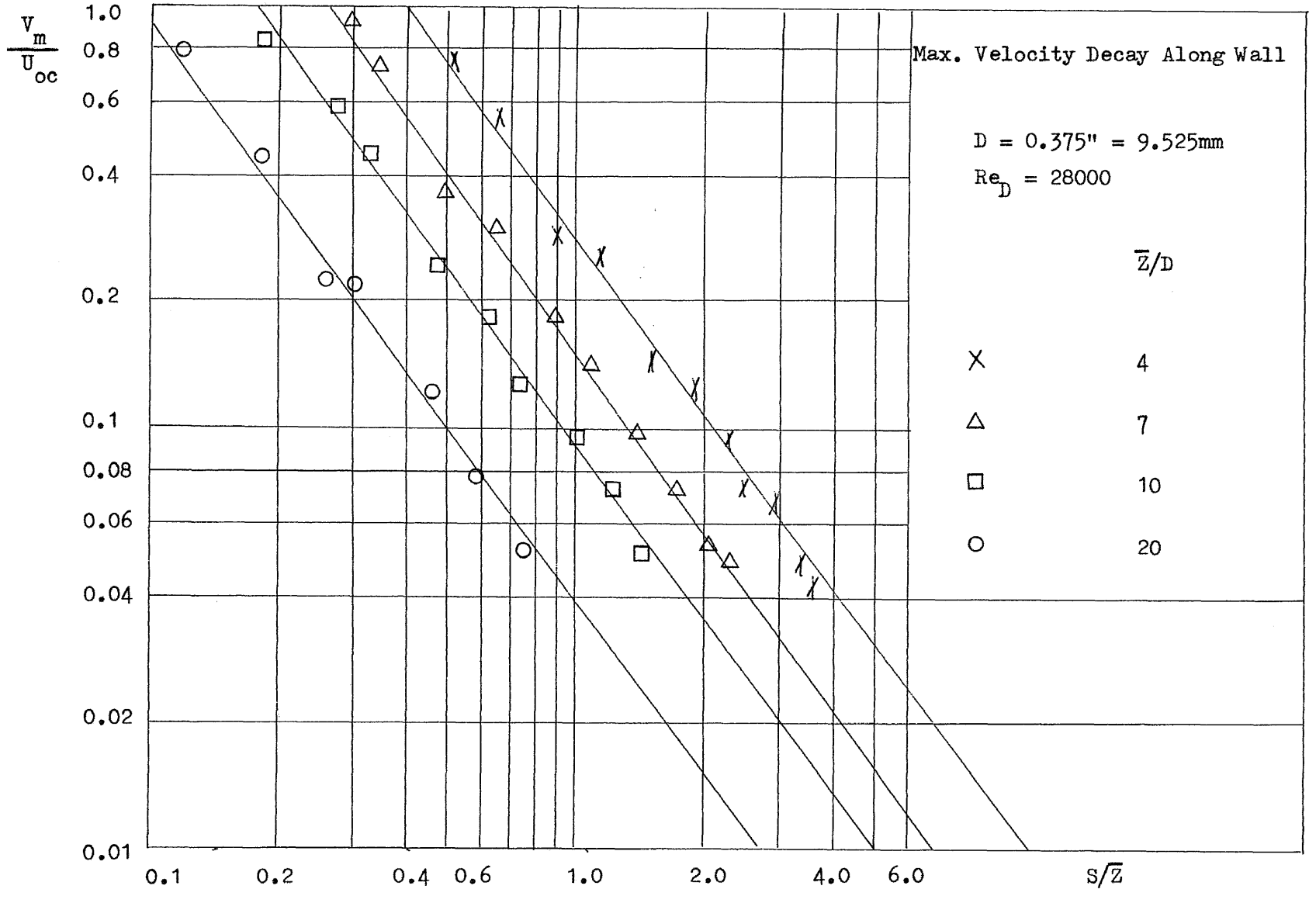
$\frac{V_m}{U_{oc}}$
1.0
0.8
0.6
0.4
0.2
0.1
0.08
0.06
0.04
0.02
0.01
0.1
0.2
0.4
0.6
1.0
2.0
4.0
6.0
S/Z
Max. Velocity Decay Along Wall
D = 0.375" = 9.525mm
Re_D = 28000
Z/D
4
7
10
20

Fig. 80

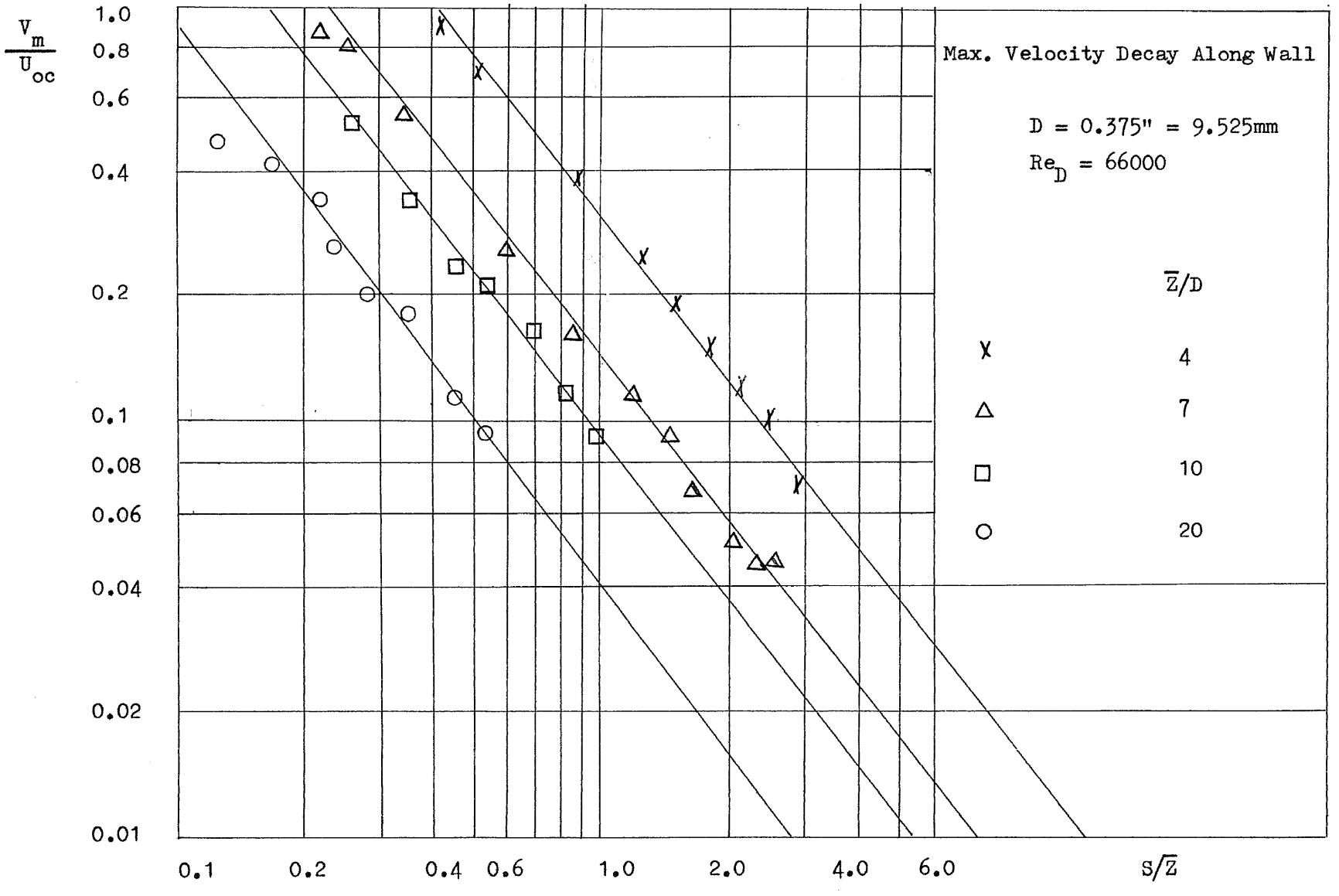
$\frac{V_m}{U_{oc}}$
1.0
0.8
0.6
0.4
0.2
0.1
0.08
0.06
0.04
0.02
0.01
0.1
0.2
0.4
0.6
1.0
2.0
4.0
6.0
S/Z̄
Max. Velocity Decay Along Wall
D = 0.375" = 9.525mm
Re_D = 66000
Z̄/D
4
7
10
20

Fig. 81

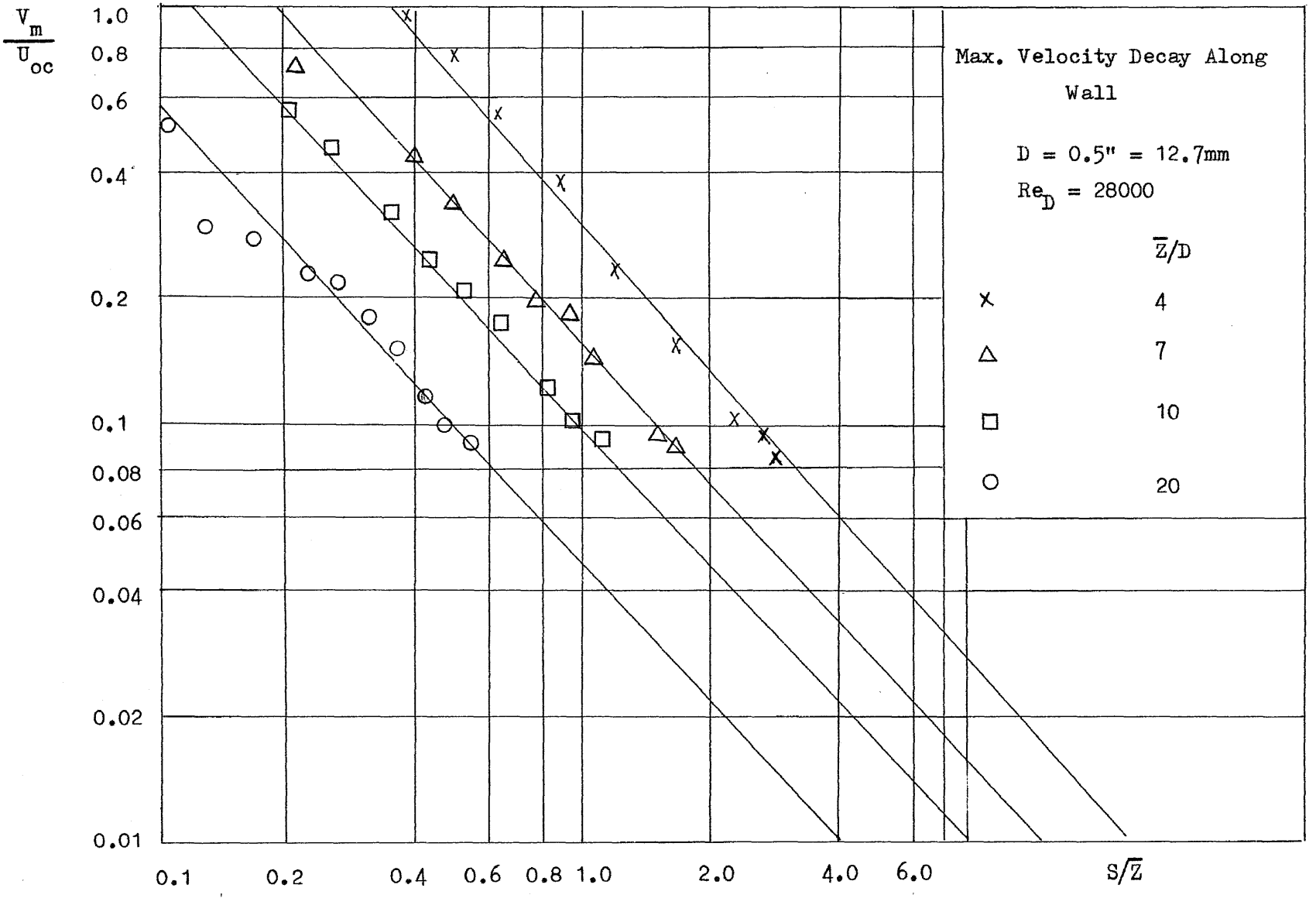
$\frac{V_m}{U_{oc}}$
1.0
0.8
0.6
0.4
0.2
0.1
0.08
0.06
0.04
0.02
0.01
0.1
0.2
0.4
0.6
0.8
1.0
2.0
4.0
6.0
S/Z̄
Max. Velocity Decay Along Wall
D = 0.5" = 12.7mm
Re_D = 28000
Z̄/D
4
7
10
20

Fig. 82

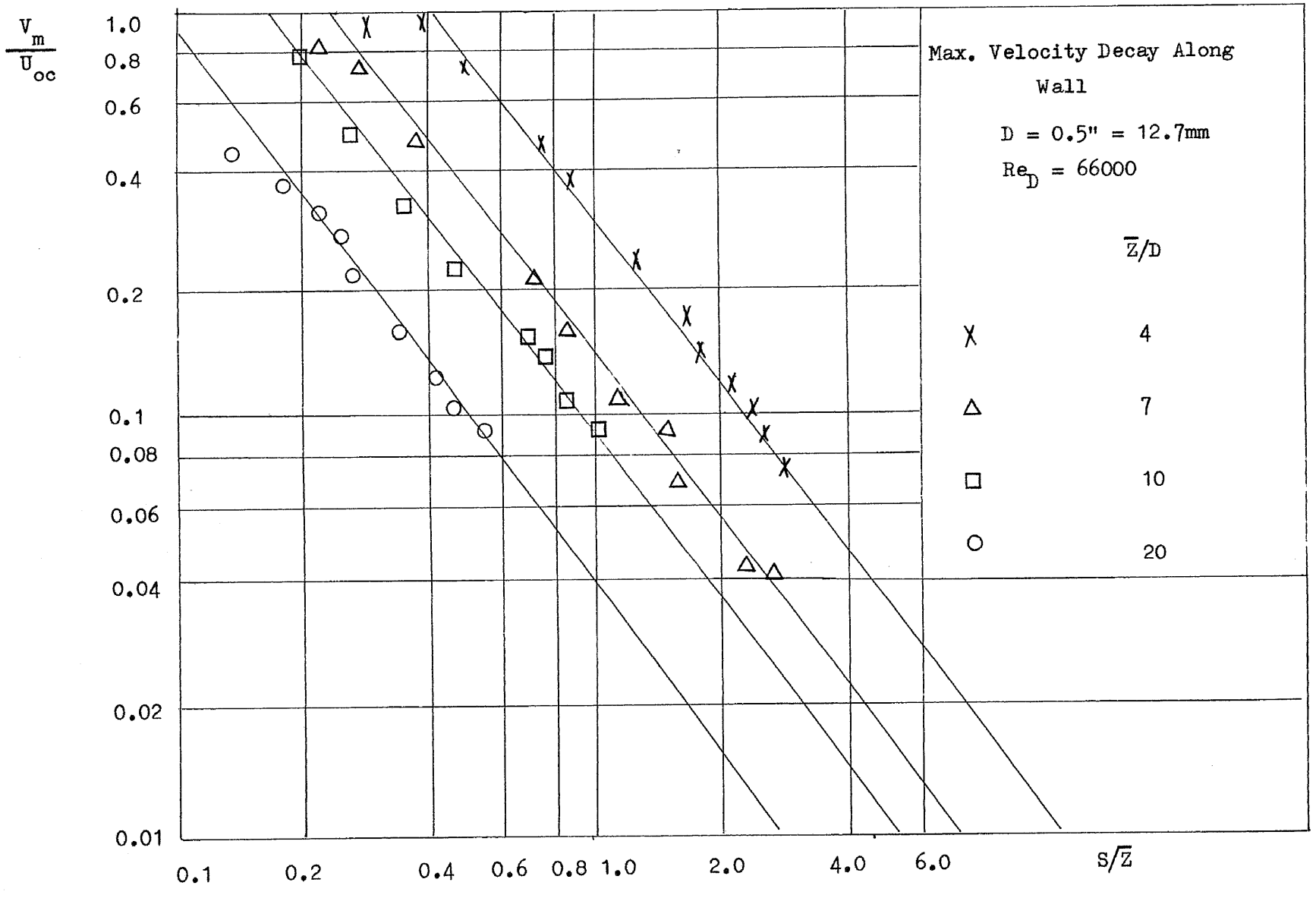
$\frac{V_m}{U_{oc}}$
1.0
0.8
0.6
0.4
0.2
0.1
0.08
0.06
0.04
0.02
0.01
0.1
0.2
0.4
0.6
0.8
1.0
2.0
4.0
6.0
$S/\overline{Z}$
Max. Velocity Decay Along Wall
D = 0.5" = 12.7mm
Re_D = 66000
$\overline{Z}/D$
4
7
10
20

Fig. 83

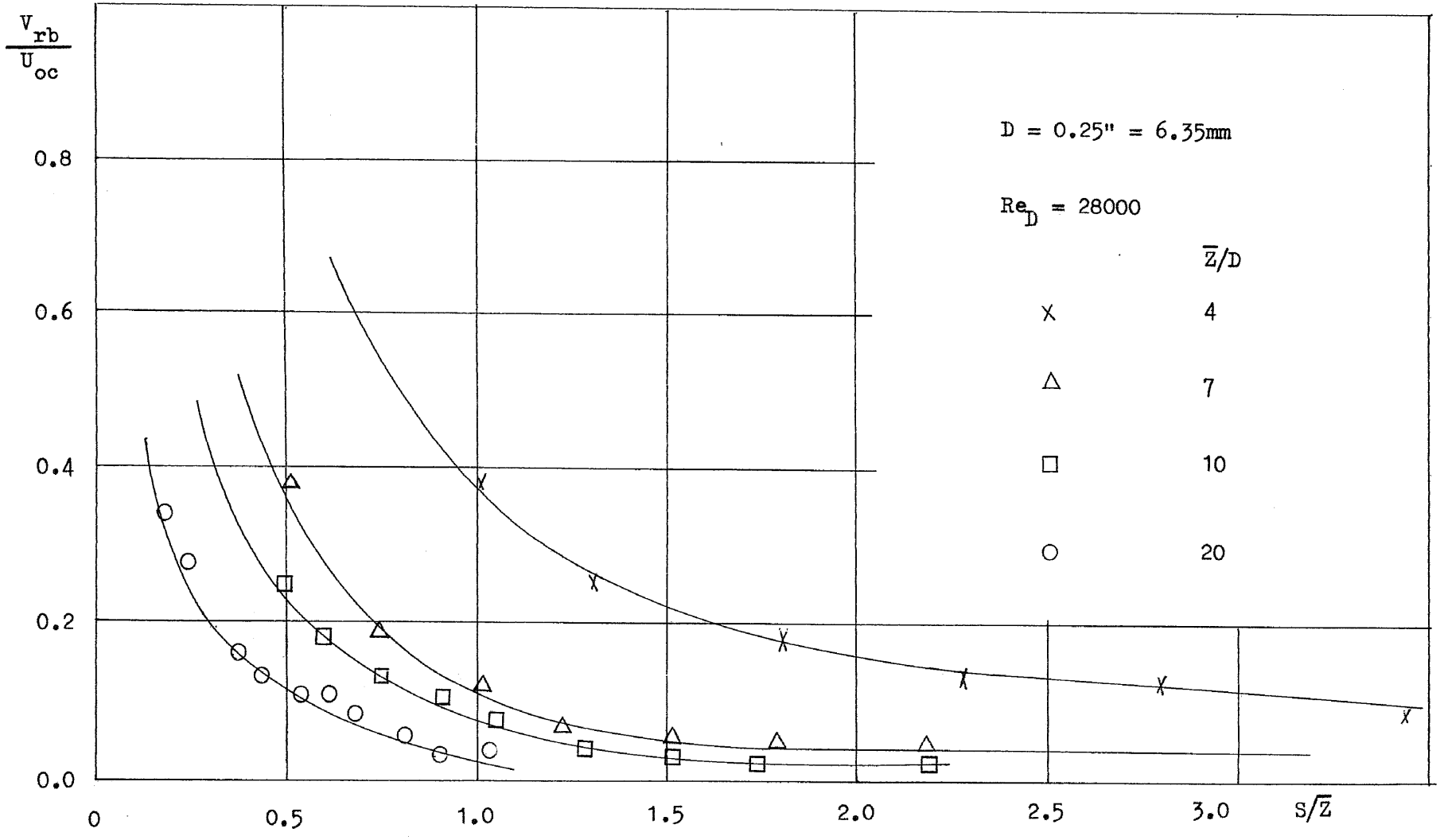

Fig. 84 Distribution of Reference Boundary Velocity of Wall Jet

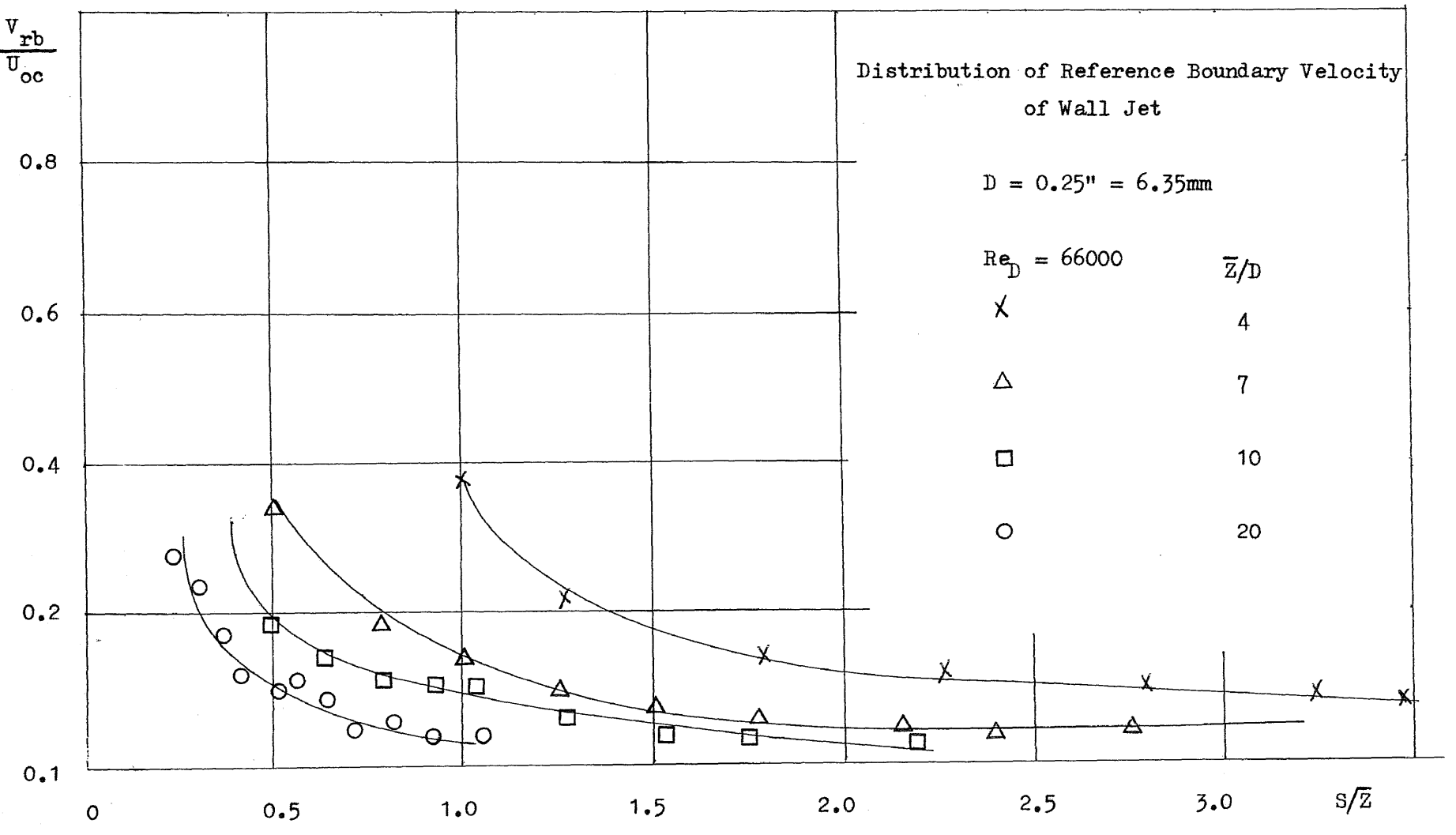
$\frac{V_{rb}}{U_{oc}}$
0.8
0.6
0.4
0.2
0.1
0
0.5
1.0
1.5
2.0
2.5
3.0
S/$\bar{Z}$
Distribution of Reference Boundary Velocity of Wall Jet
D = 0.25" = 6.35mm
Re_D = 66000
$\bar{Z}$/D
4
7
10
20

Fig. 85

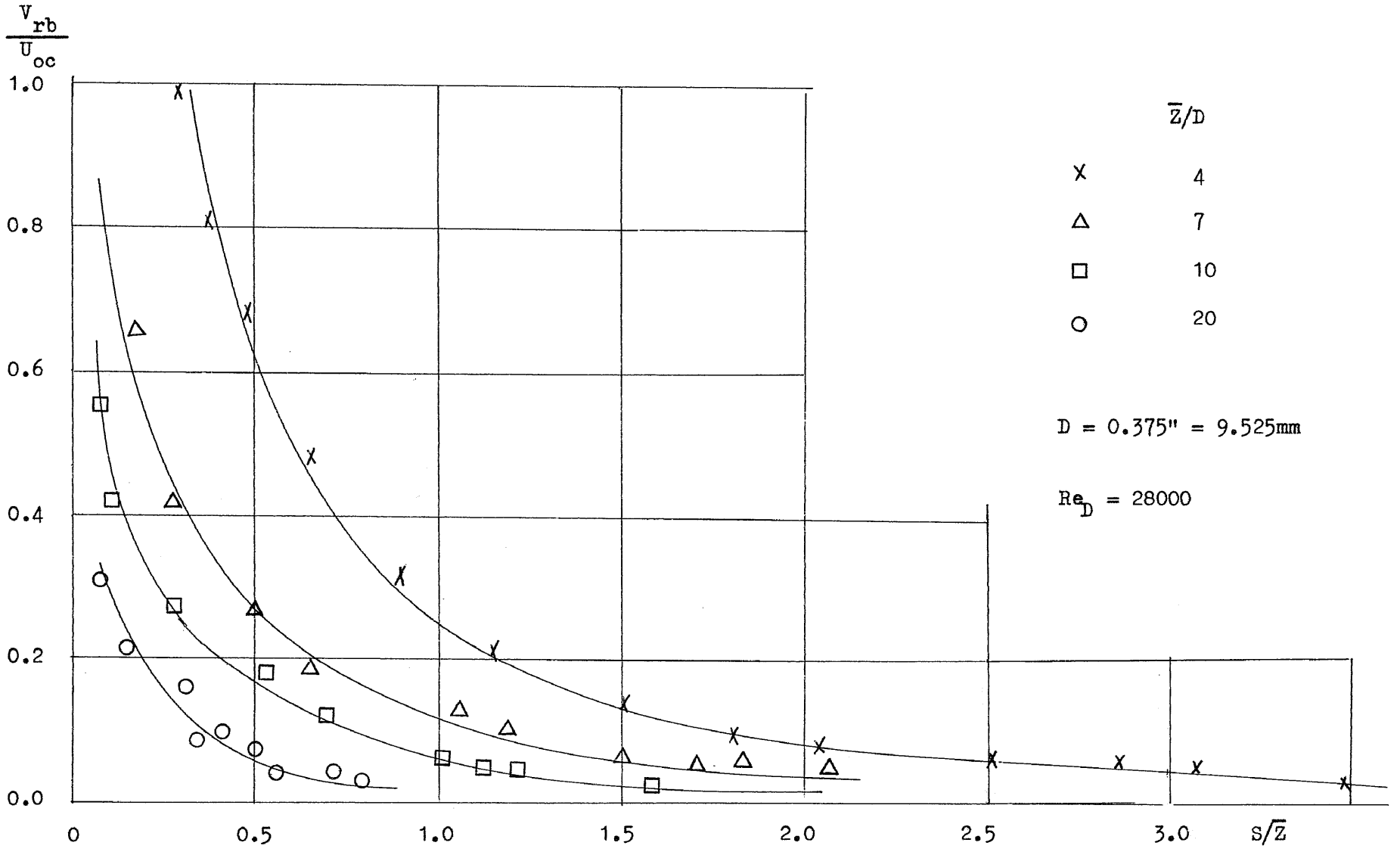

Fig. 86 Distribution of Reference Boundary Velocity of Wall Jet

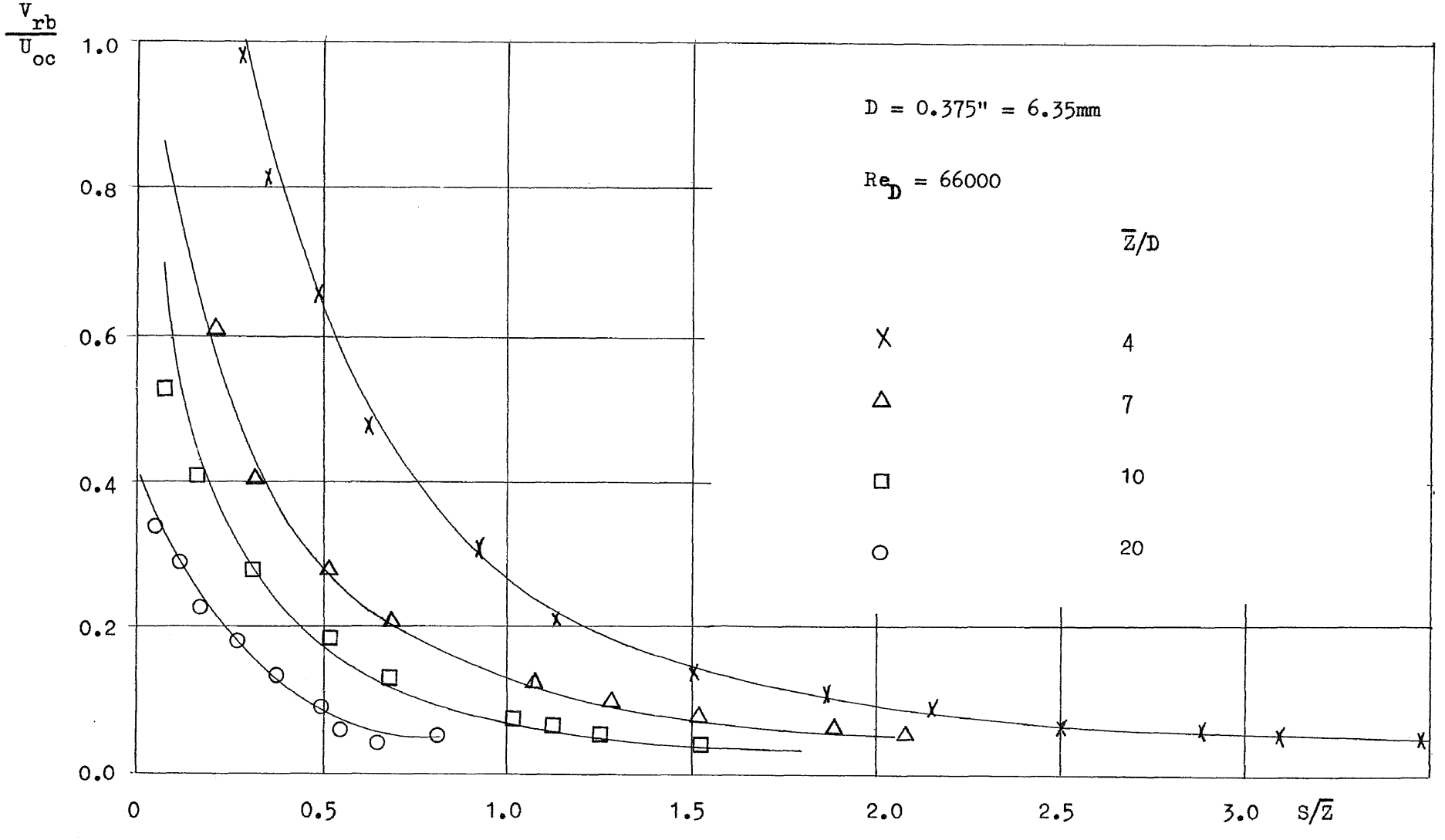

Fig. 87 Distribution of Reference Boundary Velocity of Wall Jet

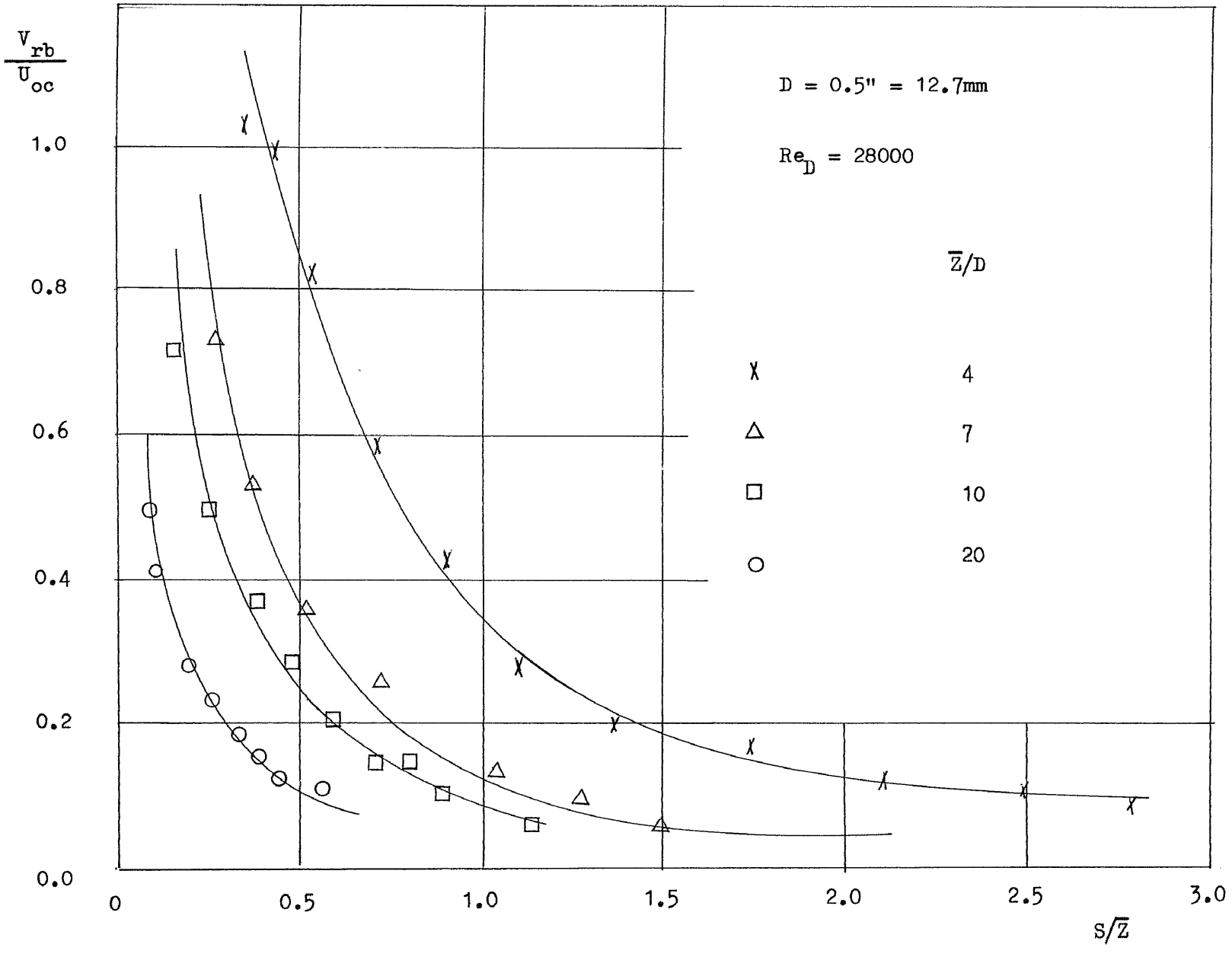

Fig. 88 Distribution of Reference Boundary Velocity of Wall Jet

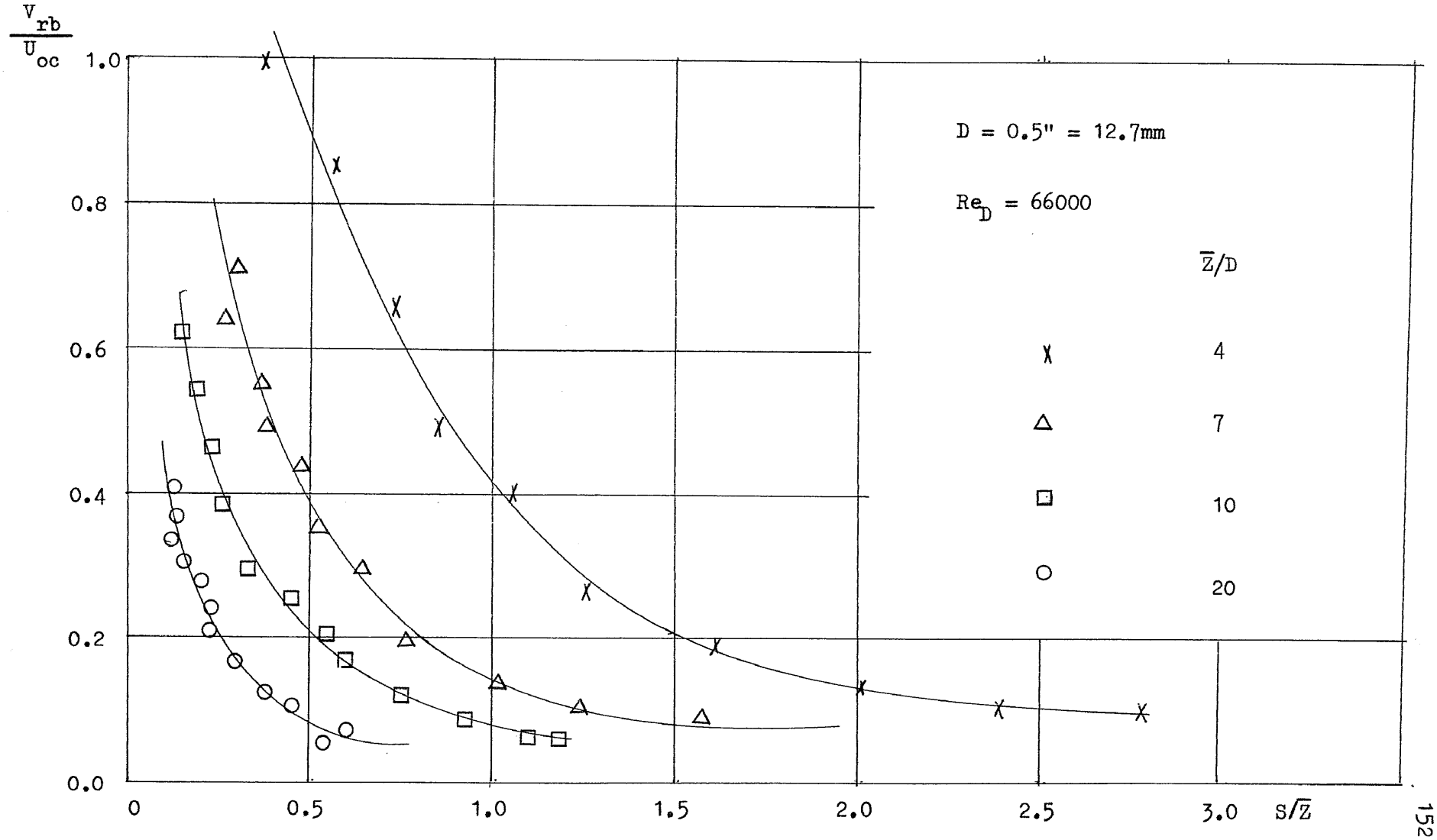

Fig. 89 Distribution of Reference Boundary Velocity of Wall Jet

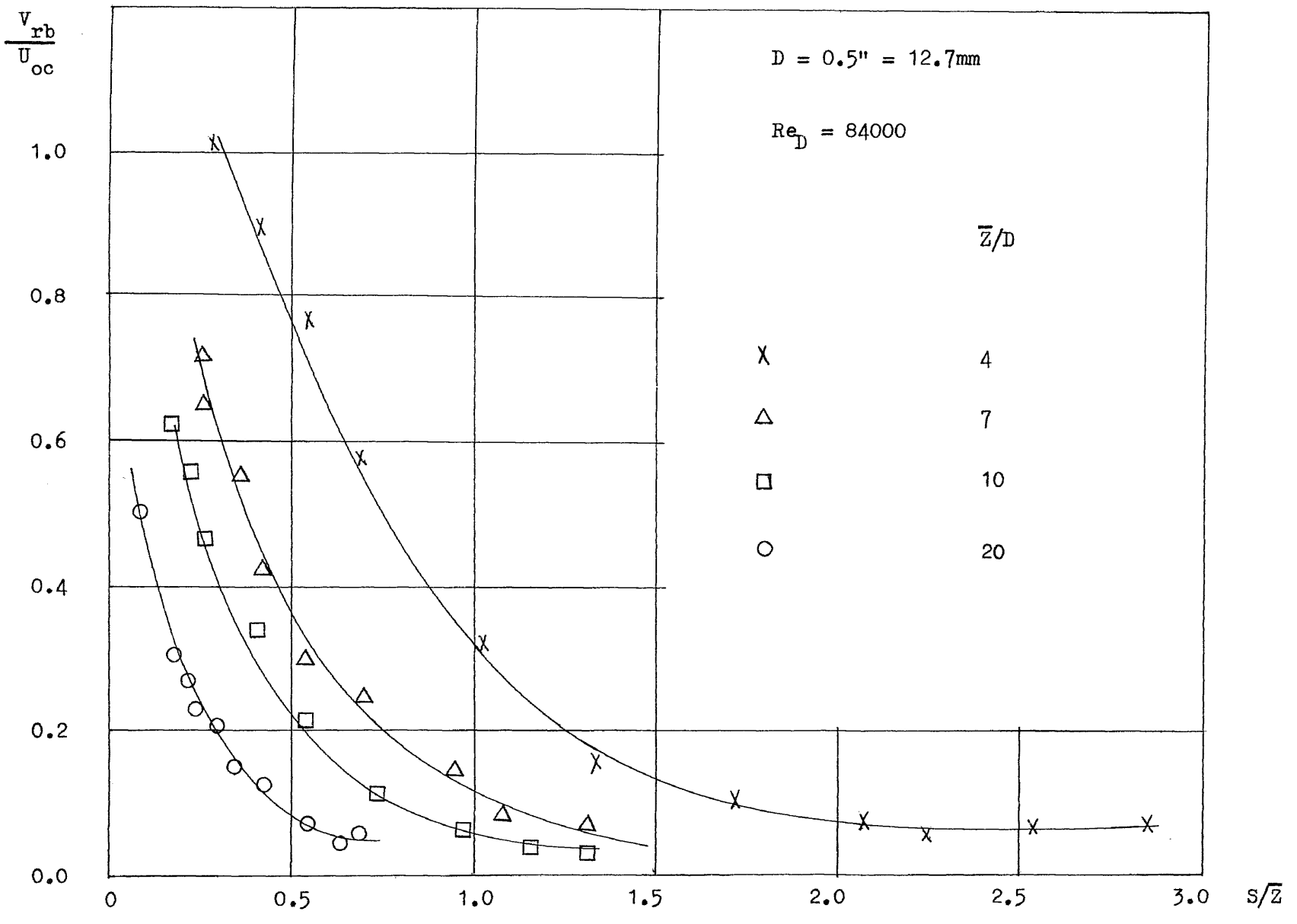

Fig. 90 Distribution of Reference Boundary Velocity of Wall Jet

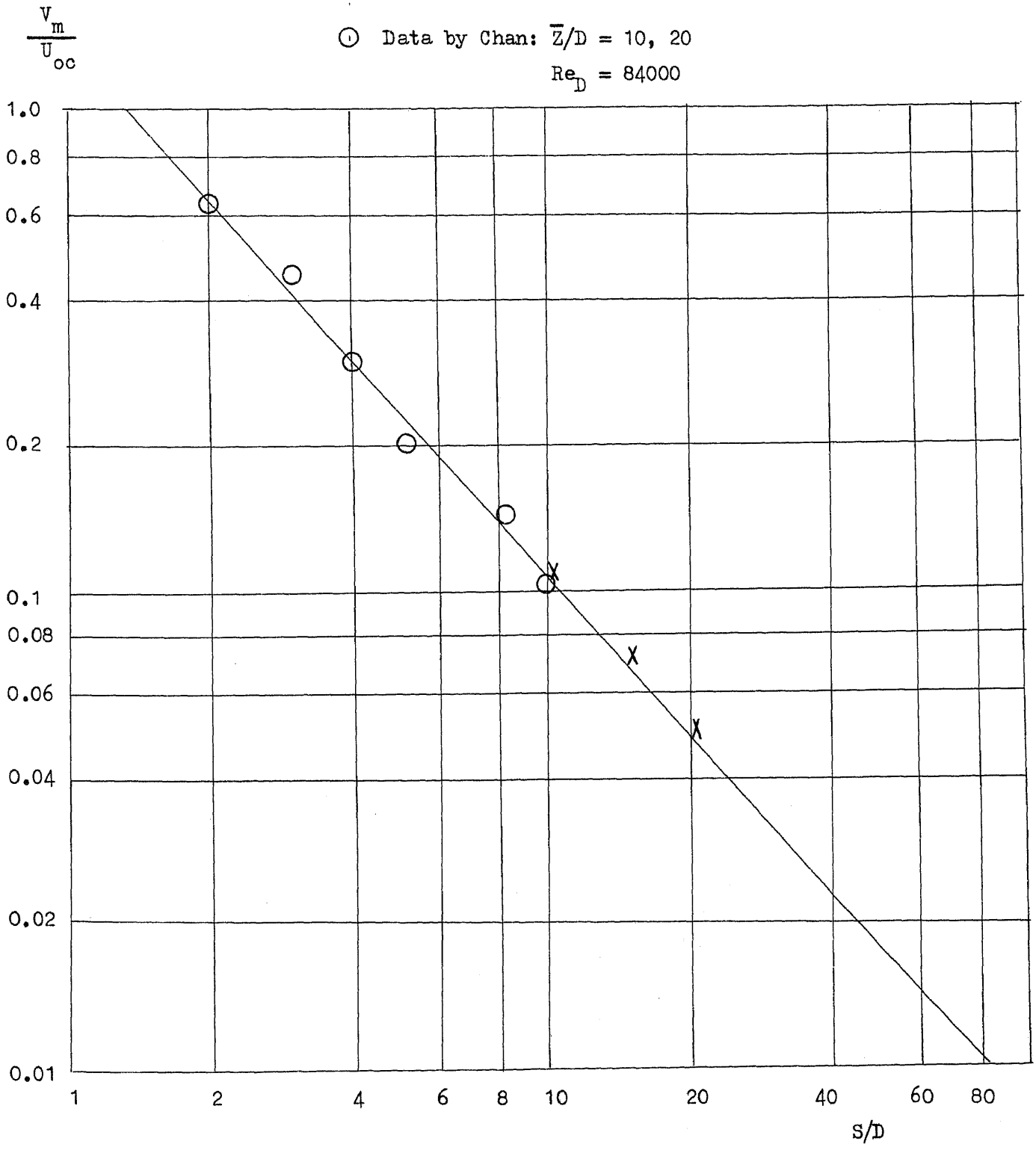

Fig. 91 Maximum Velocity Decay of Radial Wall Jet
(A Comparison)

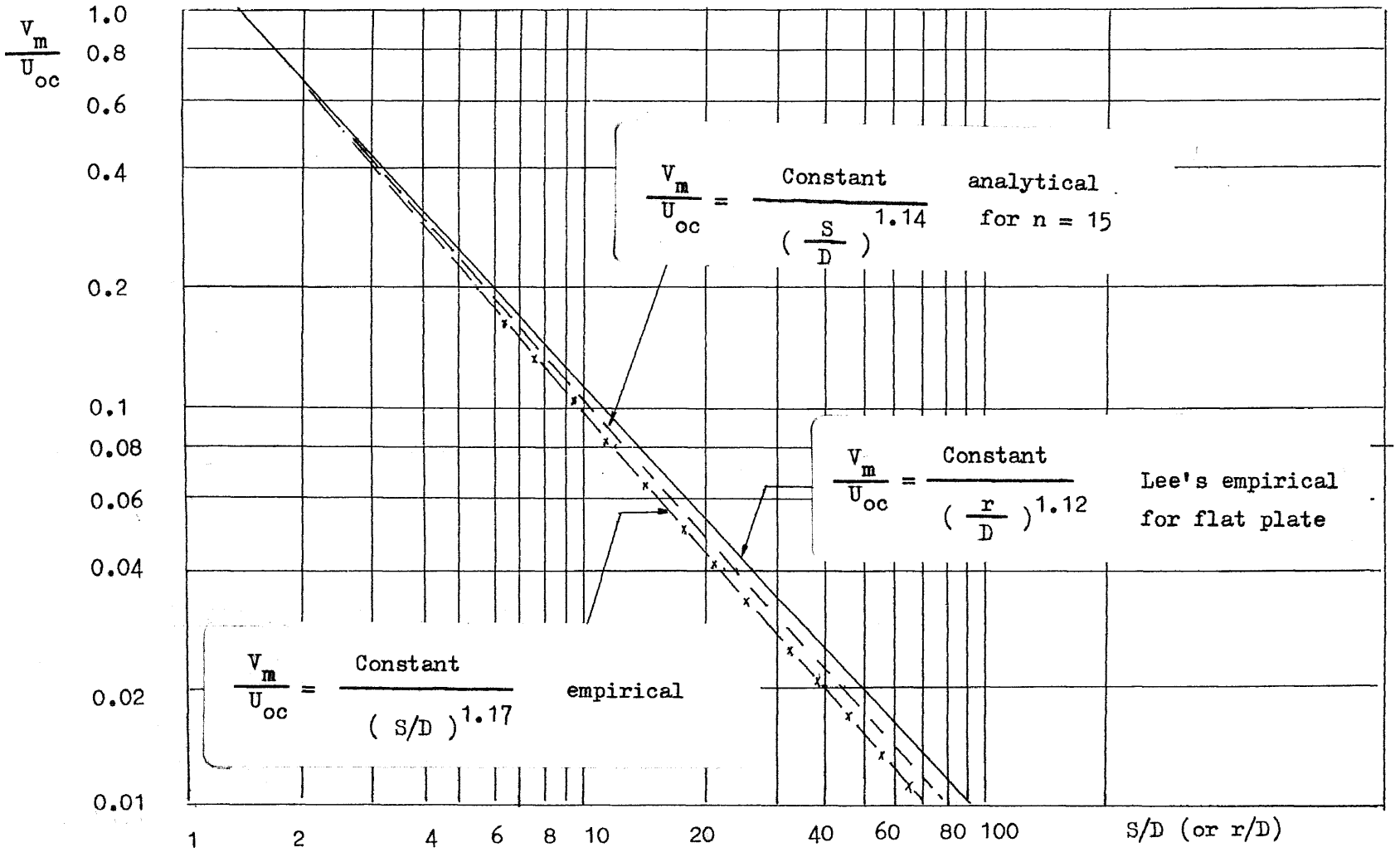

Fig. 92 Wall Jet Maximum Velocity Decay (A Comparison)

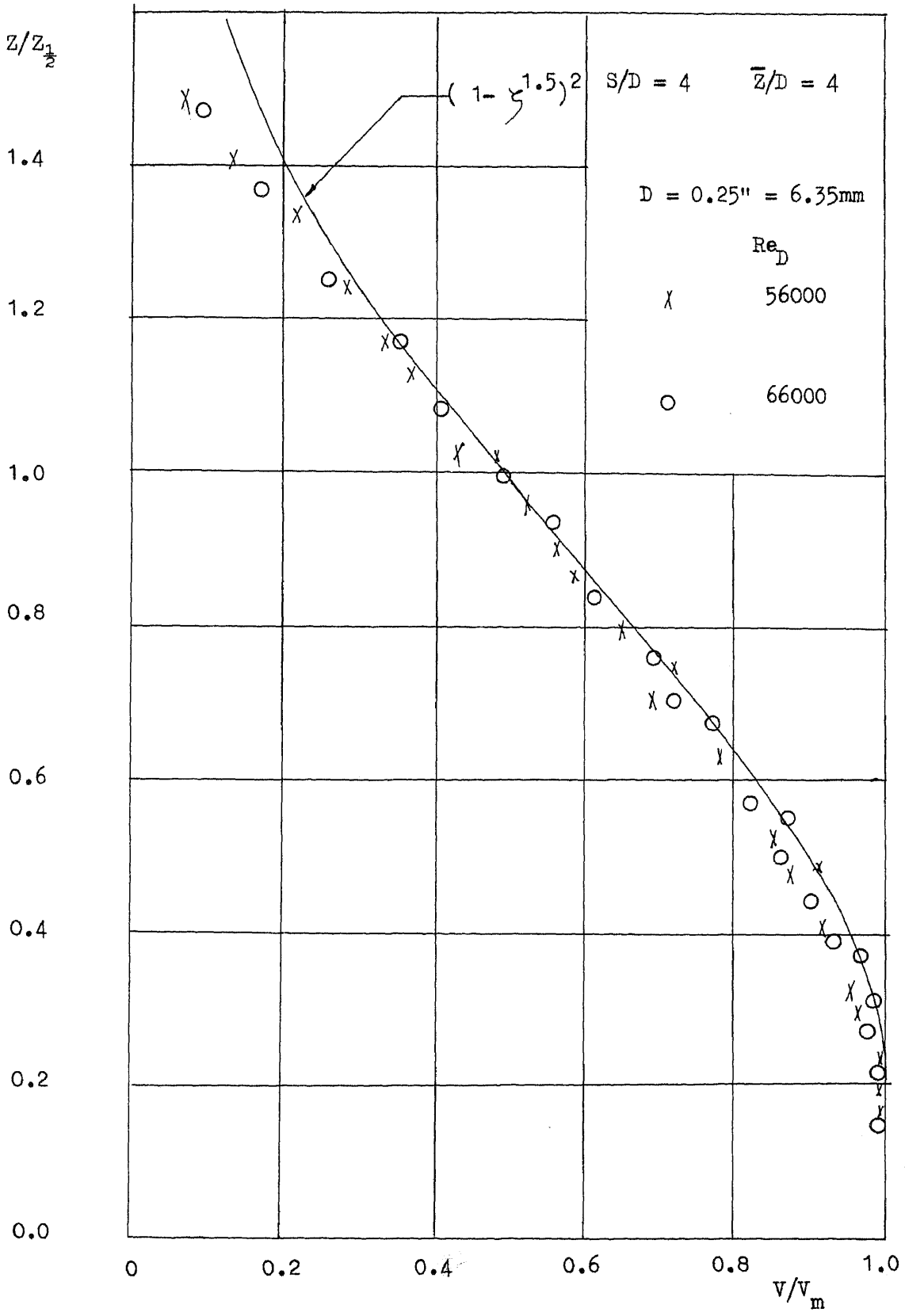

Velocity Profile of Wall Jet

Fig. 93

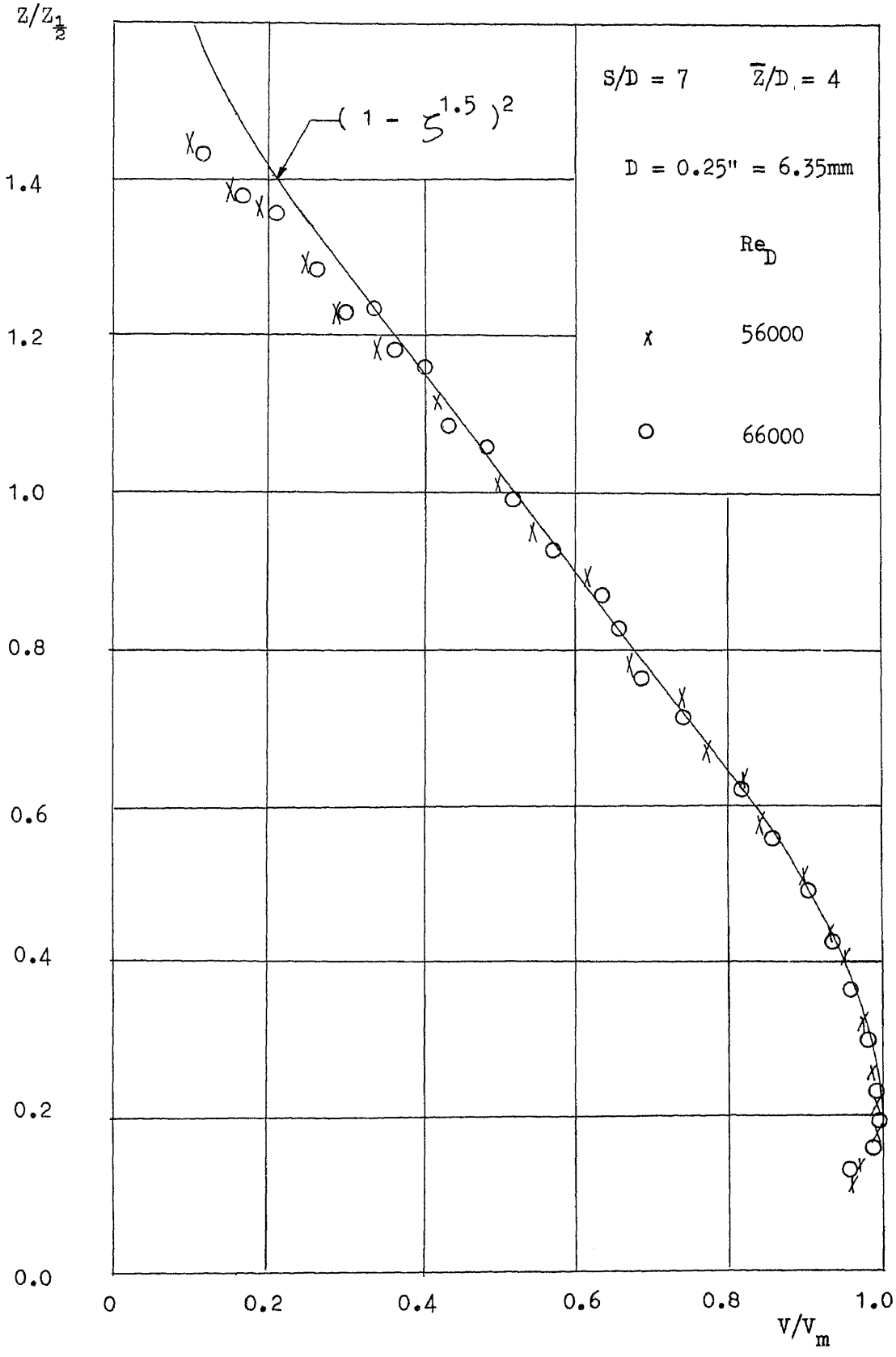

Velocity Profile of Wall Jet

Fig. 94

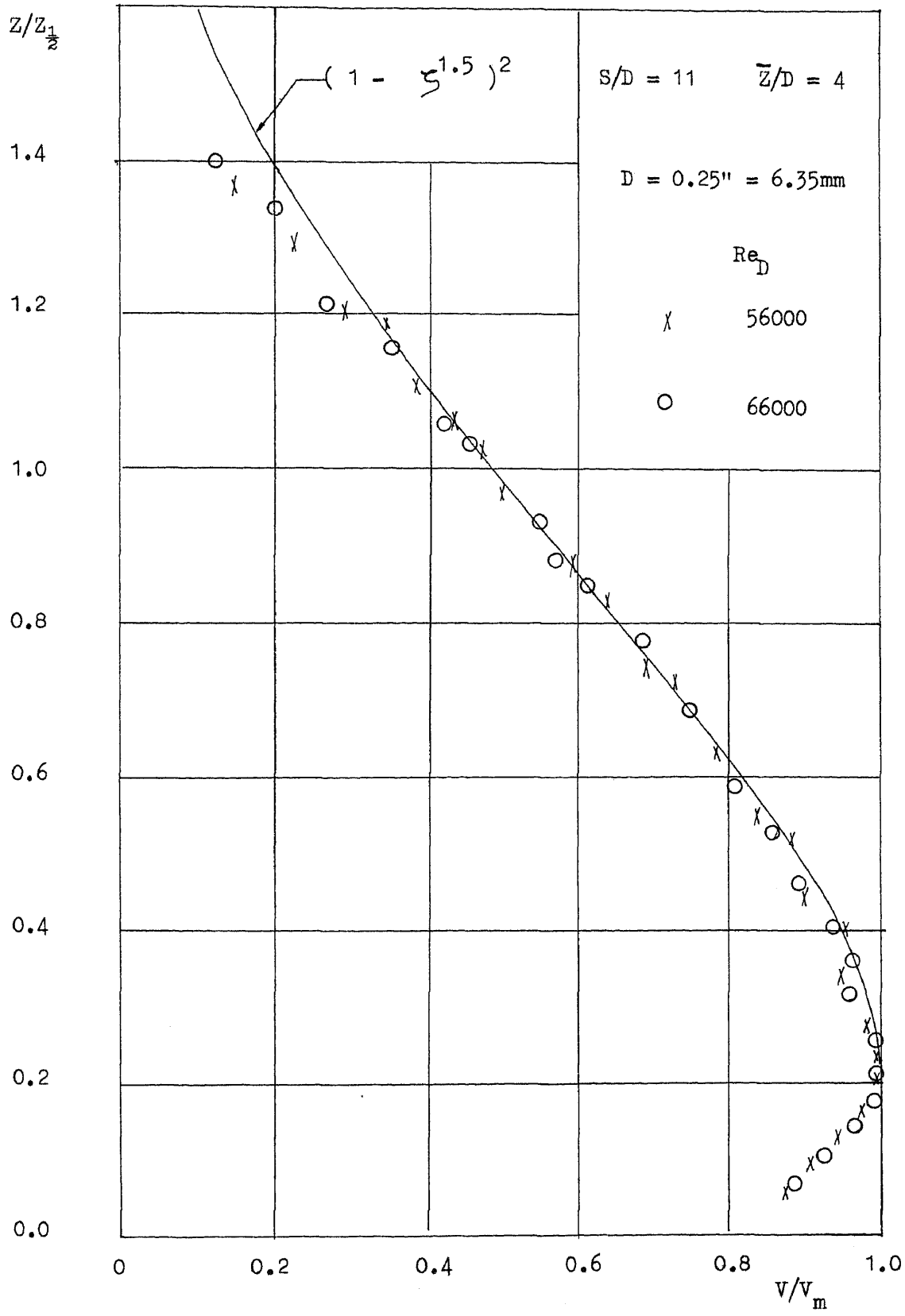

Velocity Profile of Wall Jet

Fig. 95

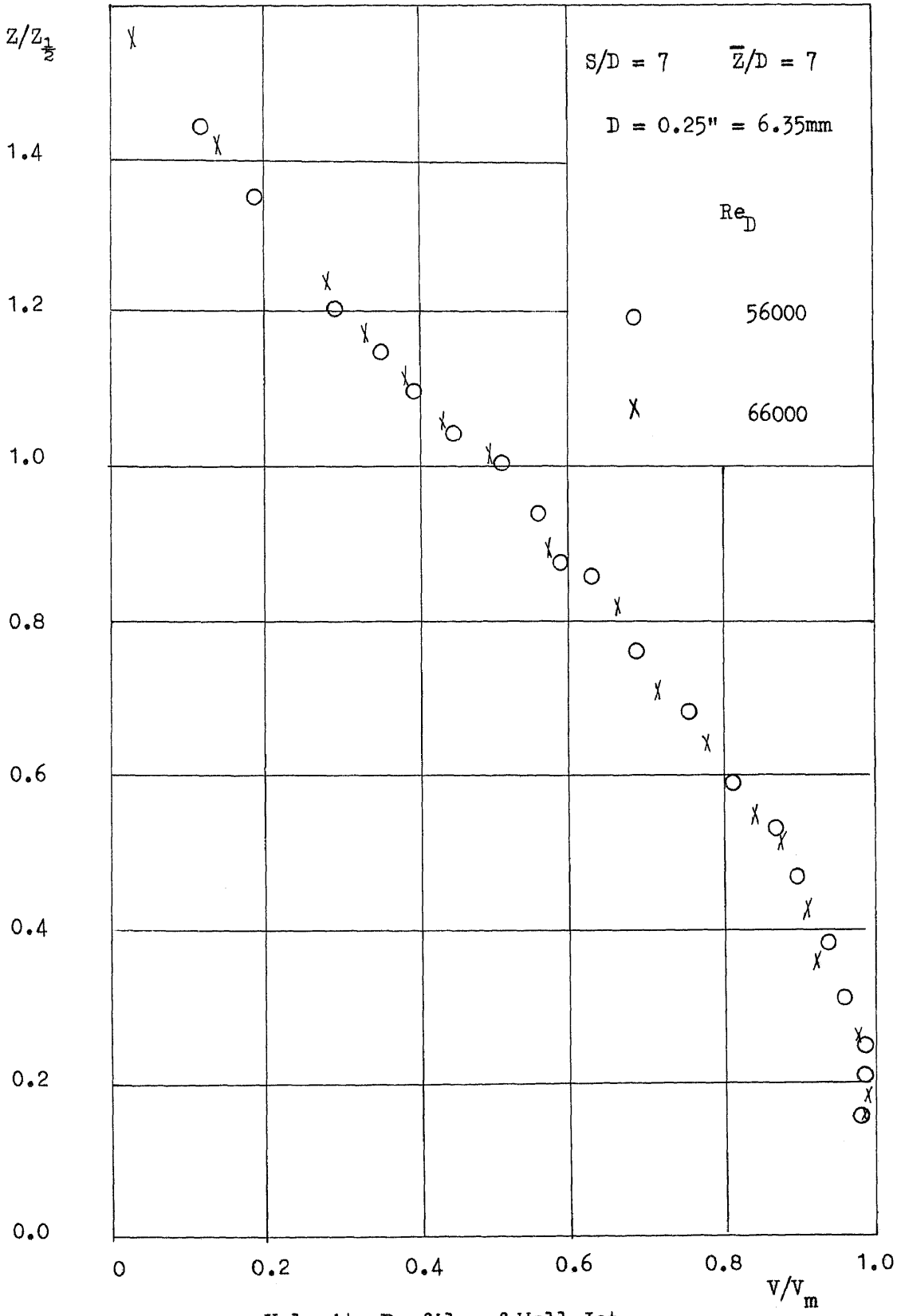

Velocity Profile of Wall Jet

Fig. 96

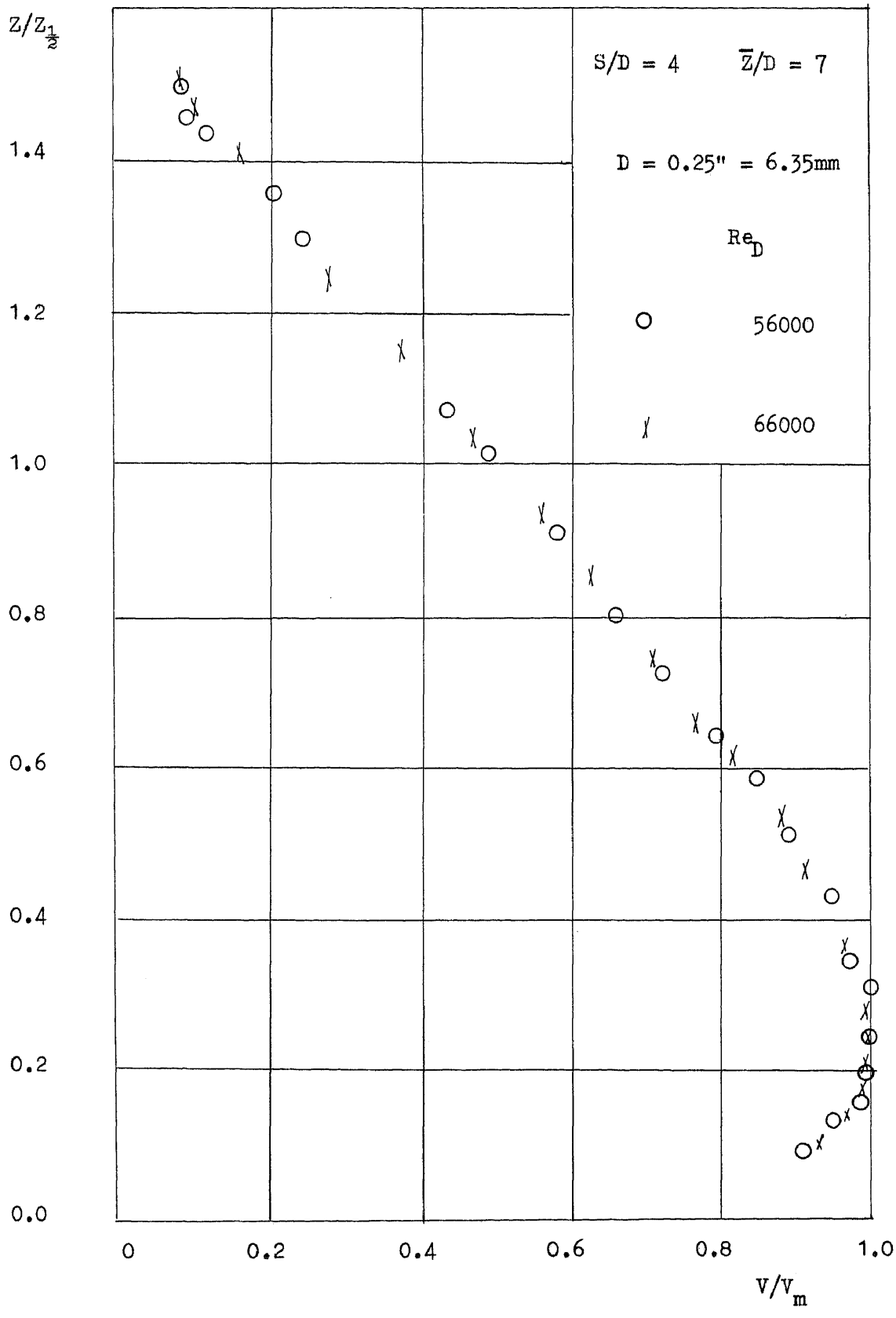

Velocity Profile of Wall Jet

Fig. 97

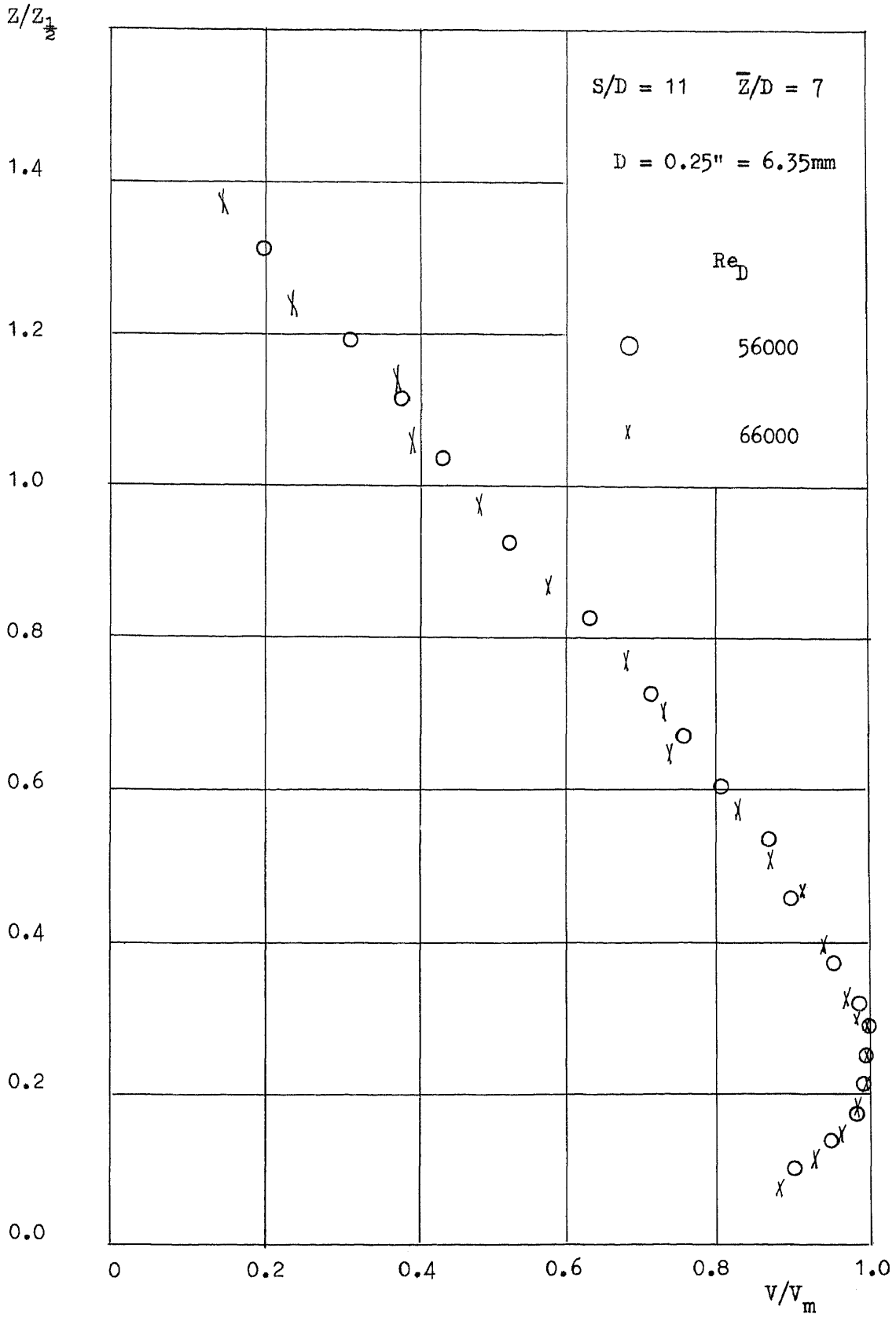

Fig. 98 Velocity Profile of Wall Jet

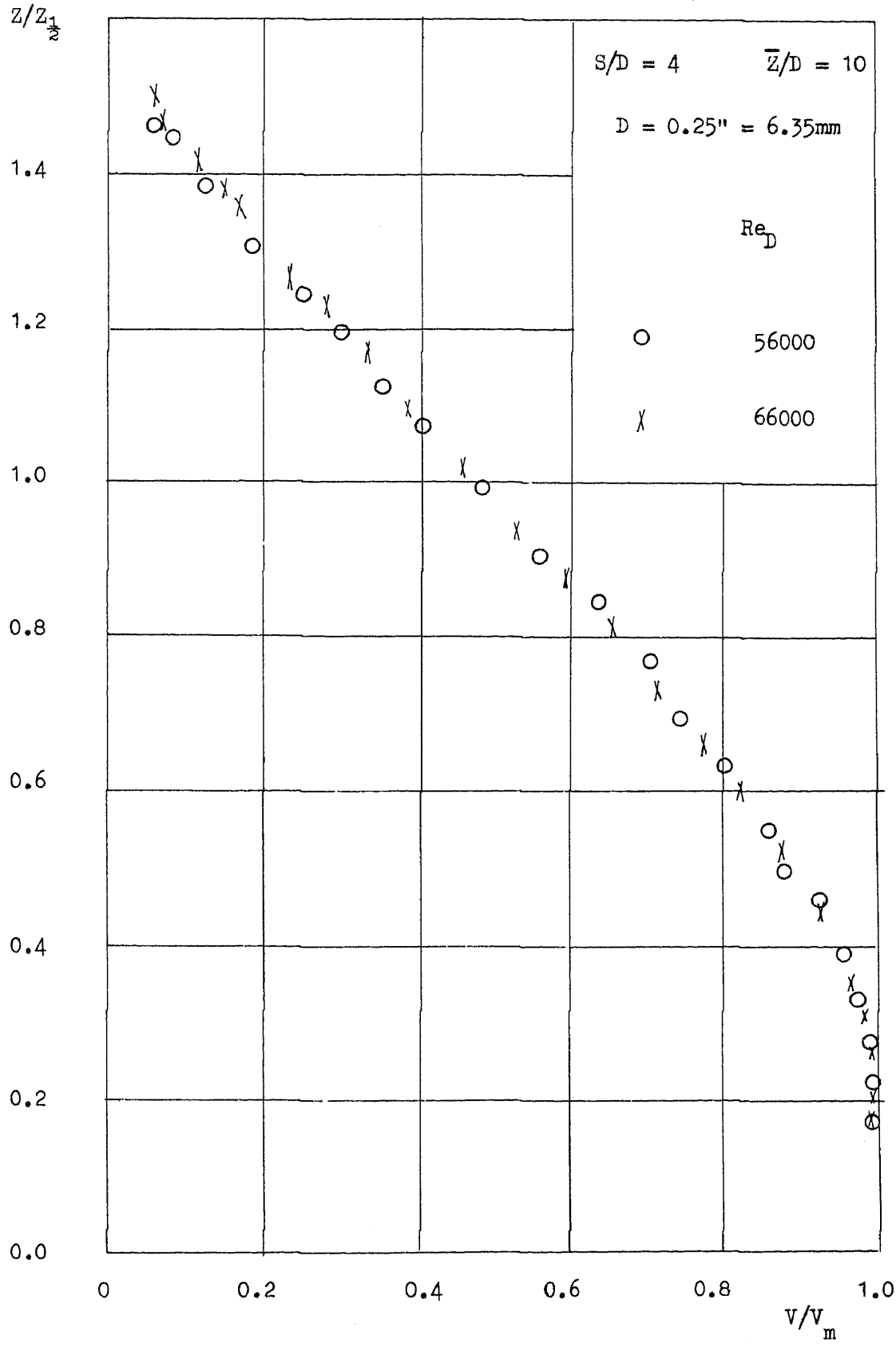

Fig. 99 Velocity Profile of Wall Jet

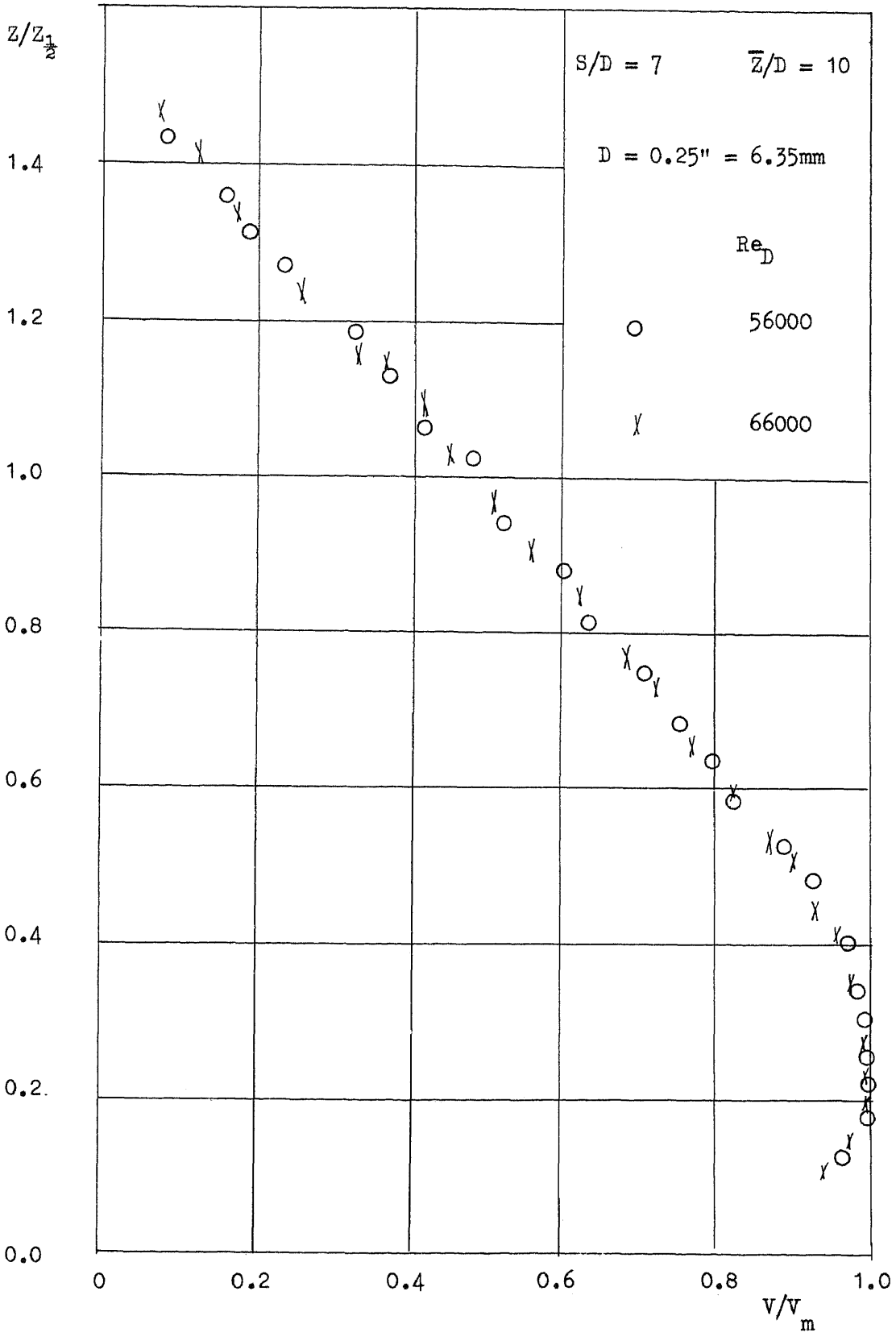

Fig. 100 Velocity Profile of Wall Jet

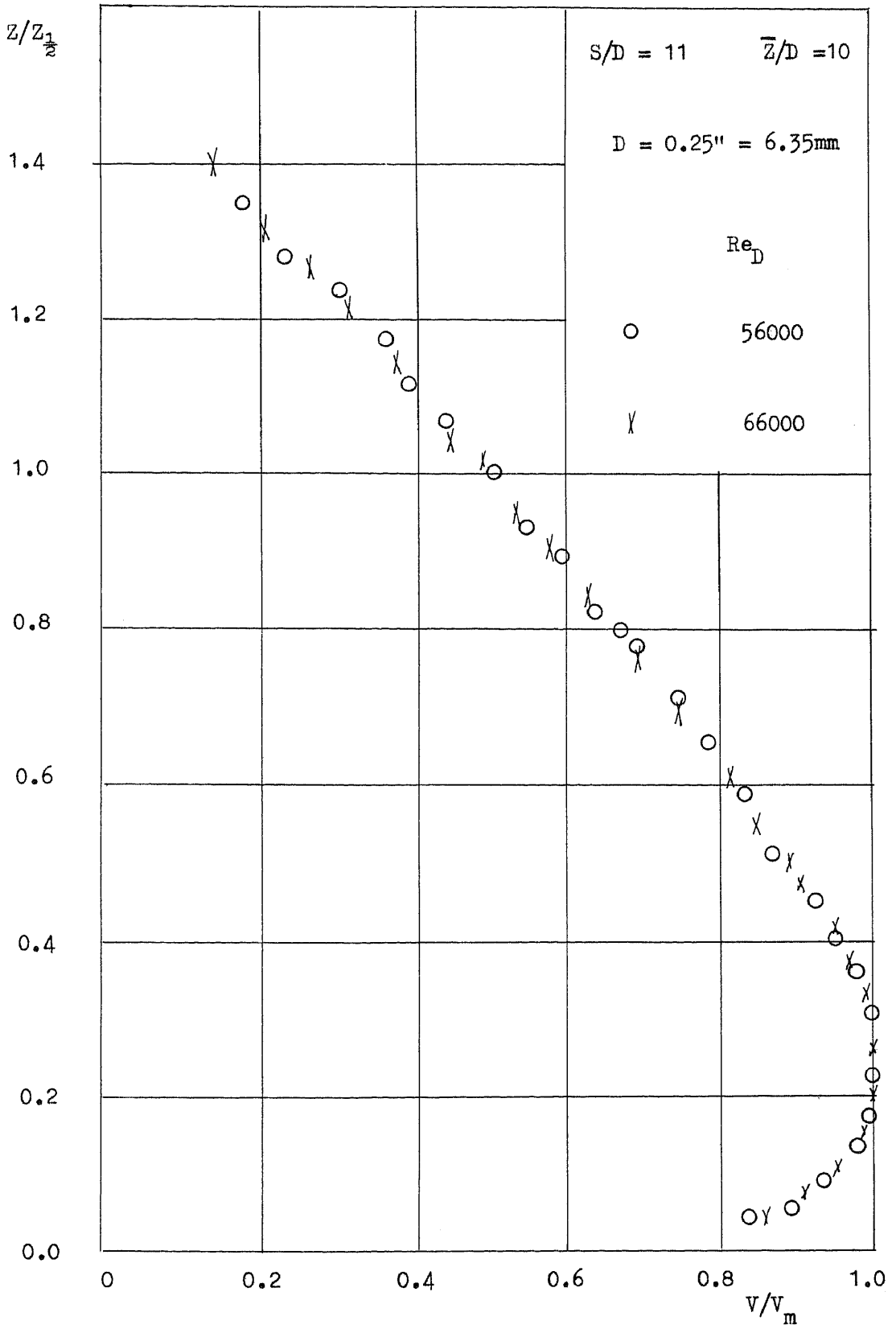

Fig. 101 Velocity Profile of Wall Jet

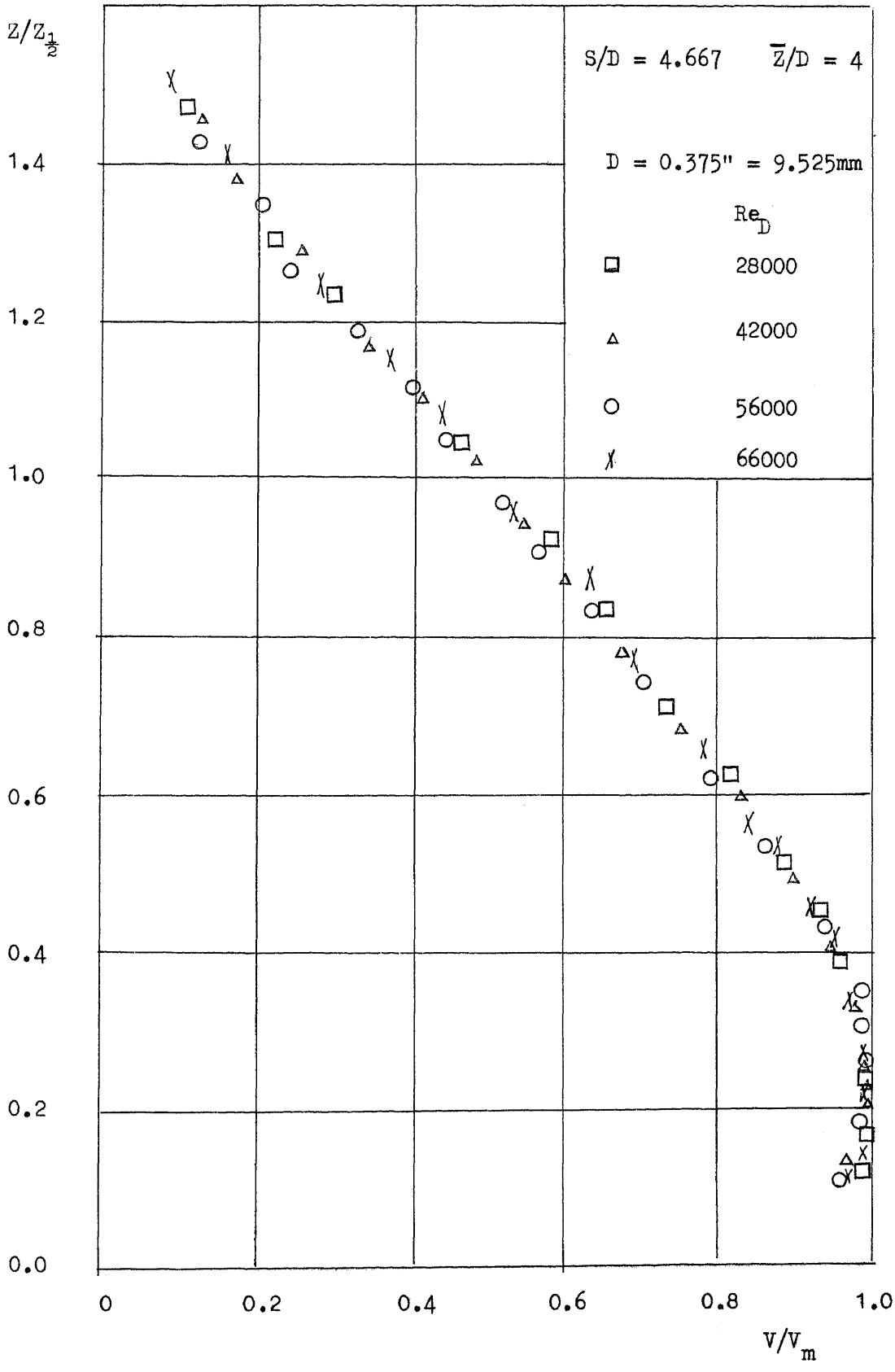

Fig. 102 Velocity Profile of Wall Jet

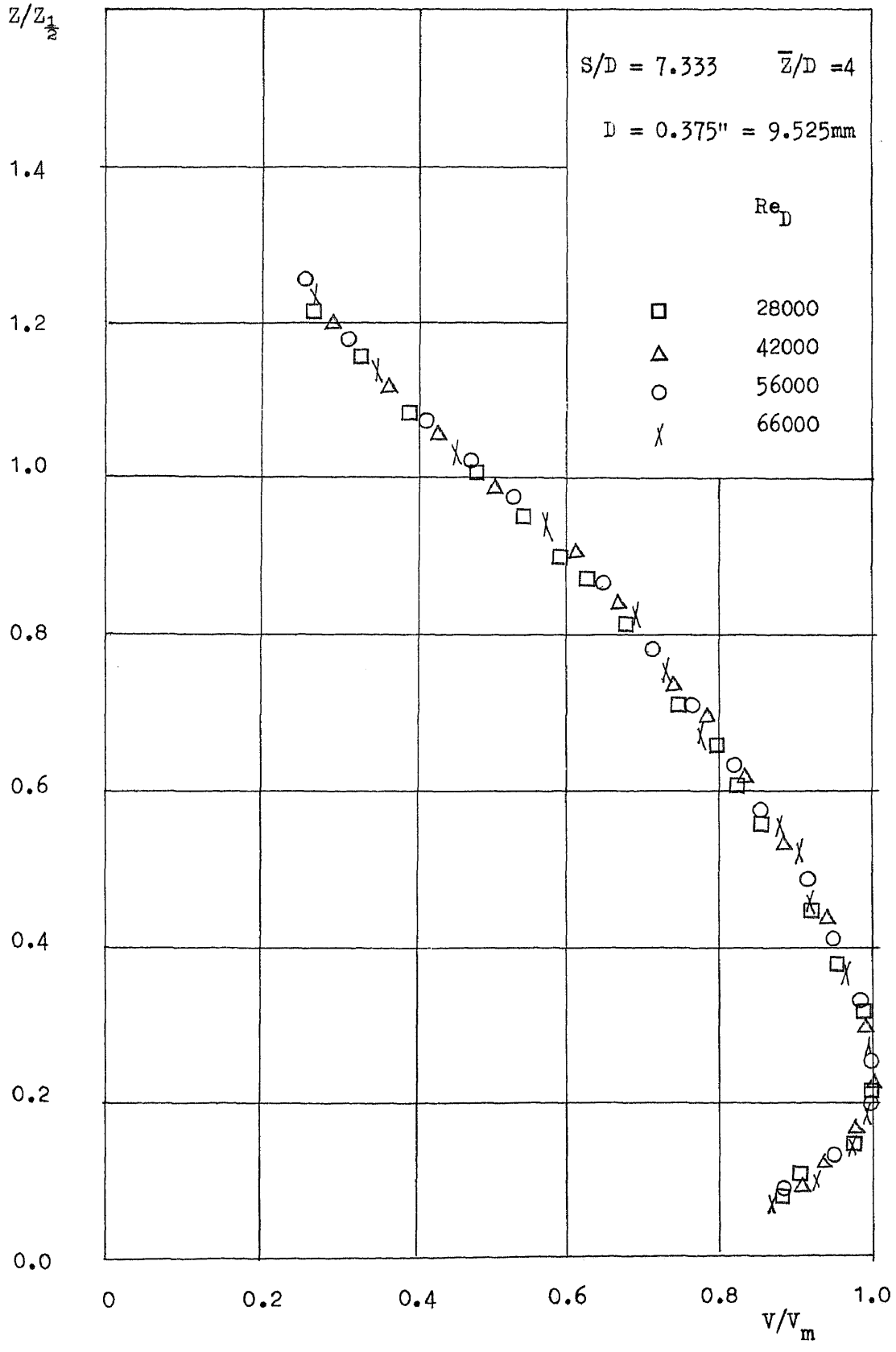

Fig. 103 Velocity Profile of Wall Jet

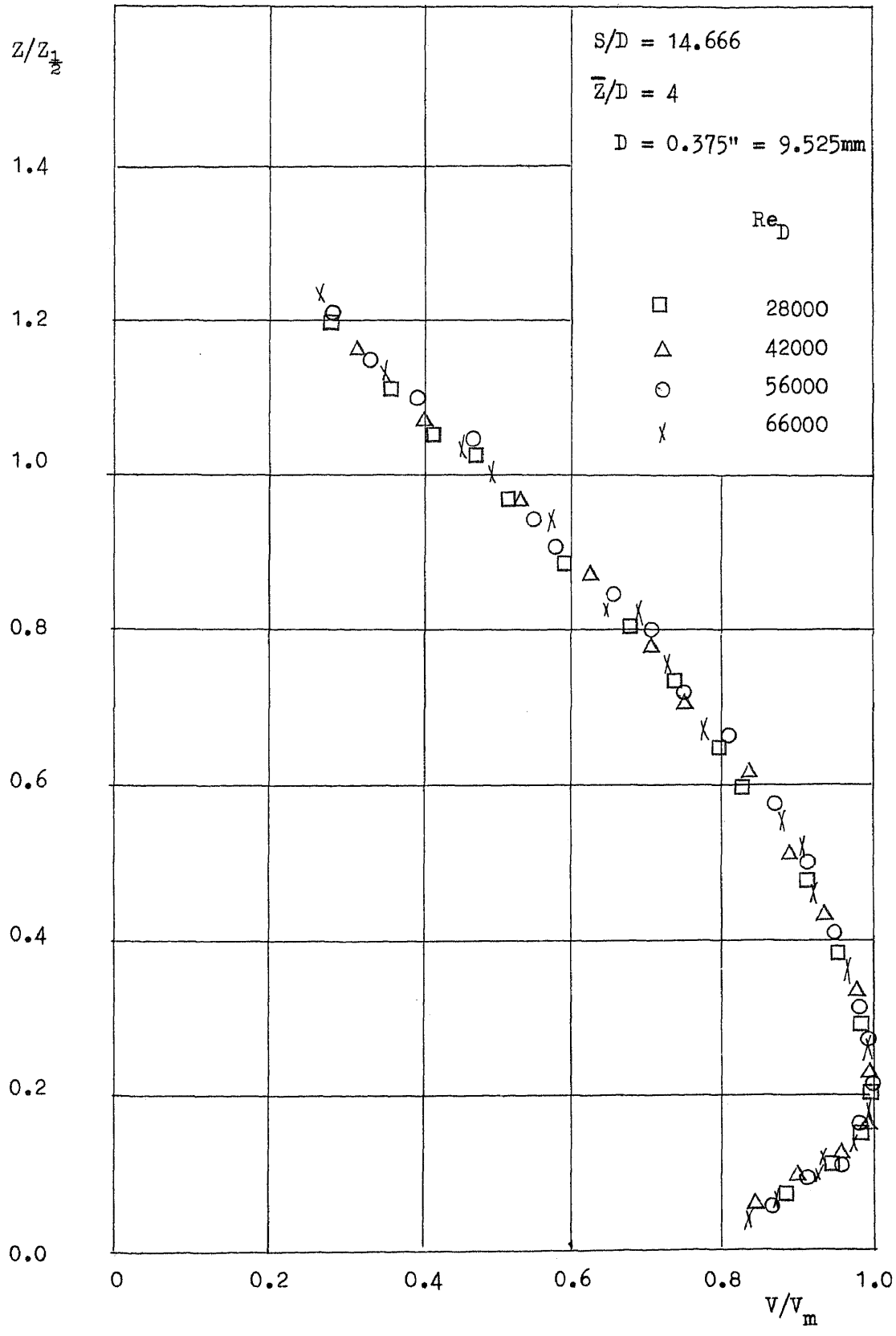

Fig. 104 Velocity Profile of Wall Jet

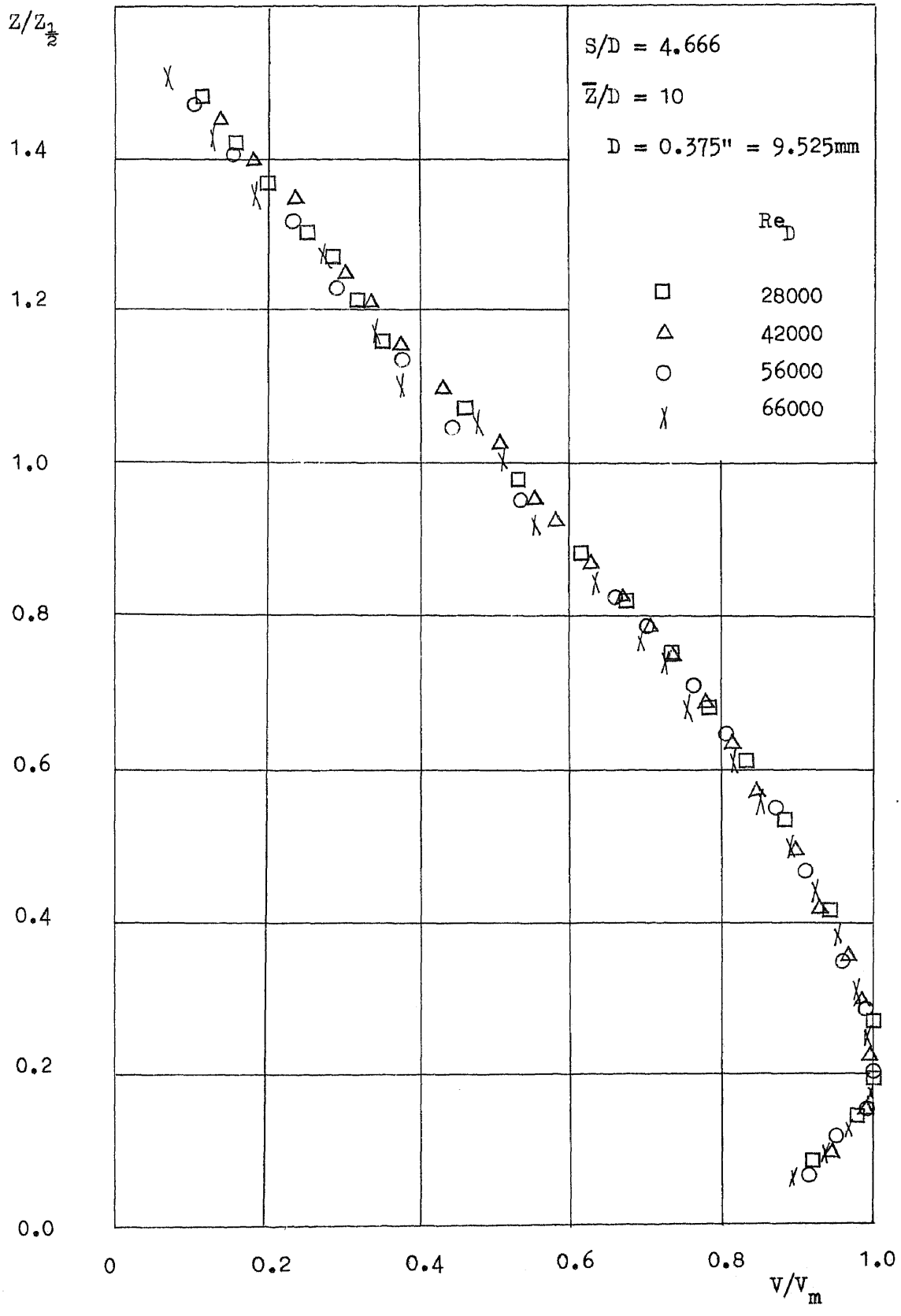

Fig. 105 Velocity Profile of Wall Jet

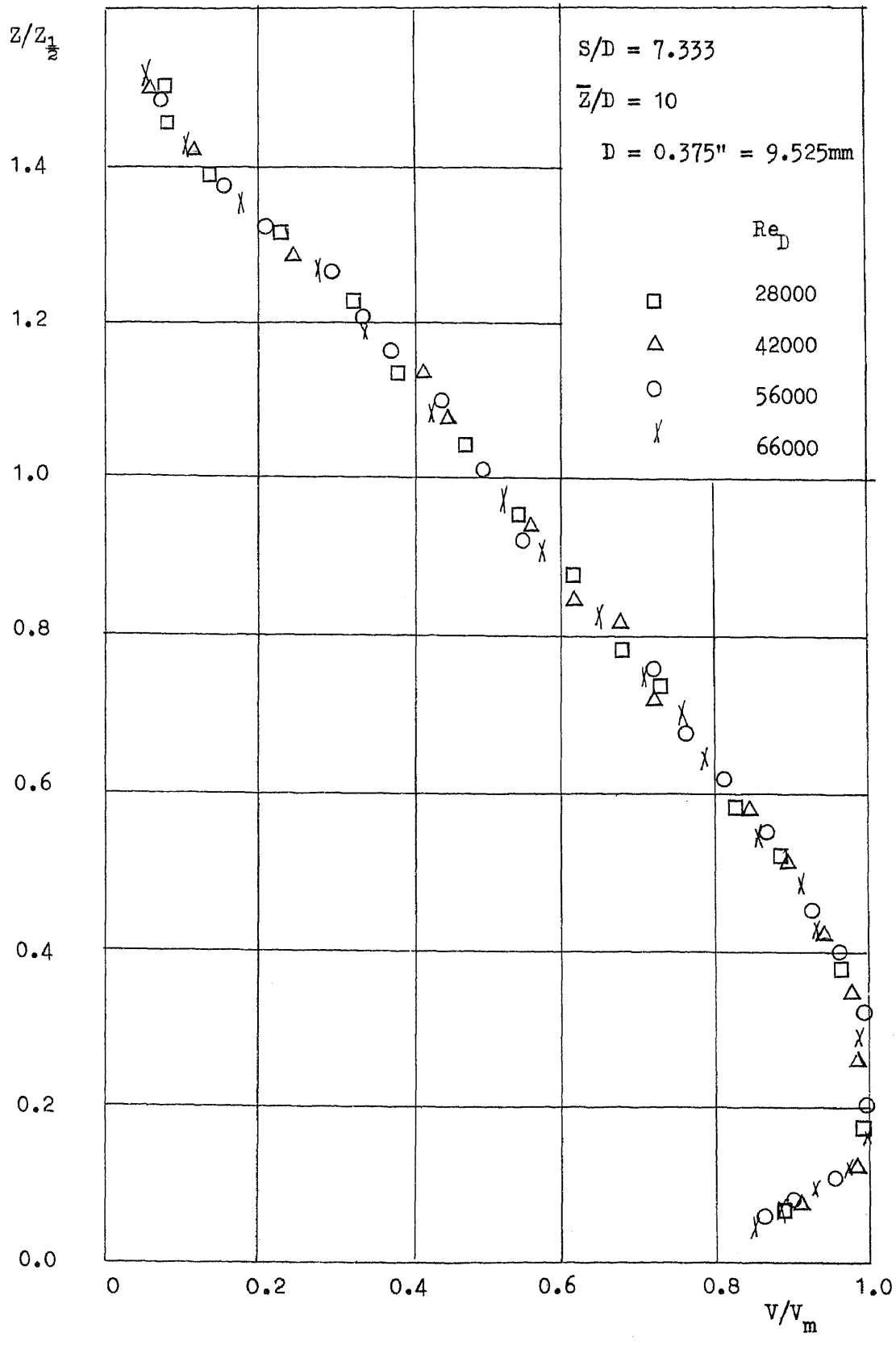

Fig. 106 Velocity Profile of Wall Jet

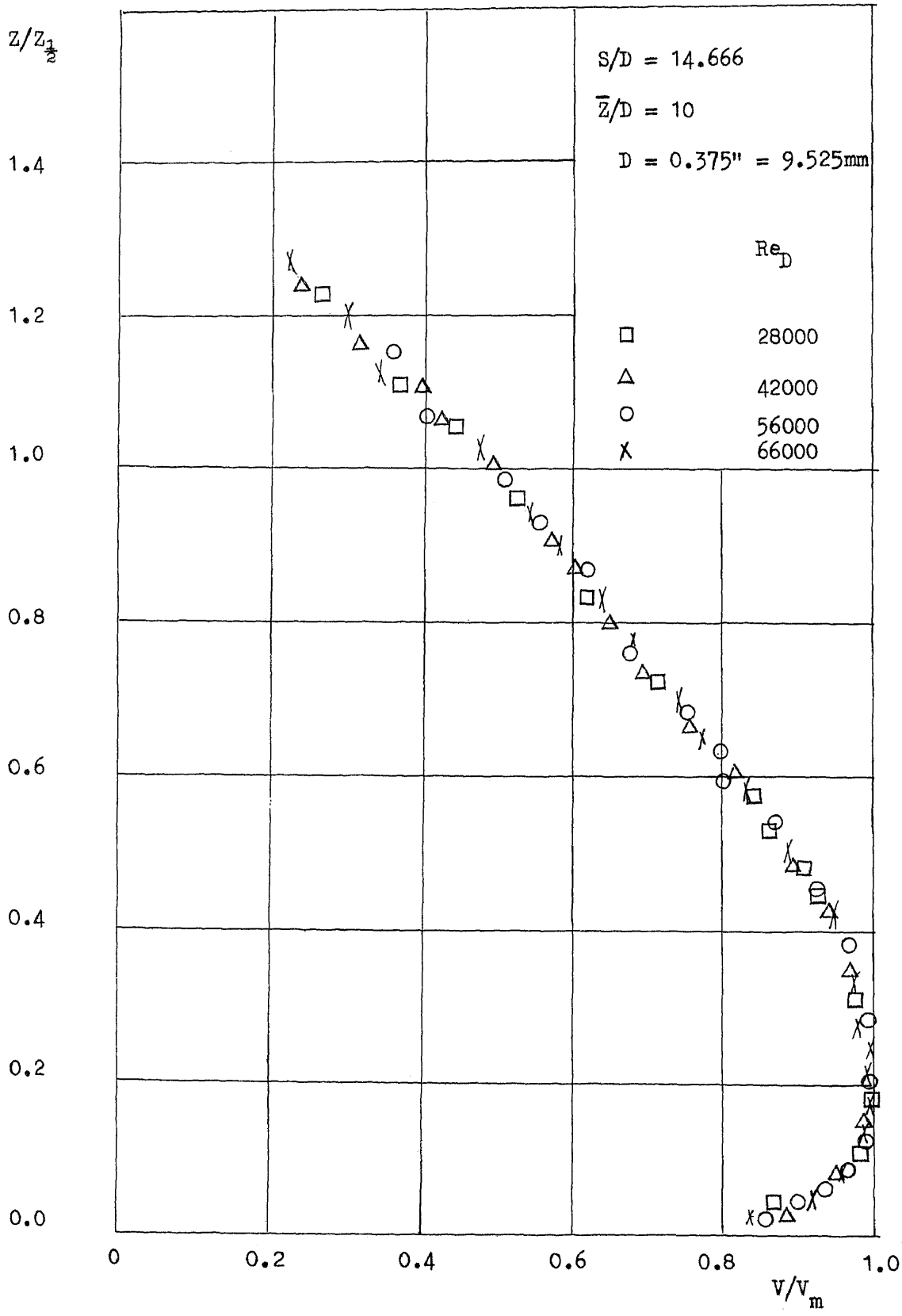

Fig. 107 Velocity Profile of Wall Jet

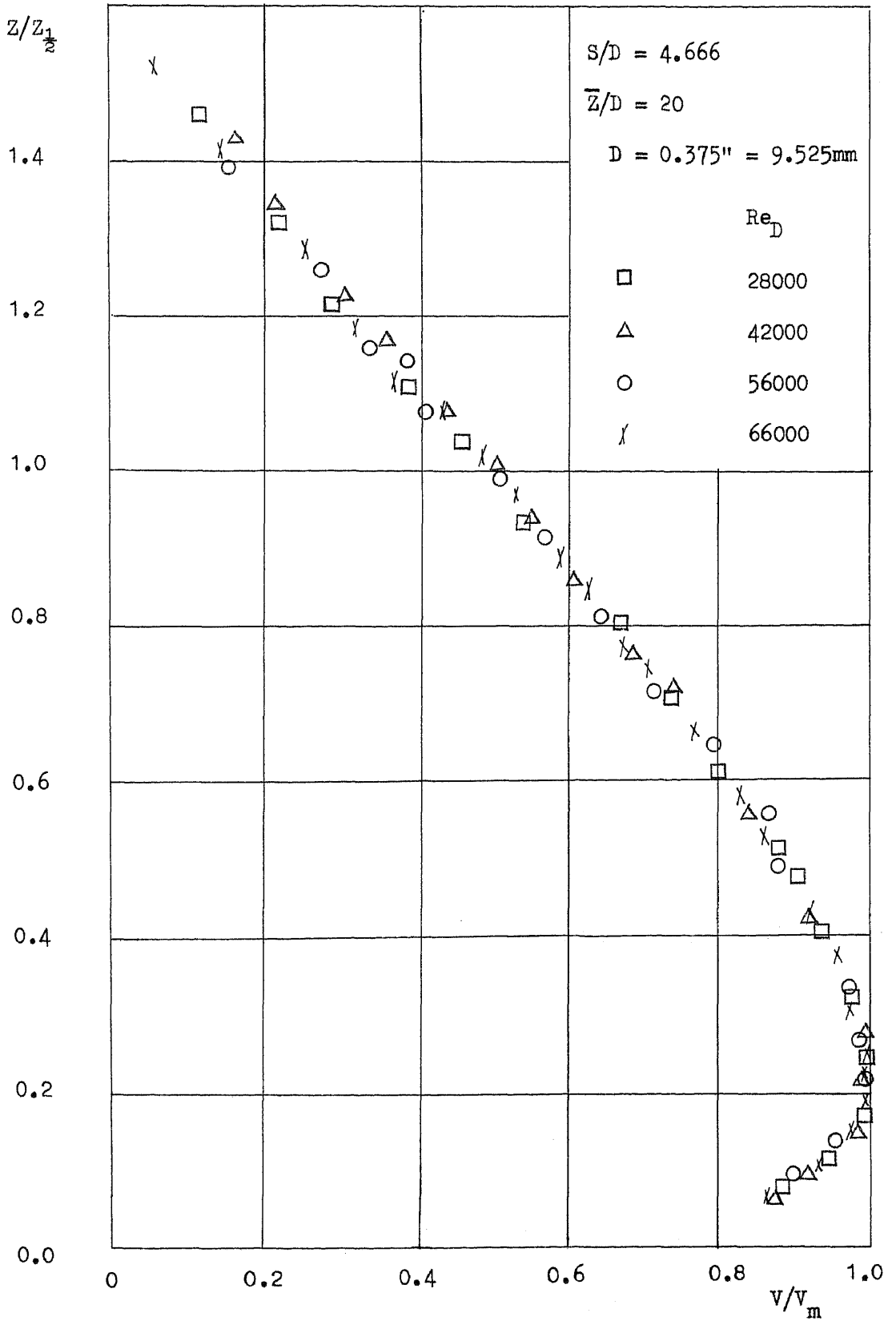

Fig. 108 Velocity Profile of Wall Jet

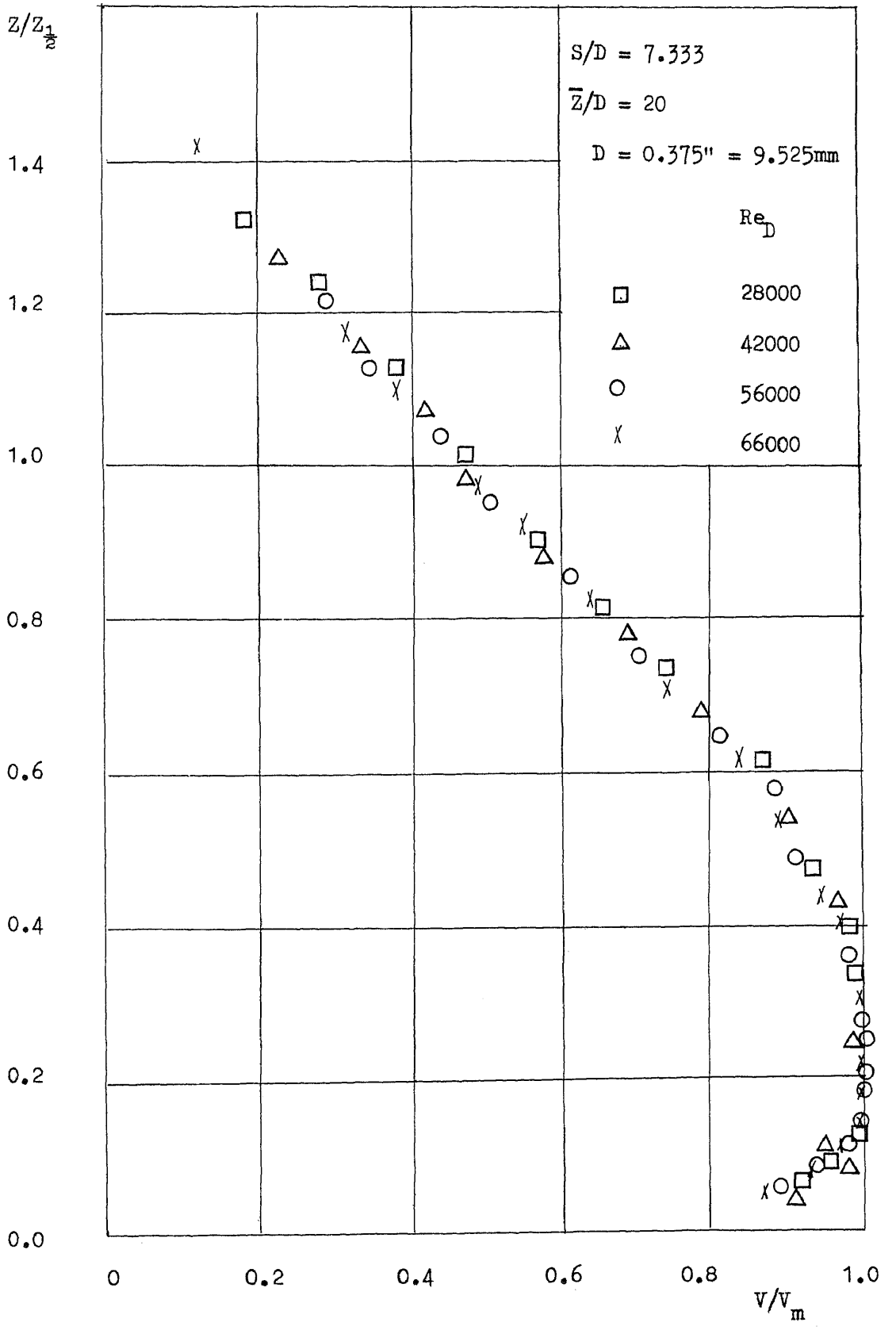

Fig. 109 Velocity Profile of Wall Jet

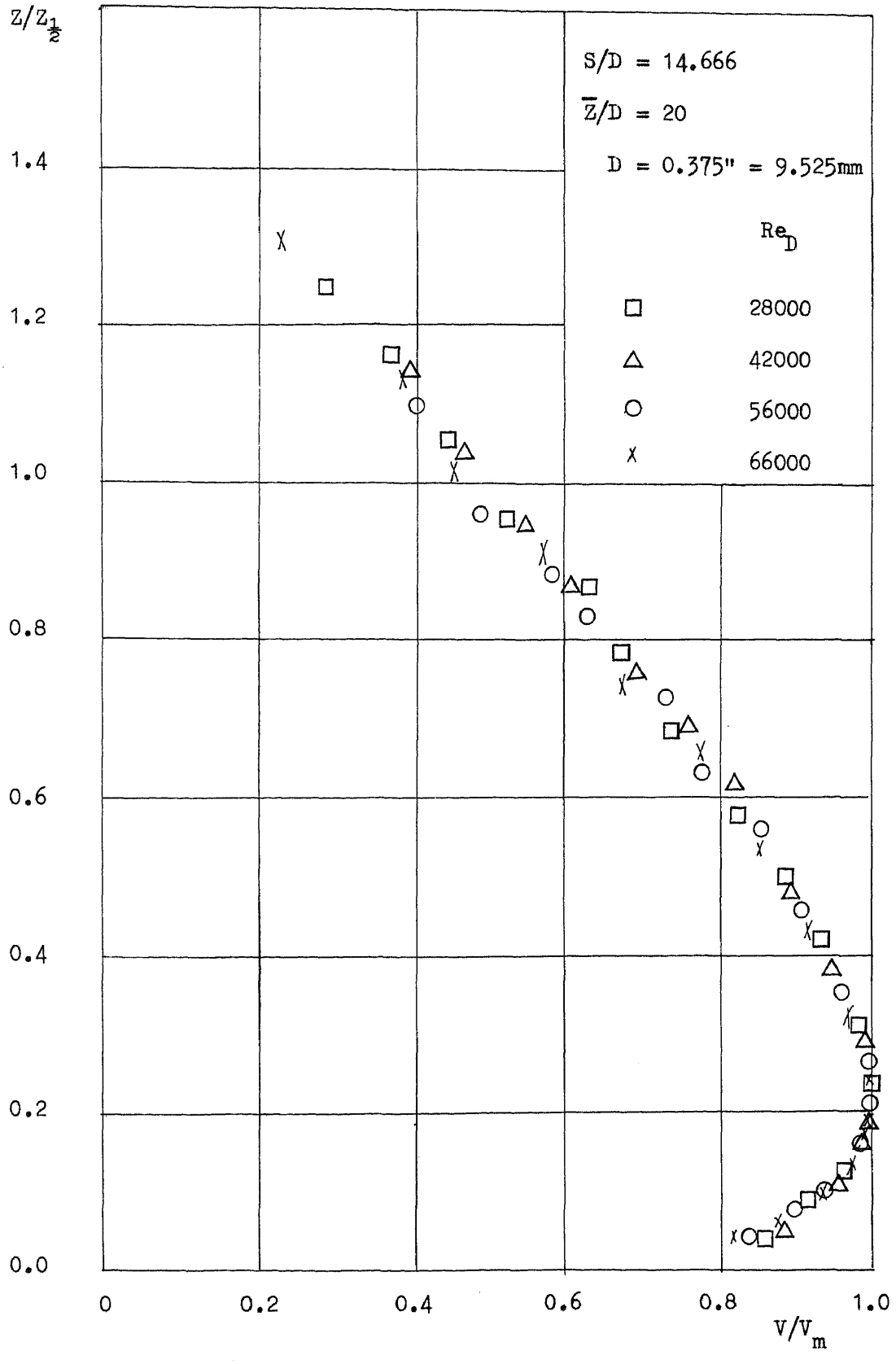

Fig. 110 Velocity Profile of Wall Jet

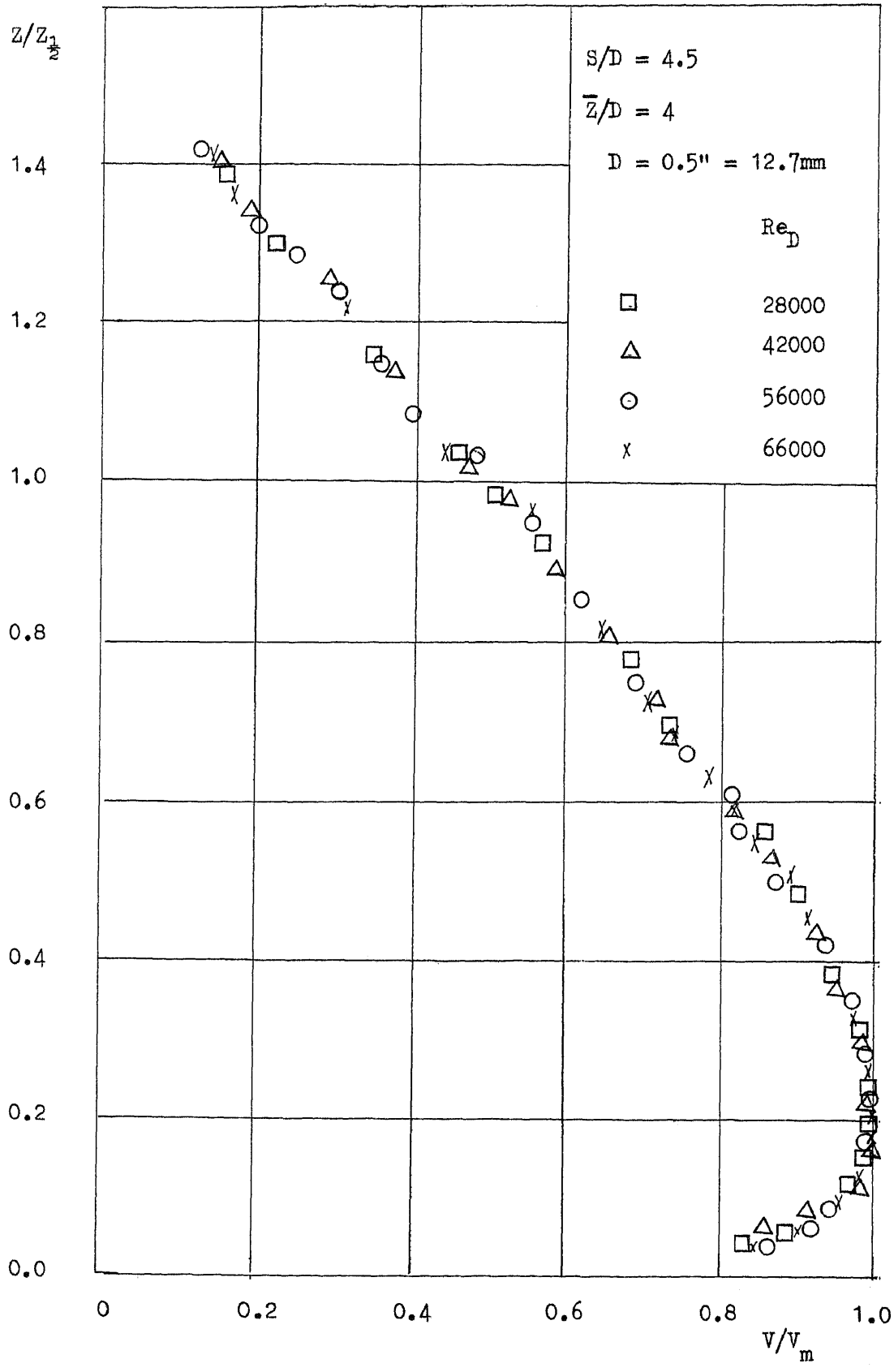

Fig. 111 Velocity Profile of Wall Jet

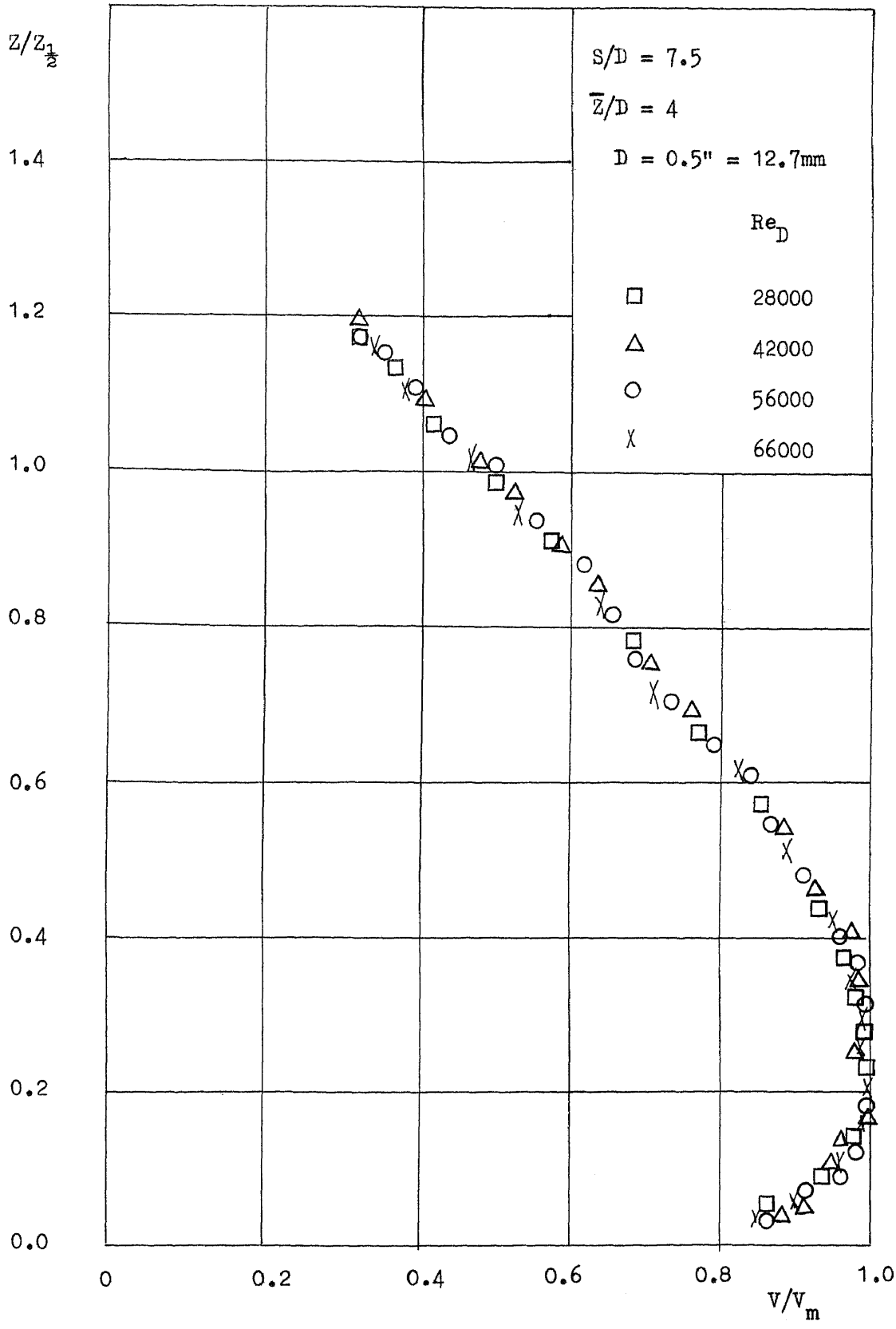

Fig. 112 Velocity Profile of Wall Jet

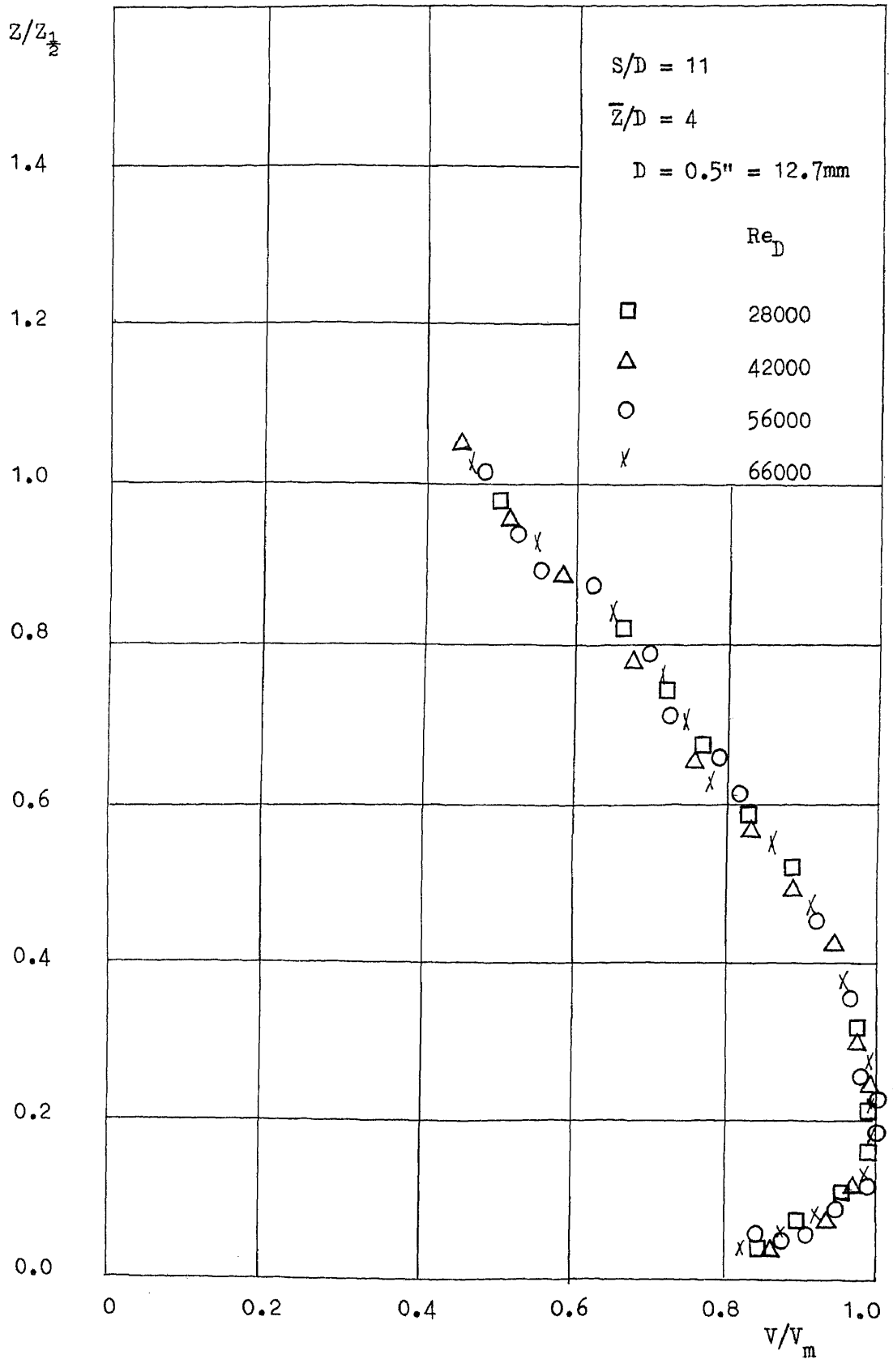

Fig. 113 Velocity Profile of Wall Jet

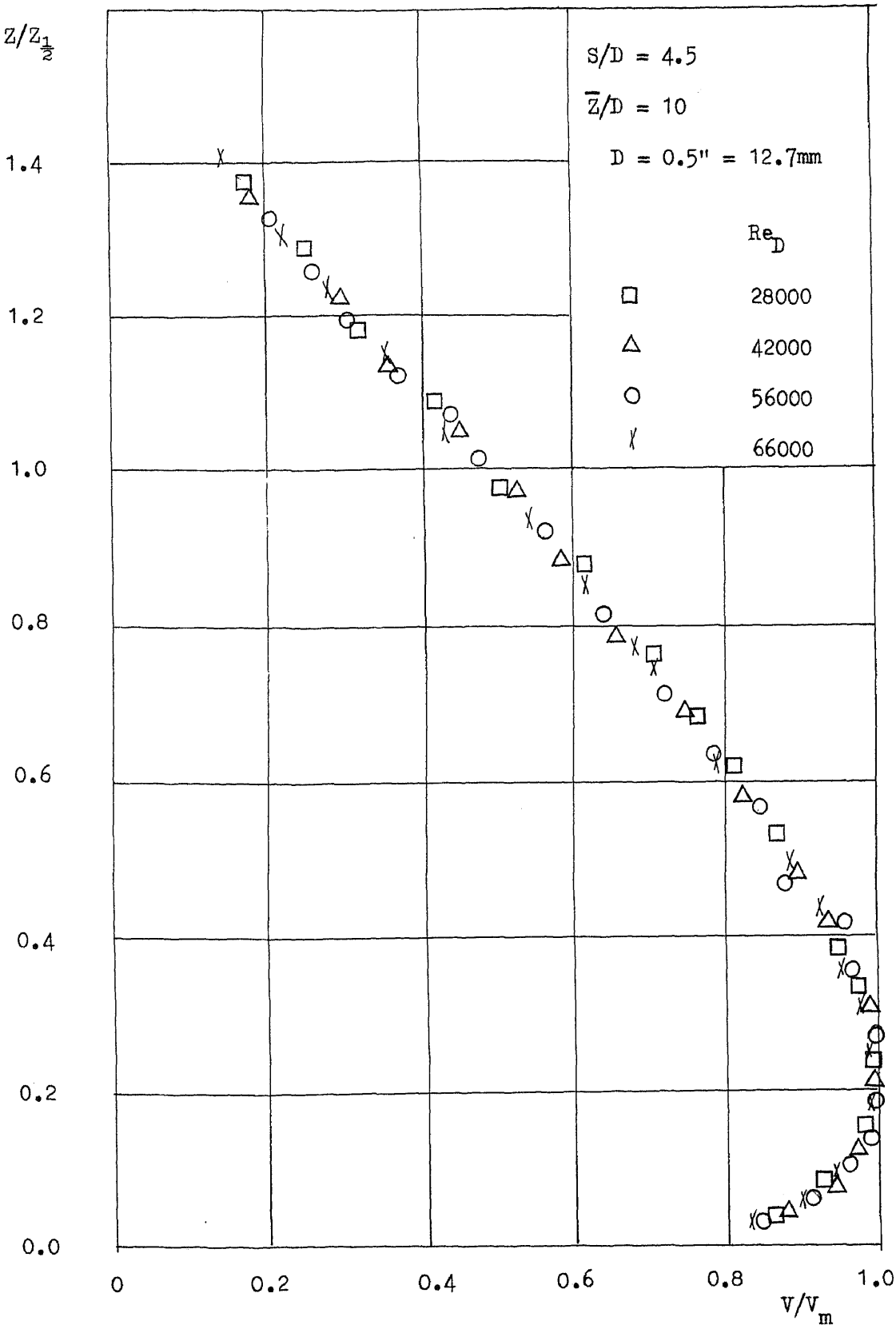

Fig. 114 Velocity Profile of Wall Jet

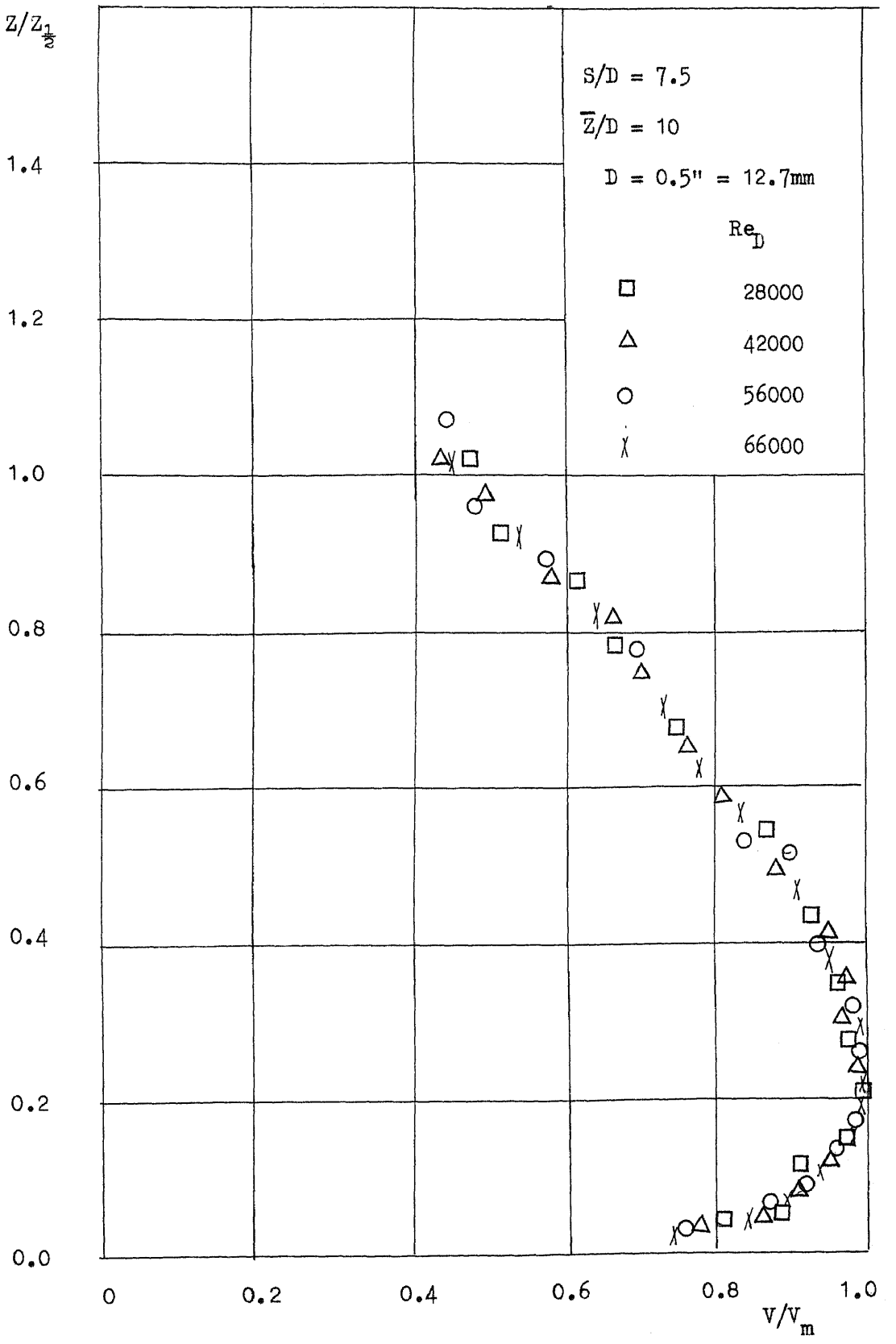

Fig. 115 Velocity Profile of Wall Jet

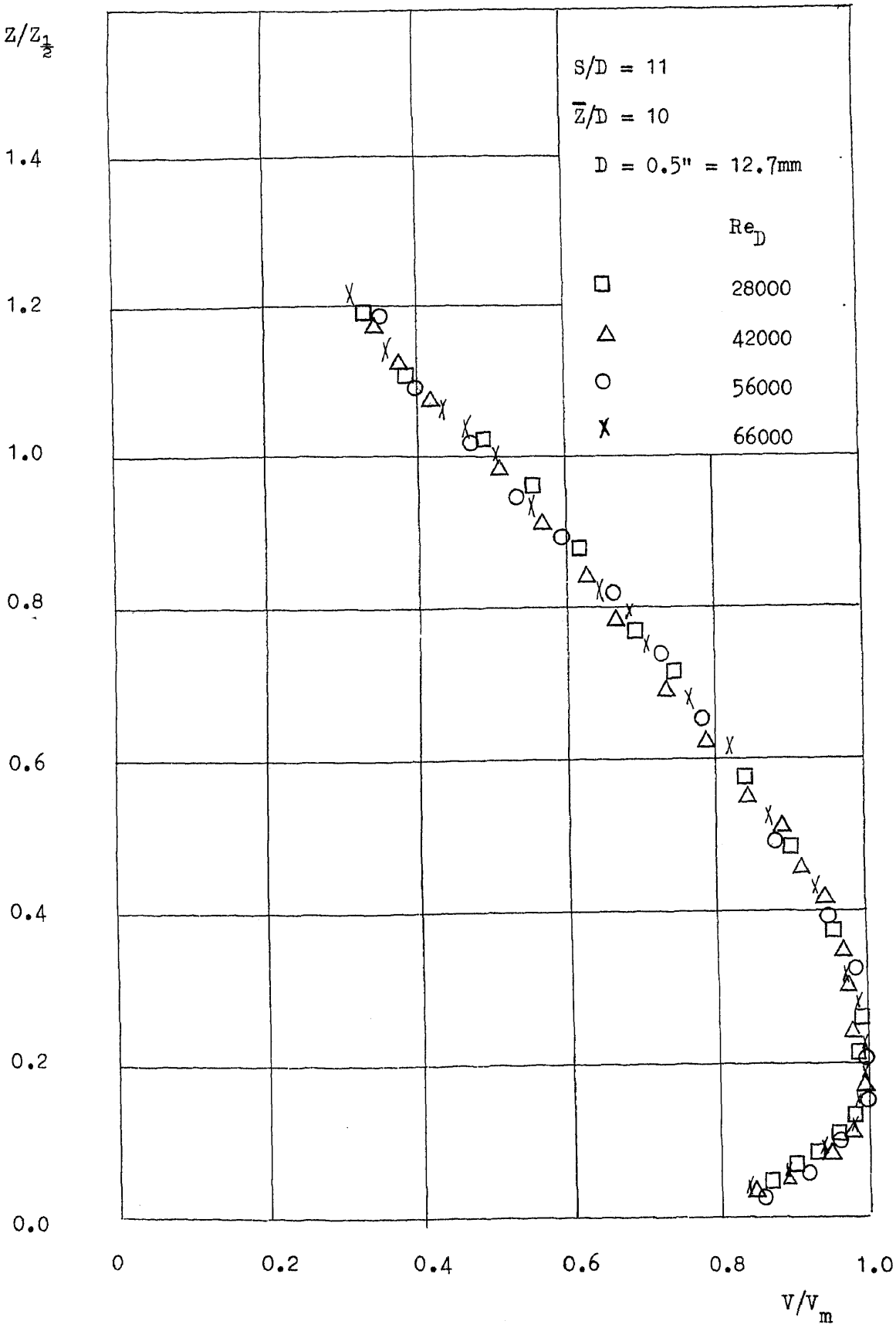

Fig. 116 Velocity Profile of Wall Jet

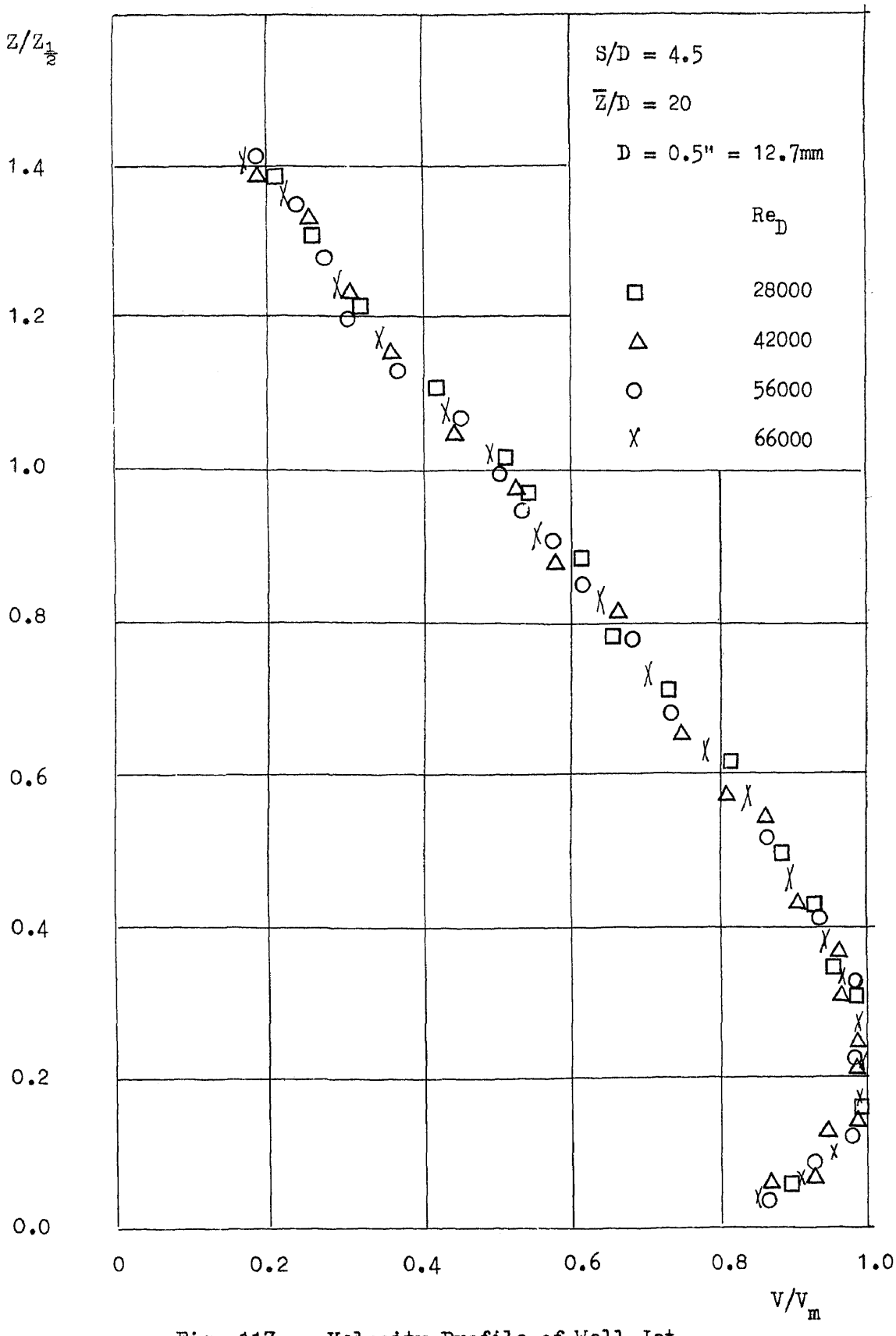

Fig. 117 Velocity Profile of Wall Jet

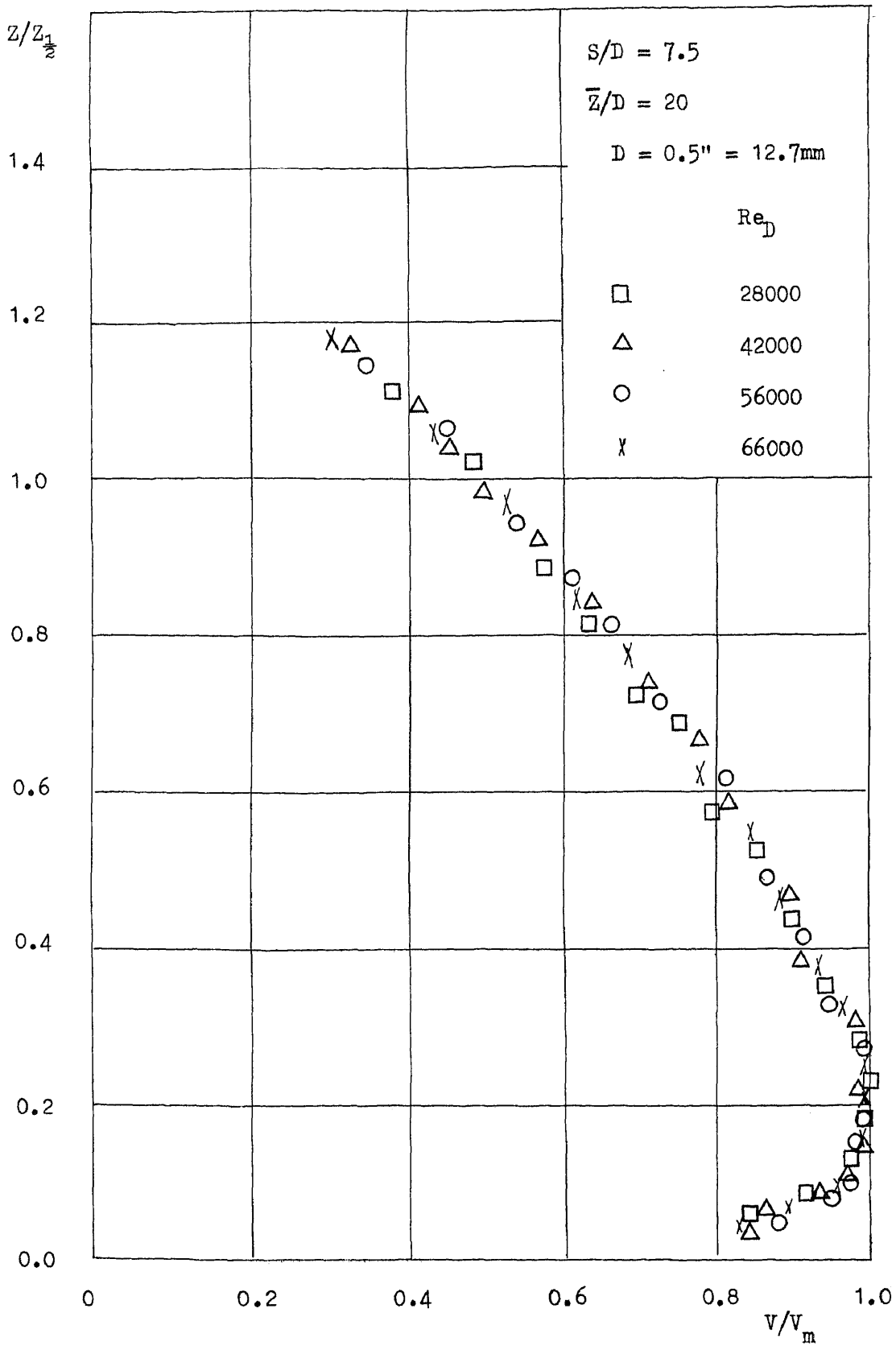

Fig. 118 Velocity Profile of Wall Jet

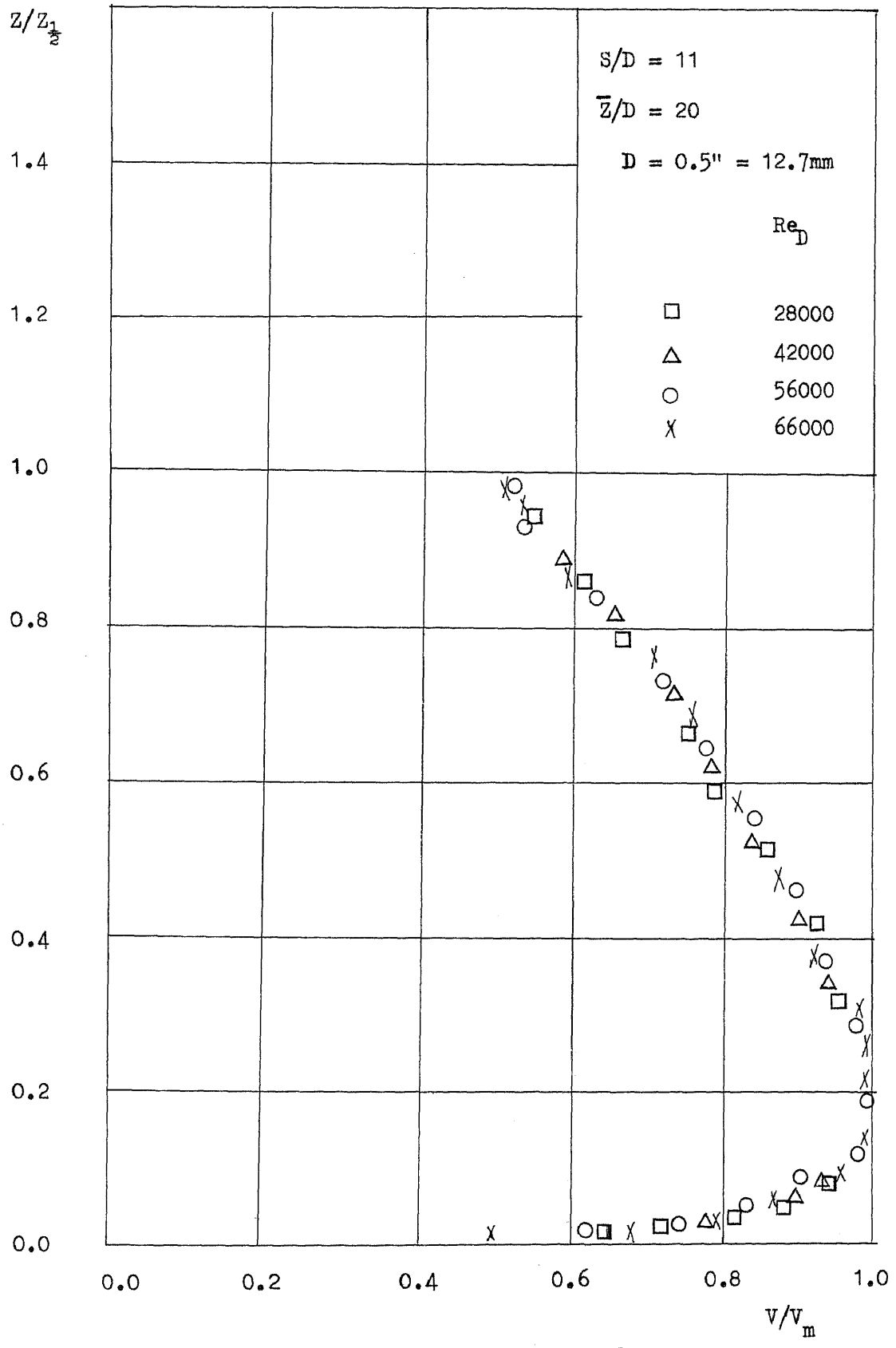

Fig. 119 Velocity Profile of Wall Jet

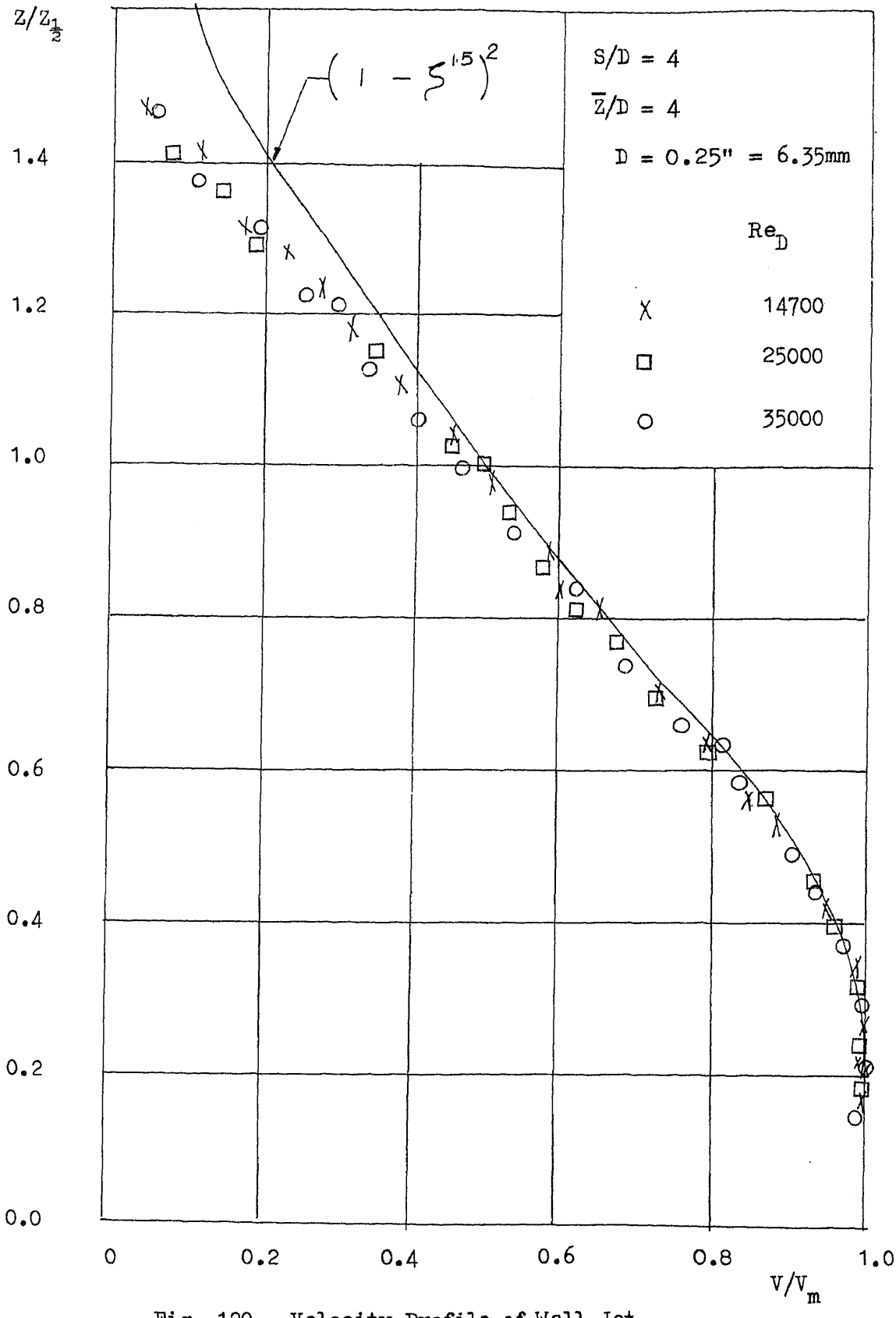

Fig. 120 Velocity Profile of Wall Jet

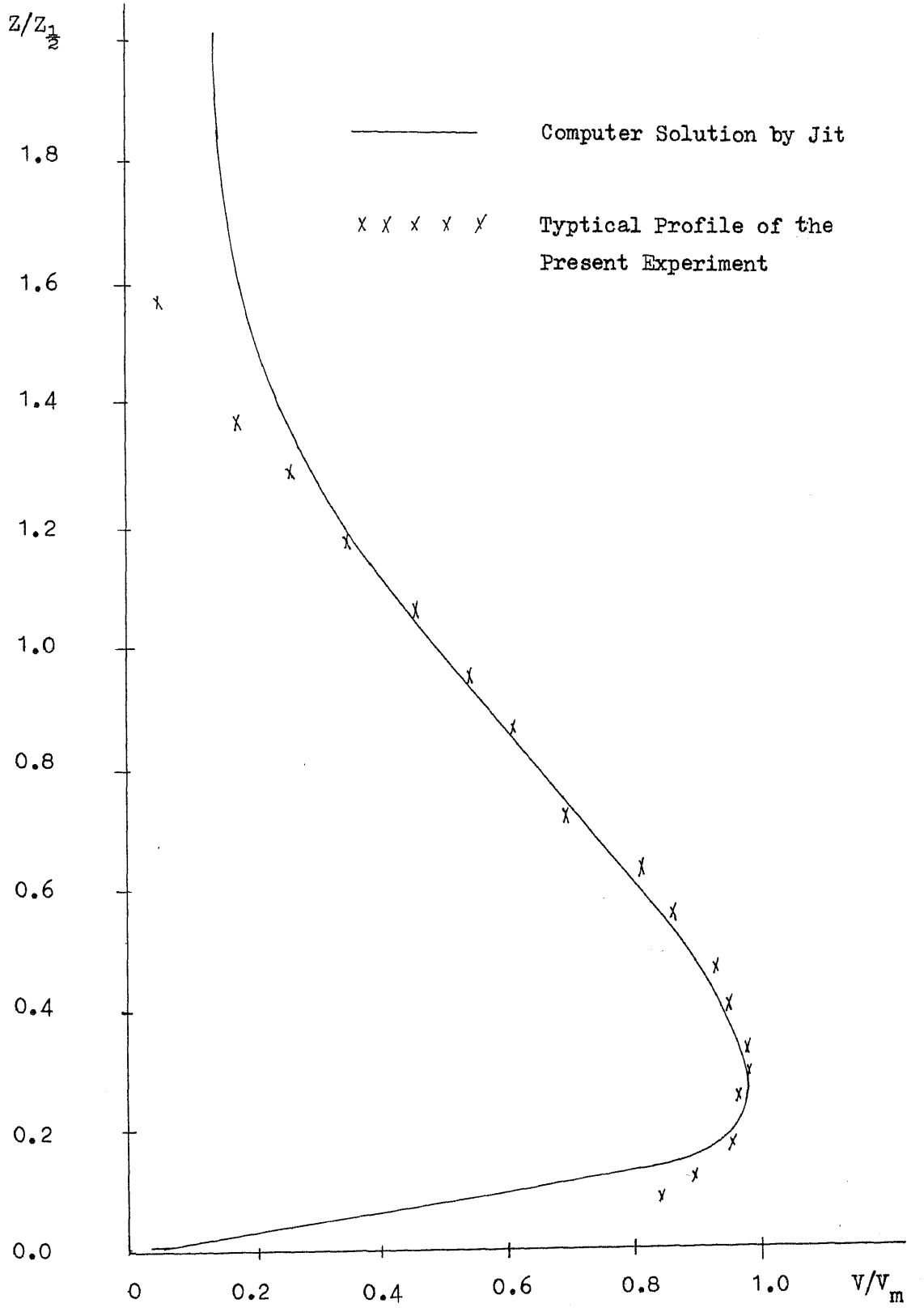

Wall Jet Velocity Profiles Comparison

Fig. 121

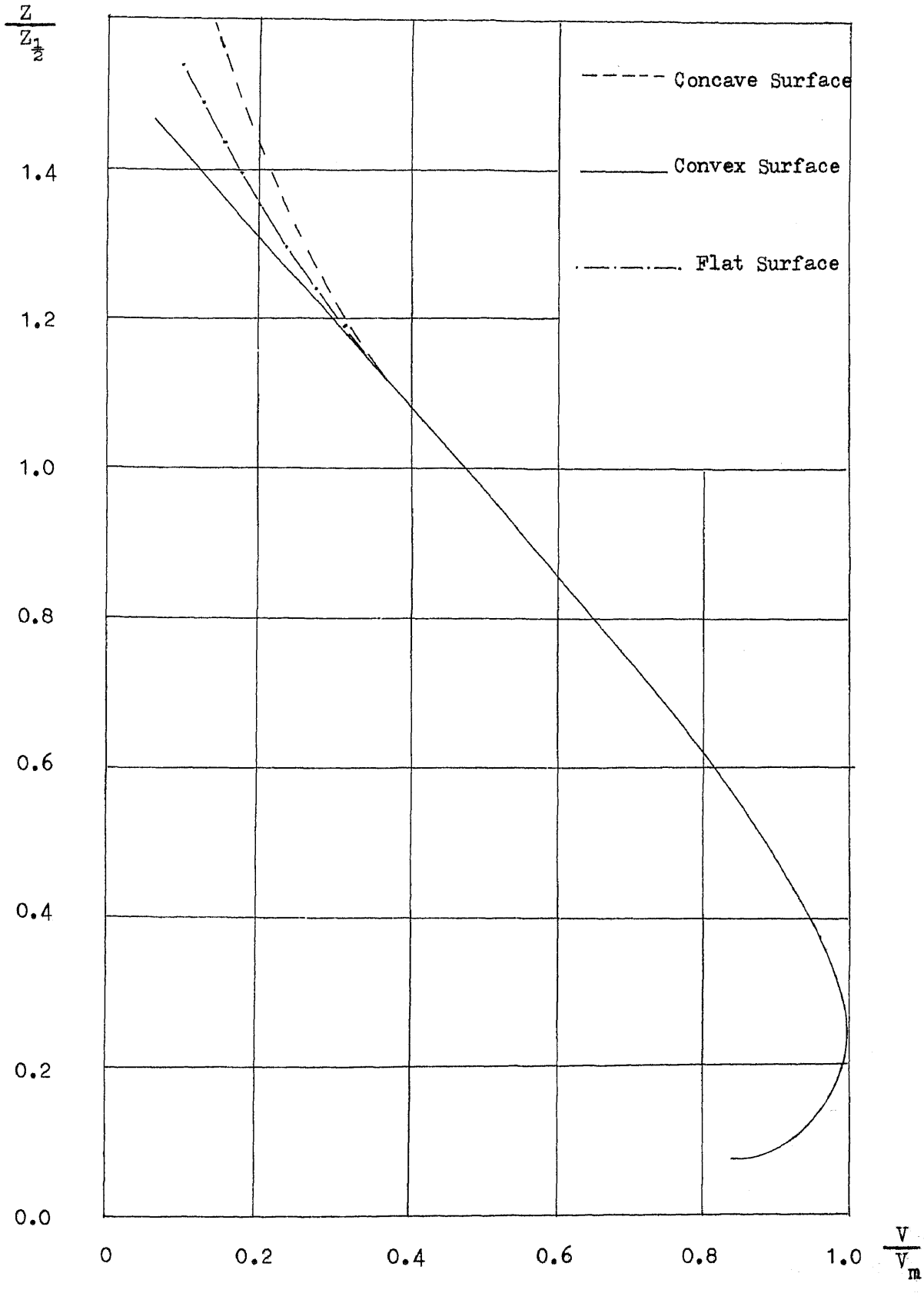

Fig. 122 Comparison of Wall Jet Velocity Profiles

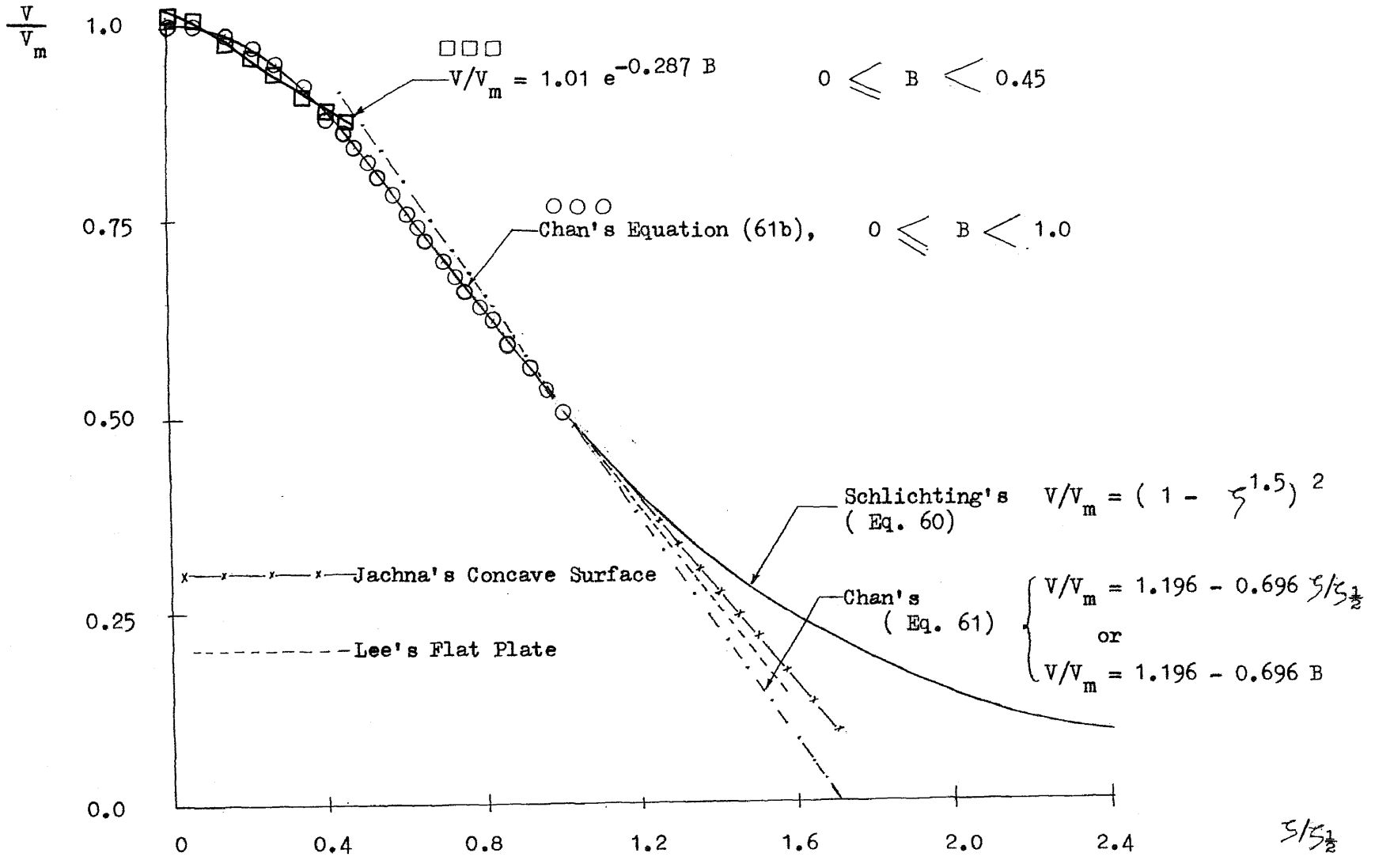

Fig. 123 Wall Jet Velocity Profiles

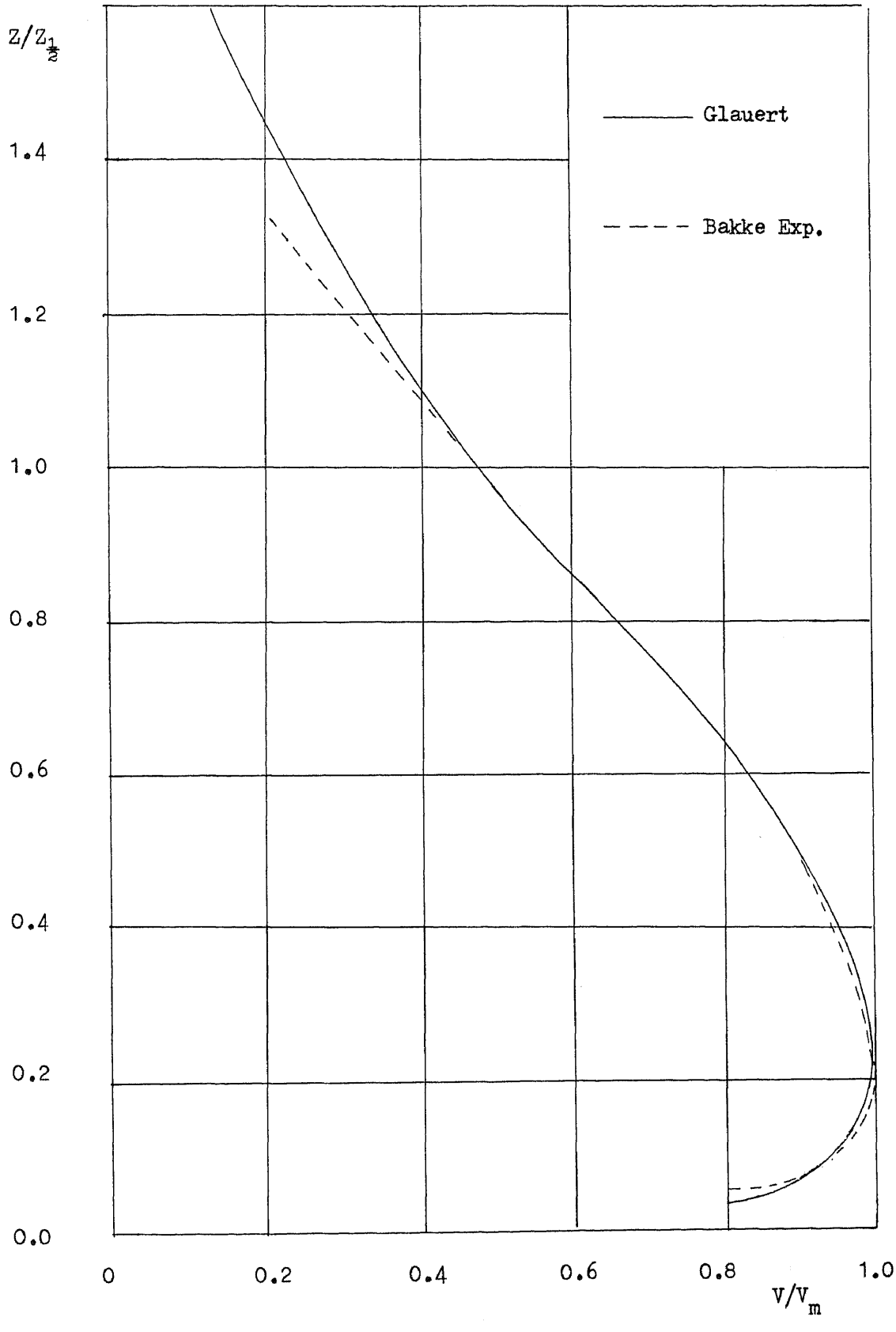

Velocity Profile of Wall Jet

Fig. 124

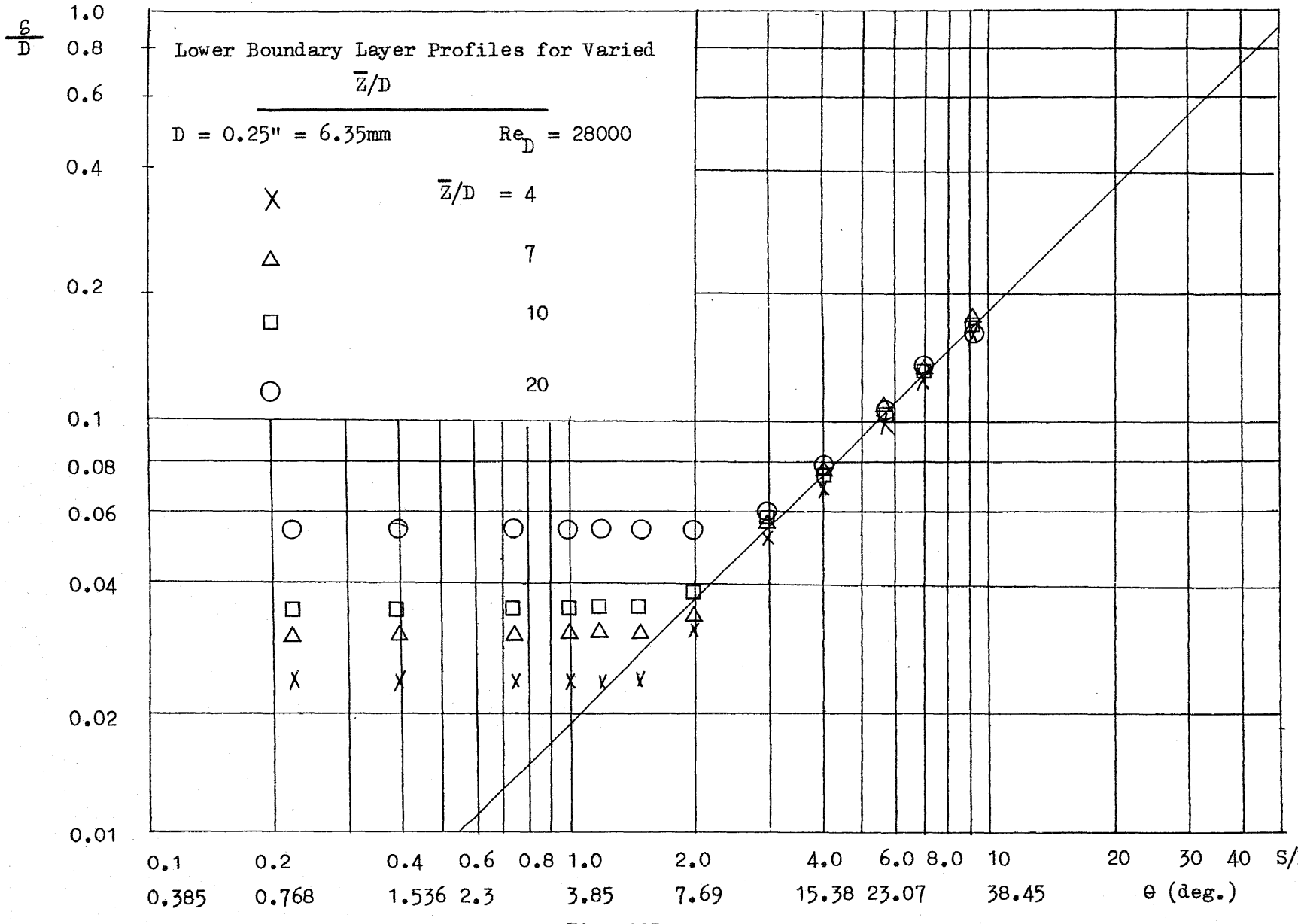
δ/D
1.0
0.8
0.6
0.4
0.2
0.1
0.08
0.06
0.04
0.02
0.01
Lower Boundary Layer Profiles for Varied
Z̄/D
D = 0.25" = 6.35mm
Re_D = 28000
Z̄/D = 4
7
10
20
0.1
0.2
0.4
0.6
0.8
1.0
2.0
4.0
6.0
8.0
10
20
30
40
S/D
0.385
0.768
1.536
2.3
3.85
7.69
15.38
23.07
38.45
θ (deg.)

Fig. 125

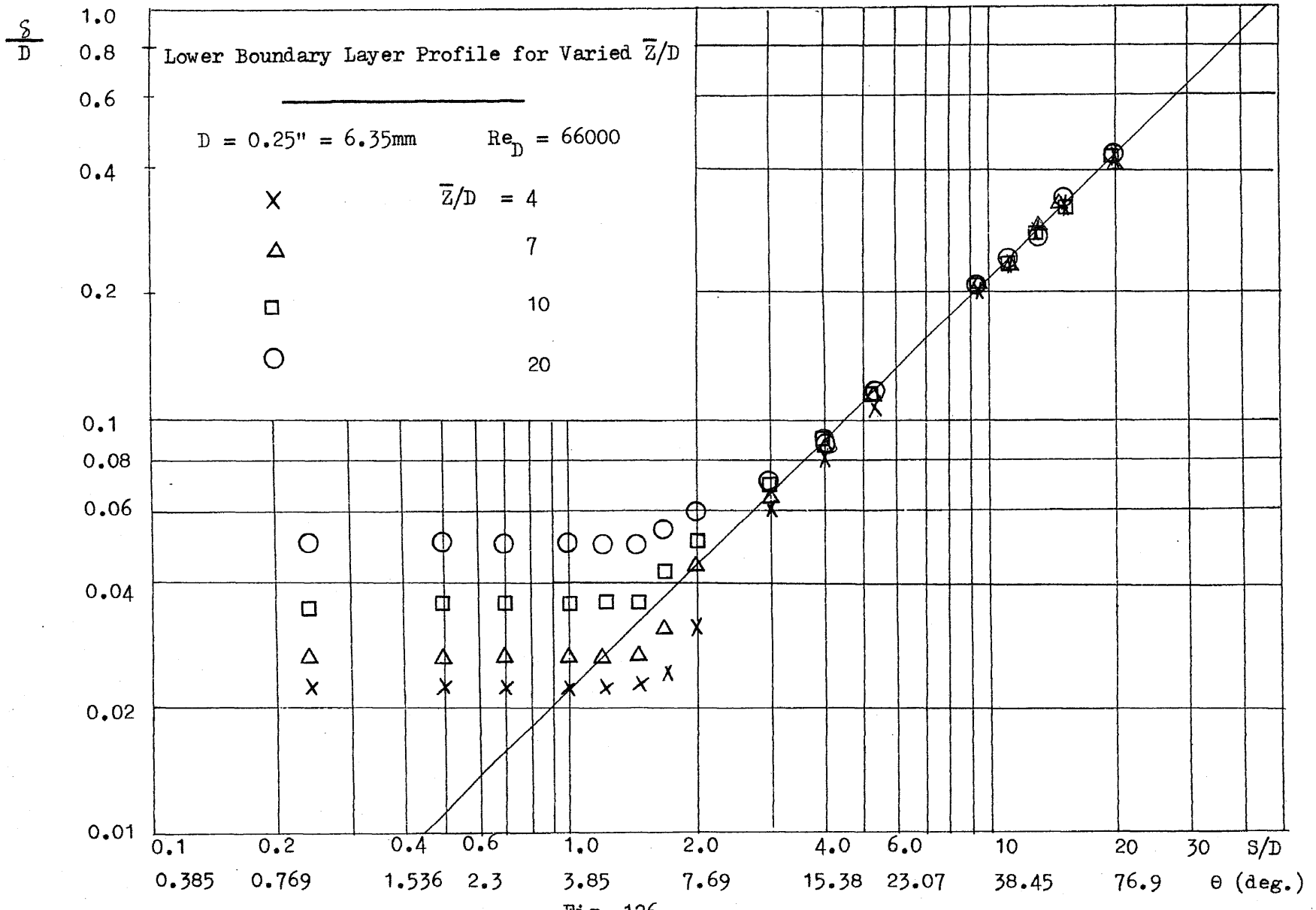
δ/D
1.0
0.8
0.6
0.4
0.2
0.1
0.08
0.06
0.04
0.02
0.01
Lower Boundary Layer Profile for Varied Z̄/D
D = 0.25" = 6.35mm
Re_D = 66000
Z̄/D = 4
7
10
20
0.1
0.2
0.4
0.6
1.0
2.0
4.0
6.0
10
20
30
S/D
0.385
0.769
1.536
2.3
3.85
7.69
15.38
23.07
38.45
76.9
θ (deg.)

Fig. 126

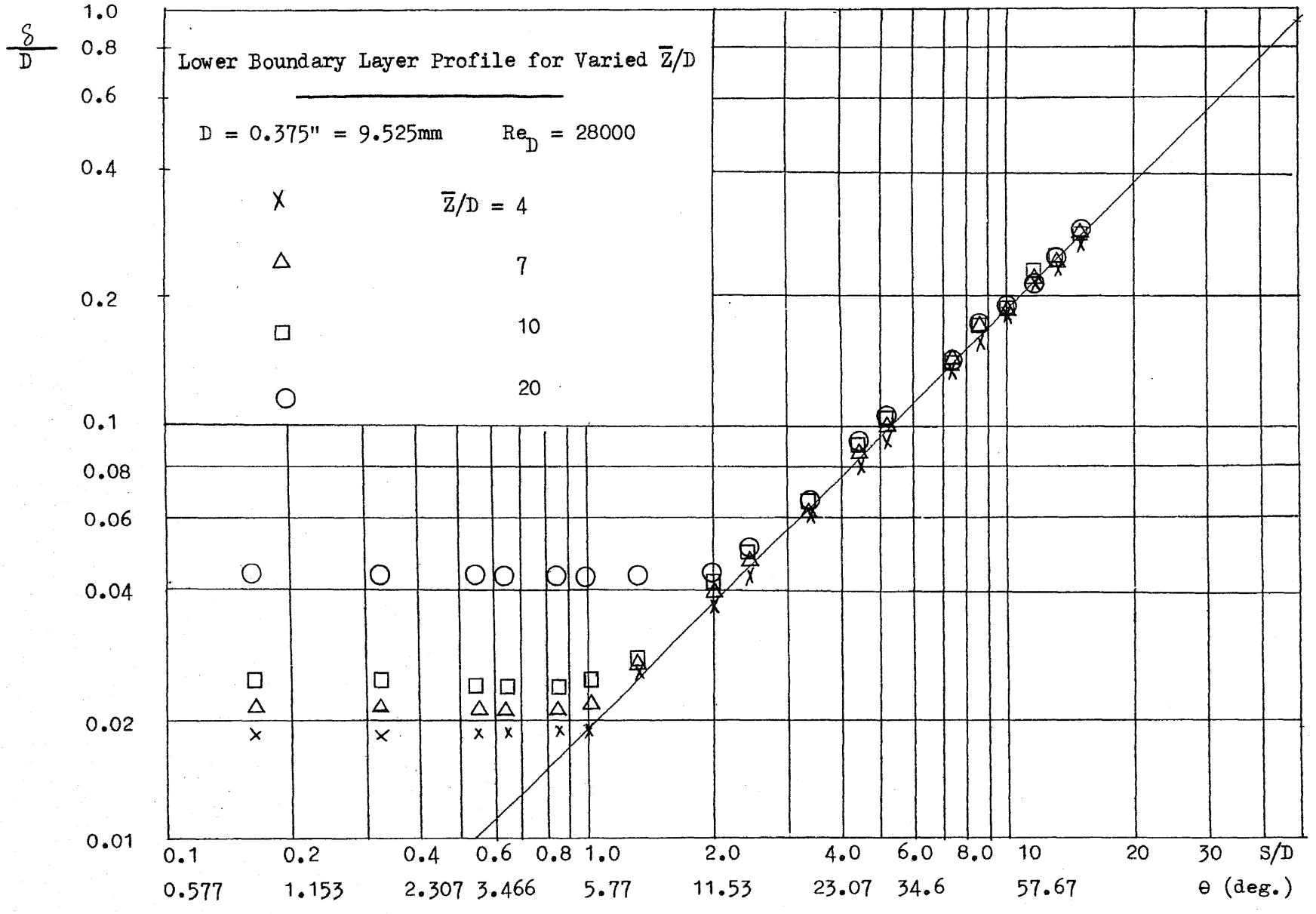
δ/D
1.0
0.8
0.6
0.4
0.2
0.1
0.08
0.06
0.04
0.02
0.01
Lower Boundary Layer Profile for Varied Z̄/D
D = 0.375" = 9.525mm
Re_D = 28000
Z̄/D = 4
7
10
20
0.1
0.2
0.4
0.6
0.8
1.0
2.0
4.0
6.0
8.0
10
20
30
S/D
0.577
1.153
2.307
3.466
5.77
11.53
23.07
34.6
57.67
θ (deg.)

Fig. 127

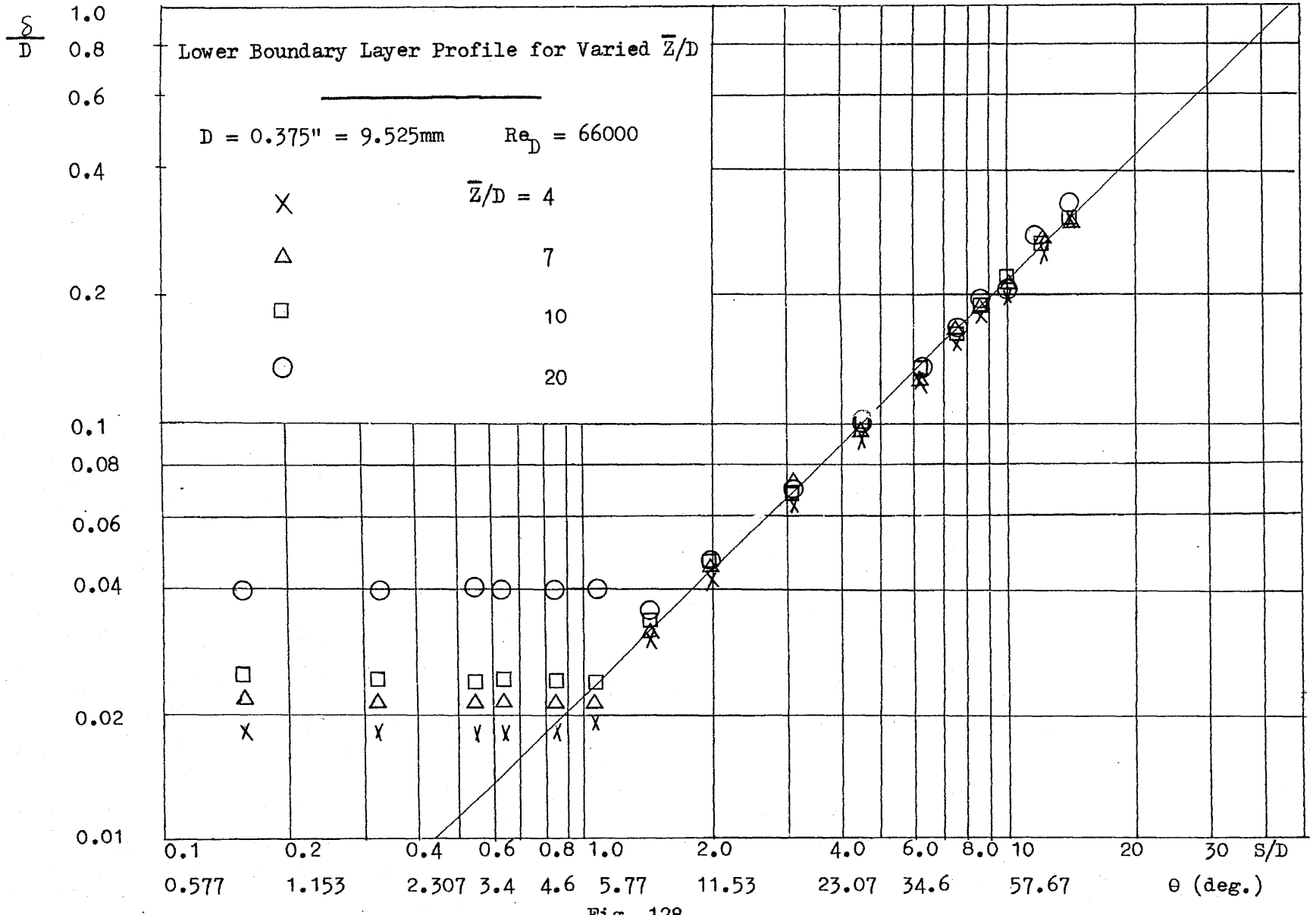
δ/D
1.0
0.8
0.6
0.4
0.2
0.1
0.08
0.06
0.04
0.02
0.01
Lower Boundary Layer Profile for Varied Z̄/D
D = 0.375" = 9.525mm
Re_D = 66000
Z̄/D = 4
7
10
20
0.1
0.2
0.4
0.6
0.8
1.0
2.0
4.0
6.0
8.0
10
20
30
S/D
0.577
1.153
2.307
3.4
4.6
5.77
11.53
23.07
34.6
57.67
θ (deg.)

Fig. 128

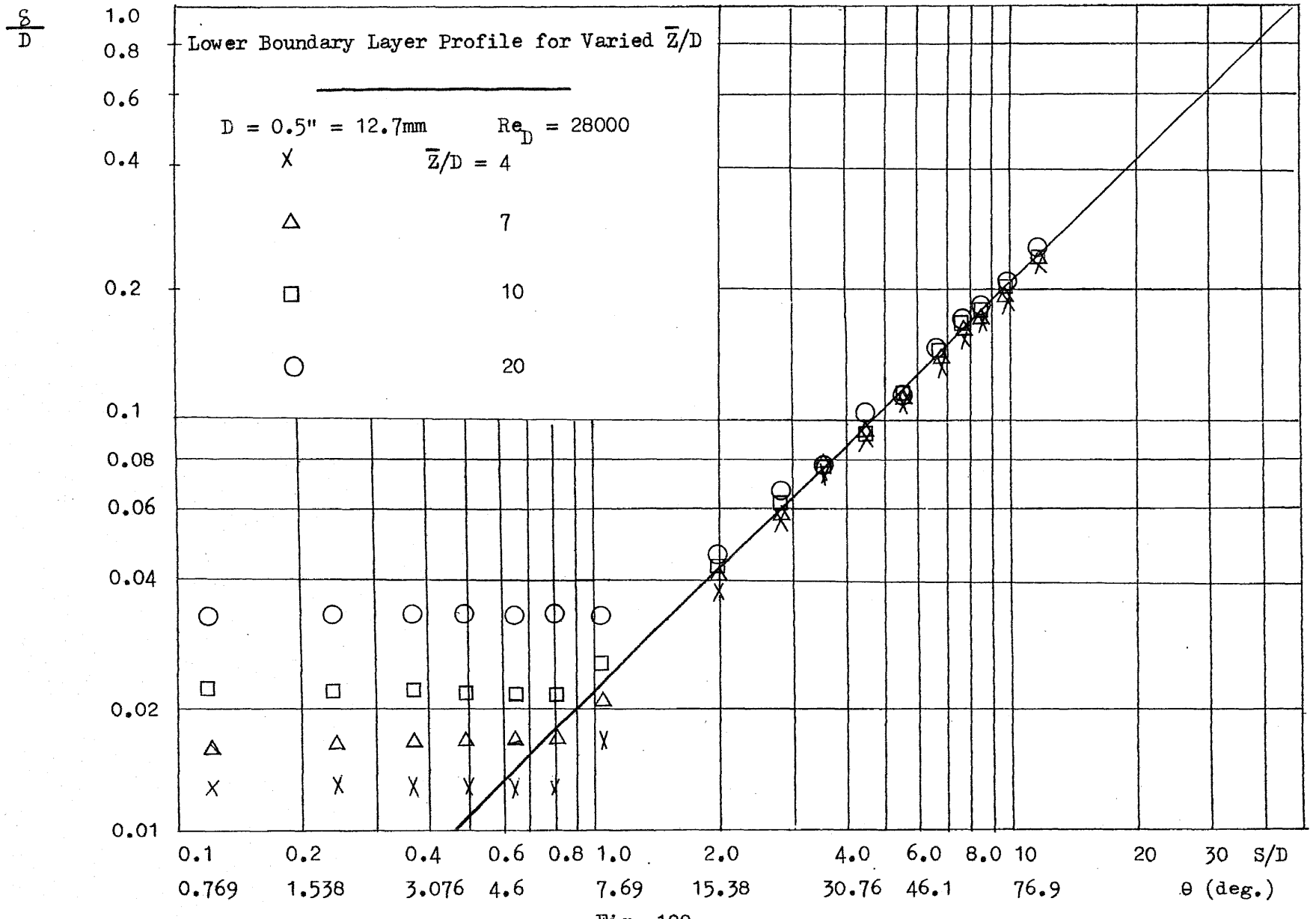
δ/D
1.0
0.8
0.6
0.4
0.2
0.1
0.08
0.06
0.04
0.02
0.01
Lower Boundary Layer Profile for Varied Z̄/D
D = 0.5" = 12.7mm
Re_D = 28000
X Z̄/D = 4
△ 7
□ 10
○ 20
0.1 0.2 0.4 0.6 0.8 1.0 2.0 4.0 6.0 8.0 10 20 30 S/D
0.769 1.538 3.076 4.6 7.69 15.38 30.76 46.1 76.9 θ (deg.)

Fig. 129

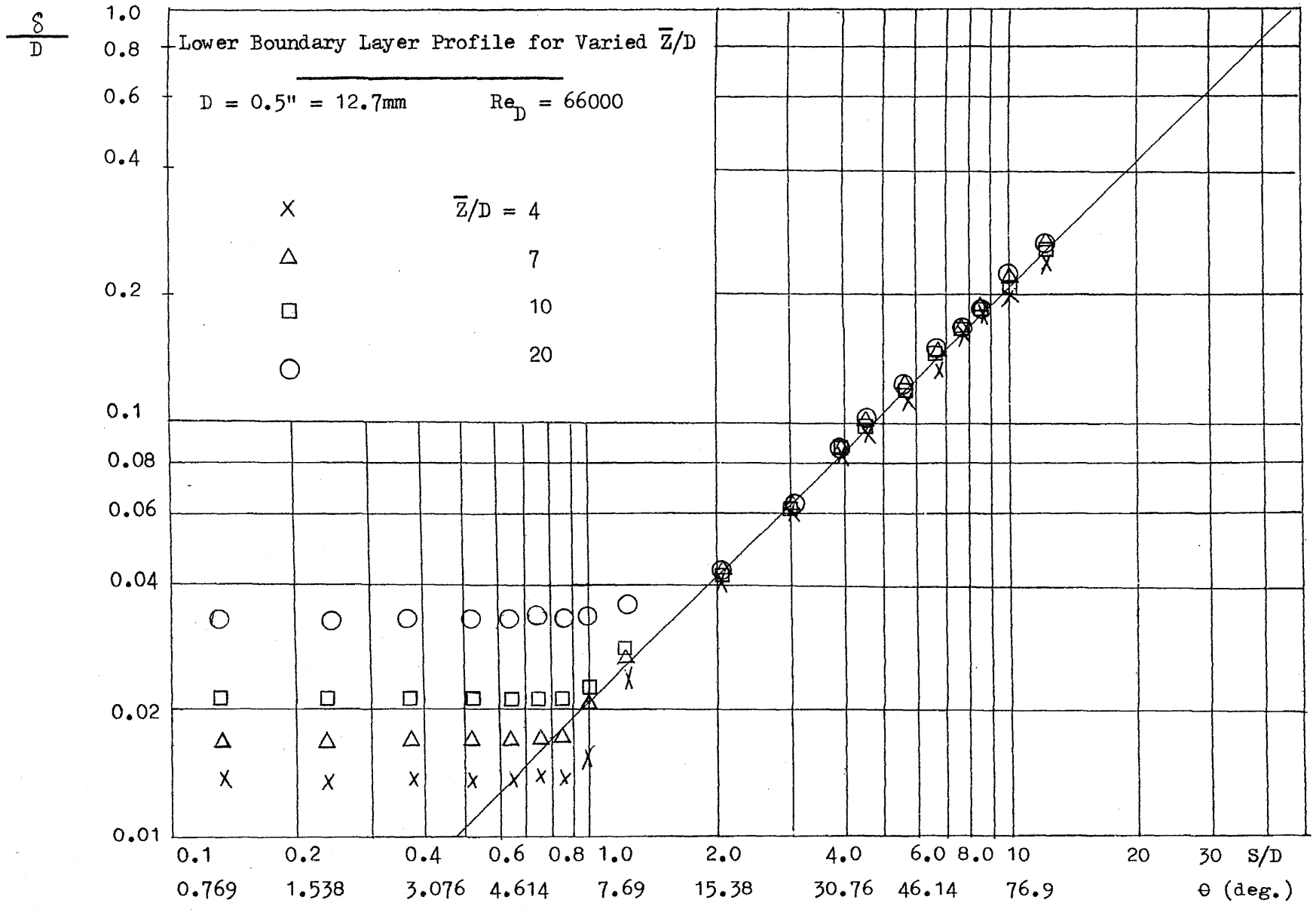
δ/D
Lower Boundary Layer Profile for Varied Z̄/D
D = 0.5" = 12.7mm
Re_D = 66000
Z̄/D = 4
7
10
20
1.0
0.8
0.6
0.4
0.2
0.1
0.08
0.06
0.04
0.02
0.01
0.1 0.2 0.4 0.6 0.8 1.0 2.0 4.0 6.0 8.0 10 20 30 S/D
0.769 1.538 3.076 4.614 7.69 15.38 30.76 46.14 76.9 θ (deg.)

Fig. 130

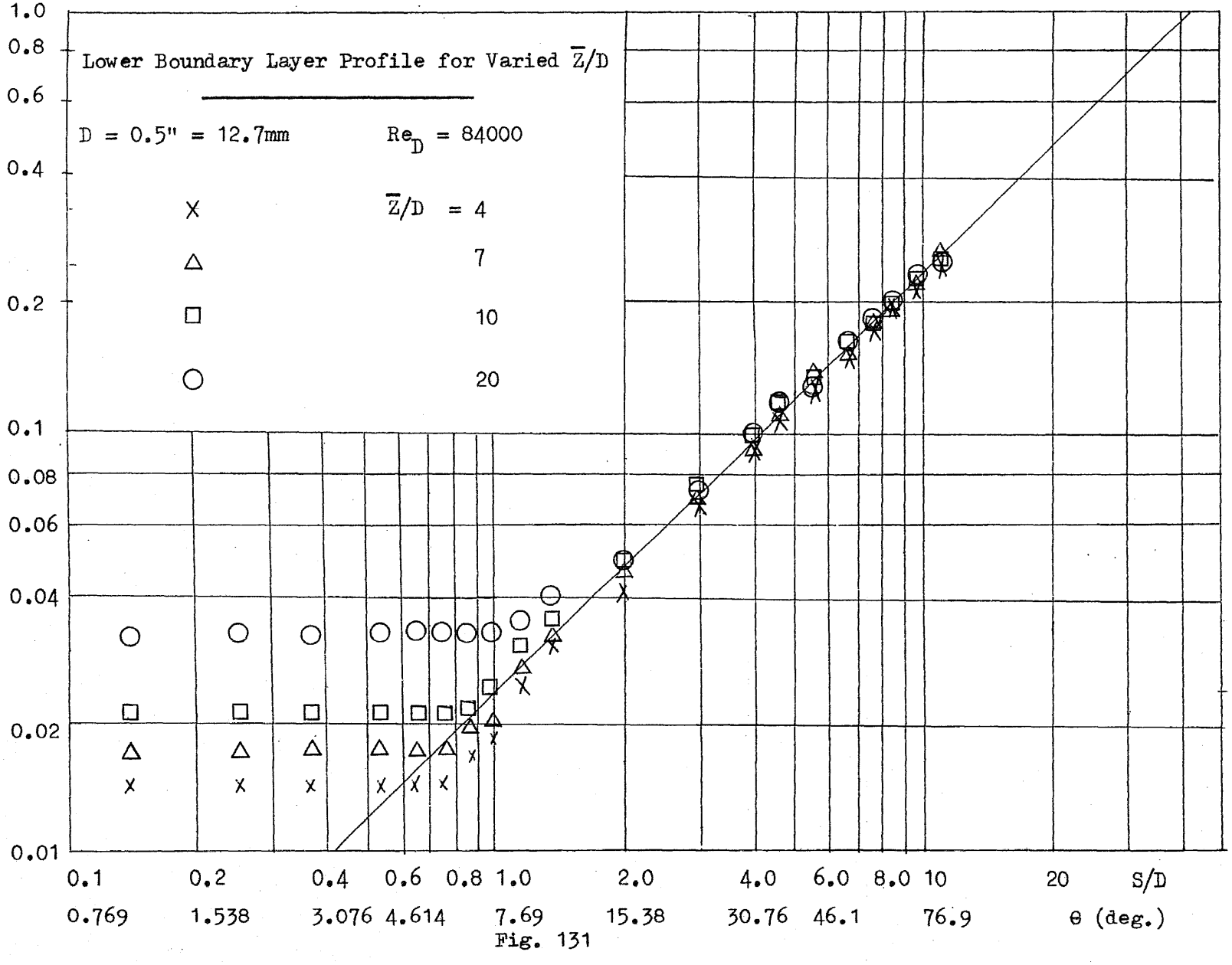
δ/D
1.0
0.8
0.6
0.4
0.2
0.1
0.08
0.06
0.04
0.02
0.01
Lower Boundary Layer Profile for Varied Z̄/D
D = 0.5" = 12.7mm
Re_D = 84000
X
Z̄/D = 4
△
7
□
10
○
20
0.1
0.2
0.4
0.6
0.8
1.0
2.0
4.0
6.0
8.0
10
20
S/D
0.769
1.538
3.076
4.614
7.69
15.38
30.76
46.1
76.9
θ (deg.)

Fig. 131

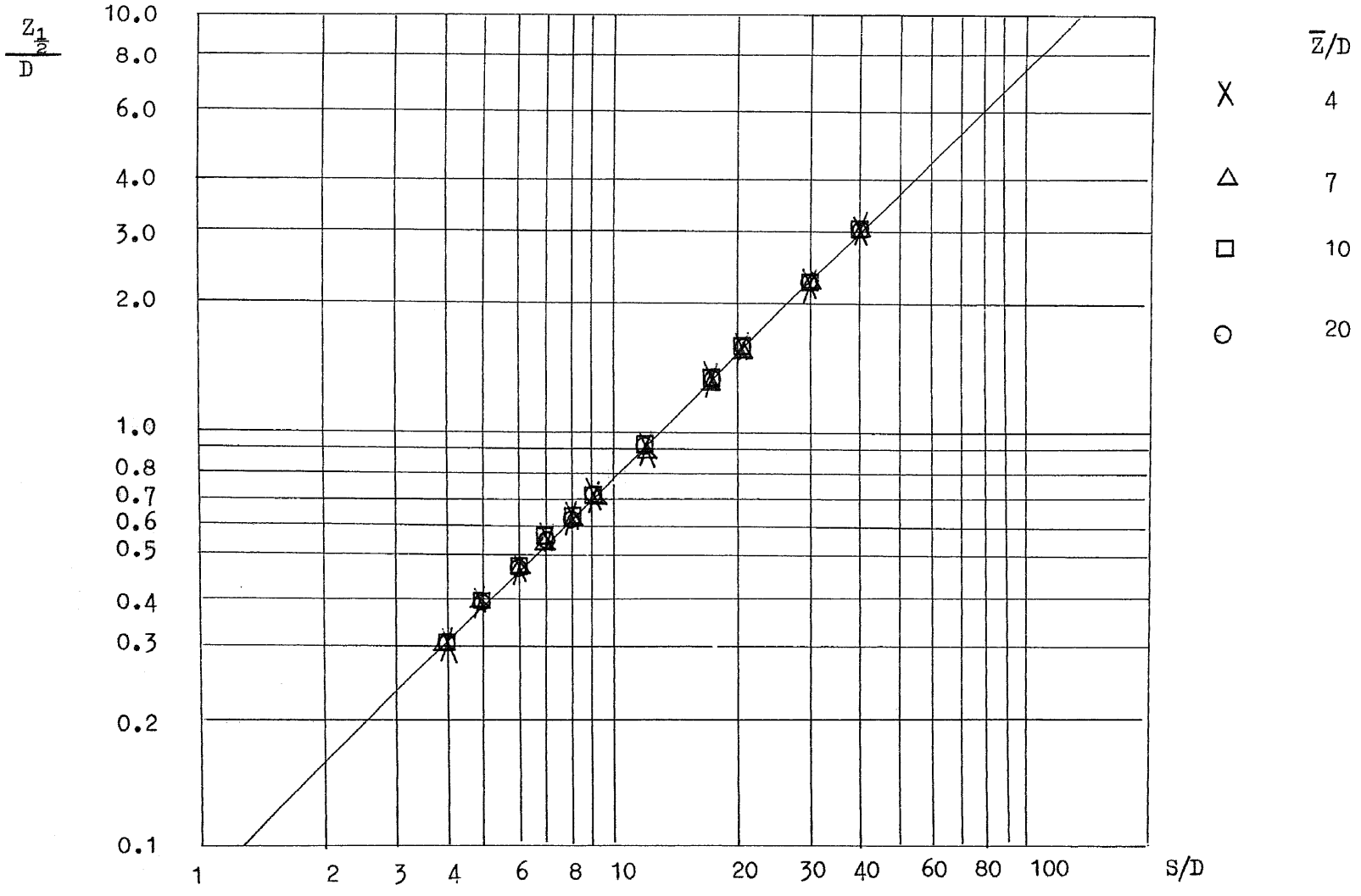

Fig. 131a Spread of Wall Jet

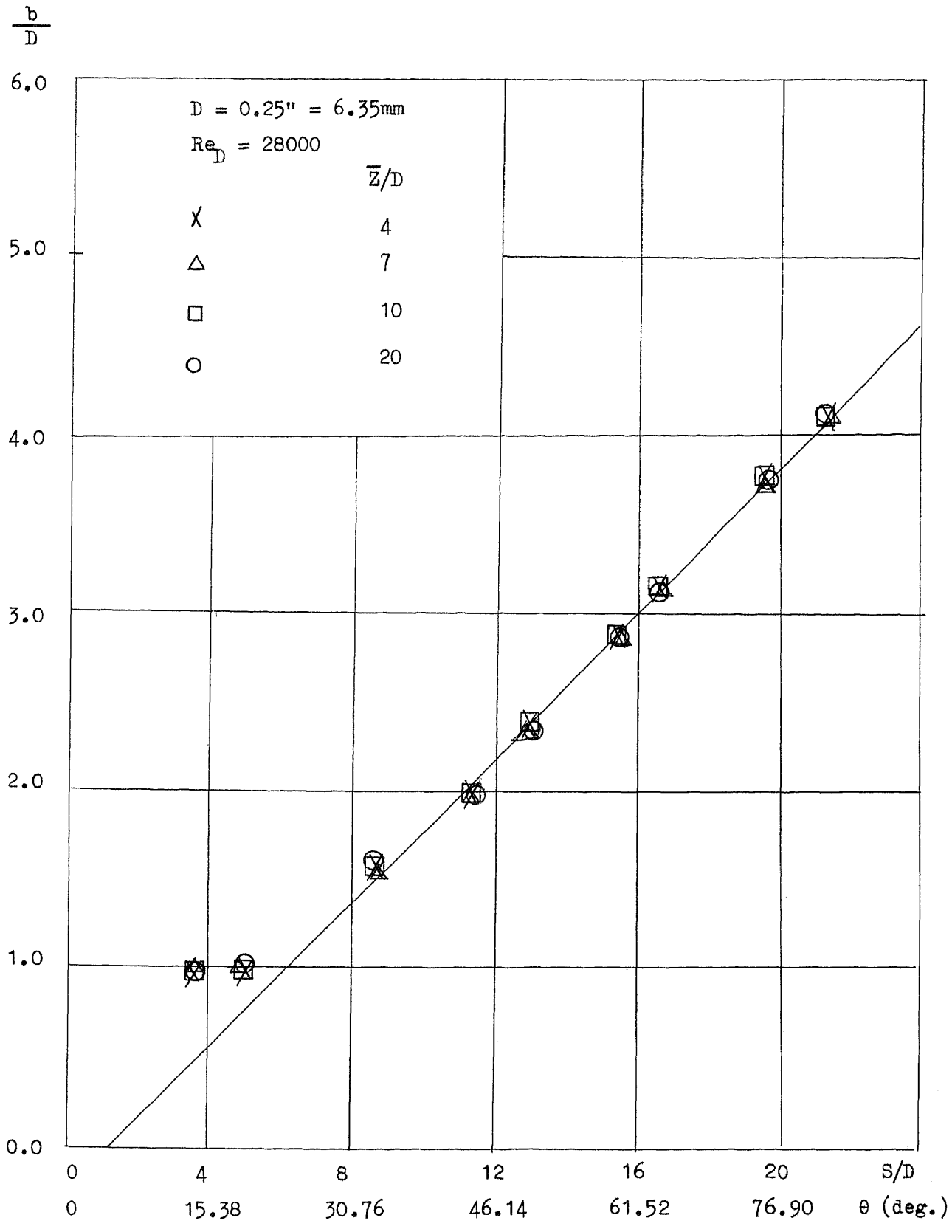

Profile of Outer Boundary Layer Growth of Wall Jet

Fig. 132

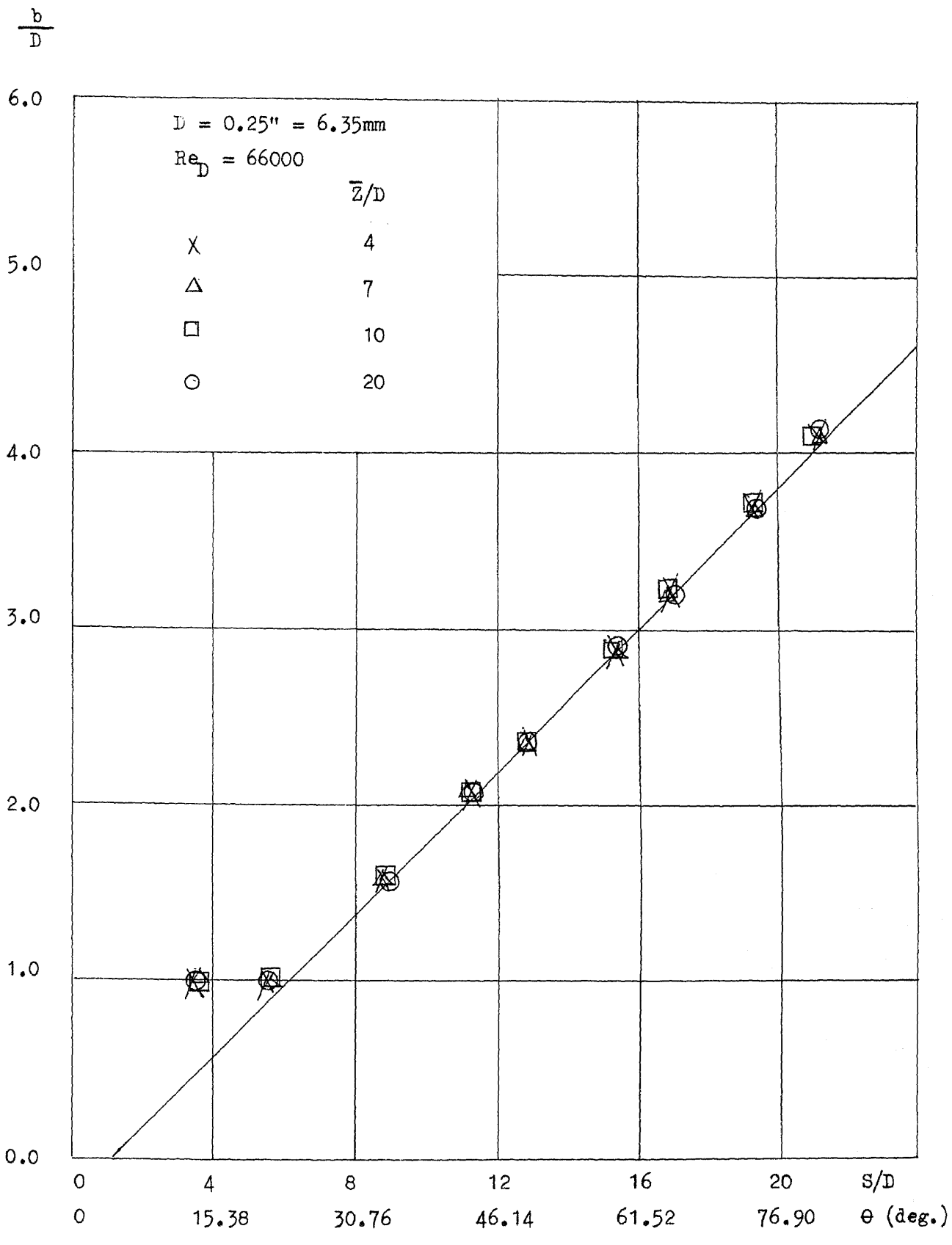

Fig. 133 Profile of Outer Boundary Layer Growth of Wall Jet

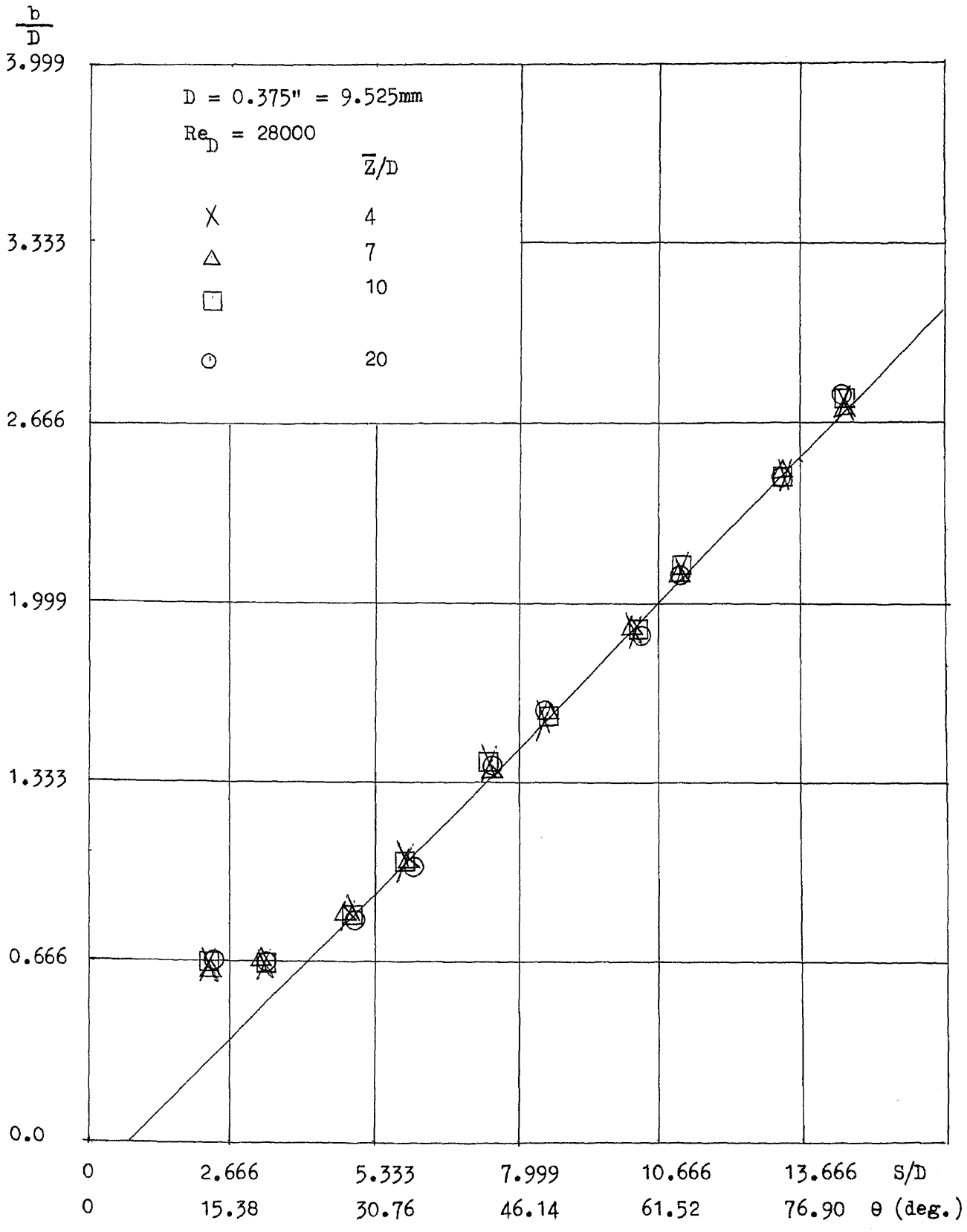

Fig. 134 Profile of Outer Boundary Layer Growth of Wall Jet

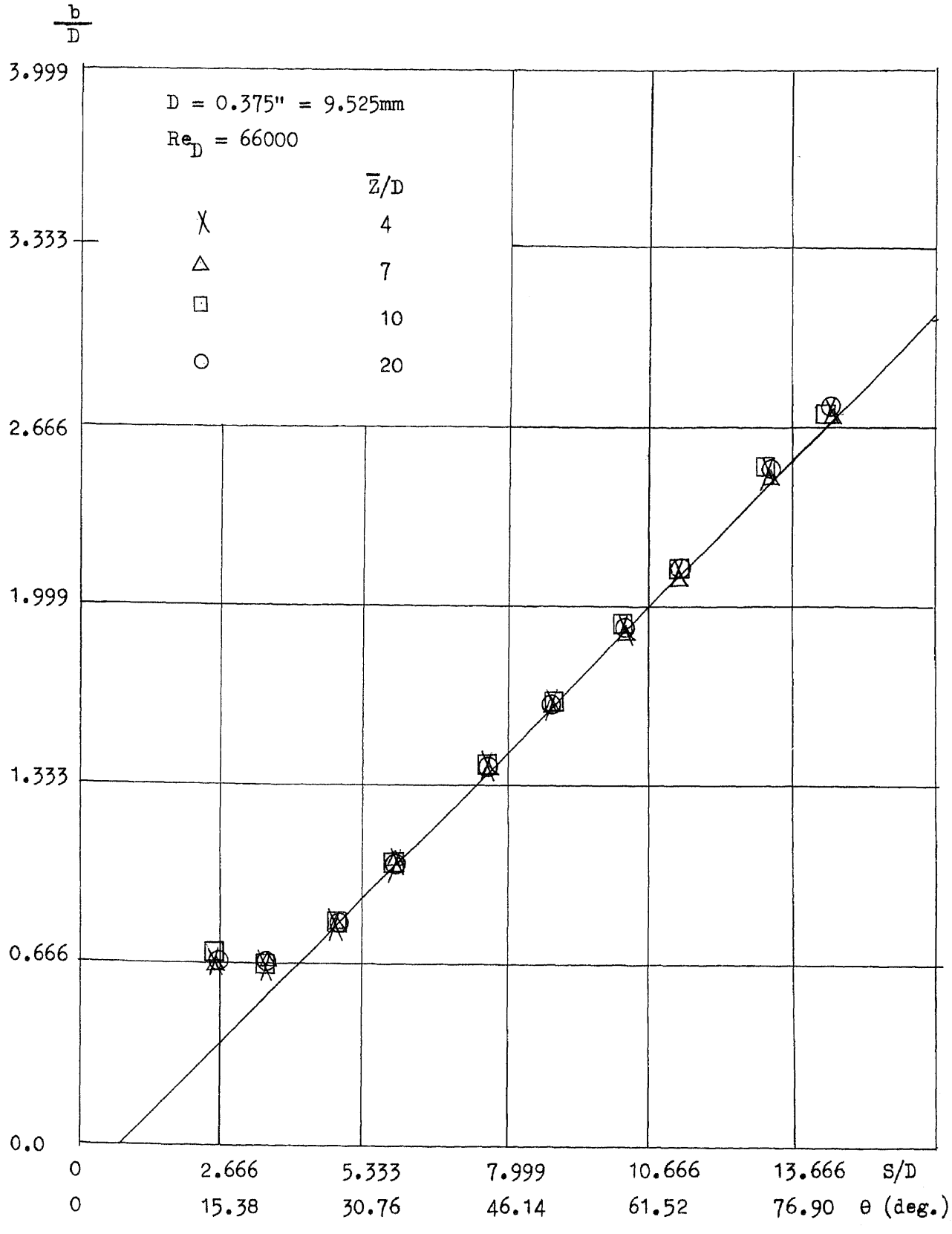

Fig. 135 Profile of Outer Boundary Layer Growth of Wall Jet

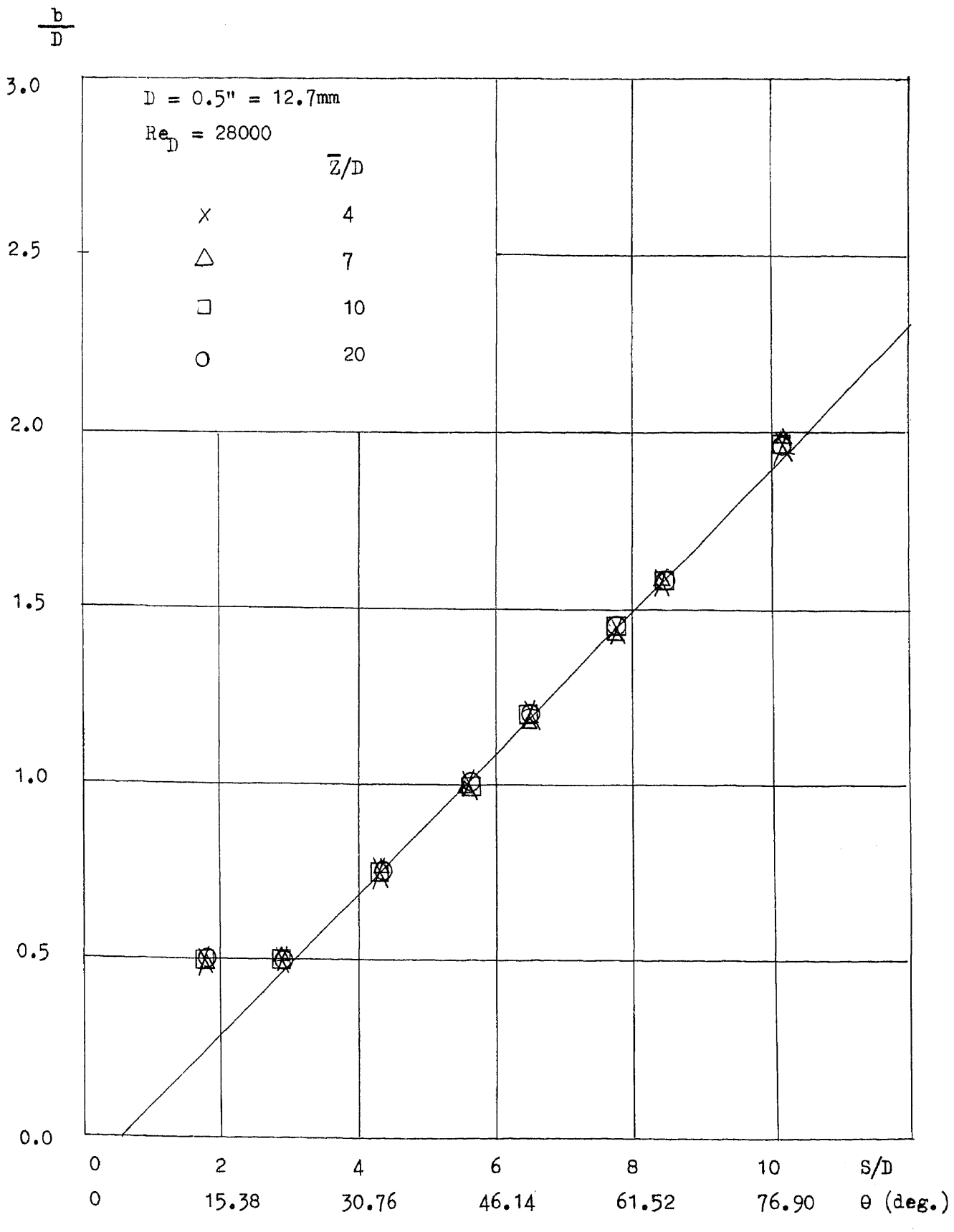

Fig. 136 Profile of Outer Boundary Layer Growth of Wall Jet

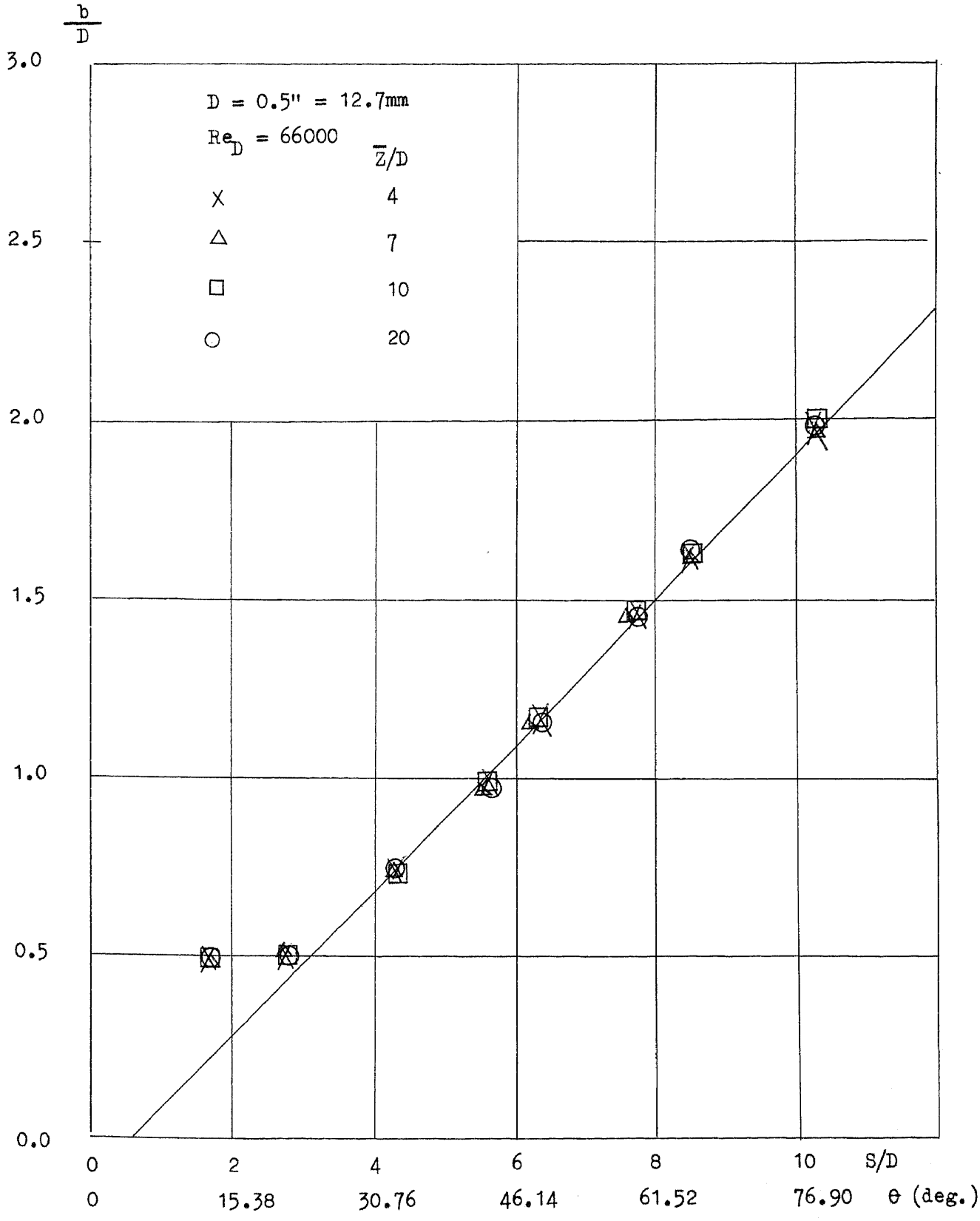

Fig. 137 Profile of Outer Boundary Layer Growth of Wall Jet

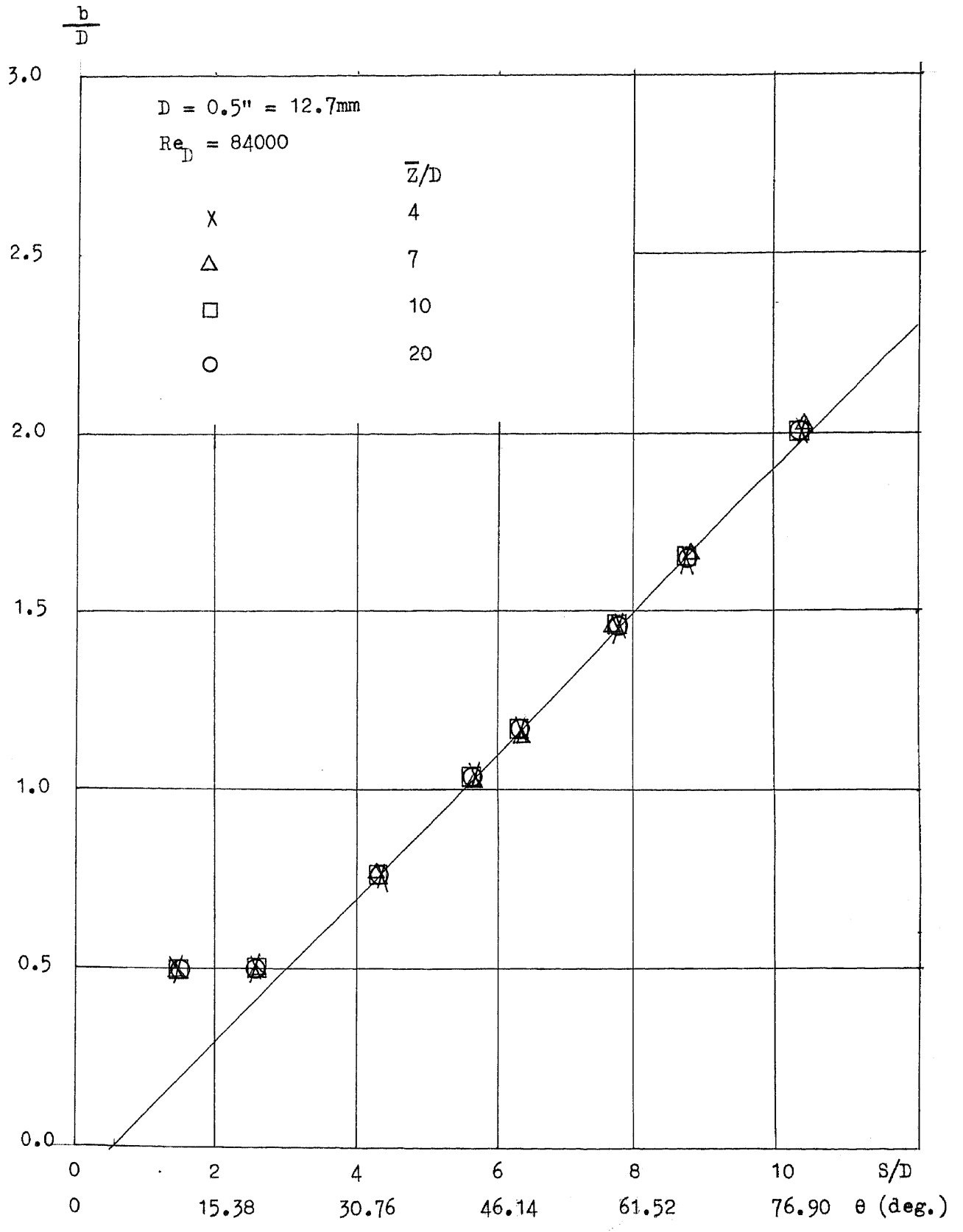

Fig. 138 Profile of Outer Boundary Layer Growth of Wall Jet

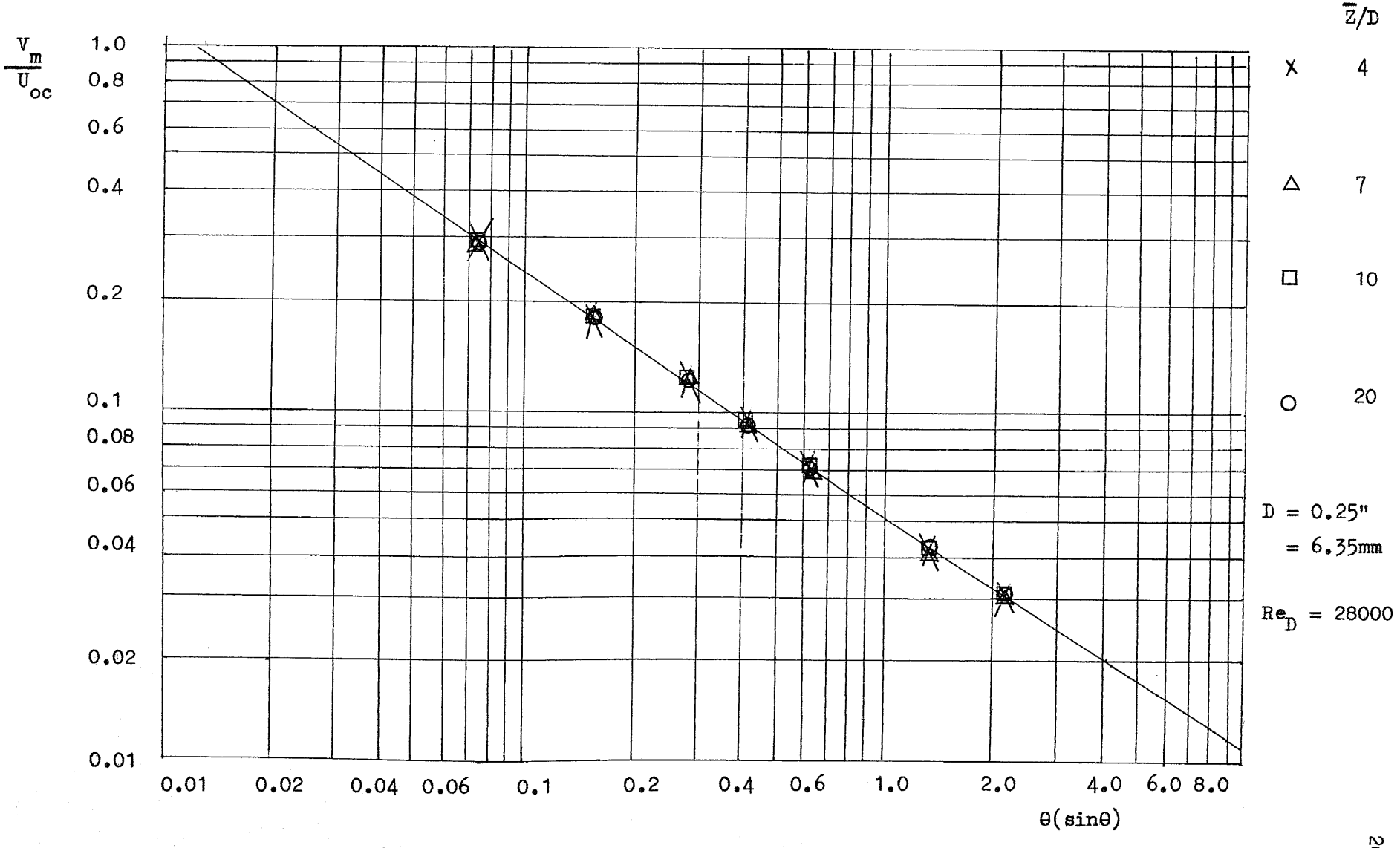

Fig. 139 Maximum Velocity Decay Along The Wall

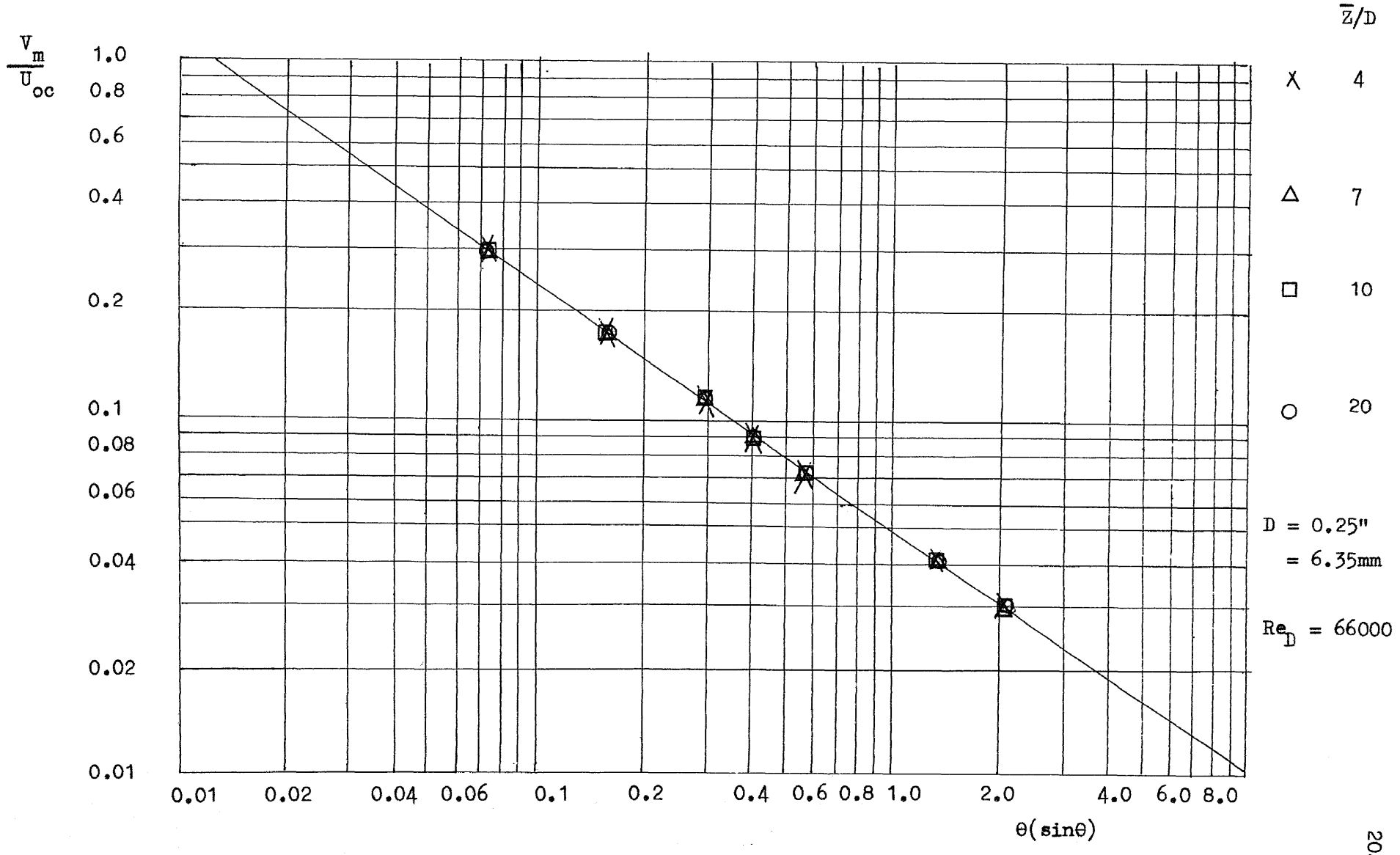

Fig. 140 Maximum Velocity Decay Along The Wall

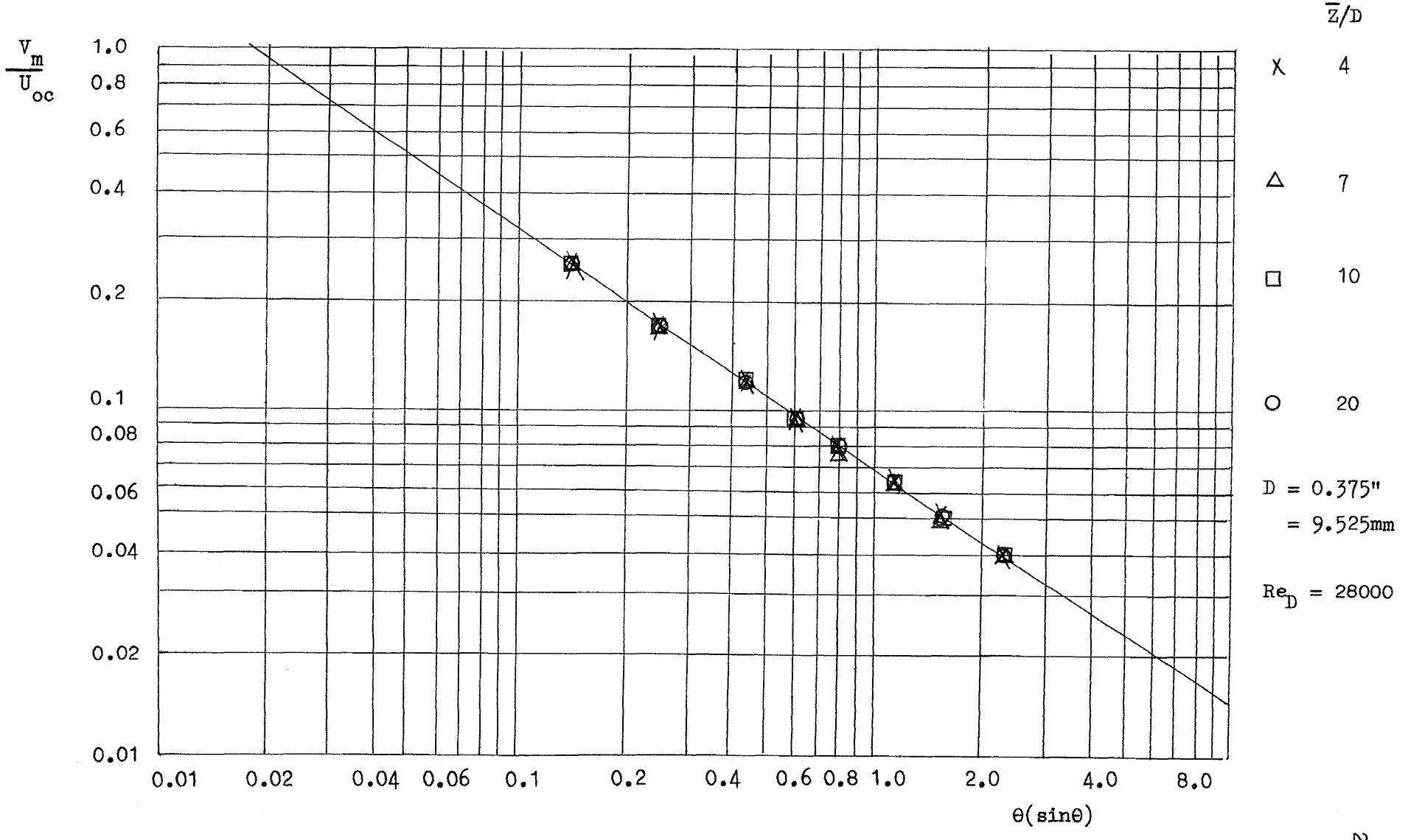

Fig. 141 Maximum Velocity Decay Along The Wall

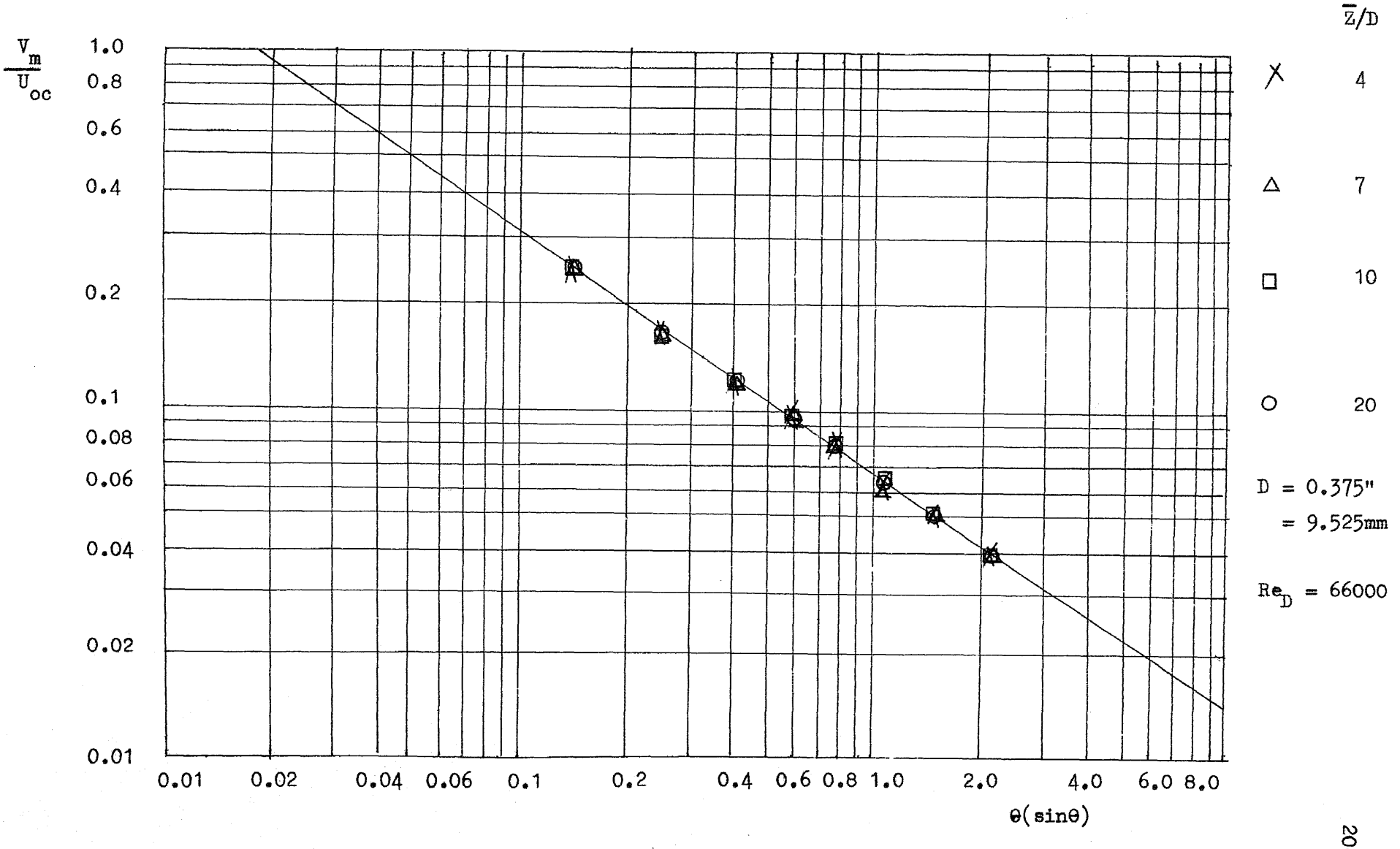

Fig. 142 Maximum Velocity Decay Along The Wall

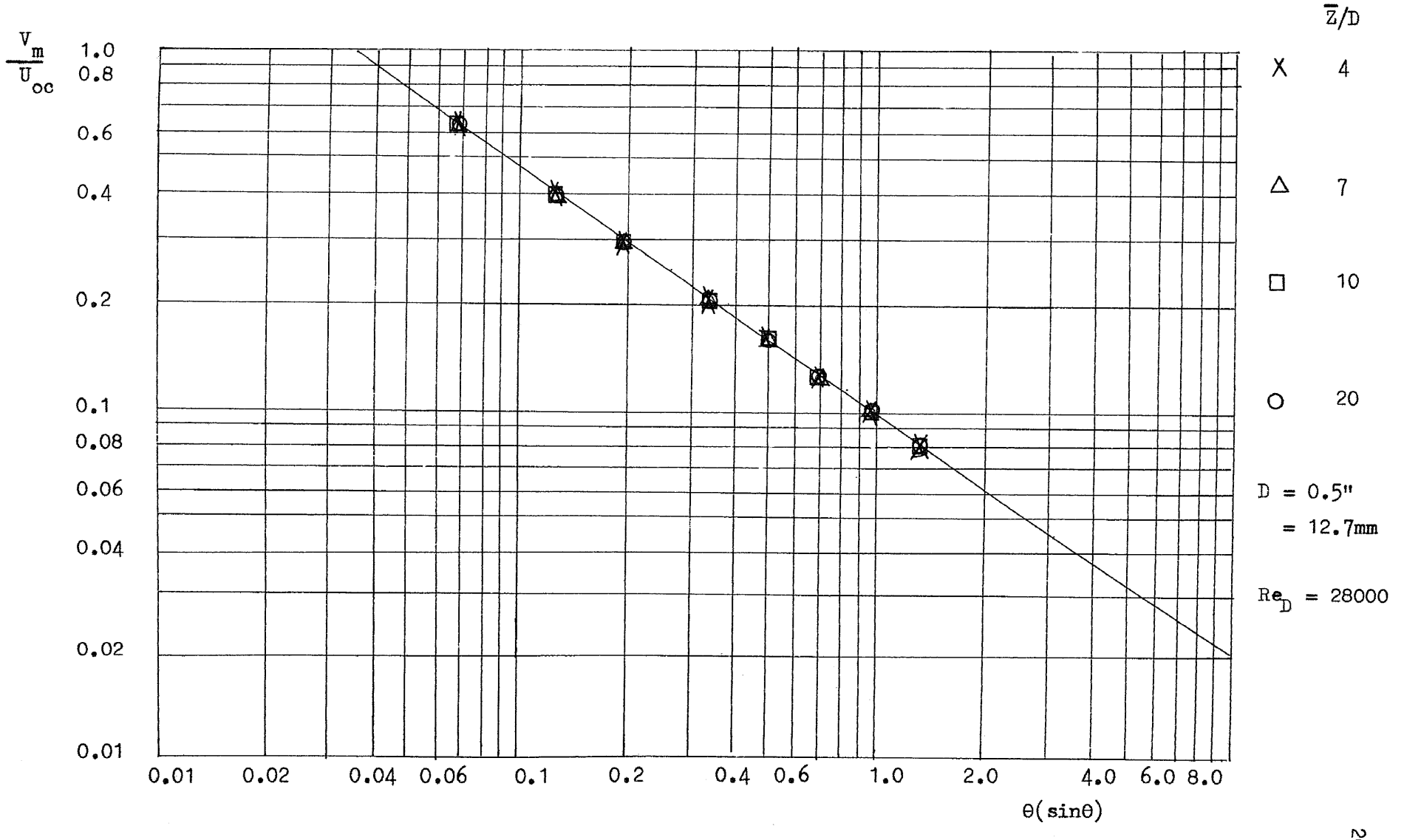

Fig. 143 Maximum Velocity Decay Along The Wall

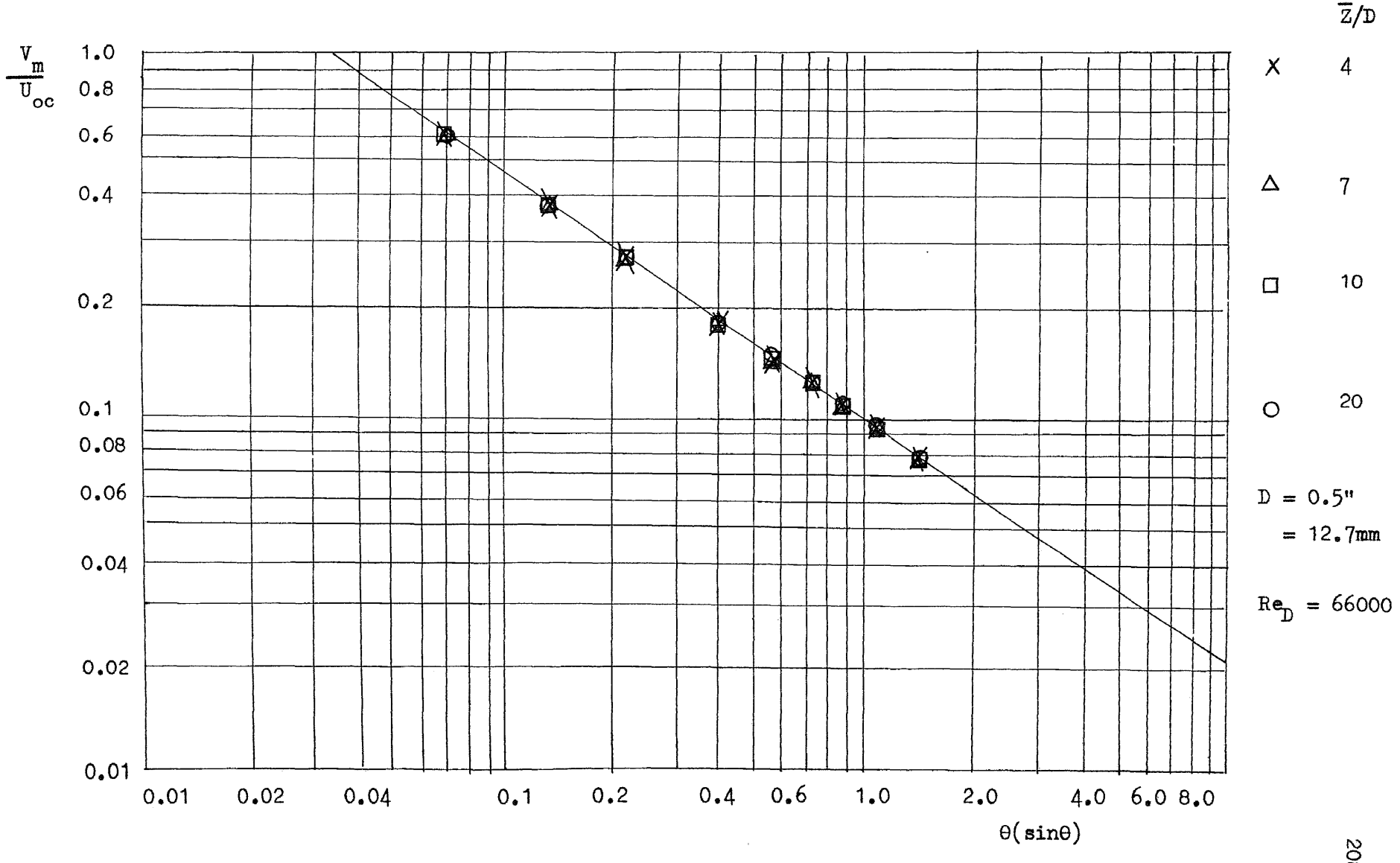

Fig. 144 Maximum Velocity Decay Along The Wall

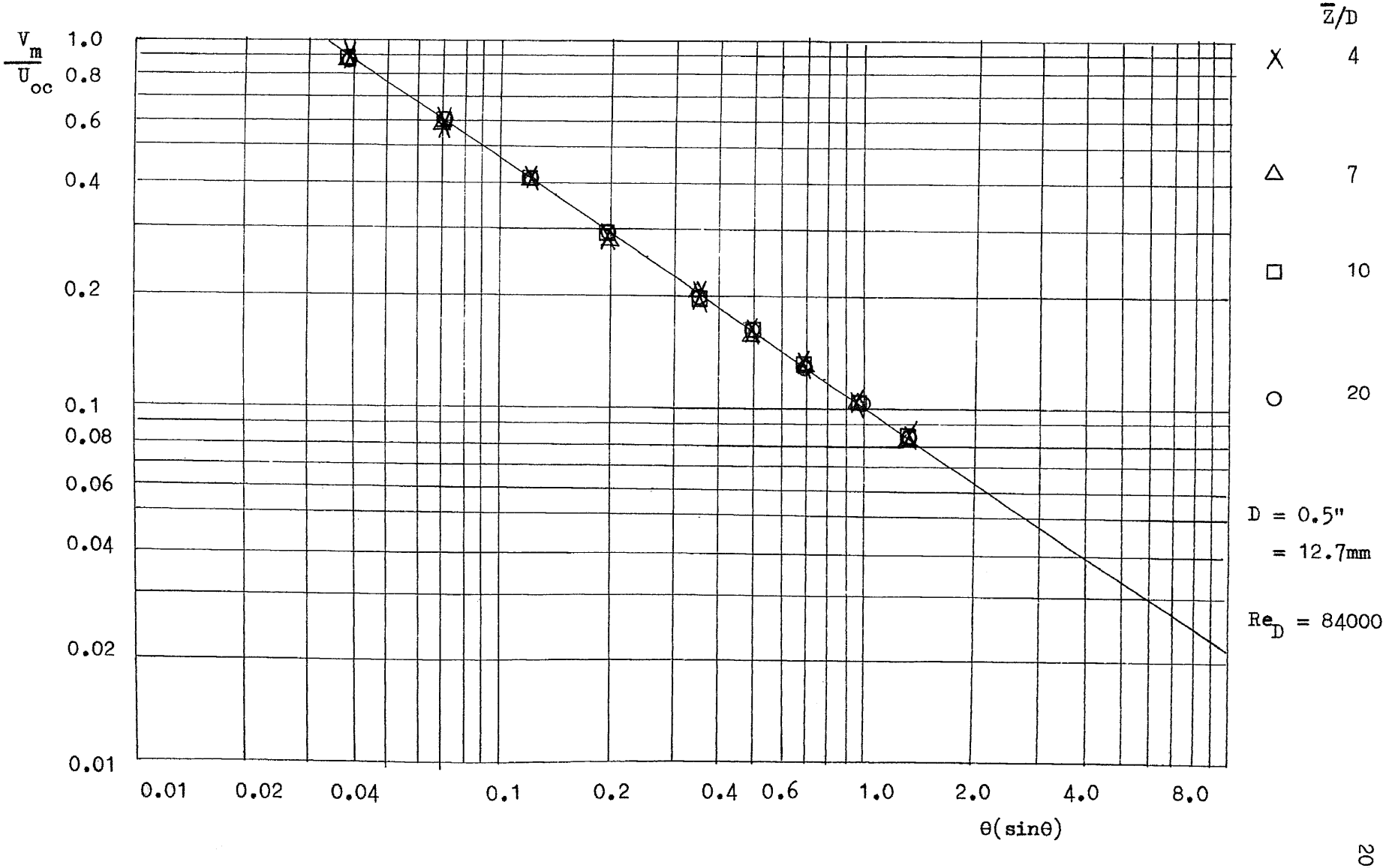

Fig. 145 Maximum Velocity Decay Along The Wall

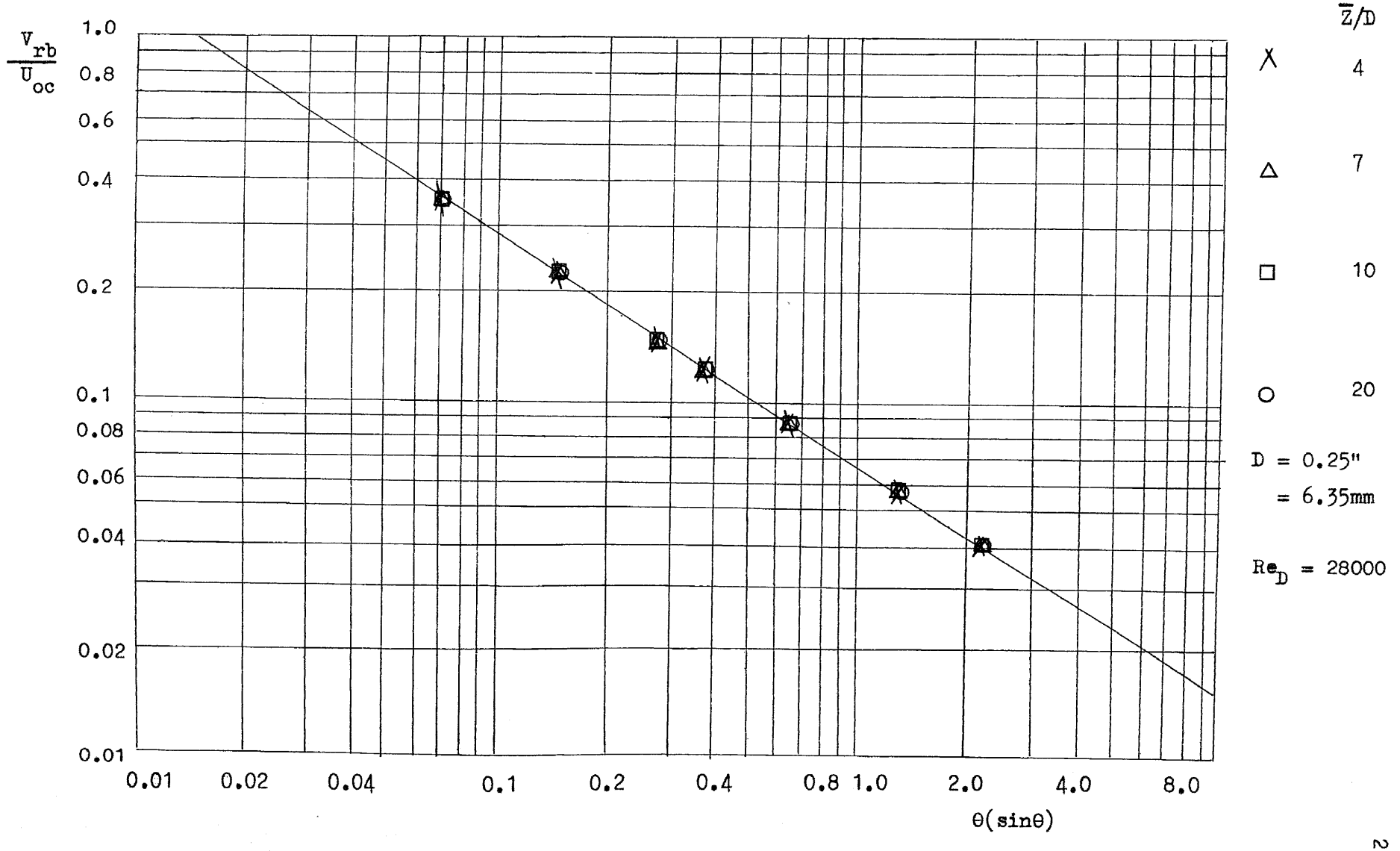

Fig. 146 Reference Boundary Layer Velocity Decay Along The Wall

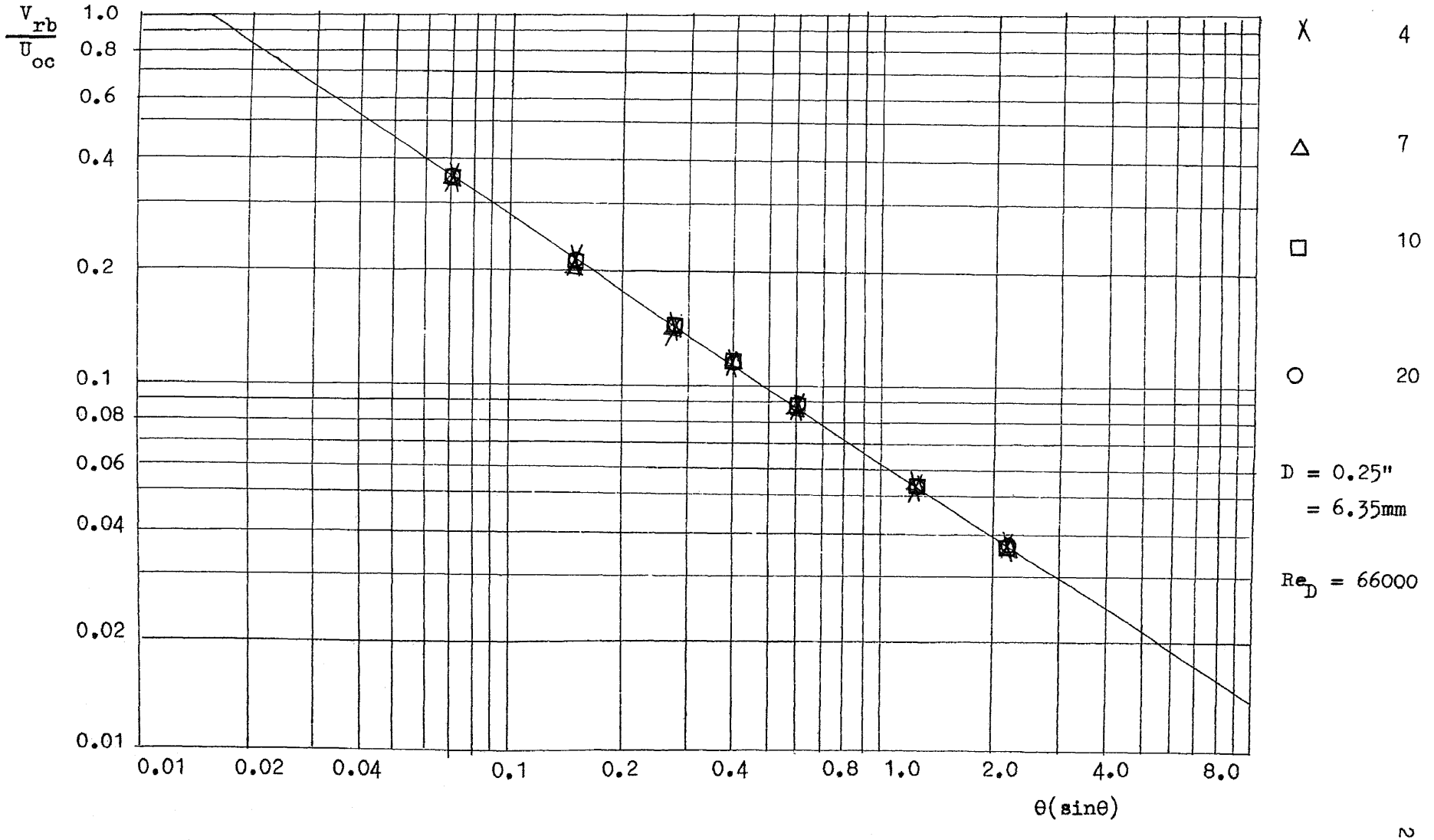

Fig. 147 Reference Boundary Layer Velocity Decay Along The Wall

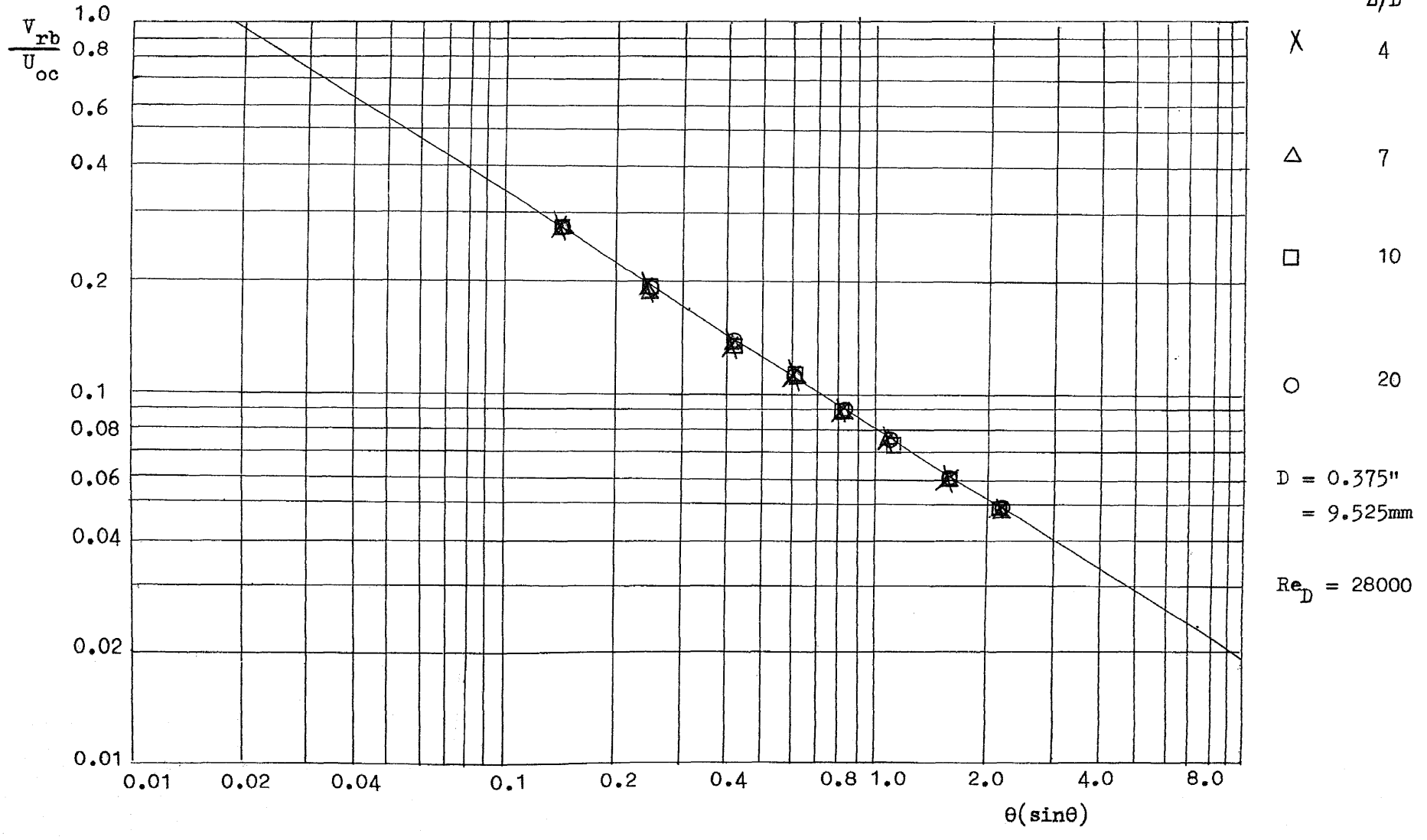

Fig. 148 Reference Boundary Layer Velocity Decay Along The Wall

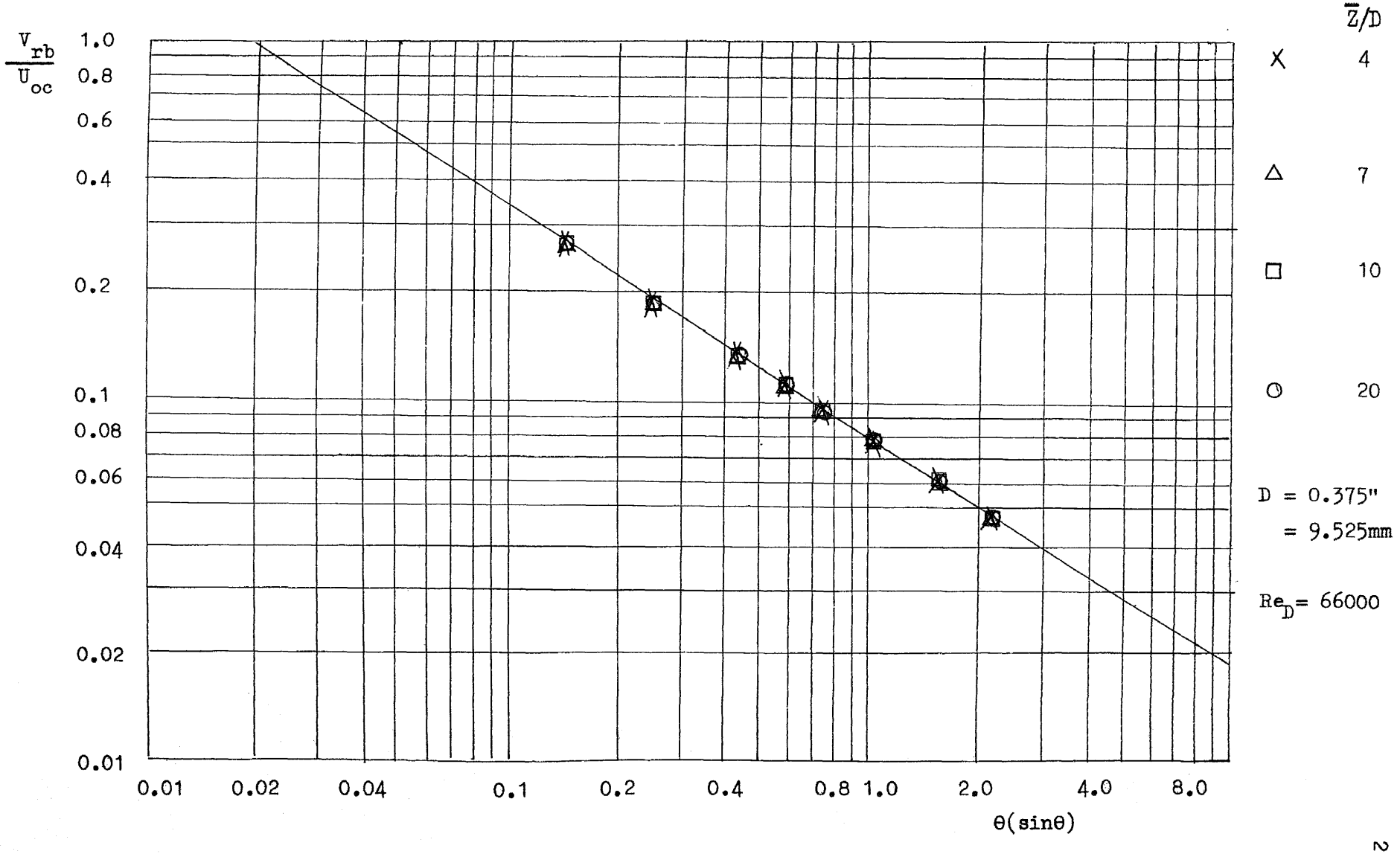

Fig. 149 Reference Boundary Layer Velocity Decay Along The Wall

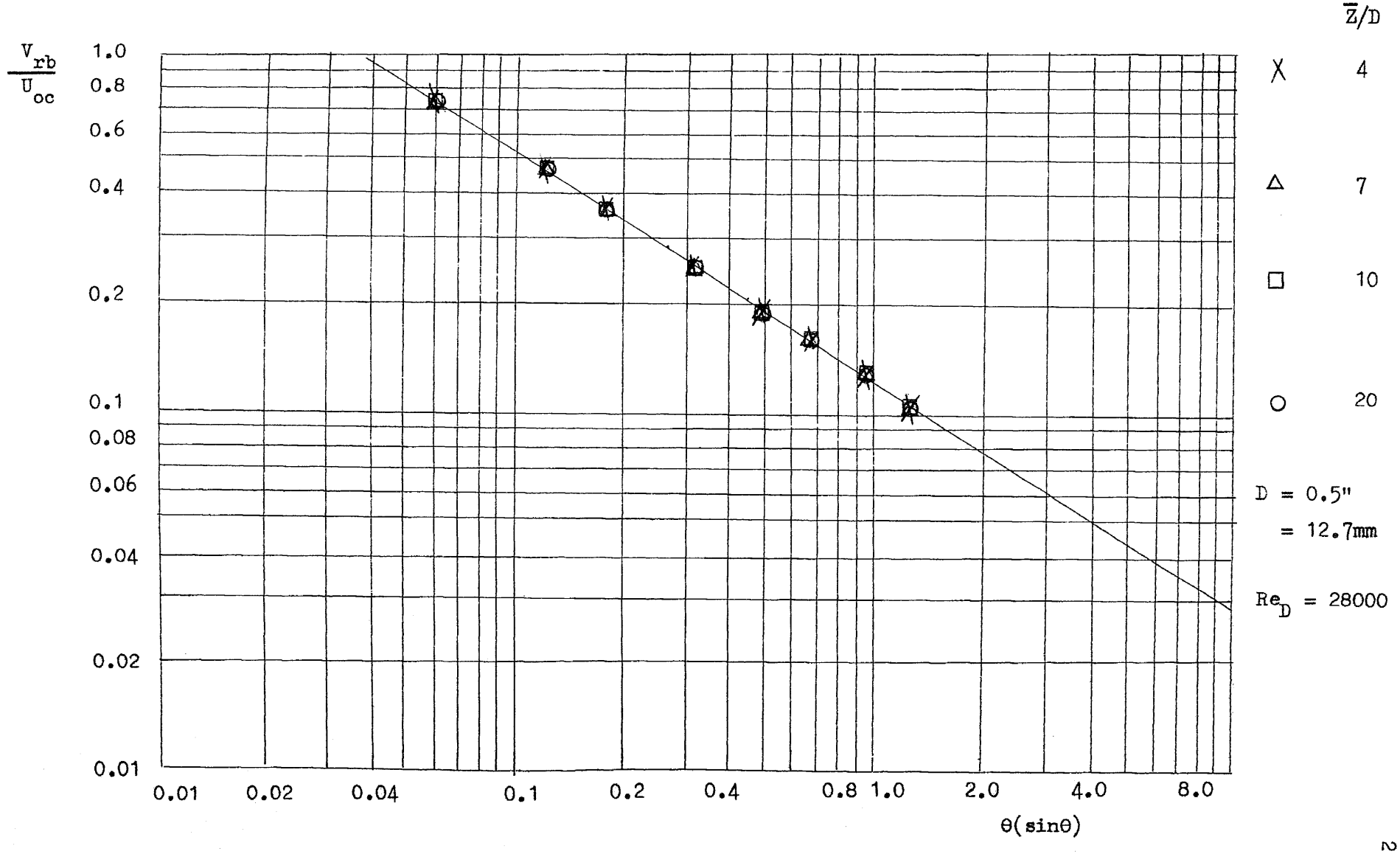

Fig. 150 Reference Boundary Layer Velocity Decay Along The Wall